CHEMPOR ’78

transport phenomena
separation processes
process economics
management sciences
September 10 th – 16 th, 1978
University of Minho
Braga
Portugal

CHEMPOR ’78

fenómenos de transferência
processos de separação
economia de processos
ciências de gestão
10 – 16 Setembro, 1978
Universidade do Minho
Braga
Portugal

CHEMPOR ’78

CHEMPOR '78

INTERNATIONAL CHEMICAL ENGINEERING CONFERENCE

University of Minho

Braga, Portugal

September 10–16 1978

CHEMPOR '78

REUNIÃO INTERNACIONAL DE ENGENHARIA QUÍMICA

Universidade do Minho

Braga, Portugal

Setembro 10–16 1978

ORGANIZING COMMITTEE

Dr. T. R. Bott, Chairman	(University of Birmingham, UK)
Dr. D. Allen	(University of Nottingham, UK)
Dr. A. Bridgwater	(University of Aston, UK)
Dr. J. J. B. Romero	(University of Minho, Portugal)
Dr. L. de J. S. Soares	(University of Minho, Portugal)
Dr. J. de D. R. S. Pinheiro	(University of Minho, Portugal)

COMISSÃO ORGANIZADORA

Dr. T. R. Bott, Presidente	(Universidade de Birmingham, GB)
Dr. D. Allen	(Universidade de Nottingham, GB)
Dr. A. Bridgwater	(Universidade de Aston, GB)
Dr. J. J. B. Romero	(Universidade do Minho, Portugal)
Dr. L. de J. S. Soares	(Universidade do Minho, Portugal)
Dr. J. de D. R. S. Pinheiro	(Universidade do Minho, Portugal)

The Conference is held under the auspices of the **Calouste Gulbenkian Foundation,** which made a generous grant, and of the **University of Minho** which provided the use of their facilities as well as technical and administrative assistance; their support is gratefully ackowledged.

The financial contribution of **The British Council, Petróleos de Portugal – Petrogal, E.P., Portucel – Empresa de Celulose e Papel de Portugal, E.P., Quimigal, E.P., CNP – Companhia Nacional de Petroquímica, S.A.R.L., EPSI – Empresa de Polímeros de Sines, S.A.R.L., Central de Cervejas, E.P., and Finicisa – Fibras Sintéticas,S.A.R.L.,** is also gratefully acknowledged.

A Reunião realiza-se sob o patrocínio da **Fundação Calouste Gulbenkian,** que concedeu um generoso subsídio, e da **Universidade do Minho,** que permitiu o uso das suas instalações e prestou assistência técnica e logística; reconhecidamente se agradece o apoio destas Instituições.

Igualmente se agradece a ajuda financeira de **The British Council, Petróleos de Portugal – Petrogal, E.P., Portucel – Empresa de Celulose e Papel de Portugal, E.P., Quimigal, E.P., CNP – Companhia Nacional de Petroquímica, S.A.R.L., EPSI – Empresa de Polímeros de Sines, S.A.R.L., Central de Cervejas,E.P., e Finicisa – Fibras Sintéticas,S.A.R.L.**

CONTENTS. INDICE

RELATIONSHIP BETWEEN RESEARCH AND PRODUCTION WITH PARTICULAR REFERENCE TO THE MAN-MADE FIBRES INDUSTRY

J R S Morris
BSc Chem Eng, F Eng, FIChemE.

National Enterprise Board, London, England

ABSTRACT

The interface between research and production is reviewed against the development of the man-made fibres industry. The impact of the growth of World population and costs of materials is demonstrated.

The development of specific polymers to meet specific needs which led to the production of Nylon and Polyester yarns is discussed with special emphasis on the part research played to meet the needs of the market place. The particular relationship of research projects and their move into production is discussed in both historical and economic terms, leading to a review of the interface and the place of the chemical engineer in relation to it.

FORMALITIES

It is a great honour to be invited to give this lecture to this distinguished gathering representing as it does the best of Chemical Engineering in our two Countries.

INTRODUCTION

Examination of the relationship between Research and Production in general terms offers almost as much scope for contentious discussion as would the general examination of relationship between men and women!

Of greater practical interest with the possibility of arriving at some conclusion of value, is an examination limited to the relationship between defined and known parties.

I therefore propose in this paper to examine the fairly closely defined topics of Research into the creation of man-made textile fibres and the Production of these fibres on the industrial scale. It will be difficult to keep to these guidelines and not wander too deeply into other closely related topics as for example, the natural fibres, textile processing, or fabric and garment making activities - but if I do I hope the digressions will have relevance.

I will first examine the Research background, then examine the production pattern which has emerged and finally make some observations which seem to me to be relevant to those of us concerned not only with knowledge for its own sake but also with its exploitation for the benefit of society generally.

RESEARCH ON MAN-MADE TEXTILE FIBRES

Human beings are by nature given to curiosity (some more so than others!) and it is not surprising that they should wonder how the spider makes his web or the silk worm his cocoon and therefore it should not be unexpected that we can find recorded as long ago as 1664 by R Hooke in his publication 'Micrographia' that it should be possible to produce fibres similar to silk by forcing a suitable liquid through small holes. But Hooke's motivation was simply knowledge and he did not pursue the idea.

After the industrial revolution, production for profit became a powerful motivating force for research in general, and in the fibres scene in particular a number of attempts to emulate the silk worm made their appearance between 1850 and 1900. The most important of these were by Chardonnet 1884 who made nitrocellulose fibres, Bemberg 1890 who made regenerated cellulose fibres from a solution of cellulose in cuprammomium, and 1892 Cross, Bevan and Beadle who made regenerated cellulose fibres from a solution of cellulose xanthate in caustic soda.

The motivation for these researches and the subsequent successful commercial exploitation of the two latter products was the profitable production of a textile fibre to compete at the expensive end of the fabric and apparel industries ie to compete with silk. The major proportion of the textile market of the time was comprised of cotton, flax, wool and silk with the highest profits derivable from the smallest section viz silk. This high profit market was the target which was attacked with significant commercial success, as research and development produced the scientific and technological information needed to make "Artificial Silk" at costs which provided the financial backers with very acceptable rewards for the risks they had taken. But for 'Artificial Silk' to be commercially successful in competition with natural silk, research and development had only to produce competitively against the expensive end of the market without the essential requirement to produce at the lowest cost technically possible.

Whilst the required targets of product quality and cost were very adequately achieved for these regenerated cellulose man-made fibres, the processes are extravagant users of energy and materials, and in our modern and more enlightened approach to total conservation of resources they can hardly be ranked amongst the best applications of scientific research and development.

I therefore pass over the next 4 decades, during which both the technology of the process and the fibres based on regenerated cellulose, were economically and technically improved, so that they were able to enter industrial uses and then into staple fibres markets where they competed with cotton, and pass on to consider the entry into the arena of another and equally powerful motivating factor for research into textile fibre ie world population growth.

The graphs 1 and 2 show the total world population and the total productions of the natural and regenerated cellulose fibres up to present day.

It is now perfectly obvious that the problem of finding textile fibres for clothing the rapidly increasing number of bodies in the world began to make itself felt in the middle of the last century, and was simultaneously attacked by increasing the production of natural fibres and by the creation of man-made fibres which we have already seen made their first impact into the costly end of the natural fibre market.

The graphs also show that the rate of increase of production of natural fibres was far less then the rate of increase of population. This situation challenged Research which has of course followed many lines of attack, the more important being:

(a) to control the growth of the world population. Fascinating as this subject may be I regard it as outside my terms of reference and time allocation.

(b) to seek out methods of creating apparel from materials other than natural or conventionally made man-made fibres. This again is an important and extremely active field of research activity the consideration of which I must also consider outside my time allocation.

(c) to increase the rate of production of natural fibres - but notwithstanding automatic cotton pickers and sheep shearers etc there has been virtually no impact made on the rate of increase due to other competing demands made upon cultivatable land by the same increasing world population. The increase that has been achieved is attributable in large measure to the efforts of research in generating higher yield per acre cultivated rather than to the cultivation of larger acreage.

(d) to make the regenerated cellulosic textile fibres available in much larger volumes and accessible price-wise to a much larger section of the total market. This has been achieved with a notable degree of success but is ultimately limited by the energy and/or materials extravagances of the present viscose and cellulose acetate processes.

(e) to seek out or create new polymers which can be converted into textile fibres more economically than by the regeneration of cellulose. This was the major research challenge during the years after World War I and results were just reaching the stage of exploitation when World War II intervened - but not before the polyamide 'Nylon' had demonstrated the ability of Research to attack and find at least one answer to the problem. By the circumstance of history Nylon was then enabled to benefit by a development during the years 1939 - 1945 which was more or less unhindered by competition.

But the economic advantages obtained by Nylon in its unusually rapid growth also served to emphasise more quickly its technical disadvantages which gave tremendous impetus in the years immediately following World War II to the search for other polymers which would be both economically and technically superior to Nylon. A large number have been examined and many - some would say too many - are being exploited today. Polyamide still survives with - polyester - polyacrylic - polyolefin and glass now established as major competitors in addition to the cellulose based man-made fibres.

In the search for all of these fibres which are now in production and also for all of those which have fallen by the wayside the motivations have been one or more of the following depending upon the involvement of the person concerned:

(a) curiosity and the search for knowledge for its own sake.

(b) the challenge to so improve the technology of production of established fibres as to secure a profitable existence in the face of competition from other established natural or man-made fibres or from new developments.

(c) the challenge to create from accessible raw materials fibres having the textile properties necessary to supply the increasing market which the natural fibres are clearly unable to meet.

Although the efforts of persons working in accordance with motivation (a) must not be underestimated in their possible long term impact upon humanity eg Archimedes, Faraday, Rutherford, and Hooke etc, by far the major human and financial resources deployed on research are in the (b) and (c) categories above, where the relationships to Production are reasonably simple and clear.

In the case where motivation has largely been attributable to (b) above the relationship of research to production is one based upon a successful and established industry and aimed at improving efficiencies, product quality and variety to maintain its position against established competition or possible new competitors.

In the case where the motivation has largely been attributable to (c) above the relationship of Research to a Production which is not yet established is one based upon a search for the optimum product to fill a known and/or established need such as that for more apparel to clothe the increased population of the world.

In the man-made fibres field the efforts of Research resulting from all the above motivations have been significantly successful when judged in terms of scientific and technological achievement. So now let us look at Production.

THE PRODUCTION OF MAN-MADE FIBRES

Although the solely scientific outcome of Research into the various aspects of man-made fibres can very rightly be granted a large measure of success, the production and commercial exploitation of those fibres has not been without problems.

Although many of the problems are not directly attributable to the quality of the scientific research work, they do none-the-less have roots in those technological aspects, and to understand what these problems are it is appropriate to compare the production processes for natural and man-made fibres and especially to examine their differences.

It is generally true to say that the polymers which nature manufactures and converts into fibres are made in relatively small production units eg the silk worm, the cotton bush, the flax plant, the sheep's back, and it is further generally true to say that the manufacturing life cycle for any one of these producing units is relatively short being usually measured in a small number of years

or even fractions of a year. Apart therefore from politically motivated intervention, the mechanism for balancing demand and supply can become effective fairly quickly, and without rendering uneconomic the continuing production from a smaller number of units or requiring massive investment to meet a relatively small incremental demand. In most instances the major asset is land the value of which is only slightly affected by the short term variations of supply and demand.

In contrast the pattern of production for man-made polymers for conversion into fibres has for simple economic reasons required large investments in a relatively small number of high output units. These high investments mean simply that a fall in demand very quickly increases the production cost to uneconomic levels, and conversely any significant increase in demand requires a further large investment to install equipment having an output sufficiently large to produce material competitively with established plants and the demand does not normally increase in such conveniently large steps. Herein you see both the problems and their causes which confront the manufacturer of polymers for man-made fibres production.

At this point it is opportune to examine some of the actual economic factors which have been and continue to be associated with business in the man-made fibres industry, in order that we may understand more precisely the nature of the problems to which I have just referred.

Because all of the man-made fibres have experienced and/or continue to experience similar economic problems the general nature of these problems can be comprehended from a specific examination of the polyester fibres. The following table shows for Western Europe the installed capacities, mill consumptions and total productions of polyester continuous filament yarns and staple fibres from 1965 to 1977. The figures are presented pictorially in graphs 3, 4 and 5.

When presented in graphical form the general trends are inescapably obvious, and reveal a situation which is an economic nonsense, and one in which existing installations can only afford to continue manufacturing if their operations can produce a positive cash flow or receive massive support from politically motivated sources.

WESTERN EUROPE POLYESTER CAPACITY AND UTILISATION (Figures in thousands tonnes)

YEAR	FILAMENT YARN		STAPLE		TOTAL		
	CAPACITY	MILL CONSUMPTION	CAPACITY	MILL CONSUMPTION	CAPACITY	PRODUCTION	%UTILISATION
1965	60	59	106	75	166	151	91
1966	81	70	140	104	221	194	88
1967	104	83	172	106	276	216	78
1968	137	121	218	150	355	311	88
1969	186	144	254	195	440	396	90
1970	239	158	307	180	546	459	83
1971	308	236	337	227	645	587	91
1972	439	226	399	283	838	657	78
1973	461	292	438	370	899	826	92
1974	522	248	466	320	988	784	79
1975	570	258	534	287	1104	682	62
1976	582	287	615	345	1197	800	67
1977	610	286	648	329	1258	730	58

Consideration of the causes which give rise to this situation - which is not unique to polyester - is more than sufficient for a separate paper but it is appropriate here to emphasise that the investment required per unit of fibre output is a very significant factor. It is well understood that production costs tend to fall as scale of output is increased, but that the capital investment to secure that additional output inevitably increases, albeit not linearly. Thus, as the total actual installed capacity rises so also does the size of an economic additional manufacturing facility increase if it is to enter the market at a competitive selling price. Insofar as Western Europe is concerned it is clear that the means of resolving this dilemma has not yet been established. There must be a pause for many years to allow the consumption requirement to catch up with capacity and hopefully to allow a system to be established which will avoid a repetition of the 1965-77 cycle of events.

DEVELOPMENT

We have seen in the foregoing that the manufacture of polymers and their conversion into man-made textile fibres is accompanied by production and economic problems which have inevitably arisen from exploitation of the knowledge provided by Research.

If the matter stopped there the whole of industrial activity would rapidly stagnate and wither. But since both parties realise this gloomy prospect, it is in their mutual interests to establish and maintain a continuing relationship, in which the Research partner must endeavour to alleviate the basic problems which are inherent in the primary application of his Research results and must move towards overcoming those problems which are unforseen before full scale production and/or which can only be totally solved on the production scale.

No matter how well based was the initial Research work, nor how well engineered was the first production unit, there is no manufacturing enterprise which has attained and maintained success without this absolutely vital relationship which is 'Development'.

To illustrate the vital role of Development I would cite one or two specific examples from the man-made fibres scene.

(a) The wet strength of regenerated cellulosic fibres: normally made viscose fibres have properties in the dry state which are very similar to cotton with which they are primarily in competition but when wetted as in laundering or even by changes in humidity the strength falls significantly below that of cotton. Thus a viscose fabric could well be permanently deformed if subjected during laundering or when otherwise in the wet state to forces which would not cause similar deformation to a cotton fabric. Clearly this represents a severe handicap vs cotton for many applications - even simple ones like bed sheeting or window curtains, and it was vital that means of overcoming this deficiency should be developed without adversely affecting the desirable properties or creating other similar or even more serious problems.

With fullscale manufacturing equipment already installed the manner by which the problem can be overcome is already subject to considerable restraints, dictated by that which is economically reasonable on the installed manufacturing plant, and the closest of relationships must be maintained between production and development to achieve what almost inevitably has to be the best compromise. In the example quoted changes in composition of the coagulating bath to affect the rate and nature of the coagulation process had to be developed to yield the more cotton-like high wet strength fibres which have successfully met the market needs - but at a slightly higher cost.

(b) Comfort from fabrics containing hydrophobic fibres.

For apparel usage and especially for clothing worn in close proximity to the body comfort is widely associated with an ability to absorb perspiration. Unfortunately a number of man-made fibres eg nylon, polyester, polyolefin are essentially hydrophobic and these fibres suffer a severe market limitation unless they can be presented with a favourable balance of acceptable properties. In fact my audience will be aware of the failure of nylon as a shirting material for this single reason which more than offset the favourable properties of easy care, stability, strength and cost.

In this case the relationship between the commercial and scientific interests is on a wider basis than in the previous example, and embraces

the whole gamut of research - development - fibre production - yarn processing and fabric structure. Its resolution involves polymer variants, fibre dimensions, yarn texturising and fabric structure, including admixture with other fibres or yarns which are able to supply complementary properties to yield a balanced end-product. Relationships have now been established not only between production and research and development but also with textile yarn manufacture and fabric construction experts.

The relationship has become at least quadripartite and the need for constant and effective communication is obvious to expedite the solving of the problems in one or more ways without time consuming expenditure or costly mistakes.

THE RELATIONSHIP

In the foregoing I have many times referred to various relationships including those between Research and Production, Development and Production, Research and Development, Production and Yarn processing, and yarns and fabric constructions.

Each of the activities is represented by people having specific abilities and interests and each contributes an essential part towards the ultimate success of the total activity of economically providing the community with an essential commodity based on the results of creative research.

The relationships in every case are those between people who must have a wider horizon than their own specifically allotted problem and who must be able to see the resolution of their own problems in the context of all the problems involved in translating the research chemists' idea to the shirt or blouse on the back of the customer.

Maintenance of proper communication between all parties is vital, to ensure a totally integrated pattern, and one in which the relationship between Research and Production is established at the earliest stage through the realisation of a Development function. The problems likely to arise, as for example the very relevant problem of matching economy of production cost with investment in polymer production plant can only be foreseen by such a liaison and the appropriate decisions then taken to alleviate.

So I have now gone full circle and from an examination of the specific relationships between Research and Production in two areas of the man-made fibres industry, it is clear that the relationship must always be an effective one between people and particularly between people involved in the Development aspects with those in the scientific and in the production and in the commercial aspects. The development arena is one where the chemical engineer must play a major part - not only in the application of his special technology but also in ensuring the proper degree of relationship between people involved in all the facets of the total enterprise.

GRAPH NO. 1

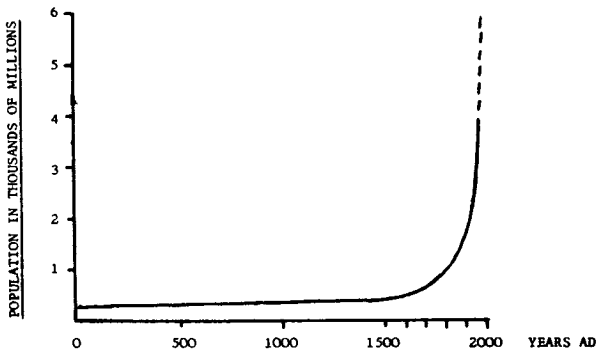

GROWTH OF WORLD POPULATION

GRAPH NO. 2

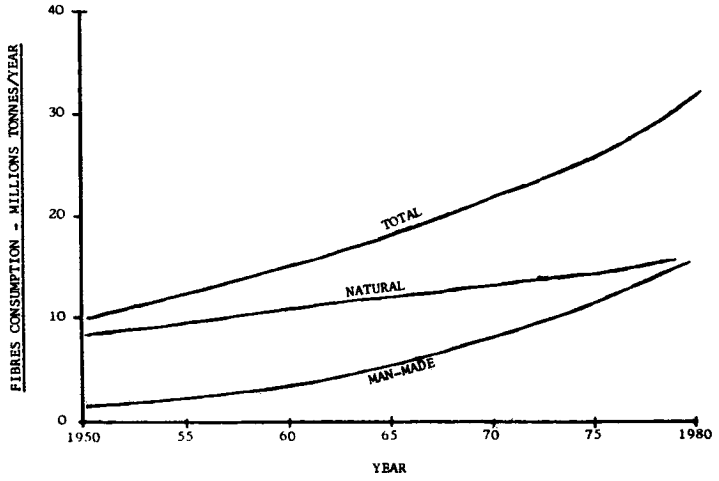

NATURAL, MAN-MADE, AND TOTAL
WORLD CONSUMPTION OF FIBRES

GRAPH NO. 3

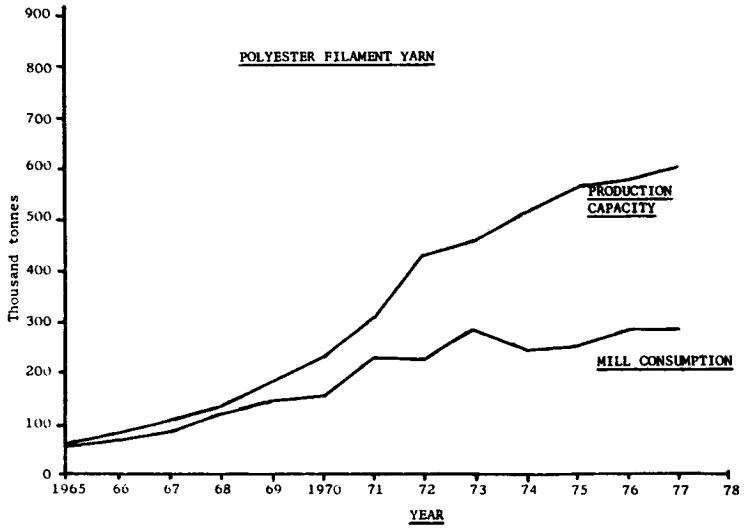

GRAPH NO. 4

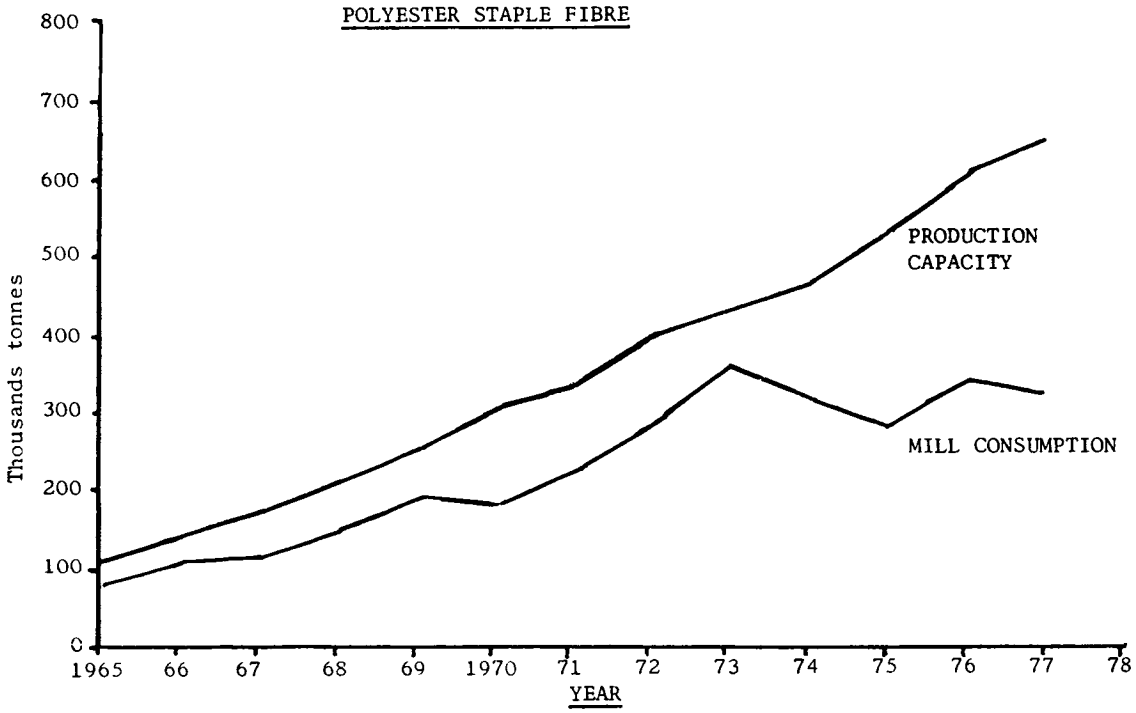

GRAPH NO. 5

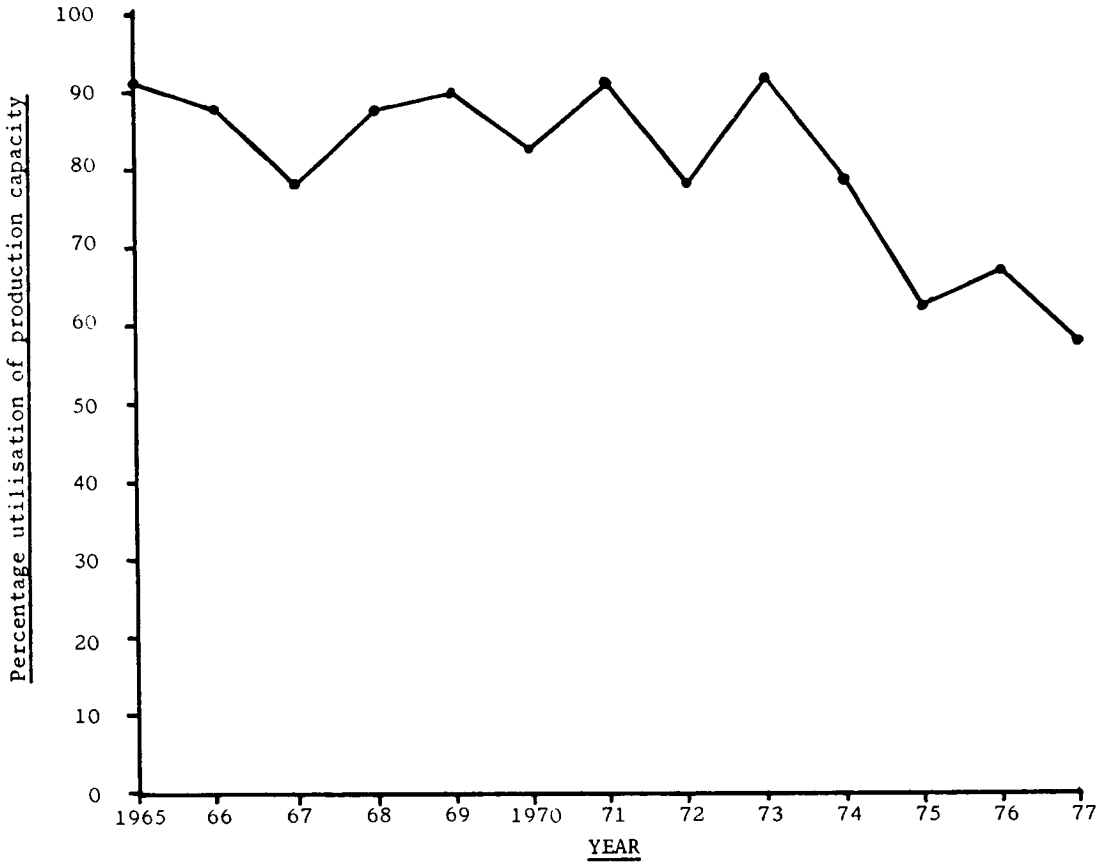

POLYESTER FIBRES

Total production as percentage of capacity

THE MANAGEMENT FRAMEWORK FOR EFFECTIVE TECHNOLOGY TRANSFER

John Dingle [1]
Carlos Beaumont [2]

1. Double L Consultants Limited, London, UK.
2. Companhia Nacional de Petroquimica, Lisboa, Portugal.

ABSTRACT

Technology transfer is an engine for social and economic development through industrialisation. It incorporates process technology, project engineering technology, production and marketing technology, and the means whereby this body of experience and expertise is translated from one environment (the "transferor's") to effective operation in another (the "transferee's").

Accelerated development of a new generation of basic industries may make heavy demands on national resources, which are commitments on the effectiveness of technology transfer. That effectiveness becomes even more crucial when, as in the petrochemical industry, the technology supports and sponsors the growth of an advanced and integrated market-orientated industrial superstructure.

Portugal's situation is distinct from that of any other petrochemical technology transferees, partly because of its unique location at a crossroads of world trade, partly because of the potential for home demand, and partly because of the nature of its industrial and social base.

Thus the transferee must be able to find and maintain an active role in the international market place. At the same time he must become the inspiration of qualitative as well as quantative growth in the home market if the technological level of the industrial superstructure is not to stagnate.

INTRODUCTION

The transfer of technology has, throughout history, affected the course of civilisation, although not always with the benefits expected by transferor or transferee. Thus, iron smelted in Africa, forged in India, shaped and tempered in Persia and Arabia, may have helped the spread of Islamic culture behind the swords of the Jehad [(1)]. A prime condition for these industrial achievements must have been the ability of "recipient" cultures to accept, efficiently utilise and eventually develop their own contributions to the application of technology. This management framework for effective technology transfer is the topic which, in the context of modern Portugal, we intend to discuss in this paper.

Technology transfer is an engine for social and economic development through industrialisation. It incorporates process technology, project engineering technology, production and marketing technology, and the means whereby this body of experience and expertise is translated from one environment (the "transferor's") to effective operation in another (the "transferee's"). A typical definition of technology transfer is "the process through which the production system of a country (public and private enterprise) acquires a technology produced in another country for incorporation in those enterprises" [(2)]. As is well known, many recipient countries have voiced their dissatisfaction with certain aspects of the mechanism of technology transfer, in which real or supposed restrictions imposed by the transferors are considered to be disadvantageous to transferees, particularly those which are "developing" countries. In consequence the international trade and development body UNCTAD is considering setting up a code of conduct governing technology transfer.

Whatever the outcome of these deliberations, at least part of the anxiety felt by recipients of the more advanced technologies, such as those

relevant to development of the petrochemical industry, is due to doubts that processes, plant designs and operational techniques worked out and implemented in countries with a very sophisticated industrial and commercial infrastructure, are altogether appropriate for transfer to countries at a level of industrialisation which is significantly lower, yet characterised by rapidly accelerating development.

In addition, ideas of what constitutes "appropriate" technology have been confused by socio-economic and political ideologies too vague or too ill-matched with the specific needs of industry and commercial realities in a country. Thus, we find opinions on "appropriate" technology transfers as diverse as the "Small is Beautiful" philosophy launched by the British economist E.F. Schumacher, which has come to symbolise the reaction against capital intensity in industrial development, and the view not uncommon in political circles, that technology as a contributor to a nation's industrial development should be chosen on the basis of that nation's political and social aspirations (3) (4) Whatever these aspirations may be, it is likely that their expression in terms of government policy will change more than once during the time over which industrial technology is commercially applied. We need, therefore, a view of technological appropriateness which is more in line with industrial practice. We suggest that the underlying principle guiding our choice of "appropriate" technology in any instance should be, that it is the most "advanced" which can be *maintained* in normal operation by normal means at the recipient site. In defining the appropriateness of technologies in this way we are only stating a necessary condition: the industrial policy adopted and the actual undertakings shall determine which sets of appropriate technologies fall within a coherent strategy of long range industrial development.

Clearly, the idea of normalcy in relation to industrial practice, i.e. normal ways of producing and marketing industrial products, leads us to consider the special position of Portugal with reference to international markets and commerce - the petrochemical business is after all, an international business.

Most of the European states have joined one of three economic unions. Their respective share of European population and of wealth generating capability as measured by gnp is shown in Table 1.

Table 1

	% population	% gnp	gnp/cap US $
EEC	33.5	49.0	5401
EFTA	4.7	7.5	5978
(in which Portugal	1.2	0.5	1570)
CMEA	46.9	35.3	2778
Non-aligned *	14.9	8.2	2024
	100.0	100.0	

Source : World Bank Atlas, 1977.

Table 2 compares Portugal with the countries of most similar population, in other economic groupings : *(see page 3)*

Thus, there is a sense in which Portugal's projected membership of EEC should be seen as a greater challenge than is its present membership of EFTA. It is a challenge which, we suggest, must be met by market-led industrial growth, which - as regards petrochemicals - throws some light on what is meant by "advanced" technology.

Table 2

	Belgium	Portugal	Greece	Bulgaria
Union	EEC	EFTA	non*	CMEA
Population million	9.8	9.6	9.1	8.7
urban %	87	26	65	58
econ. active%	41	39	38	52
gdp US$/capita	6352	1517	2140	1689 (nmp)
Production indices				
agriculture (1961/5 = 100)	116	108	154	146
industrial (1970 = 100)	108	132	151	157
Trade (a)				
Exports, % gdp	48.9	11.5	11.5	31.8 (nmp)
%av. vol. increase 1971 - 6	7.3	2.6	17.0	19.5 (b)
Imports, % gdp	52.6	26.8	27.1	36.7 (nmp)
%av. vol. increase 1971 - 6	6.7	3.2	6.7	19.5 (b)

Source: UN and OECD Statistics. Data refer to 1975 except (a) = 1976. (b) = authors' estimate. "nmp" = "net material product" not strictly comparable with "gdp" = gross domestic product.

* Some of these countries are associate members of the economic unions. Details of membership are given in Appendix 1.

Regarding its trade pattern, Portugal stands at the historic crossroads of commerce between Europe, the Americas, Africa and the Middle East. Membership of EEC will confirm West Europe as Portugal's major market place. The home demand for petrochemical products is still too small to support production at a competitive scale without exports, at least during the first years of operation, and those exports will be aimed very largely at West Europe. But, as is well-known, West Europe has, and is likely to have for the next five years, considerable overcapacity in all the commodity petrochemicals. How then, can Portugal expect to move the excess products of its nascent petrochemical industry into such a market place ?

The most obvious driver for such movements is price, and there are several examples of methods whereby relatively new producers move, or plan to move, their products into the West European market in spite of the competitive situation. The CMEA producers do so by counter-trade for plant and technology. The future producers of OAPEC intend to do so with the help of cheap raw materials. Neither however, seems to be good model for the Portuguese petrochemical industry, because - without the use of some rather unusual and probably unacceptable accountancy - neither would show an economically sound return on the investment of national resources which that industry represents. On a general examination one may conclude that the Portuguese internal market has reached such a size that it can justify and support the transfer of production technologies; the size of exports on a surplus basis only, is however much too small to allow for the transfer of international marketing technology. How to export, then, the relatively small quantities which will be necessary to push domestic production to

competitive scale ?

One possibility would be to undersell by such a margin that international operators would be attracted to trade Portuguese products; we shall see that there is no real interest in doing this. Another possibility would be to engage in joint-ventures in which the international marketing technology will be supplied by the foreign partner who, on the other hand, would gain captive participation on the Portuguese domestic market through the joint-venture.

Considering the market overall, it is easy to see in general terms that Portugal has no natural competitive advantage which would result in lower production costs. Moreover, it is seldom that any single technology is available for transfer, the production economics of which allow product selling prices to be significantly less than market prices in an over-supplied market. Thus we see that "advanced" technology has to be defined in terms of "advanced" products i.e. products which can be differentiated by their purchasers in terms of price/performance, or "marketability". We believe this favourable differentiation imposes three obligations on the management of technology transfer:

1. The feasibility of projects must be based on market realities, which may demand the integration of series of technologies;

2. The means of technology transfer must promote development of the recipient's own technological capability;

3. The recipient must plan for the organisational growth and change which will follow from technological transfer.

1. PROJECT FEASIBILITY AND MARKET REALITY.

The management of technology transfer begins with the first step of project feasibility analysis, the identification of opportunity for new capacity. Such opportunities, as future outcomes of the balance between projected demand and supply, with enough time in hand to get the "opportunity" capacity built and operating, are rarely found as neat points in time. They are more likely to appear as a kind of window with a rather fuzzy frame within which technological options have to be worked out in terms of commercial practicality.

(Figure 1)

The technological data normally available at this stage are ill-defined, for unless the new project is a copy of a plant already in operation, differences of scale, configuration, and the extent of integration with adjacent facilities are likely to make it impossible to obtain precise information on performance. In addition, a careful distinction must be made between performance data which are presented as "typical", those which will be guaranteed, and those which may reasonably be expected under normal operating conditions. The nuances of the Portuguese language contribute some semantic niceties to this problem, for the ideas of "expecting", "hoping for" and "waiting for" may all be conveyed by the same verb: *esperar*.

Somewhat similar remarks apply to the capital cost information usually available at the feasibility stage. This information, which normally originates from contractors or licensors, has a *range* of accuracy which in no way implies that the most probable project cost is represented by the median value of the range. The range of accuracy really reflects (1) the estimator's level of ignorance about differences between the experience he is using for reference and the particular project he is now costing, and (2) the contractor or licensor's interest in keeping his contractual options open as far as possible.

The overall result of imprecision in "feasibility" information is to obscure

differences between production technologies.

(Figure 2)

If we accept this as normal, we shall be better able to focus attention on what seem now to be more important aspects of technology evaluation:

(i) judging when expenditure on upgrading the precision of input data to production cost estimates is really justified;

(ii) identifying the probable effect of completion delays on our project's earning power;

(Figure 3)

(iii) matching our project's output to its real market.

(Figures 4 & 5)

The project's real market cannot realistically be separated from questions of pricing strategy, both as regards transfer pricing between production units integrated through shared ownership, and as regards building a position in the market at large. The increasing use of formula-pricing in the context of joint-ventures with technology licensors brings these questions into the domain of technology transfer.

Probably the key issue is: the extent to which the actual market may be regarded as 'free' or 'protected'. We might take the view that transfer pricing is a means of using a special sort of 'protected' market situation to promote a particular interest of one or other of the partners (such as benefitting from certain tax provisions, or building up a localised - and probably temporary - sales position). But the very same provisions which benefit one party may well disadvantage the other. Then both partners tend to resolve their dilemma by declaring that the transfer price is, in principle, the *free* market price, a concept the practical value of which depends on resolving the fiction that a market price can exist in the absence of a market. By the same reasoning it may also be seen that recourse to international market price (for instance, the spot price in some north European markets) does not solve the problem of setting equitable transfer prices *in* Portugal.

In the uncertain world of price forecasting one thing is sure: the effective market price will not be the selling price calculated from the process stoichiometry + engineering estimates + hoped-for ROI. The chances are that in the European commodity petrochemicals markets of the foreseeable future, it will be substantially less [5] so that historical ideas of what constitutes the 'viability' of projects may have to be revised.

The search for 'viability' is essentially a search for a sufficient market share. As a newcomer to the oligarchic European market, could a Portuguese producer of commodity petrochemicals expect to 'buy' a sufficient market share by means of pricing strategies alone ? It seems unlikely, because this market tends to exhibit a "kinked" price-demand elasticity so that while a small price increase is likely to produce a substantial reduction in demand, a price reduction does not raise demand very much.

(Figure 6)

Furthermore, on the home market foreign products will be disadvantaged by transportation costs and by small scale local operations due to limited individual market shares divided between several competitors and so Portuguese materials may progressively acquire a captive market for themselves. However, when turning to foreign markets, transportation and marketing costs will work against Portuguese exports. This fact introduces an abrupt downward trend in any advantage that theoretically might be achieved by increasing the scale of the projected global operation if the excess production must be placed on external markets at a discounted price.

(Figure 7)

If however, producers are able to

"differentiate" their products, for instance by specification, performance, or other services to the customer, pricing strategies designed to capture a sufficient market share have a reasonable chance of success.

This leads us back to the idea of technological integration, perhaps best explained by an example. Commodity thermoplastics such as polyolefins or pvc have many, diverse, end-uses. Each link in the chain from production to end-use increases opportunities to apply technologies (and "knowhow" which for present purposes we treat as the same kind of intellectual property) to raise the value added to the basic product. A synergy develops, when these technologies are applied in an integrated way - design of artefacts, design of fabrication equipment, selection of production techniques, selection of polymer grades, choice of process technology, polymer chemistry etc. - which, we suggest, has the potential to add more value to the overall industry operation than would be got from the sum of the activities carried out in isolation.

(Figure 8)

The conclusion begins now to become evident : through technological integration, the Portuguese petrochemical industry may induce domestic fabricators to favour production of better products, suitably developed and adapted to the end-user's convenience and preferences, and may thus build for itself a captive yet bigger internal market. By the same mechanism it does not seem possible for a Portuguese operator to secure alone and directly any profitable captive share of external markets.

2. DEVELOPMENT OF TECHNOLOGICAL CAPABILITY.

Technology transfer always involves something of the nature of a joint venture (j.v.) even when the transferor holds no stock in the transferee's project. Owners of technology often manifest an underlying current of opinion that j.v.'s are at best a compromise which is second best to developing the venture alone[6] Most of the difficulties they anticipate have to do with the allocation of financial management responsibilities, but there are technological areas where the interests of the parties may diverge, or may come to do so in time.

From the recipient's point of view it is important to get agreement on a definition of the 'scope of supply' which leaves no room for doubt as to what is covered in the technology transfer contract. It is also in the recipient's interest to make the definitions as wide as possible, and to minimise restrictions on the markets open to the products of the technology. Both demands run counter to the basic interests of the transferor: some negotiated compromise is inevitable.

Leaving aside legal protection for the recipient against claims by third parties, perhaps the most necessary management guideline is to recognise that technology which is worth having is yet capable of improvement, and consequently the recipient must (1) have access to future developments as well as to the current state of the art, and (2) must have a fair share of the benefits of any improvements to which he contributes, as a result of such access.

In practice these provisions require the recipient's technical staff to be involved in development of the basic process design philosophy and the engineering design of plant, as well as being adequately trained in operation and maintenance methods on plants as nearly as possible similar to his own. Very careful thought should be given before selecting any technology so "advanced" that the licensor is unable to meet these provisions : under-utilisation of capacity for operational reasons is just as expensive, and much more frustrating than under-utilisation for market reasons. Finally, the agreement should allow

for regular discussions between parties' specialists on research and development work. It is remarkable that while many technology transfer agreements contain this provision, the arrangements are either unworkable, or recipient organisations do not prepare themselves to take full advantage. As causes for this situation the following may be suggested :

- developing countries are normally prone to give excessive weight to "hands off" provisions stating that the transferor's guarantee shall cease to be valid if the technology is modified in any way by the transferee;

- since a new installation in these countries is generally the "one and only" in its product line, the consequences of eventually unsuccessful tampering or failed experiments may be heavy financial losses due to prolonged shutdowns;

- it is very uncommon in developing countries that sufficient emphasis and effort are put into technological R & D, and that a sufficient part of the industrial profits is diverted to finance it.

Thus, we feel that unless a long-range objective for technological development is accepted and enforced by the Portuguese industry, and adequate financial instruments and insurance are established, part of the imported foreign technology may have only a temporary beneficial effect. In fact, it will not be fully transferred, but only used as an esoteric black box during a certain time, after which its benefits will be lost.

When technology transfer forms part of a j.v. agreement, additional management problems to do with effective control of the j.v.'s marketing and financial activities may arise. It is not surprising that the transferor, seeing the j.v. as being in a sense a dilution of his technological pre-eminence, may seek to influence control to a degree out of proportion to his share-holding. Among the many possible strategems are:

- a major part of the j.v.'s output is contracted to the transferor or to a party considered likely to favour his interests, who thus controls marketing of the product. Alternatively control of production is given to the transferee, in exchange for transferor's control of a separate marketing company. In either case, control of marketing is likely to exert a dominant influence on production policy;

- an effective majority vote on the transferor's side is arranged on the Board, even though profits are divided between the partners equally;

- equal numbers of the Board members are appointed by each side; however the technology transferor has the right to appoint management.

Obviously one would hope for a partner whose views on the j.v. were more constructive than these. The recipient's criteria of choice could include:

- does the partner inspire confidence that his present and foreseeable objectives for the j.v. converge with the recipient's own ?

- is the partner willing to discuss openly potential areas of future conflict, especially on the distribution of profits, and on expansion or other activities likely to call for the future injection of additional capital ?

- is the partner willing to support and contribute to efforts the recipient may

undertake in his country to develop the technology further ?

- is it possible to agree in advance principles for the equitable termination of the j.v. if that eventually proves desirable, even though unforeseen now ?

Here we have outlined means for technology transfer to be effective in a way essential for a country which aims to use accelerated industrialisation as the motor for social and economic growth: it must plan to become technologically independent in certain fields. The alternatives - either increasing reliance on imported knowhow, or abandonment of growth - are we suppose, equally unacceptable.

3. PLANNING FOR CHANGE.

One inescapable result of technology transfer is, that changes will occur in the ways in which people are deployed in a developing industry. Another is, that the basic understandings which are common to both government and industry when industrial growth takes up a relatively minor share of national resources, are bound to change when that share of national resources becomes, as industrialisation accelerates, predominant.

The work force associated with sophisticated projects - such as oil refineries and commodity petrochemicals plants - changes not only as regards size, but, what is more important, as regards the nature of the tasks people have to do during planning, design, construction and eventual operation. Petrochemical complexes (ammonia and urea plants, ethylene plants, BTX facilities, intermediate monomer plants, polymer plants, associated facilities) have a common characteristic in that they always involve building new units, expanding existing facilities and revamping old ones. Once started, petrochemical complexes never cease to require constant technological support for, and infusion to, the operation of existing industrial units and to plan, design, construct, erect and start-up new ones. This characteristic feature allows for technological specialisation on process engineering and design as well as on project management, so that gradually, native engineering capabilities concentrate and gel to form teams inside the complex, in the petrochemical companies, and in outside independent engineering and construction firms.

In an industrial society these changes can normally be accommodated smoothly because there exists a pool of experience from which specialists are available as and when a particular project needs them. On the contrary, in semi-industrialised countries, where an industrial infrastructure of this kind is in course of development, such a pool of expertise must be created, and in a form which allows it to accommodate change acceptably. Thus, within each particular project the original (rather few) inside planners evolve and change into (rather more) designers. Later there is a temporary need for (many more) constructors. Finally the original core of the project team settles down to do the job which all along has been its destiny; to operate (and maintain in operation) the new facility. This of course includes production, distribution, marketing and the more esoteric activities that contribute to the successful development of new industry. And while much of the variation in numbers and categories of personnel can be made up from outside resources, that should be considered to be primarily a temporary expedient. What is important is that the team should develop independence as well as depth of experience and cooperative understanding, so that planning the evolution of organisational structure is an important aspect of the management of technological transfer.

In preparing this paper, we have been conscious that especially in Portugal among all the nations of West Europe, the management of technology transfer will have a profound influence on the eventual success of the industrialisation plan.

We feel we should not close our paper without commenting on the nature of 'plans' in this context.

Industry makes plans which are essentially series of hypotheses each of which is subject to tests against market response. Feedback from these tests indicates what is feasible to be achieved with the resources available.

(Figure 9)

But adjustment to changes in market response and other circumstances inevitably leads to some cyclic variation of sales and manufacturing output. Nonetheless, in a free market, the performance of these plans can be measured objectively by the Profit-and-Loss Account, and so this planning mechanism continues to be acceptable to Industry.

Governments, on the other hand, seem rather given to regarding industrial plans as statements of firm intent (about investment levels or employment, for example) which when accepted, become fixed targets to be achieved by dint of determination to overcome all obstacles.

(Figure 10)

Obstacles, including those resulting from market forces, can be eliminated by democratic negotiation - or at last, by legislation - which will control market forces [7].

In Portugal, where industry consists predominantly of small companies, we may surmise that the immediate consequences of competition within EEC would be to trigger new and stronger market forces with potentially traumatic effects on Portuguese producers.

There might seem to be an *a priori* case for government protection of the home market. But we suggest that is a step to be taken only with great caution. Reciprocal action by other trading nations would reduce the total volume of trade with consequences especially serious for a nation whose home market is relatively small. But perhaps of even greater significance for the long term development of Portuguese industry, such protection would demotivate the drive towards achieving technological independence. If that is a long term aim, no short term expedient should be permitted to stand in its way. Its achievement will depend on government and industry planners reaching a *modus vivendi* in which effective management of a consistent and selective policy of technology transfer to all levels of industry will be a necessary part.

London and Lisboa
April 1978

Appendix 1 -

Membership of European Economic Unions.

EEC : Belgium, Denmark, Eire, France, Germany (Federal Rep), Italy, Luxembourg, Netherlands, United Kingdom.

EFTA : Austria, Iceland, Norway, Portugal, Sweden, Switzerland.

CMEA : Bulgaria, Czechoslovakia, Germany (Democratic Rep), Hungary, Poland, Romania, USSR.

Non-aligned : Albania, Cyprus(1), Finland(2), Greece(1), Spain, Turkey(1), Yugoslavia(3).

Notes : (1) EEC associate members
(2) EFTA associate member
(3) CMEA associate member

REFERENCES

1. Strenger, H.J. - "Foreign Investment - a Bridge for Technology Transfer" : Chemistry and Industry 19.xi.77.

2. Quoted from a 1972 document of the Organisation of American States, in R.P. Morgan - "Technology and International Development : New Directions Needed" Chem. and Engg. News. 14.xi.77.

3. e.g. Dr. Jeremy Bray M.P., speaking at the 1976 meeting of the British Association for the Advancement of Science.

4. Antonio Barreto - "Transferts de technologie et developpement integre", Univ. Nova de Lisboa, 1975.

5. e.g. Codling, B.S. - "Olefin Pricing in Europe", Chem. Engg. Prog. July 1977.

6. cf a lecture by P. Harvey of ICI reported in Chem. and Ind. 3.xii.77.

7. e.g. Rt. Hon. Tony Benn M.P., at the 1977 UK Labour Party Conference.

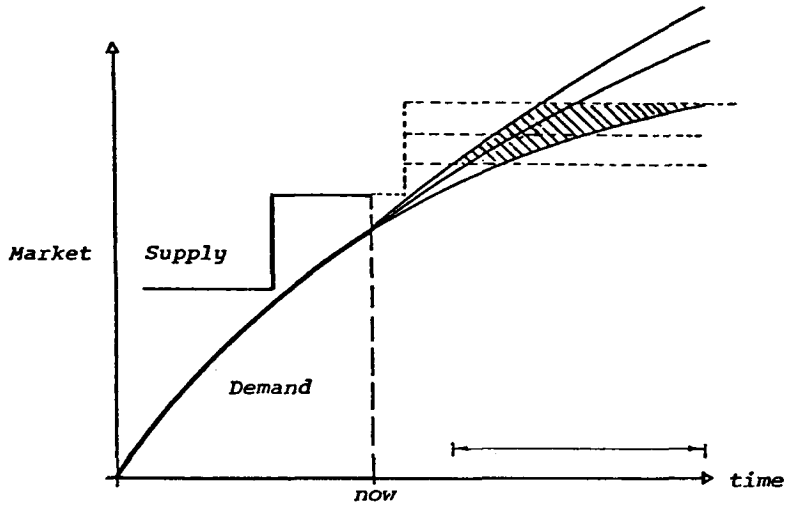

FIGURE 1 - Opportunity for New Capacity.

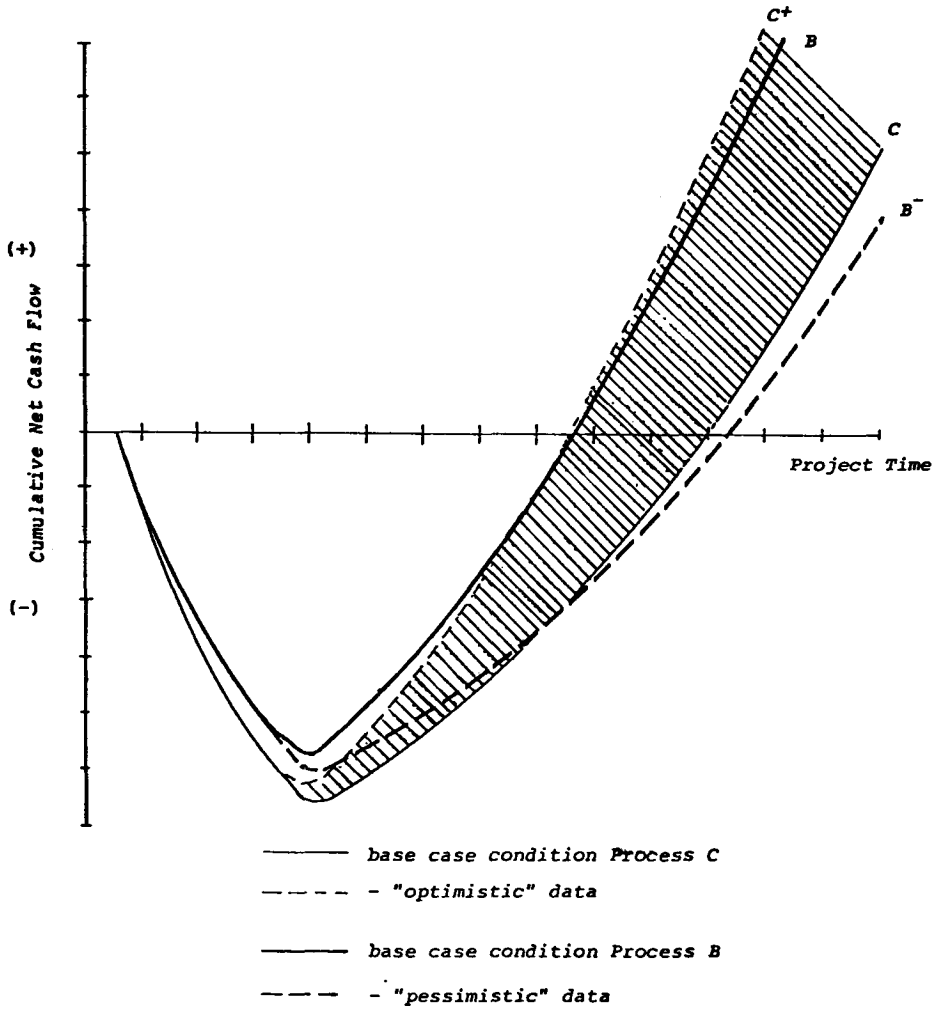

FIGURE 2 - Sensitivity to Accuracy of Data.

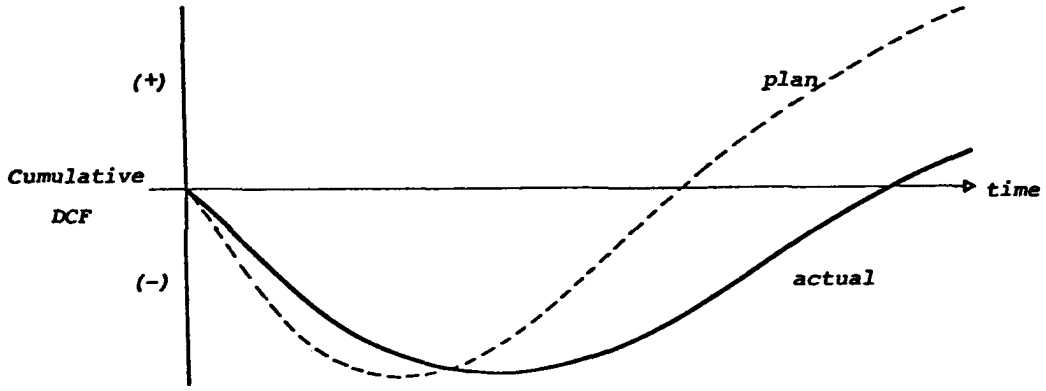

FIGURE 3 - Effect of Delays on the Venture's Earning Power over Time.

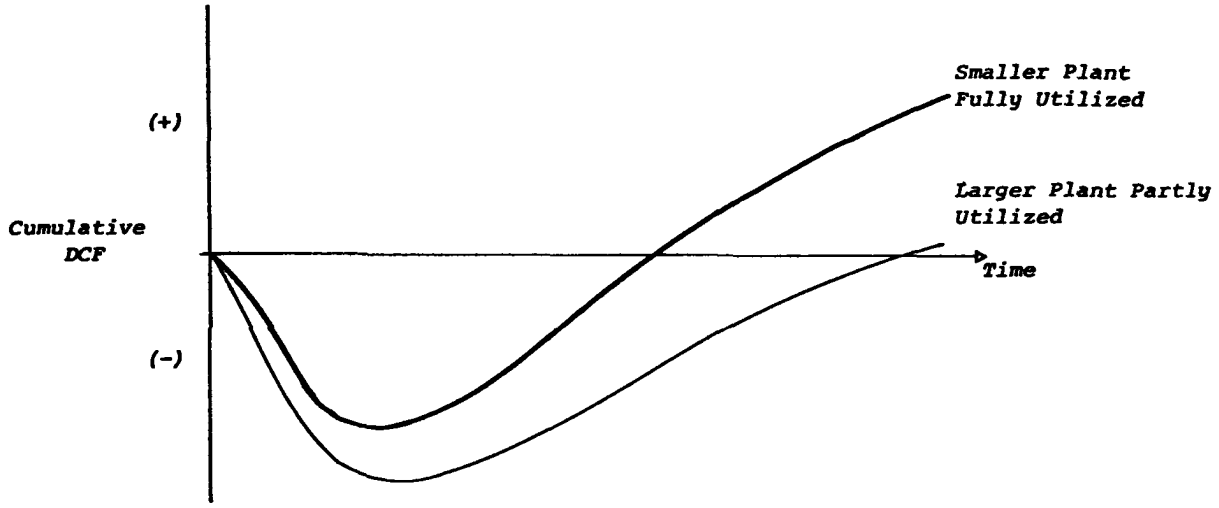

FIGURE 4 - Time Value of Earnings from Plant Operation.

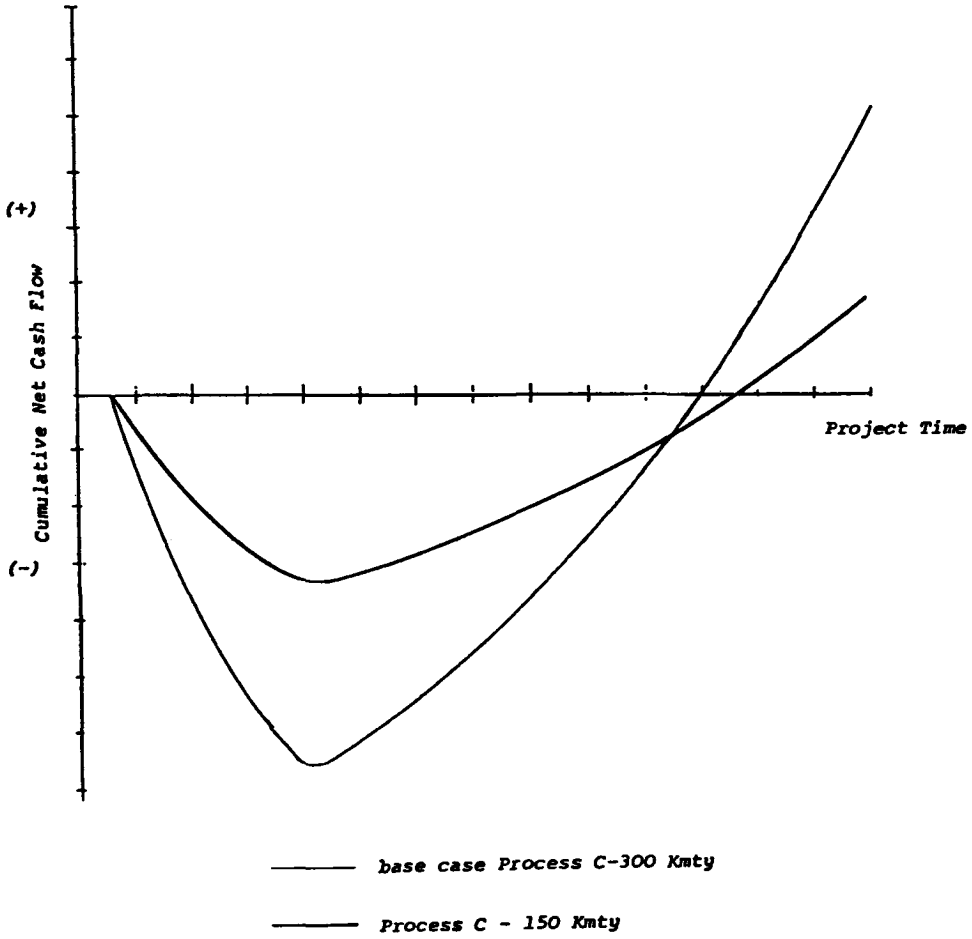

FIGURE 5 - Plant Size.

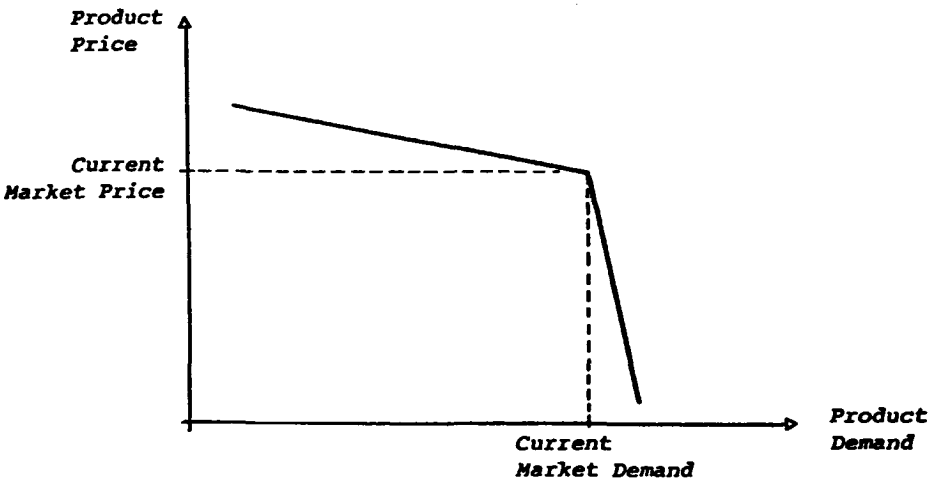

FIGURE 6 - Price-Demand Elasticity in a Special Market Case.

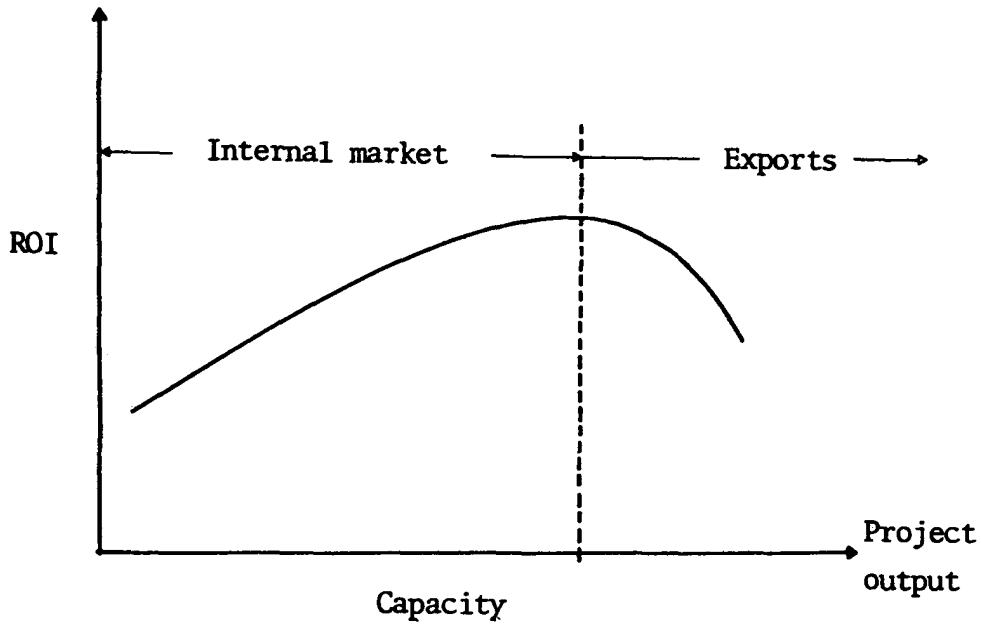

FIGURE 7 - Vanishing Economies of Scale through Export Disadvantage.

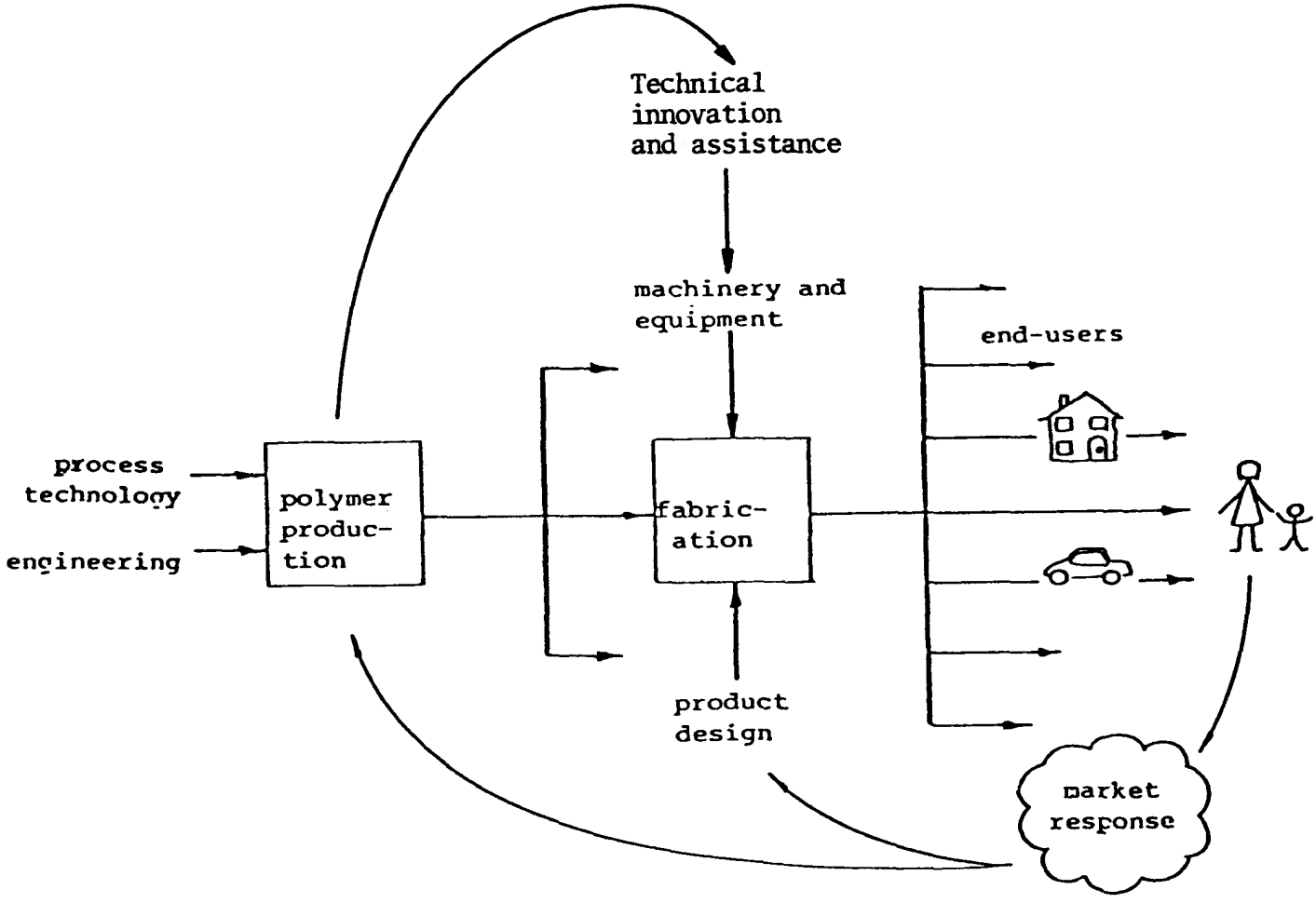

FIGURE 8 - Plastics Industry : Production-Consumption Chain.

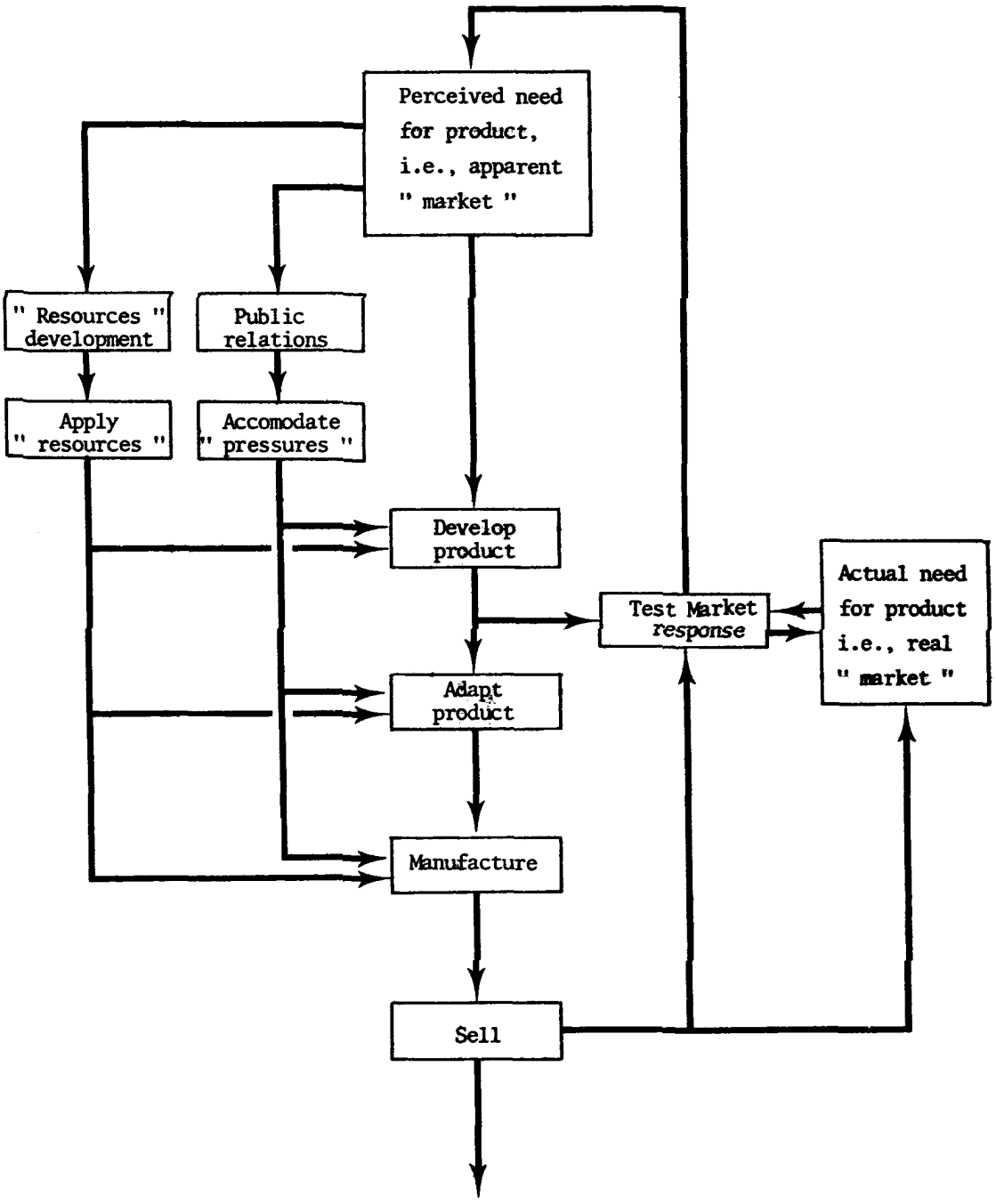

FIGURE 9 - Planning - Industry Style.

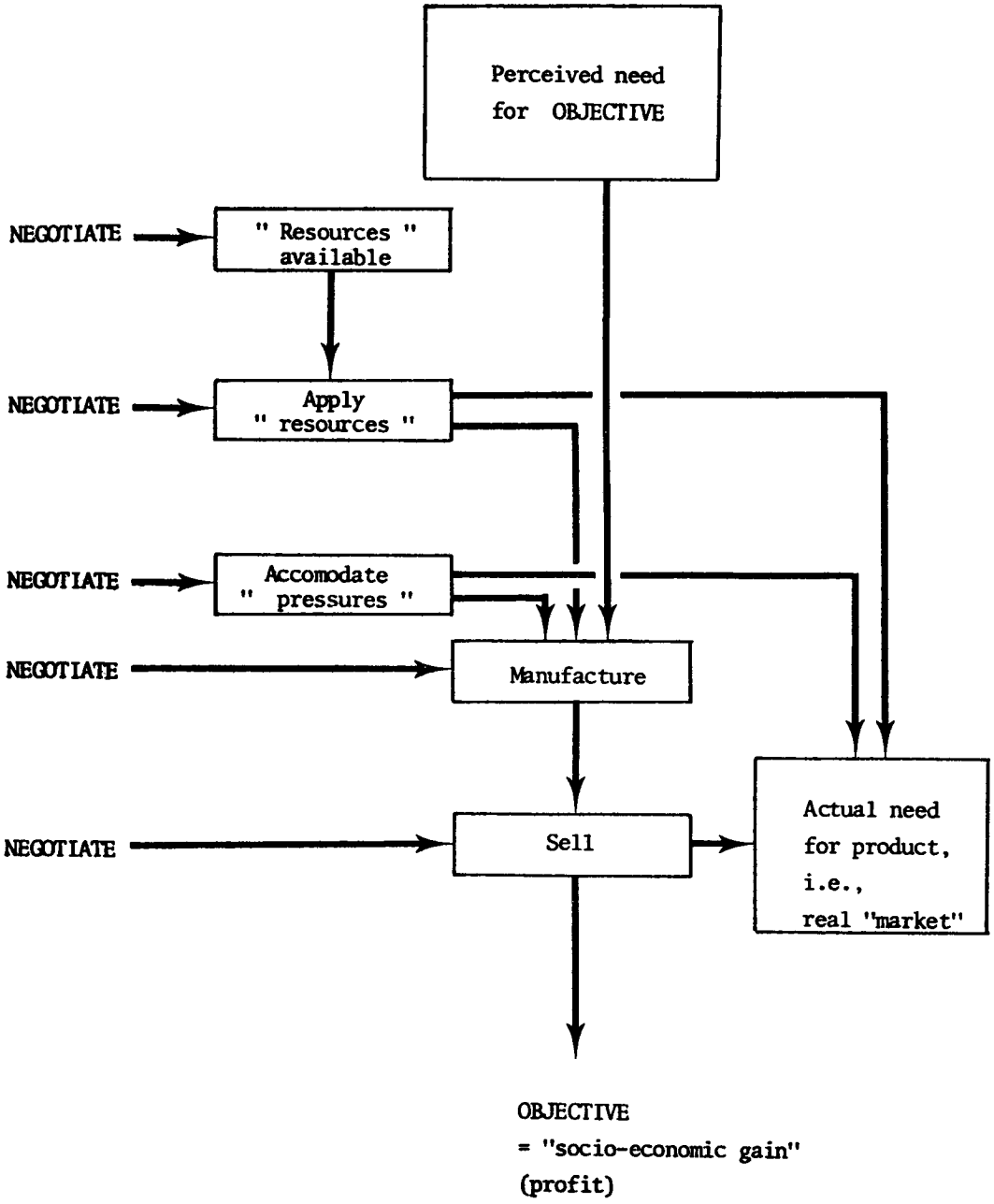

FIGURE 10 - Planning - Government Style.

NEW PERSPECTIVES ON THE ECONOMIES OF SCALE

J H Taylor P J Craven D Richards

ICI Mond Division, Runcorn
England

ABSTRACT

A study has been made of the relationship between capital and plant size for 45 projects in the United Kingdom covering a broad spectrum of plant sizes and technology.

It is concluded that for chemical plants in the 1-100 kt/year range the economies of scale for a particular single stream continuous plant are better represented by an 0.4 exponent rather than the traditional 0.6. This apparent conflict is reconciled. A lower exponent means greater economies of scale on capital. By implication this is extended to unit costs.

BACKGROUND

One of the best known and widely used rules of thumb employed by cost engineers and economic evaluators is the so called "six-tenths rule". This rule, first proposed by Williams (1) for uninstalled plant equipment, states that if the cost is known at one scale (S_1) the cost at another scale (S_2) is given by:

$$\frac{\text{Cost at scale } S_1}{\text{Cost at scale } S_2} = \left(\frac{S_1}{S_2}\right)^{0.6} \quad .. \quad .. \quad .. \quad (1)$$

In other words cost is proportional to the scale raised to an 0.6 power.

This rule was later extended to installed plants by Chilton (2) mainly on the basis of data for petroleum refinery plants. For specific items of plant equipment various power factors have been proposed and though these range widely an exponent of 0.6 is typical. For example the joint working party in the UK of "Institution of Chemical Engineers" and the "The Association of Cost Engineers" give (3) the following as typical values:

Tanks, rectangular	0.5
Pumps	0.7 - 0.9
Compressors, reciprocating	0.75
Electric motors	0.8
Towers (constant diameter)	0.7
Evaporators	0.5
Heat exchangers	0.65 - 0.95
Piping	0.7 - 0.9

The new views on the economies of scale described in this paper arose unexpectedly from the development of the "Process Step Scoring" technique (4) for estimating capital at the predesign stage.

DATA BASE

To develop the "Process Step Scoring" method it was necessary to collect capital cost data for a wide variety of chemical plants. Reliable well documented data was assembled for 45 different projects completed in the UK during the period 1963-1974. These covered a broad spectrum of processes typically encountered in the Chemical Industry. They included processes for organic solvents, intermediates and monomers, complex biologically active compounds, polymeric materials and inorganic materials. Most of the common chemical reactions were covered; for example chlorination, fluorination, oxidation, hydrolysis, amination, hydrogenation, dimerisation addition and cracking reactions. Plant sizes were evenly distributed over the range 0.3-250 kt/year.

The battery limits element of the capital was extracted and this was brought to a common time base using a capital inflation index. Fortunately all the plants were essentially completed before the oil embargo in 1973 or otherwise any conclusions on scale could have been grossly distorted by the rampant inflation experienced in the UK from around that time.

Deviations from a true scale exponent as a result of multistreaming were avoided as most of the plants were single stream or contained only minor elements of duplication which were adequately corrected for by the scoring system incorporated in the Process Step Scoring method.

REGRESSION ANALYSIS

Relating the battery limits capital cost (C) with the design capacity (S) of the plant gave not surprisingly in view of the variation of process types, a non-significant correlation. To allow for variations in the process complexity an index called the "costliness index" (I) was included as a variable in a regression analysis to fit an equation of the type

$$C = a\ I\ S^{b} \qquad \ldots\ \ldots\ \ldots\ \ldots\ \ldots \qquad (2)$$

where a and b are constants.

The costliness index is a basic parameter of the Process Step Scoring method. For a particular process it is a unique function, determined by the expression

$$I = \sum_{1}^{N} (1.3)^{X} \qquad \ldots\ \ldots\ \ldots\ \ldots\ \ldots \qquad (3)$$

where N is the number of 'significant process steps' (eg. filter, distil, react etc.) and X is a complexity score determined for each process step to take account of factors such as throughput, materials of construction, reaction time temperature, pressure and multistreaming. Costliness indices normally range from about 10 for a process to make a simple chemical such as formaldehyde, up to 200 or more for a process for a complex drug or pesticide. The method for calculating the costliness index of a process has been described (4).

Regression analysis including "I" as a variable gave a relationship (eqn 4) with an exponent of 0.39, instead of the expected 0.6:

$$C = 45\ I\ S^{0.39} \qquad \ldots\ \ldots\ \ldots\ \ldots\ \ldots \qquad (4)$$

Where C = battery limits capital in kt (adjusted to an Eng. Proc. Econ. index of 300) and S = plant capacity in kt.

The standard deviation (on capital) for this relationship was 15.2%. The correlation is shown graphically in Fig 1. The sensitivity of the standard deviation to the scale exponent was determined by repeating the regression analysis at various fixed exponents.

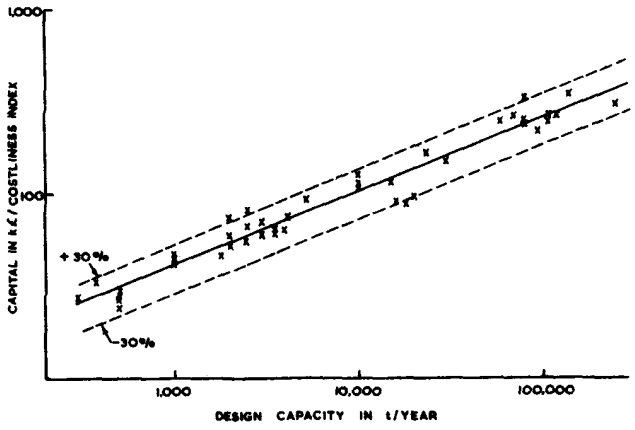

FIG. 1

Exponent	Standard deviation
0.60	37%
0.50	23%
0.40	15.5%
0.39	15.2%

Clearly an exponent of 0.4 fits the data much better than the traditional 0.6.

It could be argued that the capital is not directly proportional to I and this is why the observed scale exponent is 0.4 and not 0.6. To check this the regression analysis was repeated to fit a modified equation (eqn 5) in which I has the option of being raised to a fractional power.

$$C = d\ I^{e}\ S^{f} \qquad \ldots\ \ldots\ \ldots\ \ldots\ \ldots \qquad (5)$$

The correlation obtained (eqn 6) indicated that the capital is in fact essentially directly proportioned to I

$$C = 47\ I^{0.99}\ S^{0.40} \qquad \ldots\ \ldots\ \ldots\ \ldots\ \ldots \qquad (6)$$

DISCUSSION

The results of the regression analysis indicate that for the scale range 1-100 kt/year the capital cost for a single-stream process with a fixed costliness index varies as the 0.4 power of the scale and not as the 0.6 power as is generally accepted. The actual range of the data is 0.3-250 kt/year but because of the possibility of unknown end effects the range of confidence is limited to 1-100 kt/year.

An exponent of 0.4 means that the economies of scale are greater than would be expected using the traditional exponent of 0.6. The cost difference between using an exponent of 0.4 instead of 0.6 is large if extrapolations are being made over wide scale ranges; for example a cost of £1M for 1 kt/year would be £4M for 10 kt/year using an exponent of 0.6 but only £2.5M when using 0.4.

Why is the scale exponent we have obtained so much less than the 0.6 concluded by Williams and Chilton and which has been accepted and widely used by engineers and evaluators throughout the Chemical Industry?

The apparent conflict we believe can be explained in terms of:

i) the type of data used for correlation,
and ii) how the scale increase is achieved (eg. is it achieved by duplication of equipment or by making them larger).

Williams data was for uninstalled items of plant equipment, whereas ours is for complete plant.

Chiltons data was for complete plants but in contrast to ours was biased much more to very high tonnage (200-4000 kt/year) petroleum refinery plants. Also in Chiltons data the costliness index would not be constant for a particular process as he indicates that the scale increase could necessitate duplication of process units rather than making them larger also additional units may be needed either to deal with special problems posed by higher scales (eg. effluents) or the need for higher standards to conserve raw materials and energy. Some of the smaller plants in Chiltons data do have a lower exponent and he states that there is "a fairly smooth progression from 0.33 to 1.02".

The found exponent of 0.4 is not therefore necessarily in conflict with the conclusions of Williams and Chilton - it is for a more specific set of conditions and gives in our view a better representation of the true economies of scale (ie. making units larger) for the scale range 1-100 kt/year. We exclude from this conclusion the predominately batch processes which are often used at very low capacities (1 kt/year and less) as there are some special considerations for these.

Though an exponent of 0.4 is the best single value to cover the range 1-100 kt/year, it is probable that the exponent is not constant but progressively increasing from a value less than 0.4 (say 0.2 at 1 kt/year) up to a value higher than 0.4, ultimately reaching the traditional 0.6 at high tonnages of around 200 kt/year (see Fig 2).

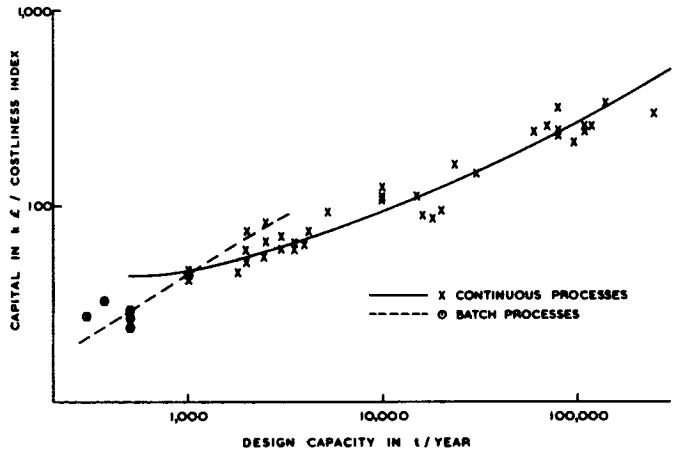

FIG. 2

The reasons for greater economies of scale at low capacities for continuous processes are probably twofold:

i) Minimum costs for some types of equipment which are not available below a certain size (eg. pumps, heat exchangers).

ii) Relatively higher installation costs, or in other words, higher installation factors (ie. Lang factors).

Evidence for a decrease in the installation factor with increasing scale was obtained by repeating the regression analyses using the basic equipment costs only instead of the gross installed costs. The relationship obtained had an exponent (0.5) closer to the traditional 0.6.

Cost of uninstalled equipment (k£)

$$= 8\ I\ S^{0.5} \qquad .. \ .. \ .. \ .. \ .. \qquad (7)$$

By division with eqn. 4 a relationship is obtained for the installation factor.

$$\text{Installation factor} = 5.6\ S^{-0.11} \qquad .. \ .. \qquad (8)$$

Thus the installation factor decreases with increasing scale; for example it is 5.6 at 1 kt/year, 4.3 at 10 kt/year and 3.4 at 100 kt/year.

A decrease in the installation factor is also implied in those engineering type estimates which use an installation factor based on the average item cost. In the following example in which the equipment is scaled up by an 0.6 exponent the calculated costs for installed equipment follow an 0.38 exponent.

	y t/year	10y t/year	
Av. equipment cost; say	£10 000	£39 800	(assuming 0.6 power)
Installation factor (5)	4.2	?.5	
Av. installed cost.	£42 000	£99 500	(ie 0.38 power)

A popular initial explanation of the low exponent allowing for scale obtained in our correlations as compared to the traditional 0.6 was that larger plants have greater economies due to learning as a result of design optimisation. To test this a regression analysis was carried out, in which the number of years in which that type of process has been operated was included as a parameter in addition to costliness index and scale. Surprisingly, it was found that the capital was almost independent of the 'learning' expressed in this way and this cannot therefore be the explanation for the low exponent. The reason why design optimisation has no detectable effect probably stems from the fact that say a 30% size reduction on equipment only produces about half that reduction in cost and also that many items of equipment (eg. storage vessels), cannot be optimised (NB 'Learning' here does not include any process improvements or modifications which alter

the costliness index such as yield increases, use of simpler materials of construction, lower stock levels).

UNIT COSTS

Most of the key components of a unit cost build-up, apart from purchased raw materials, can be related directly to the capital (9). On this basis and assuming the "six-tenths rule" for scaling capital several workers (6, 7, 8) have derived a correlation for unit cost as a function of scale, often referred to as the "minus four tenths rule":

$$\frac{U_1}{U_2} = \left(\frac{S_1}{S_2}\right)^{-0.4} \quad .. \; .. \; .. \; .. \; .. \quad (9)$$

Where U_1 and U_2 are the costs at plant sizes S_1 and S_2 respectively. (Though it is not stated this relationship should be limited to unit costs other than basic raw materials).

On the basis of our observed exponent of 0.4 for scaling capital in the range 1-100 kt/year the derived relation for unit cost becomes:

$$\frac{U_1}{U_2} = \left(\frac{S_1}{S_2}\right)^{-0.6} \quad .. \; .. \; .. \; .. \; .. \quad (10)$$

An 0.4 exponent on capital instead of 0.6 thus implies greater economies of scale on unit costs as well as on capital.

MULTI-STREAMING

It must be stressed that the 0.4 exponent that we have observed is for scaling up single stream plants of constant costliness index. If the scale up is achieved by multi-streaming, a higher exponent will result. For example for a scale up of 10 times achieved by multiplying up the number of streams by n times the original plant, the overall scale exponents for capital become:

n	Exponent
1	0.4
2	0.58
3	0.69
4	0.77
.	
.	
.	
10	1.0

Similarly for unit costs in a tenfold scale up the overall scale exponents are:

n	Exponent
1	-0.6
2	-0.42
3	-0.31
.	
.	
.	
10	0

CONCLUSION

For chemical plants in the 1-100 kt/year range the economies of scale for a particular single stream continuous process (with a fixed costliness index) are better represented by an 0.4 scale exponent rather than the traditional 0.6. Though apparently in conflict with the accepted 0.6 this can be reconciled in terms of the lower scale range and the plants being single stream.

This conclusion means that the economies of scale for capital are greater than would normally have been expected. By implication this can be extended to unit costs.

NOTATION

S = plant size in kt/year

C = battery limits capital cost in k£

I = costliness index (see eqn. 3)

N = number of process steps

X = complexity score (see eqn. 3 and ref. 4)

U = unit cost in £/t.

NOTE

The views expressed in this paper are the authors personal opinions and do not necessarily represent the views of their Company.

ACKNOWLEDGEMENTS

The authors are grateful to ICI Limited for permission to publish this paper and to their various colleagues throughout the Company for helpful discussions.

REFERENCES

1 Williams R, 1947, Chemical Engineering, June, 102 (and Dec 40).

2 Chilton C H, 1950, Chemical Engineering, April, 112.

3 The Institution of Chemical Engineers, The Association of Cost Engineers, 1977, "A New Guide to Capital Cost Estimating".

4 Taylor J H, 1977, Engineering and Process Economics, Nov, 259.

5 Kay S R, 1974, "The ICI (Petrochemicals Division) Factorial Estimating System - FACTEST", 3rd International Cost Engineering Symposium.

6 Bridgewater A V, 1974. "Rapid Cost Estimation in the Chemical Process Industries" 3rd International Cost Engineering Symposium.

7 Schuman S C, 1955, Chemical Engineering, March 180 (also May 173).

8 De la Mare, R F, 1975, The Chemical Engineer, April 227.

9 Taylor J H, Craven P J, 1978, "Economic Evaluation at the Predesign Stage", Paper to be presented at symposium titled "The Commercial Development of Chemical Engineering Projects", Nottingham University, Sept 1978.

EXPERIENCE IN USE OF THE PROCESS STEP SCORING METHOD FOR CAPITAL ESTIMATION

J H TAYLOR

ICI MOND DIVISION
RUNCORN, ENGLAND.

ABSTRACT

"Process Step Scoring" is a method for the rapid estimation of capital costs of chemical plants at the predesign stage. Following an earlier publication this paper describes:

(I) the method in outline with an example,

(II) recent developments for small scale batch plants and plants located outside the UK,

(III) the problem of published capital cost indices not fully reflecting the increasing costs of chemical plants, and

(IV) reliability and limitations of the method experienced in wide practical use over a period of four years.

INTRODUCTION

In the early stages of development of a chemical process, when ideas are changing quickly, rapid cost estimating methods are necessary to allow the potential cost of the product to be weighed along with other aspects of its evaluation, such as market price, hazards, environmental constraints and competitive strength. The traditional methods of estimating capital, which involve flowsheeting and chemical engineering design, followed by a mechanical engineering cost estimate are too cumbersome to cope with this rapidly changing scenario, since they require a level of definition in process design commensurate with the accuracy of the mechanical design method. Generally this cannot be realised in the early days in the life of a project.

Several workers (1-6) have proposed methods for the rapid estimation of capital at the predesign stage. One of these methods is the so-called "Process Step Scoring" method which was developed in 1972-75 and first published (6) by the present author in "Engineering and Process Economics" in 1977. This paper describes the method in shortened version with an example, and then goes on to describe some more recent thoughts and developments and the impressions gained from four years experience in wide practical use.

DESCRIPTION

Since details of the "Process Step Scoring" method have already been published, a shortened description of the method only is given here together with an up-date of the key relationships.

"Process Step Scoring" only requires a simple flow diagram such as the one in Fig 1 indicating the process steps (eg. react, filter, store A) and giving throughputs, reaction times etc. The capital cost for this can then be derived in a matter of minutes at a level of accuracy that is good enough for most preliminary evaluations. Also no knowledge of chemical engineering design is needed, so the method can be used by pure chemists.

The basic principle of the "Process Step Scoring" method is the postulation that the capital cost of a plant is related to a costliness index (I), expressing the complexity and nature of the chemistry involved in the process, and to its size by a relationship of the form:

Capital cost = constant X costliness index X (capacity)^p where p is a fractional power.

The costliness index, which is a unique function for a particular process is determined by the expression:

$$I = \sum_{1}^{N} (1.3)^{y} \qquad .. \; .. \; .. \; .. \; .. \; .. \; (1)$$

where N is the number of 'significant process steps' and y is a 'complexity score' determined for each process step to take account of factors such as throughput, materials of construction, reaction time, temperature, pressure and multistreaming.

Costliness indices normally range from about 10 for a plant to make a simple chemical such as formaldehyde up to 200 or more for a plant for a complex drug or pesticide.

In principle the "Process Step Scoring" method relates capital cost directly to the chemistry involved in the process without considering engineering aspects of the type of equipment

required. In this respect it differs from other published quick costing methods. Another significant feature is that each process step is scored independently for throughput, corrosion etc.

The found relationship between battery limits capital (C) in k£, costliness index, and plant size (S) in kt/year for a plant in the UK is:

$$C = 45\ I\ S^{0.39} \quad .. \ .. \ .. \ .. \ .. \ .. \ (2)$$

(For an Engineering and Process Economics (EPE) capital index in the UK of 300).

The Capital (C) includes all installation costs, together with the necessary on-costs for an "in-house" design, construction and commissioning.

Eqn. 2 was derived by carrying out a regression analysis on 45 projects completed in the UK during 1963-74. These covered a broad spectrium of plant sizes and types of technology encountered in the Chemical Industry.

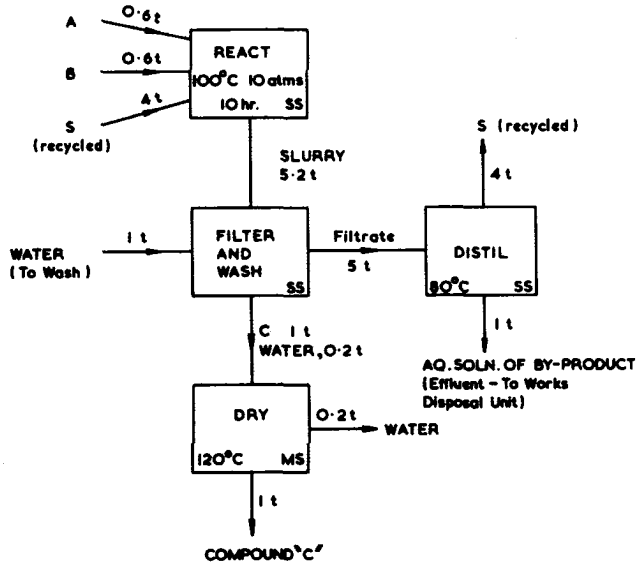

FIG 1 HYPOTHETICAL FLOW DIAGRAM FOR THE REACTION A + B → C IN A SOLVENT S

An alternative "direct analogy" type of approach not employing the derived relationship, eqn. 2, is to compare the costliness index (I) with that (I_1) of a similar process of known capital cost (C_1) and capacity S_1; the required capital cost being given by:

$$C = C_1 \left(\frac{I}{I_1}\right) \left(\frac{S}{S_1}\right)^{0.39} \quad .. \ .. \ .. \ .. \ .. \ (3)$$

This approach avoids the uncertainties associated with the variations on costs from one country to another and it also eliminates the personal factor in assessing the significant process steps - one of the main difficulties in applying the method.

The scope of the "Process Step Scoring" method covers complete new plants in the capacity range 0.3-250 kt/year. These can be for manufacturing either organic or inorganic chemicals, but they must use process operations which are reasonably typical of those common in the Chemical Industry.

EXAMPLE

Suppose that it is required to estimate the capital cost for a plant to manufacture 8 kt/year of Product "C" by reacting "A" and "B" in a solvent "S".

The various stages in estimating the cost are as follows:

1) Define the process to be costed by a simple block flow diagram (Fig 1) showing the main process steps, relative throughputs (ie. t/t product), temperature, pressures, materials of construction, reaction (or storage) times, multi-streaming and any special conditions, such as explosion hazards.

2) List the "significant process steps" and score each of these on throughput, materials of construction etc. according to the rules given in Table 1. For Product "C" the various process steps and their respective scores are given in Table 2.

3) Convert the score for each process step into a costliness index using the conversion Table at the foot of Table 1.

   The sum of these gives the costliness index for the process. Thus for Product "C" it is 21, see Table 2.

4) Estimate the battery limits capital using eqn. 2. Thus for Product "C" this Capital

   $= 45 \times 21 \times 8^{0.39}$

   = £2.1M (EPE index = 300)

5) Add allowances where necessary to cover inflation, off-sites, site development, location of plants outside UK and use of existing equipment. Thus for Product "C", assuming a typical notional allowance for off-sites of 30%, the total fixed capital required for a UK plant is £2.7M (for an EPE index of 300).

SMALL PLANTS

Generally speaking plants of under 1 kt/year are predominantly batch whereas those larger are mainly continuous. The design criteria for batch processes differ considerably from those for continuous processes. For example a continuous process generally requires a piece of equipment for each unit operation, whereas in a batch process several operations (eg. react, distil, decant) can be carried out in the same (but larger) equipment.

The original development of the "Process Step Scoring" method was largely concerned with continuous plants. More recent studies of batch plants with capacities of 1 kt/year or less have led to the conclusion that the costs of this type of plant are better represented by eqn. 4:

$$C = 45\ I\ S^{0.6} \qquad .. .. \quad (4)$$

This is the same as eqn. (2) but the exponent is 0.6 instead of 0.39. Using eqn. (4) the scope of the method is extended down to 0.1 kt/year.

With small plants appreciable use is often made of *existing equipment and/or an established building.* Eqn. (4) gives the cost for a completely new plant built up from the ground. In a real life situation therefore with a very small plant of say 0.1 kt/year the cost could be much less than indicated (eg 50% or less).

PLANTS OUTSIDE UK

As indicated the basic "Process Step Scoring" relationship (eqn 2) was derived on the basis of UK based plants. The translation of a capital cost for a UK plant into a cost for an equivalent plant overseas is difficult because of lack of reliable up-to-date comparative data. Also any proposed location factor such as for example the USA:

$$\text{Location factor} = \frac{\text{Cost in USA in \$}}{\text{Cost in UK in £ x \$/£ exchange rate}}$$

is, in the present rapidly changing economic environment, quickly invalidated as the location factor is a function of both the current exchange rate and the relative rates of inflation in the two countries concerned.

The approach adopted to extend "Process Step Scoring" for costing overseas plants, was to find the most reliable cost comparison data available and then inflate the cost from that date by using published capital inflation indices for the two countries concerned. For example using the definitive comparison of UK and USA capital costs made by Cran (7) in 1973, the value of the numerical constant in eqn. 2 for the USA (in k$) was estimated at 93 (June 1978 index). Similarly the values of the constant for Japan (k Yen) and West Germany (k DM) were estimated at 19,300 and 182, respectively. (June 1978 index).

Though these derived constants for USA, Japan and West Germany are an approximate guide, it must be stressed that the best approach for users of "Process Step Scoring" outside the UK is to determine the value of the constant by direct analogy using eqn. 3, with an actual cost or preferably range of costs, of known pedigree for their particular location.

INFLATION INDEX PROBLEM

As indicated the "Process Step Scoring" method was developed on the basis of plants completed during 1963-74. The costs were then brought up-to-date using the EPE capital inflation index, which agrees closely with other available indices for inflating UK capital costs. Though this is apparently satisfactory, our experience suggests that during the rampant inflation in the UK, following the oil embargo in 1973 and in the aftermath of the Flixborough disaster in 1974, capital costs for chemical plants have been rising *significantly more than that indicated* by the capital inflation indices.

Why are the published capital inflation indices not adequately reflecting the escalation of the costs of chemical plants? It is often not appreciated that the capital indices are built-up not from costs for complete plants, but are based on mainly Government statistics for costs of basic construction materials and labour. Inflationary factors that are not covered by the indices are, for example,

(i) more sophisticated designs to meet tightening safety and environmental requirements together with the ever increasing need to conserve raw materials and energy,

(ii) varying profit margins, as the supply/demand situation changes,

(iii) productivity trends.

To allow for these the capital inflation index should be modified by multiplication by an additional factor which we refer to as 'factor X'. There is insufficient evidence to give a definitive value for this factor and also it will *depend on the circumstances in question. It is* suggested on very limited data that a typical value for the UK is at present somewhere in the range 1.1 to 1.3 (for an index with a base year of 1970). The value will tend to be at the higher end of the range for plants employing mainly specialised equipment particularly if these are in limited supply or require individual fabrication.

RELIABILITY IN USE

The measured accuracy for "Process Step Scoring" for estimating the battery limits capital of a given process at a specified capital cost index was:

95% Confidence limits +36% and -26%

Standard deviation 15%

This should be regarded as an idealised accuracy for a definitive set of conditions. In a practical situation it has been found that when the project is at an early stage there are several other additional sources of error/uncertainty that can arise. These are:

(1) Changes in the process with increasing knowledge as the project proceeds. Generally these result in the process becoming more complicated and therefore more expensive than originally envisaged but sometimes developments enable the process to be significantly simplified.

(2) Errors in the allowances added to the battery limits capital to cover off-sites and site development. Depending on the actual site chosen these can range from 10% to 50% or more of the battery limits capital.

(3) Errors in identifying the "significant process steps". A common error among Chemical Engineers and others is to think in terms of the equipment needed whereas they should be thinking in terms of each operation (react, filter, distil etc) that is performed on the material flow, completely dissassociating their minds from the equipment that is needed.

(4) Errors in forecasting forward inflation together with the "factor X" problem ie. the uncertainty as to whether capital inflation indices are fully reflecting the true inflation of chemical plant.

(5) For plants outside the UK, errors arising from the location factor used and its sensitivity to exchange rate changes.

(6) Variations in design charges; for example contract design instead of in-house or when the plant is being built overseas, particularly when there are language problems and maybe process changes needed to meet the local conditions.

In spite of these various sources of error the "Process Step Scoring" method has proved a valuable technique for use in the preliminary economic evaluation of R&D projects. The possible sources of error that have been indicated are usually not critical in an early economic evaluation of an R&D project. In comparing various process options, for example, most of the errors will be common and cancel out. When using the estimated capital for a new product, together with estimates of raw materials and other unit costs, to obtain a likely manufacturing cost, the range of uncertainty on this is usually small compared to the uncertainty on the sales and market price that can be potentially achieved.

In the preliminary stage of a new project when the process is poorly defined the "Process Step Scoring" method has in our experience given more reliable results than engineering estimates. This is because cursory assessment of the plant equipment required, often grossly underestimates the complexity of the process thus leading to an estimated cost which is much too low. Errors of this type are less likely with the "Process Step Scoring" approach, because costs for a specified process step are determined by correlating directly with costs achieved in practice for steps of analogous complexity - thus analyses of the fine details of the step are already built into the method.

LIMITATIONS IN USE

Though in the early stages of an R&D project, "Process Step Scoring" is the preferred estimating method in terms of speed, minimal use of resources, flexibility, and (in our experience) reliability, there are some circumstances in which it cannot be used and an engineering type estimate is therefore needed.

The main limitations on practical use have been found to be:

(i) Process optimisation studies (eg. is it preferable to separate by filtration or distillation)

(ii) debottlenecking, extension or modification of existing plants, and

(iii) specialised operations such as fibre spinning, electrolysis or plastic extrusion.

CONCLUSIONS

During four years of practical use by numerous evaluators on a wide variety of R&D projects, the "Process Step Scoring" method has proved a valuable technique for early economic assessment. Reliability in use has proved adequate bearing in mind the many uncertainties that accompany any new project. The main problem is whether published capital indices are adequately reflecting the increasing costs of chemical plants resulting, in particular, from the trend to more sophisticated designs to meet modern requirements on environment safety and conservation of raw materials and energy.

NOTATION

I = costliness index (see eqn. 1)

N = number of process steps

y = complexity score (see eqn. 1 and ref. 6)

C = battery limits capital cost in k£

S = design capacity of the plant in kt/year.

NOTE

The views expressed in this paper are the author's personal opinions and do not necessarily represent the views of his Company.

ACKNOWLEDGEMENTS

The author is grateful to ICI Limited for permission to prepare and publish this paper and to his various colleagues throughout the Company for helpful discussions. Material from the original article in "Engineering and Process Economics" is included and the author is indebted to the Elsevier Scientific Publishing Company for permission to reproduce this.

REFERENCES

1 Zevnik, F C and Buchanan, R L, Chemical Engineering Progress, 1963, 59(2), 70

2 Stallworthy, E A, The Chemical Engineer, 1970, June, 182

3 Wilson G T, British Chemical Engineering and Process Technology, 1971, 16(10), 931

4 Allen, D H and Page, R C, Chemical Engineering, 1975, March 3rd, 142

5 Bridgewater, A V, "Rapid Cost Estimation in the"Chemical Process Industries", 3rd International Cost Engineering Symposium, 1974

6 Taylor, J H, Engineering and Process Economics, 1977, Nov, 259

7 Cran J, Process Engineering, 1973, April, 109

TABLE 1

Scoring for complexity of significant process steps

	Score												
	−3	−2	−1	0	1	2	3	4	5	6	7	8	9
Relative throughput (*t*/*t* product)	0.2	0.35	0.6	1	1.7	3	5	8	14	23	40	67	110
Reaction time in h (reaction, crystallisation, etc)				3	5	9	14	25	42	69	120		
Storage time in weeks				1	2	3	5	8					
Temperature extreme (°C) Min				20	−25	−75	−125						
Temperature extreme (°C) Max					500	1100	1700	2300					
Pressure extreme (atm) Min				1	0.1	0.01							
Pressure extreme (atm) Max					10[a]	50[a]	200	700	1500				
Materials of construction				MS[b]	SS[c], Keebush RLMS[d], EbLMS[e], PVC	ELMS[f] Inconel Nickel Monel PbLMS[g]	Titanium Hastelloy	Precious metals Tantallum					
Multistreaming. No. of streams				1	2	3	5	7	11				

Special conditions:
(a) Explosion, dust, odour or toxicity problems. Score 1 if a major problem.
(b) Reactions in fluid beds. Score 1.
(c) Distilling materials of similar b.pt. Score 1 if b.pt. difference <5°C and Score 2 if <1°C.
(d) Tight specification e.g. Score 1 if distillation is to reduce 'key' component to 10 ppm level.
(e) Film evaporation e.g. in Luwa. Score 1.

Conversion of score to costliness index

Score (S)	−3	−2	−1	0	1	2	3	4	5	6	7	8	9	10	11	12	13	14	15	16
Costliness index (*f*)	0.4	0.6	0.8	1	1.3	1.7	2.2	2.8	3.7	4.8	6.3	8.1	10.6	14	18	23	30	39	51	66

[a]For liquid phase reactions only. All others score = 0. [b]MS = Mild steel. [c]SS = Stainless steel. [d]RLMS = Rubber lined mild steel. [e]EbLMS = Ebonite lined mild steel. [f]ELMS = Enamel lined mild steel. [g]PbLMS = Lead lined mild steel.

TABLE 2

Calculation of costliness index for process in Fig. 1

	Throughput	M of C	Reaction/ storage time	Pressure/ temp.	Other	Total score	Costliness index
Storage/handling							
A	−1	0	1	0	1 (toxic)	1	1.3
B	−1	0	2	0	0	1	1.3
C	0	0	3	0	0	3	2.2
S (Recycle)	2½	1	0	0	0	3½	2.5
S (Make up)	−3	1	1	0	0	−1	0.8
Process							
React	3	1	2	1	0	7	6.3
Filter	3	1	0	0	0	4	2.8
Dry	0	0	0	0	0	0	1.0
Distil	3	1	0	0	0	4	2.8
							21.0

RISK ANALYSIS IN PROJECT EVALUATION

S.S. Alves

University of Birmingham, Birmingham, England.

ABSTRACT

This report deals with the analysis of the risk involved in industrial projects and the application of the results of risk analysis to decision making.

Consideration of the risk involved is of utmost importance in project appraisal. Most often, even in large investments, risk is evaluated only qualitatively, which is not satisfactory. Non-probabilistic methods sometimes used to express risk, such as sensitivity analysis or the calculation of a pessimistic and an optimistic case, do not actually quantify uncertainty and can be misleading. Hence, the need for a probabilistic approach to risk analysis is suggested.

The Monte-Carlo technique for deriving the probability distribution of the project profits from the distribution of the project variables is discussed and briefly compared with other techniques. An example is then used to show the possible contribution of risk analysis to decision making.

It is concluded that, although of questionable accuracy, Probabilistic Risk Analysis can be a very useful tool in decision making, mainly by stimulating and systematizing a careful consideration of the risks involved in a project.

INTRODUCTION

The decision to invest in a new plant is a very important one, because it is not easily reversible and because it involves a great deal of money and many people. On the other hand, it is also a very difficult decision to make, because of all the uncertainties involved in the estimation of the project outcome. A drop in product price or demand, or an unexpected technological problem may make uneconomic projects that looked attractive at the start.

Investment decisions are usually based upon a best estimate of the project economic performance, uncertainty being considered more or less carefully, but only in a qualitative manner. Methods, such as sensitivity analysis or profit calculation in a pessimistic and optimistic case, sometimes used to give a feeling for the uncertainty involved, are helpful by just doing so, but do not offer any measurement of risk and can be misleading. Only a probabilistic approach to risk analysis enables risk to be quantified.

The probabilistic approach to risk analysis has become popular since the early sixties in the academic circles. This, however, has only been accompanied by very little acceptance by executives and companies, three main reasons being currently given: difficulty of the analysis, lack of preparation among management and impossibility of testing the results of risk analysis. However, there are some clear advantages in the use of probabilistic risk analysis. Even if of doubtful accuracy, it is certainly more accurate than a simple, qualitative assessment of risk. An explicit, exhaustive examination of all the factors of uncertainty and how they affect the project outcome makes people think more carefully about the numbers they are putting down or on which they are basing a decision. On the other hand, if risk analysis is expressed in a language (probabilities, in this case) common to the engineer, the marketing personnel and the executives, communication is improved between the various levels of expertise.

Once uncertainty has been quantified, a second problem then arises in project evaluation, and this is the synthesis of risk and profit to obtain a single measure of project desirability. When comparing two projects, it often happens that the most profitable is also the most risky. What criterion should be used to choose between them? The answer depends upon the investors' attitude towards risk and profit. The mathematical description of attitudes towards risk and profit is dealt with by Utility Theory. Unfortunately, due to many problems, its practical applicability to risk analysis is unlikely in the near future and very much open to research, and therefore it is left out of the scope of this paper.

UNCERTAINTY AND ITS IMPORTANCE TO THE PROJECT OUTCOME

Project Evaluation: An Example

Most often, project appraisal is based on a feasibility study, where a single-valued best estimate of the project economic performance is given. Let us turn to a simplified, semi-fictitious example which will be used throughout to clarify the exposition.

A company is interested in investing in a plant for D-α-phenylglycine and derivatives, raw materials for various antibiotics, mainly ampicilin. 260 tons/year is considered to be a suitable capacity. The plant would be located somewhere in South America, where the demand for ampicilin is still growing quickly. The chronogram of the investment and a summary of the best estimate of its economic outcome are shown in Table 1.

Table 1 (units = millions of some currency)

Years	0	1	2	$3 \leq i \leq 8$
Events	Pilot plant research, Engineering	Buildings, some equipment	Finish installation, start-up	Full production
Expenditure	C_0 8.0	C_1 23.5	C_2 22.0	$V_i S_i + F_i$ 48.5
Sales Revenue	-	-	-	$P_i S_i$ 83.2
Before tax Cash Flow	$-C_0$ -8.0	$-C_1$ -23.5	$-C_2$ -22.0	$(P_i-V_i)S_i-F_i$ 34.7
After tax Cash Flow X_i	$X_0 = -C_0$ -8.0	$X_1 = -C_0$ -23.5	$X_2 = -C_2$ -22.0	$X_i(1-T_i)x$ $((P_i-V_i)S_i-F_i)$ 20.8
Discounted Cash Flow r=0.1	X_0 -8.0	$\frac{X_1}{1-r}$ -21.4	$\frac{X_2}{(1+r)^2}$ -18.2	$\frac{X_i}{(1+r)^i}$	$NPV=\sum_{i=0}^{8} \frac{X_i}{(1+r)^i}$ 27.2

The discount rate r, such that NPV = 0, is the discounted rate of return, R = 24%

The meaning of the symbols is as follows:

- C_i = capital cost
- P_i = product price = 320/Kg
- V_i = variable costs = 97.7/Kg
- F_i = fixed costs = 23.1 x 10^6/year
- S_i = sales volume = 260,000 Kg/year
- T_i = income tax rate = 0.4
- r^i = rate of discount = cost of money = current interest rate = 0.1
- X_i = after tax cash flow
- Subscript i refers to year i
- NPV = Net Present Value

All values are based on prices at year zero. Salvage value was considered negligible. Units are some fictitious currency.

Table 1 shows that the Net Present Value of the project using a discount rate equal to the interest rate at which money is available, is positive. Even if, as many companies do, "our" company has the policy of only accepting projects with a rate of return higher than, say, 20%, the project still looks attractive. But how reliable are the figures in Table 1? All the factors involved in the cash flow calculations are more or less uncertain and the real life profits may in the end turn out to be very different from those estimated in the feasibility study.

Factors of Uncertainty and their Effect on the Overall Profit

Factors of Uncertainty

Every economic variable in a project has some

uncertainty attached to it. When analysing the risk involved in a project, all of the following should be considered:

(a) Installed cost of fixed investment
(b) Working capital
(c) Initial start-up expense
(d) Fixed and variable costs
(e) Product price
(f) Sales volume
(g) Income tax rate
(h) Research, installation and start-up periods
(i) Economic life
(j) Effect of inflation on tax

Other kinds of uncertainty may also be important. For example, when choosing a plant location, it can be relevant to consider the political and social situation to assess the risk of nationalisation or strikes.

Obviously, not all of these variables are equally uncertain or have the same impact on the overall project profit. Usually, the most important factors of risk can be singled out for further analysis on a qualitative examination of the project. To illustrate this, consider the example of the phenylglycine project.

Uncertainty in the Phenylglycine project

The technology to produce the product is well known by the company, so that the uncertainties in the installed cost are fairly small. Except with new technologies, this is usually the case. The installation and start-up period is also known accurately enough and its impact in the profits is small. Usually, the further into the future the analyst has to forecast, the greater the uncertainty involved. And so we come to the major uncertainties in the phenylglycine project.

(a) The first one is competition. Supply of an important derivative of D-α-phenylglycine is irregular and difficult to obtain. However, it is possible that this will give incentive to other investors in the field and it may happen that, in three years time supply will exceed demand. The effects would be felt on sales volume S_i and product price P_i.

(b) The demand for ampicilin is growing in South America. The possible discovery of antibiotics of wider spectrum and better properties could however threaten this trend, and thus also reduce the demand for the raw materials, phenylglycine and derivatives, again affecting P_i and S_i. Still, the company may rely on the usual delay in the penetration of new discoveries into developing countries.

(c) The major derivative of D-α-phenylglycine to be manufactured is a difficult salt which liberates HCl. This, together with various organic solvents, makes the choice of resistant materials for a considerable part of the plant virtually impossible. The life of some expensive centrifuges is estimated inbetween 2 and 3 years. The average economic life of the plant, n, is thus quite difficult to predict.

(d) Variable cost, V_i mainly dependent on the price of raw materials, fixed costs F_i and income tax rate T_i complete the list of most uncertain variables in this project.

This case, where product price and sales volume are the two most uncertain variables, is quite typical of chemical plants.

Sensitivity Analysis

In the previous section, the most uncertain economical variables in a project were singled out. But it can happen that a smaller variation in a more accurate variable, say capital cost, has a greater effect on the rate of return than the wildest variation to be expected from a very uncertain factor, say variable costs. A sensitivity analysis will show the cause effect relationships between the variables and the rate of return and single out the variables with greater impact on the profits.

To make a sensitivity analysis, each factor is varied at the time, the others being kept at their most likely values, and the rate of return (or some other measure of profit) is calculated each time. The effect of each single factor on the project economic performance is thus determined. One way of expressing it is $\partial R/\partial(\%X)$ where X is the factor being varied and %X is its percentage variation from the most likely value.

A sensitivity analysis was carried out on the phenylglycine project, the results of which are given below in Table 2. This table shows that price and sales-volume are the variables with greater impact on the rate of return. Being also the most uncertain, it becomes clear that they are critical for the success of the project. All other variables have a less dramatic effect on the outcome.

Traditional Methods of Dealing with Uncertainty

Once the feasibility study has shown that the project meets the company's minimum standard of profitability, some sort of assessment of the risks involved is made, where intuition usually plays a major role.

In the case of the phenylglycine project, for example, the experienced decision maker will probably have the feeling that price and demand are crucial, even is a sensitivity analysis is not

Table 2 Sensitivity Analysis

Factor varied X	Variation	Rate of Return R	∂R/∂(%X)
None	-	24.0%	-
Capital cost	+20%	18.7%	0.342
Capital cost	-20%	32.4%	
T	+20%	18.7%	0.265
P	+20%	38.6%	0.812
P	-20%	6.1%	
V	+20%	20.0%	0.212
V	-20%	28.5%	
S	+20%	35.0%	0.562
S	-20%	12.5%	
F	+20%	20.3%	0.210
F	-20%	28.7%	
n	+ 1	26.7%	0.220
n	- 1	21.2%	

carried out. Hence he will concentrate on estimating how likely price and demand are to fall below the expected. A sensitivity analysis would help him a great deal, if only by telling him that a 20% drop in product price is sufficient to make the project unprofitable at the 10% cost of capital. This will give the decision maker a feeling for the risk involved, but will not tell him either what will happen when several variables vary at the same time or how likely the project is to be unprofitable.

A technique sometimes used to see how the profits vary with a change in several variables is to do the project economic calculations for multiple cases, usually a pessimistic, a most likely and an optimistic case. To calculate, say the pessimistic case, pessimistic values are used for the most important variables, and this can be misleading, as it is extremely unlikely that all the variables will change unfavourably at the same time. Suppose that in the pessimistic case, the sales revenue is below break even point. It looks discouraging, but, if the probability of this happening in only 1 in 1000, then the risk may be insignificant and well worth taking. Unfortunately neither in the sensitivity analysis nor in the calculation of multiple cases is there anything suggesting the probability of each rate or return. In the end, it will be the executive's intuition that will weigh everything in a qualitative manner to give him an assessment of the risk.

All that has been said points, therefore, towards the need for a probabilistic approach and a procedure that will give the uncertainty involved in the profits by examining the uncertainty of the project economic variables.

Probability Distribution of the Economic Variables of a Project

The first step in the calculation of the project risk is the determination of the probability distributions of the individual variables that affect profits. The best people to attribute probabilities to the values of each variable are the experts in the corresponding field, e.g., marketing personnel will estimate the demand distribution and the project engineer will estimate the probability distributions of such variables as capital cost, operating costs and economic life of the project.

Probability Distribution of the Project Outcome

The Problem

Once the probability distributions of the various factors of uncertainty in a project have been determined, the problem is to obtain the probability of the project rate of return or some other measure of probability. This means obtaining the probability distribution of a function of random variables of known distributions, $R=f(P,V,F,n,T,....)$. Three types of methods have been proposed to solve this question: Monte-Carlo simulation, decision tree analysis, and probability theory methods (ref 1).

Monte-Carlo Simulation

Monte-Carlo simulation is the most used of the three methods, mainly for practical applications (ref 1). Its application to economical risk analysis has become popular since the beginning of the 60's.

Through the use of random numbers the Monte-Carlo technique simulates a "world" that obeys the probability distributions of the variables. For example, consider the probability distribution of fixed costs in the phenylglycine example:

Interval	F_{rep}	$P(F_{rep})$
$15 \leq F < 20$	17.5	0.05
$20 \leq F < 25$	22.5	0.70
$25 \leq F < 30$	27.5	0.25

(all quantities in millions)

where F_{rep} is the representative value of F in the respective interval, i.e., if $15 \leq F < 20$, then $F_{rep} = (15+20)/2 = 17.5$ for the subsequent calculations.

A random number Rnd is generated between 0 and 1 (either using a computer random function or random tables) and selects:

F_{rep}	= 17.5	if	$Rnd \leq 0.05$
F_{rep}	= 22.5	if	$0.05 < Rnd \leq 0.75$
F_{rep}	= 27.5	if	$Rnd \geq 0.75$

Thus the probability of F_{rep} =17.5 being selected is $p(F_{rep} = 17.5) = p(15 \leq F < 20)$. Random numbers, one for each variable, together with the known probability distributions of the variables, simulate a set of circumstances that determine all the variables in a project: they simulate a "reality" where the project has been implemented. Each time a "reality" is simulated, the rate of return of the project can be calculated. If this procedure is carried out a large number of times (say, 100 or 200), the frequencies of the rates of return obtained approach the probability distribution. The greater the number of simulations, the better the accuracy (refs 2,3, 4,9).

The requirement for a large number of random outcomes normally leads to computer solutions. A simple, non-versatile, computer program applying Monte-Carlo simulation to the phenylglycine project, using the probability distributions of the variables shown in the appendix, was run. The results of 140 runs are summarised in Fig 1. The height of each block is the probability that R lies within the corresponding interval in the abcissas. Economic conclusions from this graph are drawn in another section, below.

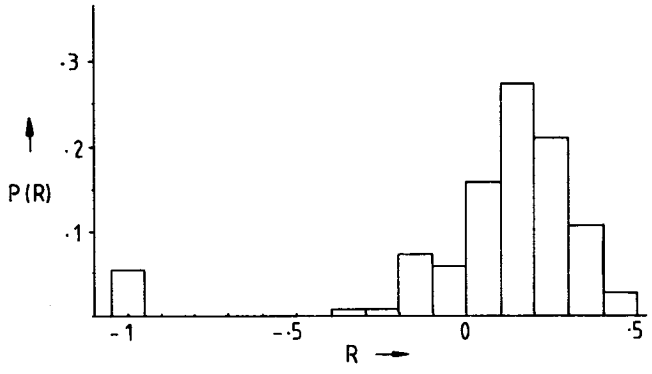

Fig 1

Monte-Carlo simulation has been criticized (refs 5,6) for being a cumbersome way of studying a problem, since it requires developing the model and the input data and then writing and running the computer program. The need of computer facilities is indeed an important disadvantage, mainly for small decisions or small companies. With some complex investment decisions, the execution time required may make the cost of a Monte-Carlo simulation very high even for big companies.

These shortcomings of the Monte-Carlo technique are however usually smaller than those of the other methods available and often smaller than its own advantages, namely that it is conceptually simple, needs little computer storage, is easy to program, and it is commercially available at many different levels of sophistication and price (ref 1).

Other techniques

Other methods of obtaining the probability distribution of the project outcome from the probability distribution of the variables are Decision-Tree Analysis and Probability Theory Methods.

Decision-Tree Analysis whose application to risk analysis is described by Magee (refs 7,8), calculates the probability distribution of the rate of return by calculating the joint probability of all possible rates of return obtained by using different combinations of values of the project variables. For practical application, this method also implies the use of a computer, requiring less execution time, but more storage than Monte-Carlo simulation.

Under the name of probability theory methods come those which try to avoid lengthy calculations and the need for a computer by resorting more fully to probability theory theorems. The main disadvantages lie either in the assumptions needed, which often make these methods inaccurate, or in the complexity and often theoretical difficulties involved in the more refined versions (refs 5,6,10).

Appraisal of the Probabilistic Approach to Risk Analysis

From the result of risk analysis, fig. 1, the decision maker can assess the risk involved in the proposed project. He can conclude that:

(a) The expected discounted rate of return is only 8%, i.e., in an "average" sort of future, the return on capital is much below the minimum 20% acceptable according to the company's policy, and even below the 10% cost of money. The "average" project is viable if the company can provide their own funds, but it would be more profitable to put the money in the bank.

(b) There is a small but considerable risk ($p \approx 0.05$) that the project may be unviable, i.e., sales revenue below break even point. This corresponds to the cases where the

demand has fallen to very low levels, due may be to obsolescence of the ampicilin process using the salt of phenylglycine or may be due to some world wide objection to the use of ampicilin or still sue to very strong competition from a better medicine (unlikely but possible).

To try and discuss what was in fact gained or lost by doing such a risk analysis, the following points should be examined.

(i) how accurate are the results,

(ii) how much of the results could have been intuited by the executive without any risk analysis being made at all,

(iii) what is the cost of risk analysis itself.

(i) ACCURACY: The results of both the Monte-Carlo and the Decision-Tree techniques are, in practical terms, as accurateas the estimates of the probability distributions of the individual variables. The accuracy of these latter is, on the other hand, a very open matter and, at least to some extent, an unsolvable question, since the results of each particular risk analysis can never be tested in practice, due to the statistical nature of the forecast and the uniqueness of the future. A possible test would be to compare the average accuracy of many singled valued feasibility studies with that of many risk analyses, in many different situations. All that can be said at the moment is that risk analysis is likely to be more accurate than an executive's intuition of risk, because it combines various levels of expertise in the determination of uncertainty, it stimulates careful consideration of all the uncertainties involved, and it derives from them the uncertainty of the outcome in a fairly accurate manner.

(ii) HOW MUCH COULD HAVE BEEN OBTAINED FROM INTUITION. For an experienced executive, it would be clear that price and demand are critical for the success of the project. The small probability of a commercial disaster would also be in his mind. He would still consider however the rate of return of 24% calculated in the feasibility study as the likely one, i.e., acceptably high, when the expected rate of return calculated by risk analysis is only 8%, below the cost of money. Unless some powerful motives not included in the analysis, such as, e.g. a long-term company strategy where penetration in South America is crucial, come into play, the project will be rejected by the Board of Directors.

Thus, risk analysis can give a significant contribution to decision making, indeed, making all the difference and reversing decisions.

(iii) COST OF PROBABILISTIC RISK ANALYSIS: An experienced engineer, computer facilities, one day collecting data and one day for programming and calculations should be enough for the risk analysis of a project considerably more complicated than the example presented. The analysis of combinations of interrelated projects can be far more difficult and even defy a reliable solution.

As a conclusion it can be said that probabilistic risk analysis, however of discussable reliability, is a valuable tool for decision-making, mainly in big companies.

APPENDIX

DATA USED IN THE EXAMPLE OF MONTE-CARLO SIMULATION

Probability distribution of the variables

V	p(V)	S	p(S)	F	p(F)
70-90	0.20	0-1.1	0.05	15-20	0.05
90-110	0.40	0.1-0.2	0.10	20-25	0.70
110-130	0.30	0.2-0.24	0.20	25-30	0.25
130-190	0.10	0.24-0.28	0.50		
		0.28-0.32	0.15		

T	p(T)	N	p(N)	P	p(P)
0.3	0.3	6	0.05	210-250	0.05
0.4	0.5	7	0.10	250-290	0.10
0.4-0.5	0.2	8	0.4	290-310	0.20
		9	0.25	310-330	0.40
		10	0.20	330-350	0.25

Other variables as in the feasibility study shown in Section "Projection Evaluation: An Example"

LIST OF SYMBOLS

C = Capital cost
F = Fixed costs
m = Number of years in economic life of a project
NPV = Net Present Value
P = Product price
p(x) = Probability that variable x has value x
R = Discounted rate of return
r = Discount rate
Rnd = Random number between zero and one
S = Sales volume
T = Tax rate
V = Variable costs
X = General variable

Subscripts

i = refers to year i
rep = representative value of a variable in an interval.

ACKNOWLEDGEMENT

The author wishes to thank Dr. T.R. Bott, Birmingham University, for his encouragement and

most helpful criticisms.

REFERENCES

1. Berger, R.W., Engineering Economist, 1972, 17 (4), 241.
2. Hertz, D., Harvard Bus. Rev., Jan-Feb 1964, 95.
3. Hertz, D., Harvard Bus. Rev., Jan-Feb 1968, 96.
4. Hess, S.W., Quigley, H.A., Chem.Eng.Progr. Symp.Ser. 1963, 42, 55.
5. Hillier, F.S., "Evaluation of risky interrelated investments", North-Holland Pub.Co., 1969.
6. Hillier, F.S., Engineering Economist, 1972, 17 (1), 1.
7. Magee, J.F., Harv.Bus.Rev., 1964, 42 (4), 126.
8. Magee, J.F., Harv.Bus.Rev., 1964, 42 (5), 79.
9. Malloy, J.B., Chem.Eng.Progr., 1971, 67 (10), 68.
10. Reymand, E.L., Ind.Eng.Chem., 1966, 58 (7), 61.

CAPITAL COST ESTIMATION IN EARLY STAGES OF CHEMICAL PROCESS DEVELOPMENT.

A.V.Bridgwater

Chemical Engineering Department,
University of Aston,Birmingham,England.

ABSTRACT

Many rapid methods of estimating capital cost have evolved in recent years. These may be broadly classified as module or unit cost estimating methods where estimates of delivered equipment cost are subjected to conventional factor estimating: and step counting methods where the overall cost of a process step is correlated with factors representing process complexity.

These step counting methods have now achieved respectability with evidence of their applicability and reliability for cost estimating at early stages of project development. Their history is briefly reviewed and the most recent developments for both the petrochemicals and pollution control industries are described. Examples of application are included and compared.

INTRODUCTION

There are many factors that influence a decision whether to invest in a new plant. Capital cost is only one of the economic, political and social aspects that need to be considered, but is often regarded as particularly significant. This is due to the size of the sum of money and the short period over which it has to be paid; the need to spend it before any return is obtained and the con sequent greater uncertainty; the conventional relationship between net income and investment to give profitability; and the capital intensive nature of the process industries.

This importance and consequent interest in capital costs has led to considerable research and development both into more sophisticated and detailed cost estimating procedures utilising computers and also into rapid estimating methods where preliminary capital cost estimates are valuable for screening alternatives, making preliminary evaluations and for assessing novel processes. These latter preliminary or screening methods are particularly valuable at the research and development stages of a project when decisions to proceed or not need to be taken at each stage of development. Other uses include provision of cross checks for detailed estimates, optimisation of novel processes and assessment of new technology. These are illustrated later.

This paper briefly describes and critically reviews some of the more significant rapid capital cost estimating methods. These are never claimed to give better than $\pm$ 20% accuracy and some may not improve on -40% + 60%. This accuracy of estimating is quite acceptable, and used sensibly many of the methods have considerable value.

Traditional cost estimating techniques

A) Ratio estimating

There is a well established relationship between capital cost and plant capacity which is usually expressed as

$$\frac{C_1}{C_2} = \left(\frac{Q_1}{Q_2}\right)^x$$

where C_1 = capital cost of plant 1

C_2 = capital cost of plant 2

Q_1 = capacity of plant 1

Q_2 = capacity of plant 2

x = scale factor, typically 0.6 or 0.67. This is empirically derived for a particular plant process operation or piece of equipment (see (1)).

If any four of the five variables are known, from historical information, then the fifth, usually C_2, may be calculated. Alternatively the relationship may be expressed as a cost model.

$$C = K\,(Q)^x$$

where K is a constant for a particular plant or item of equipment (see (1)). The concept of economy of scale is derived from this, where the capital cost per unit produced reduces as the plant size increases.

there area number of difficulties in using this approach for cost estimation as follows:

1) Data : it is necessary to know the capital cost of an identical plant at a given capacity, as well as the correct scale factor x. It is only possible to estimate capital costs with such historical data.

2) The scale factor x is not constant for all sizes of plant. A typical graph of plant size versus capital cost is shown in Figure 1. Generally scale up or scale down by more than a factor of 5 should be avoided. This problem can be overcome by differentiating between the direct capital costs which can be

considered as subject to the economy of scale rule and the indirect or fixed element. The relationship can be expressed as:

$$C = D\left(\frac{Q_1}{Q_2}\right)^x + F$$

where D = the variable element of capital cost
F = the fixed element

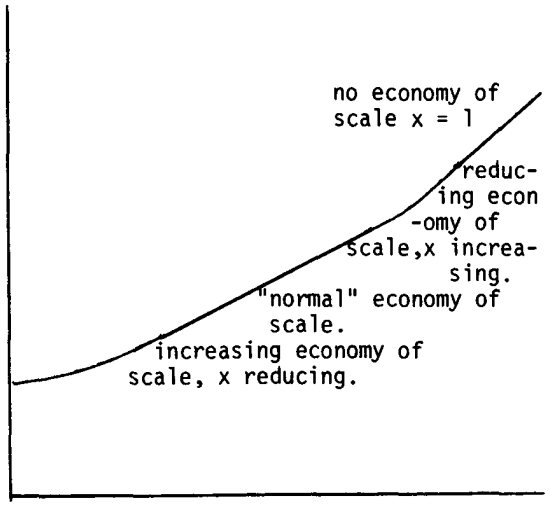

FIGURE 1.

3) Cost index; as historical data is employed, it is necessary to use a cost index to give a current cost, and thus no account is taken for example of developing technology changes in design standards, new legislation or macroeconomic factors.

B) Factor estimating

One of the earliest researchers into short cut methods was Lang (2) who related total plant investment to delivered equipment cost by deriving factors for processes handling different phases. These are the well known Lang factors which are derived in Table 1.

This principle is widely employed in a variety of forms for cost estimation at all stages of project development. When employed for preliminary cost estimating a number of well known problems emerge, such as:

1) The depth of information required: considerable information is necessary to obtain delivered equipment cost,such as fully detailed flowsheet and equipment specification. This can be overcome to a certain extent using the unit cost approach (see later).

2) Special problems with materials of construction other than mild steel. This requires other materials to be reduced to a mild steel equivalent basis, then multiplying by the appropriate factor(s),finally adding the incremental cost of the special materials.

3) Variation of Lang factor with plant size capacity or throughput. Little information is available but the problem can be overcome by using individual factors related to equipment unit cost (e.g. 3), however, this requires even more information.

4) Choice of appropriate factor. Considerable experience is needed to adjust the components for a given situation and/or to choose the appropriate factor if detailed factoring is used.

5) Technology change. Since the factors were first promoted, considerable advances in technology have occurred which will affect the significance of each component in Table 1. There is little information available on the extent of the change.

The Lang factor approach at its simplest is thus fraught with problems and uncertainty, and is not easy to use for preliminary estimating. In the hands of experienced and well informed cost engineers, the technique can be refined and computerised to the ultimate extent of having factors available for every item of equipment in every situation. In this context factor estimating is capable of giving the most accurate detailed estimates that a contractor or his client could expect. Not surprisingly details of such factors and the methods of useage are highly confidential.

"SHORT CUT" METHODS OF COST ESTIMATION.

The problems of using either of the above two methods for preliminary estimating, particularly for novel processes where there is no historical data, have been outlined above. Many methods for overcoming these difficulties have been proposed which are based on the principle that the average cost of a process step or unit can be related to the process parameters of, for example, capacity, temperature, pressure, and materials of construction.

Earlier cost estimation procedures attempted to obtain the delivered equipment cost which could then be multiplied by the appropriate Lang factor to give the total capital cost. This is referred as unit estimating and several examples of this approach are included. Later work tried to avoid the problems associated with any factor estimating by relating total capital cost, rather than delivered equipment cost, to the process parameters. This produced the step counting or functional unit approach for which a number of examples are also included.

Hills method

One of the earliest examples of short-cut estimating procedures was that of Hill (4) for obtaining the capital cost of fluid petrochemical processes. He employed "standard units" as a basis which are defined as major pieces of process-

equipment, and the degree of complexity is reflected by the number of standard items associated with major pieces of equipment, which may be either one or two "units".

example of one unit include mild steel column, reactor, evaporator, blower, liquid feed or product storage.

TABLE 1: Ratio factors for estimating capital-investment items based on delivered-equipment cost.

Item	Percent of delivered-equipment cost for: Solid processing plant	Solid-fluid-processing plant	Fluid-processing plant
Direct costs			
Purchased equipment-delivered (including fabricated equipment and process machinery)	100	100	100
Purchased-equipment installation	45	39	47
Instrumentation and controls (installed)	9	13	18
Piping (installed)	16	31	66
Electrical (installed)	10	10	11
Buildings (including services)	25	29	18
Yard improvements	13	10	10
Service facilities (installed)	40	55	70
Land (if purchase is required)	6	6	6
Total direct plant cost	264	293	346
Indirect costs			
Engineering and supervision	33	32	33
Construction expenses	39	34	41
Total direct and indirect plant costs	336	359	420
Contractor's fee (about 5% of direct and indirect plant costs)	17	18	21
Contingency (about 10% of direct and indirect plant costs)	34	36	42
Fixed-capital investment	387	413	483
Working capital (about 15% of total capital investment)	68	74	86
Total capital investment	455	487	569

A "unit" is ascribed a value of $30,000 when incorporated into a process producing ten million lb per year. Other plant capacities are considered by application of the six tenths rule (see capacity-cost ratio). The capital cost for any petrochemical process may be found therefore by the following formula:

$$\$\ C = F \times IEC \times CCI$$

where C = estimated capital cost

F = appropriate factors to account for piping, building, electrics, instrumentations, etc. (i.e. Lang factor).

IEC = installed equipment cost, $

$$= N \times \left(\frac{Q}{10}\right)^{0.6} \times 30{,}000\ \$$$

N = total number of "units"

examples of two units include stainless column, furnace, compressor, refrigeration unit, solid or gaseous feed or product storage.

Q = plant capacity, million lb per year

CCI = Marshall and Stevens construction cost index base 185 for 1954/5.

This technique provided a short curt for obtaining the delivered (or installed) equipment cost which was the basis of most of the factor methods of estimating. Although Hill recognised that the cost of units could be averaged, he still preserved two levels - simple (one unit) and complex (two units). It is not difficult to see Hill's "units" becoming functional units: disregarding the two levels, if the factors were applied to

each "unit" before summing, this would effectively give the total capital cost of each "unit", and the method would become a sophisticated functional unit approach. Alternatively, by a change in definition and emphasis each "unit" could become a main plant item which leads to the module or unit estimating approach. Hill's technique might there fore be seen as the point of divergence and consequent development of two techniques of capital cost estimation and his proposal thus assumes a certain significance.

Unit estimating procedures to obtain delivered equipment cost.

A number of procedures have been developed to derive the delivered equipment cost of a chemical plant in order to apply an overall factor to give the total capital cost.

One relatively simple approach is that due to Wilson (5) who proposed the following:

$$C = f.N.(AUC).F_M.F_P.F_T$$

where C = Capital cost of plant, £, in 1971.
f = Investment factor, dependent on dominant phase, (q.v. Lang factor) and AUC, and is obtained graphically. (Figure 2).
N = Number of all main plant items except pumps.
AUC = Average unit cost of main plant items.
$= 21.V^{0675}$ where V = capacity, tons per year.
F_M = factor for materials of construction which ranges from 1.0 for mild steel to 2.0 for titanium. A weighted mean value may be used (Table 2).
F_P = factor for design pressure, which is applicable only outside the range 15-115 psia and is obtained graphically. (Figure 3).
F_T = factor for design temperature outside the range 0-100°C and is obtained graphically. (Figure 4).

A cost index would also need to be included for current costs.

The object of the study was to try and combine the advantages of functional unit estimating and factor estimating. As the correlation was derived from a study of only 16 processes and an accuracy of ± 30% claimed for only 13 of them, the method might be considered to have a low level of credibility. In practice cost estimates from this procedure seem to come out a little high.

The method is simple to use and only requires the total number of main plant items in the process. For preliminary estimating, however, even this level of information requirement may not be available.

The same principle and approach was adopted by Page(6), but is more sophisticated and requires more information. It is, however, claimed to give more accurate results. To illustrate the procedure

f. Investment factor

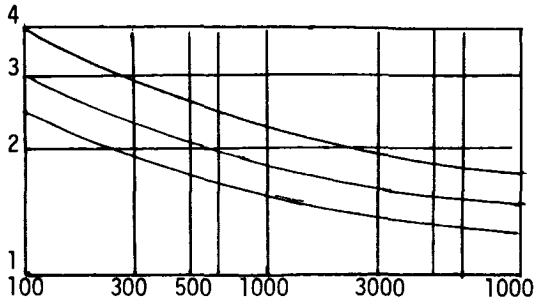

Figure 2.

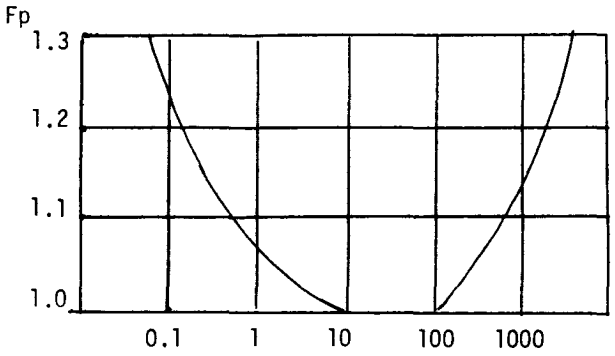

Figure 3.

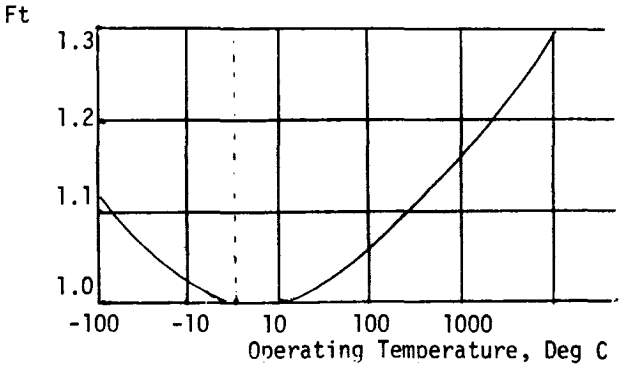

Figure 4.

1.0	for mild steel
1.07	for aluminium and bronze
1.1	for cast steel
1.3	for stainless steel
1.5	for higher grades of stainless steel
1.55	for hastelloy C.
1.65	for monel
1.7	for nickel and inconel
2.0	for titanium

TABLE 2 - Materials of Construction Factors.

and complexity a summary is given:

The initial information required is:

1. Process flowsheet identifying main plant items and process streams.
2. Total process stream input, ibmol/yr.
3. Extreme process temperature and pressure conditions encountered.
4. Material of construction of main plant items.
5. Operating phases of each main plant item.
6. Whether any unusually high or low direct or indirect initial costs are expected.

The order of estimating procedure is:

1. CAP : Determine total process input, ibmol/yr
2. n : Obtain number of main plant items from flowsheet.
3. FF : Calculate flow factor from flowsheet and equation provided.
4. PF : Obtain number of volume items from operating phase data and calculate phase factor from equation provided.
5. TP : Calculate plant throughput from equation provided.
6. EXP : Calculate cost-weighted plant capacity exponent from knowledge of main plant items, table and equation provided.
7. BIC.TP: Construct a plant log-log plot through the point where TP = 2.5 x 10^6 x BIC = \$7000. Line has a gradient of EXP.
8. BIC : Read off basic item cost from plant line knowing plant TP.
9. SF : Determine plant (F_t) max and (F_p) max from extreme conditions and figures. Calculate (F_m) mean for main plant items provided using data provided. Derive SF from equation provided.
10. DEC : Calculate using equation provided.
11. Investment: Divide DEC by a suitable percentage factor of 15-30% for grass-roots or battery-limits capital cost. For a plant with average initial costs the factor is 21%.
12. Updating: Use equipment cost index to update from the reference cost date: base M & S June 1972 value of 331. (USA base) or EPE (US)June 1972 value of 110.

Similar temperature, pressure and materials of construction factor are employed as in the Wilson method. Although high levels of accuracy are claimed, in practice this technique has been found to be unwieldy and not easy to use.

Functional unit or step counting procedures to obtain total capital cost.

The concept of "number of steps" in a process influencing costs was first suggested by Wessel (7) in proposing a correlation for labour costs. Later Hill (see above) assigned costs to "standard units" which is seen as the precursor of the functional units employed by Zevnik and Buchanan, and in methods described in this paper and the process steps used by Taylor.

TABLE 3 Explanation and Definition of Functional Unit.

A functional unit is a significant step in a process and includes all equipment and ancillaries necessary for operation of that unit. Thus the sum of the costs of all functional units in a process gives the total capital cost.

Generally a functional unit may be characterised as a unit operation, unit process, or separation method that has energy transfer, moving parts and /or a high level of "internals". Both main process stream, recycle and side streams are considered.

Pumping and heat exchange are ignored as they are considered as part of a functional unit unless substantial loads (e.g. gas compressors) or unusual circumstances (e.g. refrigeration) are involved.

Storage is ignored, unless mechanical handling is involved (i.e. for solids) as the cost of storage is relatively low and tends to be a constant function of the process.

Multistage operation is ignored.

Simple "mechanical" separation where there are no moving parts is ignored (i.e. cyclone, gravity settler) as the cost is usually relatively insignificant.

A functional unit is a significant step in a chemical process which includes all equipment fully installed and ready for that step to operate. A more detailed explanation and definition is given in Table 3 which encompasses all development work on this principle of estimating except for Taylor who defines his steps by example.

To illustrate the concept of a functional unit, an example of an acetic anhydride process is given which is used later to exemplify the various estimating techniques described. The outline process is shown in Figure 5. Each step comprises a significant operation and includes all equipment and ancillaries for operation of that unit. The detailed flow diagram is shown in Figure 6 for comparison.

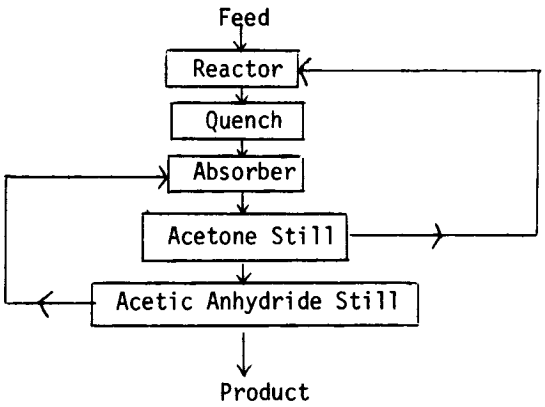

FIGURE 5.

FIGURE 6

Detailed Flowsheet of Acetic Anhydride Process.

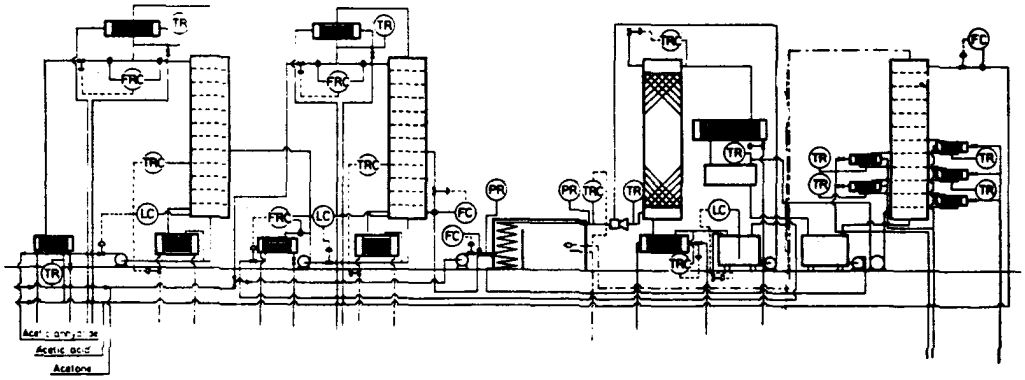

The principleof the estimating method is that the average cost of a functional unit in a process is a function of various process parameters:

Capital cost per functional unit= f(Q,T,P,M,CCI)

where Q = capacity or throughput
T = temperature
P = pressure
M = materials of construction cost index

Although there may be major differences between different units, for example, a distillation unit and compressor, these differences are averaged out over the process as a whole. The advantages and justification for the approach are:

1. With the information available at this level of estimating, there is no indication of relative costs of different items.

2. The costs of the items in any case are immaterial as it is the overall capital cost that is being estimated.

3. *Justification may be claimed on grounds of* equiprobability.

4. It appears to work well.

It is interesting that the concept is rapidly gaining acceptance with its adoption as a valid preliminary estimating procedure by many international companies.

A) Zevnik and Buchanan.

One of the earliest applications of the function unit method of capital cost estimation was due to Zevnik and Buchanan (9). They developed an essentially graphical technique for obtaining the cost of one functional unit based on plant capacity, maximum pressure, maximum temperature and materials of construction. This cost per functional unit (CPF) is then multiplied by the number of functional units, a utilities factor of 1.33 and a cost index based on ENR construction cost index, base 100 in 1939, divided by 300.

The cost per functional unit (CPF) is read from a graph of CPF versus plant capacity for a range of complexity factors (CF) calculated from the following expression:

$$CF = 2 \times 10^{(F_t + F_p + F_m)}$$

where F_t= temperature factor, read from a graph of F_t versus maximum (or minimum) process temperature.

F_p= pressure factor, read from a graph of F_t versus maximum (or minimum) pressure.

F_m= materials of construction factor, read from a table of factors from 0 for mild steel and wood to 0.4 for precious metals.

The overall procedure can be expressed as a series of equations depending on plant capacity, temperature, pressure, cost index, and number of functional units:

a) for "gas phase" processes within battery limits, plant capacity above 10 million lb p.a. (4464 long tons p.a.), and temperature and pressure above ambient.

$$\$C = 400.Q^{0.6}\ \frac{N.ENR.}{708}\ 10^{(0.1 \log P_m)+(1.80 \times 10^{-4}(T_m-300))} + (F_m)$$

where C = estimated capital cost
Q = plant capacity, long tons per year
ENR = ENR cost of construction index base 100 in 1913
P_m = maximum process pressure, atmosphere
T_m = maximum process temperature, deg K
F_m = materials of construction factor
0 for mild steel and wood
0.1 for aluminium, brass, some stainless steel
0.2 for monel, nickel, some stainless steel
0.3 for hestelloy
0.4 for precious metals

b) for plant capacities below 10 million lb p.a. (4464 long tons p.a.) the equation becomes:

$$\$ C = 930.Q^{0.5} \quad \ldots\ldots\ldots\ldots\ldots\ldots$$

c) for subambient temperatures, the temperature factor becomes:

$0.57 - (1.90 \times 10^{-2} T_{min})$

in place of: $1.80 \times 10^{-4} (T_m - 300)$

d) for subambient pressures, the pressure factor becomes:

$0.1 \log (1/P_{min})$

in place of: $0.1 \log (P_m)$

Zevnik and Buchanan's definition of functional unit "refers to all equipment necessary to carry out a single significant process function". There were difficulties in applying this definition which is evident from the inconsistencies in the worked examples, although the authors do confess to an "unconscious bias". There were also problems both in the reliability of published data and also in the boundaries of plant under consideration - whether a battery limits cost or greenfield site cost was being derived.

The authors claim an accuracy of ± 25% which they suggest could be equalled or bettered by a well calibrated user/system adaptation.

Recent attempts, however, to use their method have proved relatively unsuccessful (5) with results tending to be a little high. This is thought to be due to the inaccuracy of the correlation and the suspected high level of intuition employed in derivation.

B) Taylor.

Since this estimating procedure is being presented at this conference, it will not be described again. It is, however, important to note that more information is required for this method than the others described, as each step is considered individually.

C) Current work.

Work continues in developing more representative and accurate models for estimating capital costs at early stages of project development.

For gas phase processes only, including both organic and inorganic chemical products the following equation is proposed (8).

$$C = 986.\ N.\ Q^{0.616}\ \frac{EPE\ (UK)}{300}$$

where C = capital cost in UK, £, battery limits
N = Number of functional units
Q = Plant capacity, tonnes/y.
(if a multiproduct process, then average capacity is used)
EPE = Engineering and Process Economics Cost Index for U.K. (Base 100 in 1970, and value 300 mid-1978)

Accuracy claimed = ±20%.

This was derived from multiple regression analysis of 103 processes over the last 10 years. The equation has a multiple correlation co-efficient (R^2)of 0.955. This model is only one of a series that have been developed, and which will be reported in the near future.

A sufficient number of data sets were used to highlight one aspect of the overall problem of employing published data, and this is an understanding of the basis of the capital cost quoted. It seems that contractors tend to publish installed equipment costs and ignore engineering and design costs etc., while plant purchasers or clients tend to quote total capital cost which can be up to 40% higher.

For liquid and/or solid handling processes the following equation is proposed:

$$C = 76.9\ N \left(\frac{Q}{s}\right)^{0.675}\ \frac{EPE\ (UK)}{100}$$

where C = Capital cost, £, battery limits
N = Number of functional units
Q = Plant capacity, tonnes/y.
s = reactor "conversion"
= $\frac{\text{weight desired reactor product}}{\text{weight reactor input.}}$

hence $\frac{Q}{s}$ = process throughput, tonnes/y.

Accuracy claimed = ±25%

valid for $\frac{Q}{s}$ above 60,000

and $C = 6750\ N \left(\frac{Q}{s}\right)^{0.30}\ \frac{EPE\ (UK)}{300}$

for $\frac{Q}{s}$ below 60,000

Although the above model was the best fit with the data, an acceptable correlation was obtained with a linear model thus:

$$C = \left[195900 + 0.636 \left(\frac{Q}{s}\right)\right] N.\ \frac{EPE\ (UK)}{100}$$

This is explained by capital costs having a fixed element for design and some overheads which tends to be unrelated to capacity, together with a variable element relating to economy of scale. This effect is evidenced by the reduced scale factor at low plant capacities when the significance of the fixed element increase. A better representation of the situation is likely to lie between the linear and exponential relationship.

By including factors for temperature and pressure, the multiple correlation coefficient was raised to 0.94 with the following equation:

$$C = 94.N.\left(\frac{Q}{s}\right)^{0.665} e^{(2.58\times10^{-7}Q)}\ T^{-0.022}\ P^{-0.064}\ .\frac{EPE\ (UK)}{100}$$

where C = capital cost, battery limits, £
N = Number of functional units
Q = Plant capacity, tonnes/y
s = Reactor "conversion"
T = Maximum temperature, deg C
P = Maximum pressure, atm
Accuracy claimed ± 20%

Valid for $\frac{Q}{S}$ above 60,000

Of particular relevance and at least of equal importance is the principle involved that capital cost is a function of number of steps and basic process parameters, in particular capacity or throughput. This principle can be applied to any special situation to derive a model that is valid for that industry or group of processes.

Two examples are included here:

A) Refuse sorting and treatment processes:

$$C = N.(425900 + 612\ Q).\ \frac{EPE\ (UK)}{300}$$

where C = capital cost, £, battery limits
N = number of functional units
Q = plant capacity in tonnes refuse feed per day
multiple correlation coefficient (R^2) = 0.935.

B) Non-biological effluent treatment:

$$C = 312.N\ Q^{0.453}\ \frac{EPE\ (UK)}{260}$$

where C = total installed capital cost, £, battery limits basis, fully automated plant. Buildings not included.
N = number of effluent treatment steps. Effluent treatment steps are:

- Acid/alkali neutralisation
- Chrome reduction, aqueous (if gaseous sulphur dioxide is used, add a half step)
- Cyanide oxidations to cyanate, aqueous (if gaseous chlorine used add a half step)
- Demulsification
- Filter press
- Ion exchange
- Lime reagent preparation
- Settlement
- Water recycle system

Q = design throughput, gallons per hour
EPE = Engineering and Process Economics cost index (UK).

The capital cost includes all equipment, materials, labour, civils, installation, commissioning and cubicle for the control panel. Reagent warehousing would cost about 20% more, and complete enclosure up to 100% more. Piping, sumps and work outside the plant perimeter would cost extra.

Application of capital cost estimation procedures described.

To illustrate how the techniques described above are employed, and compare the different results, the acetic anhydride process shown earlier is costed. Another flow sheet and plant layout is given in Figure 7.

The process parameters are as follows:

Capacity	20,000 t.p.y. 16.p.y.
Number of functional units	5
Number of main plant items	26
Reactor conversion	0.126
Maximum process temperature	714°c
Maximum process pressure	1.7 atm
Materials of construction	lower grade of stainless steel
EPE(UK) cost index,mid 1978,	300
ENR cost index, mid 1978 estimated	2700

All estimates are presented in £ mid 1978 for a battery limits plant. Conversion from US $ has been accomplishedby updating to mid 1978, using US $1.8 = £1 and a location factor of 1.1 (US/UK)

Hill

$\$_{1955}$ C = f.IEC. Cost index
f is calculated from factors provided in the original paper (q.s.)
= 3.1

$$\$_{1955}IEC = 30{,}000.\ 9.\ \left(\frac{20000}{4245}\right)^{0.6}$$

= $656843

$£_{1978}IEC$ = 1022850

$£_{1978}C$ = 3.1.1022850

= £3170800.

N.B. This would be expected to be high, as applying a cost index over 20 years only considers increases in costs and ignores technological progress. There is no way of measuring this latter factor and is one of the known limitations of cost indices.

Wilson

$$C = f.N.\ (AVC)\ F_M\ F_P\ F_T$$

$$£_{1978}AVC = 21\ V^{0.675}$$

$$= 21.\ (20{,}000)^{0.675}$$

(taking V as the plant capacity instead of average equipment item throughput due to lack of data)

= 16804

$$C = 1.80.26.16804.1.2.1.0.1.09\ .\frac{300(EPE,UK,1978)}{100\ (EPE,UK,1971)}$$

= £2730900.

Zevnik and Buchanan

$$\$C = 400.N.Q^{0.6}\ \frac{ENR}{708}$$

$$10^{(0.1\ \log P)} + (1.80 \times 10^{-4}(T-300)) + (FM)$$

$$= 400.5.(20000)^{0.6}\ .\frac{2700}{708}.\ 10^{(0.023 + 0.075 + 0.1)}$$

+ $4576602

= £2311400

Taylor

Significant process steps, and their parameters, are:

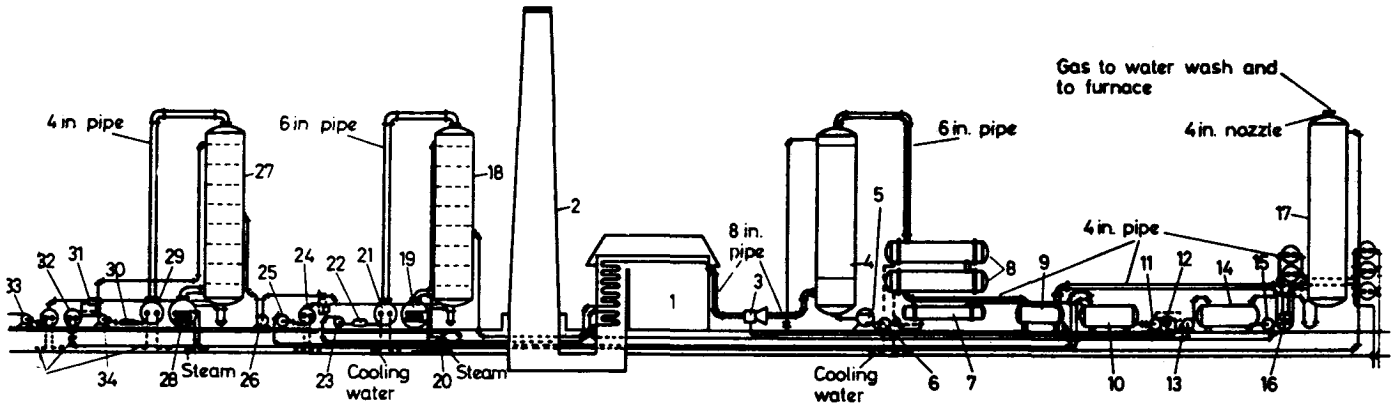

FIGURE 7. Acetic Anhydride Plant, General Plant Layout.

	score a	b	c	d	e	f	g	h	Total	Costliness Index
Feed storage	-	-	2	0	0	0	0	0	2	1.7
Reaction	2	0	-	1	0	2	0	0	5	3.7
Quench	3	-	-	1	0	2	0	0	6	4.8
Absorber	1	-	-	0	0	1	0	0	2	1.7
Crude product storage	-	-	2	0	0	1	0	0	3	2.2
Acetone still	3	-	-	0	0	1	0	0	4	2.8
Acetic anhydride still	1	-	-	0	0	1	0	0	2	1.7
Product storage	-	-	2	0	0	1	0	0	3	2.2
									TOTAL:	20.8

a relative throughput, t./t.product
b reaction time in hours
c storage time in weeks
d temperature extreme. ^{o}c
e pressure extreme
f materials of construction
g multistreaming
h special problems

Costliness index (CI) for whole process = 20.8.

£ capital cost = $42000.(Q)^{0.39}$ .CI. $\frac{EPE\ (UK)}{280}$

where Q is plant capacity in thousands of tonnes

= $42000.\ (20)^{0.39}$ .20.8. $\frac{300}{280}$

= £3010800.

Alternatively,

£ capital cost = $115000.N.\ (Q)^{0.26}\ \frac{EPE(UK)}{280}$

where N is the number of steps and
Q is the capacity in thousands of tonnes

= £2147900

Alternatively,

£ capital cost = $1120000,\ R.(Q)^{0-3}\ \frac{EPE\ (UK)}{280}$

where R is the number of reactions and
Q is the capacity in thousands of tonnes

= £2947800.

Timms

$£C = 986.\ N.Q^{0.616}\ \frac{EPE\ (UK)}{300}$

= £2199300.

Bridgwater
(This is not strictly applicable as it is only for liquid/solid based processes, but is included for illustration).

$£C = 76.9.N.\ (\frac{Q}{s})^{0.675}\ \frac{EPE(UK)}{100}$

= $76.9.6.\ (\frac{20000}{.126})^{0.675}\ .\frac{300}{100}$

= £3736500

Alternatively,

$£C = N\ 195900 + 0.636\ (\frac{Q}{s})\ \frac{EPE(UK)}{100}$

= 4452900

Alternatively,

$£C = 94.N.\ (\frac{Q}{s})^{0.665}.\ e^{(2.58x10^{-7}Q)}.\ T^{-0.022}.\ P^{-0.064}.\ \frac{EPE(UK)}{100}$

= $94.5.(\frac{20000}{0.126})^{0.0665}\ e^{\frac{5.16 \times 10^{-3}}{714}}\ .1.7^{-0.064}.3.$

= £3,407,100.

(N.B. The figures are expectedly high as solid handling functional units seem to cost about 50% more than gas handling steps.)

Comment

There is, therefore, a range of answers from £2147900 to £3170800 with a mean value of £2645600 (ignoring the estimates from the model for liquid-solid systems). The "error" on the average value is thus -19% +20%. If a conclusion were required, it might be that for preliminary capital cost estimating, as many methods as possible should be used and an average taken!

Conclusions

Interest in step counting methods for capital cost estimation is continuing to develop. There is probably not yet a "best" method, but the principle is demonstrated to be valid and progress in this area should be studied.

Acknowledgments

Permission to reproduce the flow diagrams of the acetic anhydride process from "The Manufacture of Acetic Anhydride" by G.V. Jeffreys, published by the Institution of Chemical Engineers, is gratefully acknowledged.

References:

1) Bridgwater, A.V., 1977, Effluent and Water Treatment Journal (May, July, September, November).

2) Lang, H.J., 1948, Chemical Engineering, June.

3) A new guide to capital cost estimation, 1976, (Institution of Chemical Engineers).

4) Hill, R.D., 1956, Petroleum Refiner, 35 (8) 106-110.

5) Wilson, G.T., 1971, British Chemical Engineering and Process Technology, 16 (10) 931-934.

6) Allen, D.H., and Page, R.C., 1975, Chemical Engineering, March 3rd, 142-150.

7) Wessel, H.E., 1952/3, Chemical Engineering, July 1952, June 1953.

8) Timms, S.R., 1977, Research in progress.

INVESTIGATION OF THE ECONOMICS OF THE NITROBENZENE PRODUCTION

C. McGreavy
A.O.L. de Q. Novais

Department of Chemical Engineering,
University of Leeds, Leeds, England

ABSTRACT

An investigation of the general features which identify the structure of optimal operating policies for a mixed acid nitration process is reported. The plant is multipurpose in that it can be used for several products, but attention is confined to exploring the best operating states for producing mononitrobenzene. From a parametric sensitivity study, it has been established that the molar feed ratio (MFR) of nitric acid to benzene is the most important variable. This suggests that the best strategy for determining the optimal conditions is to fix MFR before searching for the best operating temperatures for the reactors, which are the other principal variables.

INTRODUCTION

The profitable operation of an existing chemical plant results from the judicious balance between two essentially different sets of factors conveniently classified as external and internal. In practice, both are recognized as implying some degree of flexibility, with the former being more restrictive than the latter. External factors, such as cost of raw materials and other utilities, or unit selling prices of main and by-products usually appear as constraints which have to be met. Others, such as the level of demand, scheduled time and rates for delivery are more flexible in as much as they can, to some extent, be subject to negotiation prior to contract. Once the terms of contract have been agreed, the internal factors represent the only area where further adjustment may be made. These factors comprise what may be broadly classified as operating and design variables. Major alterations in the type and capacity of equipment, or even in the arrangement of existing equipment, will involve additional running costs and time lags which alter the balance of costs. The consideration of such factors, though providing potential scope for adjustment, will be undesirable in a situation where delays in production and/or delivery may be

penalised and will consequently be better investigated and dealt with while orders are still being sought and negotiated.

On the other hand, alternative operational policies of the equipment, though not causing great changes in the running costs, are still associated with different degrees of efficiency. Thus, in a situation where the external factors and design variables are fixed, the study of operating conditions will represent an area of further improvement.

This paper deals with the effect of operating conditions on the profitability of a mixed acid nitrobenzene plant. It is one aspect of a much more extensive study and so inevitably is based on a number of fixed conditions which have been arrived at, for the present discussion, by examining the problem in a wider context. More detailed analysis can be found in reference (1). With the restraints implied by this larger framework, the following considerations define the terms of reference of the problem,

(i) Although attention is confined to nitrobenzene, the plant is multi-purpose, i.e. other products can be produced using the same equipment, e.g. nitrotoluene.

(ii) Because of this, an inventory model is required such that the solution leads to a definition of an optimum production rate for each process (and hence throughputs), as well as number of runs and running times.

(iii) The inventory model can be solved for an arbitrary set of prices, cost and demand level, which means that the magnitude of the quoted numerical values should also be regarded as arbitrary. This in no way limits the significance of the points to be discussed, which are quite general in scope.

(iv) Taking the production rate as a parameter, the best operating conditions for each individual process may be investigated on the basis of an annual cash flow after tax, without regard to the remaining processes. But as suggested in (ii), only by solving the inventory model can the overall optimum individual production rates be defined for a given market situation. The unit manufacturing cost could be used instead as a performance

index, but it would be less comprehensive in that taxes, which are normally based on sales volume, would not be accounted for.

(v) For the nitrobenzene process, as well as for the others, the main operating variables must be identified by means of extensive parametric sensitivity analysis. This showed that the principal variables are the molar feed ratio, nitric acid to benzene (MFR) and the reactor temperatures TR1 and TR2 in vessels R1 and R2 respectively. Closer examination of the problem revealed that the most appropriate strategy for searching the optimal combination was to fix MFR, since this showed the greatest sensitivity and then treat the reactor temperatures as a subproblem.

(vi) Detailed plant simulation is conveniently carried out using a flowsheeting program (2), and the appropriate information flowsheet can be developed from the process flowsheet shown in figure 1. Each unit computation is based on a mathematical model which, together with general mathematical subroutines, allows an optimisation algorithm (the simplex method of direct search) to be used (3) to search for the best set of operating states. There is naturally a close correspondence between the process and information flowsheets, so that the results can be interpreted in terms of operational conditions without ambiguity. Consequently, there is no explicit requirement to give the information flowsheet as well.

PROCESS DESCRIPTION

The process flowsheet of the plant for nitration of benzene is shown in figure 1. The feeds are concentrated sulphuric acid (98 wt.%), concentrated nitric acid (96 wt.%) and benzene. Other inputs to the system are cooling water for the reactors, process water for the washers and electricity for the motors which operate the agitators and centrifuges.

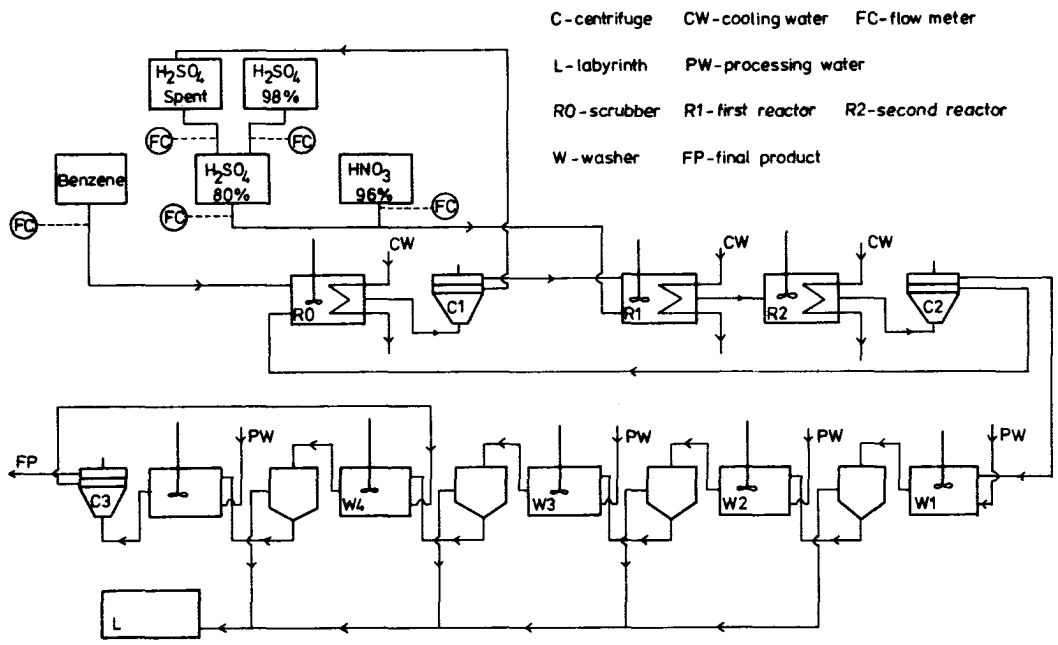

Fig. 1. Process flowsheet of nitrobenzene plant.

The benzene is admitted to the scrubber, where it is mixed with the recycle stream (an acid mixture containing unreacted nitric acid, sulphuric acid and water)and some entrained organic phase.

The scrubber, as well as the remaining reactors, is cooled by means of water. Also, all the reactors are agitated. From the scrubber, there is a mixture of aqueous and organic phases which are separated in a centrifuge, Cl. The aqueous phase, diluted sulphuric acid, (spent acid), goes to storage. Part of it is sold as a by-product; part of it is premixed with 98 wt.% sulphuric acid. The organic phase, composed of the organic reactant with some nitroderivative and some entrained aqueous phase, enters the first reactor. In addition this reactor admits the nitrating mixture formed with 80 wt.% sulphuric acid and 96 wt.% nitric acid.

The bulk of the reaction takes place in this reactor which is followed by another which takes the reaction nearer to completion. The reaction mixture is finally separated in a centrifuge, C_2. The resulting aqueous phase forms the recycle stream and the organic phase, being composed of nitrobenzene, dinitrobenzene, unreacted benzene and some entrained aqueous phase is purified.

The second section of the plant, where purification is carried out, comprises four washers and a labyrinth. Each washer consists of two sections, the first is the mixing vessel, where the product is thoroughly mixed with process water, and the second is the settling and separating vessel, where the two phases are separated by gravity. The labyrinth is a tank which receives the aqueous phase with some entrained organic phase, from the washers.

The washers are followed by a fifth washer where the settling and separating vessel is replaced by a centrifuge, C_3. This centrifuge separates the final product from the aqueous phase which is fed back to the fourth washer in place of process water, giving rise to a second recycle stream. The process water to the second washer is added of 10 wt.% caustic soda for a more thorough elimination of any acid present in the product stream.

OPTIMISATION STUDIES -

Using a demand of 2000 tonnes/year means a production rate of nitrobenzene equivalent to 300 kmol/day of benzene. This quantity is a constraint and the question which needs to be investigated is: what are the operating conditions which will achieve this production level most effectively? As already noted, the index of efficiency is assumed to be the annual cash flow after tax, y, and the most significant variables have been shown to be MFR and TR1 and TR2 by parametric sensitivity tests. The problem so defined is an optimisation which reduces to the investigation of the selection of these variables so as to maximise y.

The permissible range of variation of the independent variables during optimisation will normally be bounded, since there are safety regulations which must be met with regard to chemical and mechanical restrictions on the materials of construction and the need to prevent hazards such as loss of toxic materials by evaporation, etc. For example, under normal pressure nitric acid is partially decomposed above 86°C and consequently an upper limit must be set on the operating temperatures of the reactors, especially no. 1, where the higher acid concentrations are to be found. Also, an upper limit on MFR will be necessary to prevent an undesirable excess of unreacted nitric acid in the system which can cause

excessive corrosion.

To illustrate the valuable insight which can be revealed by carrying out such studies, the following cases are examined to show how the essential structure of the problem can be identified.

CASE 1 -

Linear constraints representing upper and lower bounds are imposed on the variables in the form

$$0 \leq \text{MFR} \leq 1.20 \qquad (1)$$

$$20^{\circ}\text{C} \leq \text{TR1} \leq 80^{\circ}\text{C} \qquad (2)$$

$$20^{\circ}\text{C} \leq \text{TR2} \leq 90^{\circ}\text{C} \qquad (3)$$

The optimum ($y^{*} = -3.0 \times 10^{4}$ £/year) in the subregion defined by these constraints is at TR1 = 77°C, TR2 = 89°C and MFR = 0.99.

CASE 2 -

The temperatures TR1 and TR2 are preset at

$$\text{TR1} = 43^{\circ}\text{C} \qquad (4)$$

$$\text{TR2} = 62^{\circ}\text{C} \qquad (5)$$

The problem then reduces to a one-dimensional search over MFR defined by condition (1).

The optimum ($y^{*} = -9.2 \times 10^{4}$ £/year) is found at MFR = 1.01.

CASE 3 -

The variable MFR is fixed at 1.01. The search in the ranges for TR1 and TR2 as governed by conditions (2) and (3) leads to the optimum ($y^{*} = -6.4 \times 10^{4}$ £/year) at TR1 = 73°C and TR2 = 89°C.

CASE 4 -

A case similar to case 3 is considered with the MFR fixed at 0.99 which results in values similar to case 3 which is in agreement with case 1.

Of these four cases, 1 is the most general since no judgement need be exercised on the level of the independent variables, apart from the boundaries described by conditions (1), (2) and (3). The temperatures are found to approach the upper boundaries very closely and MFR indicates slight deficiency in nitric acid with respect to the stoichiometric ratio. The result is confirmed in case 4, where MFR is preset.

By restricting the temperatures to values well below the safety limits (case 2), the most profitable operation of the plant is found with a slight excess of

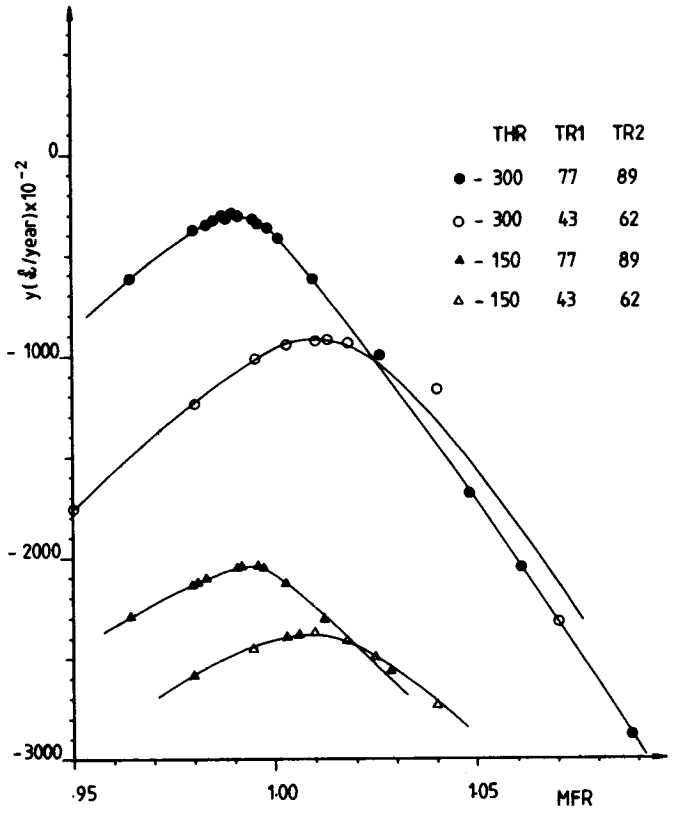

Fig. 2. y versus MFR for various throughputs and reactor operating temperatures.

nitric acid, MFR = 1.01, although the value of y^* is lower than in case 1. This conclusion is reasonable, in that the less expensive reactant, nitric acid, is used in excess to obtain higher degrees of conversion. That the reverse happened in case 1 suggests that higher degrees of conversion are obtained by higher temperatures in the reactors, with the steady state operating conditions resulting in the presence of unreacted benzene. Given the fact that the normal boiling point of benzene is 80.1°C, such a policy may be undesirable. With case 3, the possibility of obtaining higher values of y^* with MFR = 1.01 can be explored. Again, the temperatures approach the upper boundaries closely. Difficulties can arise because the numerical procedure on which the optimisation algorithm is based has to be terminated within a preset tolerance, so the differences between TR1, TR2 and the upper limits in cases 1 and 3 are not significant. The general pattern of behaviour is of a common trend in the temperatures for different MFR, although the specific value of the maximum y^* depends on MFR. To assess whether this effect is specific to this level of throughput, THR = 300 Kmol/day, a study similar to cases 1 - 4 can be examined for THR over the range 150/450. In figure 2 is shown the plots of y versus MFR for THR = 150 and 300, for two different sets of temperatures. For every THR, similar behaviour is observed. As THR increases, the MFR which leads to maximum y for a given set of temperatures remains constant and the differences between the y^* for a given THR, also increase. As can be seen in figure 2,

while the difference between y^* for THR = 150 Kmol/day is approximately 3.50×10^4 £/year, for THR = 300 Kmol/day it is 6.20×10^4 £/year.

If it is accepted that it is desirable to operate the plant with a slight excess of nitric acid, it is possible to investigate the effect of alternative operating temperatures, e.g. intermediate to cases 2 and 3. This study is illustrated in figure 3 where lines of constant y are shown across the whole range of TR1 and TR2, together with some observed values.

It can be seen that y is slightly more sensitive to TR2 than to TR1, and that for a fixed MFR, the maximum y is to be found at the intersection of the upper boundaries. Such graphs (and similar ones for different MFR) can be very useful in assigning operating temperatures to reactors 1 and 2, in that they provide a mechanism for defining conditions in terms of an economic index.

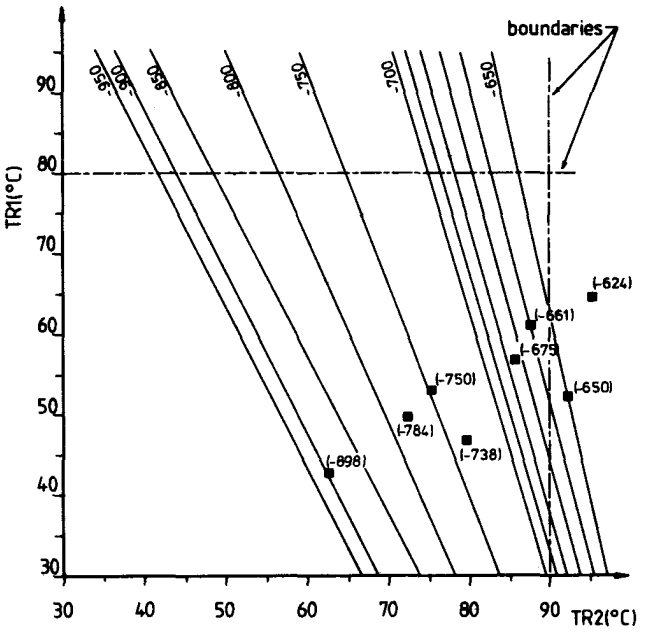

Fig. 3 - Lines of constant y on the plane (TR1, TR2) for THR = 300 Kmol/day and MFR = 1.01
[y] - (£/year) x 10^{-2}
■ - observed values of y.

CONCLUDING REMARKS -

The above optimisation studies have necessarily been somewhat brief and simple. No reference has been made to the difficulties which are always present in the preliminary stages of establishing valid models for the simulation. In fact, this represents considerable effort, but is rewarded by the insight which is gained. In particular, the relative significance of the most important variables can be identified and point to strategies of operation which are not intuitively obvious.

It should also be stressed that although the discussion has been centred on an economic index, it is not the only one

which could be used, e.g. the same approach could be used with conversion, heat load, or composition of streams which the operator may require to analyse. In fact, for every case so far mentioned, whether it is an optimum or not, the use of a flowsheeting program provides a full description of the profile of the plant shown in figure 1, besides the evaluation of y. A study similar to that depicted in figures 2 and 3 could be applied to other indices. The curves shown in figure 2 and figure 3 represent sections on the surface y = y (MFR, TR1, TR2) at constant (TR1, TR2) and MFR respectively. They are meant to provide a local exploration which will reveal the characteristics of the optimum in relation to neighbouring states. This will ultimately determine whether a given set of operating conditions is acceptable from the point of view of implementation. It can be seen that y has a very sharp optimum with relation to MFR, which in fact is enhanced as THR increases. The operating temperatures also influence y, but to a lesser extent, and this suggests that MFR should be fixed before the temperatures. Because MFR measures the molar ratio between nitric acid and benzene feeds and only mass flows are directly controlled (see figure 1), maximum profitability will be achieved for a given range of operating temperatures, when changes in throughout are compensated for by corresponding changes in nitric acid mass flow.

Useful results from such studies are dependent on reliable representation of the process units in the computation modules for the flowsheeting program. Considerable effort has therefore to be expended in confirming the basic structure has been identified. However, even if the availability of data does not permit absolute predictions to be made, the qualitative behaviour can be recognised which permits strategies for process improvement to be identified. In addition, insight as to operational policy can be gained which would normally take years on a plant.

NOTATION

MFR - molar feed ratio nitric acid : benzene.

THR - throughput, mass flow of benzene, Kmol/day.

TR1 - operating temperature of reactor 1, deg. C.

TR2 - operating temperature of reactor 2, deg. C

y - annual cash flow after tax, £/year.

superscript * - optimum value.

ACKNOWLEDGMENT

The authors wish to thank the Calouste Gulbenkian Foundation, Lisbon for the support it provided to enable Mr. A. Novais to participate in the present work.

REFERENCES

(1) NOVAIS, A, Ph.D. Thesis, Department Chemical Engineering, University of Leeds, 1978.

(2) JOHNSON, A.I. and associates; "GEMCS manual and application studies", Department of Chemical Engineering, McMaster University, Canada, 1970.

(3) NELDER, J.A., MEAD, R., Comput. J., 1965, 7, 308.

THE ESTIMATION OF THE TRANSPORT PROPERTIES OF FLUIDS
PART I. PHILOSOPHY AND METHODS

C.A. Nieto de Castro
W.A. Wakeham

Imperial College, London, England

ABSTRACT

The estimation of the thermophysical properties of fluids and fluid mixtures has been, for many years, the subject of a considerable research effort owing to its significance in the design of many items of process plant. In this paper attention is concentrated upon the transport properties of fluids and a hierachy of estimation schemes is established. It is argued that the most reliable estimation schemes are founded on a rigorous theoretical analysis of the fluid state and confirmed by means of a series of measurements on a limited number of carefully chosen fluids and fluid mixtures. Lower levels of estimation scheme are ordered according to their degree of departure from this optimum.

It is shown that the highest level of estimation procedure is, at present, only applicable to the transport coefficients of dilute, non-polar gases. However, the success of this procedure indicates the approach which should be adopted in future measurements of the transport properties of fluids to develop more applicable correlation schemes of the same type. In addition, the ordering of estimation schemes permits the develpment of an algorithm for the selection of the best procedure for the evaluation of transport coefficient data for a particular fluid.

1. INTRODUCTION

The design of any chemical process plant invariably requires a knowledge of the thermophysical properties of the fluids involved in the process. In particular, the design of equipment for heat or mass transfer operations is based upon values for the transport properties for the fluids. It is evidently impossible that experimental measurements of these properties could ever be carried out over the entire range of thermodynamic states for every pure component and for multicomponent mixtures of arbitary composition. Consequently, it will always be necessary to have means available whereby, at best, the available experimental data may be employed to generate the required properties, or, at worst, entirely empirical estimates of their values may be made.

It is the purpose of this paper to present an underlying philosophy for the development of data generation and correlation schemes for engineering design. It is shwon that a hierachy of estimated procedures can be established based upon their degree of reliance on fundamental theory, and accurate experiment. This hierarchy naturally leads to the establishement of an algorithm for selection of an estimation procedure in particular cases. A corollary to the existence of various estimation schemes is the increase in the uncertainty of the generated physical property data as the procedure departs more from a sound theoretical basis. In a companion paper (1) the consequences of these uncertainties for the design of process plant equipment are discussed and shown to be technically and economically significant. Thus, efforts to develop fundamental theories of the fluid state and perform accurate experimental measurement of fluid transport properties are shown to be justified in an engineering context as well as from the viewpoint of basic science.

2. THE ESTIMATION PROCEDURE

The overwhelming body of experimental measurement of the transport properites of fluids have been carried out for thermodynamic states close to room temperature and atmospheric pressure upon simple molecular species. The reasons for this are, first the relative simplicity of the experimental procedures under these conditions, and second the possibility of a fundamental interpretation of the data in terms of molecular theory. Even within these constaints it is only in the last ten years that reliable experimental data for the transport properties of the simplest, pure molecular species have become available. For engineering design purposes therefore the experimental measurements which have been carried out have appeared to have little direct relevance. That this is not in fact the case forms the cornerstone of the philosophy of transport property estimation procedures advanced here. In order to define the elements of this philosophy it is essential to identify the various levels of estimation which exist. Accordingly, the next four sections define the different approaches to the estimation of fluid transport properties. Since it is clearly impossible and unproductive to list every variant of a particular approach, examples have been selected in order to emphasize the essential features of each level of estimation procedure.

2.1 EXPERIMENTAL DATA

The first recourse in any attempt to generate thermophysical property data should always be to direct experimental measurements for the fluid

transport property required. It must be added as a rider that any experimental data employed should be of well characterized accuracy which is commensurate with the requirements of the design. In the event that the experimental accuracy is poorer than can be tolerated in the design, it is possible that an estimation procedure would give more reliable data. Furthermore, for fluid mixtures, only in exceptional cases will the experimental data refer to identically the same composition as that required. In these circumstances the data can be used in conjunction with a suitable theory to evaluate data at the required composition.

2.2 THE PREDICTIVE SCHEME (CLASS I)

The predictive scheme is defined as that which has a rigorous theoretical framework and which requires as input information only physically meaningful quantities derived from a minimum set of experiments or calculated from other fundamental sources.

The most successful approach of this type is provided by a scheme designed for the transport properties of dilute gases. Since this scheme represents the optimum estimation scheme which should be aimed at for all states of fluids it will be described in some detail.

The kinetic theory of gases initiated by Boltzmann (2) and developed by Chapman and Enskog (3) early in this century provided a complete formal description of the macroscopic properties of such gases in terms of the properties of their constituent atoms.

Because these molecular properties were not known the utilization of this theory for the explicit evaluation of macroscopic properties was not possible immediately. Nevertheless the theory did provide a framework for the correlation for the low density viscosity, thermal conductivity and diffusion coefficient data available. In recent years considerable advances have been made in this field. On the one hand accurate measurements of the viscosity of the pure monatomic gases and their mixtures have been made (4-6) and on the other it has been possible to derive the molecular properties of the constituent molecules from these measurements, in particular the intermolecular pair potential (7-8).

These developments have had consequence for both basic science and engineering design. For example the experimental data for the viscosity of the monatomic gases has been used, together with the Chapman-Enskog theory, to demonstrate that the majority of thermal conductivity data for the same gases are in error by as much 10% even near room temperature (9). From this observation it can be inferred that data for more complicated molecules which have been less frequently studied are in error by at least a similar amount. In Ref. 1 it is shown that errors of this magnitude are of great significance to the optimum design of process plant.

A further development which has stemmed from the conjunction of accurate experiments and theory for simple molecules is the extended law of corresponding states (10). It follows directly from the hypothesis that all the interactions of the monatomic species conform to the same universal intermolecular potential that there exist several functionals of that intermolecular potential function. These are defined by the Chapman-Enskog theory, and serve to describe the transport properties of all the pure monatomic gases as well as their binary mixtures. These universal functionals have been determined and two scaling parameters characteristic of each binary interaction which secure this universality have been obtained (10). Concurrently, other work has shown that the fundamental hypothesis of the extended law of corresponding states is valid to a considerable degree of accuracy (5, 11-13).

The importance of this development is twofold. First the existence of universal functionals for the interactions of the monatomic transport properties of pure gases and binary mixtures over a range of temperature far wider than that which can be achieved experimentally. Secondly, the Chapman-Enskog theory demonstrates that the calculation of any of the transport properties of any multicomponent gas mixture of arbitary composition can be effected over a similarly extended temperature range from a knowledge only of the binary interaction functionals. Thus from a body of viscosity data obtained for binary mixtures of monatomic gases over a limited temperature range it is possible to predict any transport property of any mixture of the same gases over a much wider temperature range.

In order to make further advances towards a complete treatment of polyatomic gases the Wang-Chang-Uhlenbeck kinetic theory of dilute polyatomic gases must be involved (14). It has been shown that to a very high degree of accuracy for both the viscosity and diffusion coefficient of such gases the presence of internal energy in such molecules is negligible (15). Consequently, the formal expressions for these two transport coefficients remain the same therefore contain the same functionals of the intermolecular potential. Thus, by extending the hypothesis of the universality of the intermolecular potential among the monatomic species to these more complicated molecules they can be encompassed in the same scheme. This extension has been carried out to some ten polyatomic gases and their binary mixtures with great success (5). Following the preceeding arguments again we see that it then becomes possible to predict the viscosity of any low density gas mixture containing up to 11 components over a wide temperature range. Indeed the viscosity of over 2000 gas mixtures of arbitary composition can now be predicted in this way, and the temperature range covered for CO_2 for example, extends from 130K to the dissociation limit. The Chapman-Enskog theory shows, and experimental tests confirm that the accuracy of these predictions is comparable with that of the original measurements ($\pm$0.5%).

This example shows how the use of rigorous theory together with a relatively small number of judiciously chosen experiments can be used to generate a much greater body of experimental data. As such it forms the optimum predictive procedure for design purposes. Generalizations of this approach to other thermodynamic fluid states should be the aim of future work.

2.3 THE THEORETICALLY-BASED ESTIMATION SCHEMES

The foregoing type of procedure has been referred to as predictive since all the necessary quantities for the evaluation of the viscosity of a particular gas mixture were derived from accurate experiments and used in a rigorous theoretical framework. It is possible to discern two types of scheme which lie somewhat below this in order of preference.

In the first type (Class II) an exact rigorous theory for the transport coefficients of the fluid exists formally, but there is insufficient experimental information available to make use of the theory. In this case the procedure involves not estimation of the transport coefficients themselves but of some intermediate, often molecular, quantity on which they depend. This estimated value is then used within the rigorous theoretcial framework.

An example of this approach is provided by the Mason and Monchick theory of the thermal conductivity of polyatomic gases (15,16). According to their apporach the Wang-Chang-Uhlenbeck theory of transport in polyatomic gases is cast into a form containing experimentally accessible, though not often available, internal energy relaxation times in addition to the viscosity of the gas or gas mixture which may be obtained as before. If experimental relaxation times are not available they are estimated by means of a suitable physical model and then used in the rigorous theory. A further example is afforded by the use of assumed intermolecular potential models for the evaluation of dilute gas viscosity data for polar gases. Here, the Wang-Chang-Uhlenbeck kinetic theory provides the rigorous theoretical framework again, but in this case the pair interaction potential for molecules of the gas is estimated (17).

Evidently, the uncertainty in the transport properties evaluated in these ways is dependent upon the sensitivity of the particular transport property to the quantity estimated and the reliability of this estimate. Thus, whereas the uncertainty in the estimate of the internal energy relaxation time in the first case may be large, this may not be totally reflected in the final uncertainty of the transport coefficient. On the other hand errors in the guessed intermolecular potential and/or its parameters will certainly have a direct effect upon the uncertainty of the estimated transport coefficient.

Procedures of this type would be improved to predictive methods when the estimated quantites are derivable from experiment. That this is not yet possible is, in most cases, owing to the lack of reliable experimental data rather than any defect in the underlying theory.

A second class of theoretically inspired methods (Class III) occurs when a formal theory of transport in the fluid state exists but where its application to the interpretation of experimental data or estimation of properties is not possible because of a combination of mathemtical difficulty and inadequate knowledge of other necessary physical quantities. In this class we may cite as an example the situation for the transport coefficients of simple liquids. Statistical mechanical theory of liquids developed by Bearman and Kirkwood (18) among others expresses their transport coefficients in terms of many-particle distribution functions and intermolecular potentials. Since neither of these quantities are known the theory cannot be applied in its present form. Thus, other approaches have had to be adopted. On the one hand theories of transport in liquids have been developed based on simple models for the liquid state such as the Eyring theory(19) and the Van der Waals theory (20). On the other hand, attempts have been made to simplify the complete theory by physical arguments (21). In either case the resulting 'theoretical' expression for the transport coefficients is less than rigorous and so any parameters it contains are likely to be physically meaningless. Usually, such parameters are obtained from a fit to experimental data for a particular fluid, although some entirely empiricalmeans of estimating their values for fluids or fluid mixtures are available.

Since this type of estimation scheme is weakly founded on theory and dispensable parameters have to be obtained by comparison with experiment or guesswork, the reliability of these schemes is considerably less than those discussed earlier, and their general application restricted to fluids for which some experimental data exist.

2.4 EMPIRICAL ESTIMATION TECHNIQUES

The final subset of estimation methods is defined as that for which there is presently no theoretical justification, but which are based upon observations of relationships between the transport coefficients of fluids and other macroscopic quantities for the same fluids (Class IV). Such methods would involve, for example, a correlation between the viscosity of a pure liquid and its partial molar volume (22). Such correlations are formulated on a considerable body of data over a moderate temperature range and then applied universally to all fluids.

Such procedures have obvious deficiencies in terms of the accuracy of their estimates, furthermore, no indication is usually given as to the mechanism by which the procedure may be extended to any number of components without further heuristic assumptions. Their sole advantage lies in the fact that they may be applied to any chemical compound.

3. THE PHILOSOPHY

Section 2.2 has defined the optimum predictive scheme for the transport properties of fluids. Although a scheme of this type presently exists only for the viscosity and diffusion coefficient of dilute gases, its success suggests the direction for future work in the field of the development of correlation and estimation techniques and the philosophy governing such work.

First a series of careful coefficient measurements of high accuracy should be carried out on relativiely simple pure fluids and binary mixtures. These measurements should then be interpreted in terms of a rigorous theory so as to determine quantities depending on the two species in the binary mixture. Subsequently these measurements and the associated theory should be used to predict the transport

properties of multicomponent mixtures of these fluids which should then be compared with accurate experimental measurements. These tests together will serve to identify the minimum set of experimental measurements necessary to add a new fluid to the overall scheme. For example in the case of dilute gases the minimum set of measurements required for the generation of the viscosity of a multicomponent mixture of arbitrary composition containing the new fluid, comprises the viscosity of the pure fluid and its binary mixtures with the other components over a range of temperature. Subsequently, the experimental measurements can be extended to progressively more complex molecules incorporating modifications into the theory as they become necessary.

Within the context of this philosophy therefore measurements on pure, simple fluids are a prerequisite to the development of reliable estimation schemes and are not carried out solely for their scientific interest. Furthermore, in specific cases such measurements can serve to extablish the reliability of experimental techniques before they are used for more complex molecules. It is argued that this strategy must form the gasis of all long term research in the field of the transport properties of fluids.

Since such a programme is likely to be of long duration it is recognised that less satisfactory extimation methods must be used for many fluids at present, and for some considerable time in the future. However, in the spirit of our philosophy it becomes possible to chart a route to the most suitable estimation procedure for the transport properties of a particular fluid mixture.

4. THE ALGORITHM

It is not our purpose here to develop any new correlation scheme but rather to rationalize the choice of a scheme for a particular problem in the light of the foregoing remarks. Consequently, Tables I-IV list the possible sources of data for the viscosity and thermal conductivity of fluids. The sources are grouped according to the classification of section 2. The list is not intended to be exhaustive, in particular we cite only one empirical method in each case from a considerable field, nevertheless the method selected in each case is chosen to be the best in a particular class defined in section 2. The accuracy of each estimation method is included. Sufficient bibliographic information is included to allow the reader to obtain details of a particular scheme.

Figures 1 to 4 then provide a flow chart for the determination of the most suitable extimation procedure for the viscosity and thermal conductivity of gases and gas mixtures from among the various possible schemes. Figures 1 and 2 deal exclusively with pure components, which form a necessary prerequisite to the estimation of mixture properties. Three density regions are identified: the low density zone near atmospheric pressure, the moderate density zone, corresponding to the region for which a virial equation of state including the third virial coefficient is adequate, and a high density region corresponding to still higher densities. Figures 5-8 present corresponding algorithms for viscosity and thermal conductivity of liquids. Figures 5 and 6 deal only with pure components, whereas figures 7 and 8 give a similar chart for the liquid mixtures.

5. SUMMARY

Algorithms have been presented for the selection of the most appropriate route to the extimation of the transport properties of fluids. They have been developed with respect to a well defined philosophy which serves to identify the reliability and desirability of the use of particular types of scheme. It has been argued that the basis of the most successful correlation scheme indicates the direction of future experimental work on the transport properties of fluids.

One of us (CANC) acknowledges the leave of absence from Instituto Superior Tecnico, Lisbon and the financial support from INVOTAN, Lisbon, Portugal.

TABLE I

Sources of viscosity data for the gaseous phase (Typical claimed accuracy quoted in parenthesis)

M = Monatomic, NP = Non Polar Polyatomic, P = Polar Polyatomic

PURE COMPONENT		EXPERIMENTAL	PREDICTION CLASS I	ESTIMATION		
				Semi-empirical CLASS II	Semi-empirical CLASS III	Empirical CLASS IV
LOW DENSITY	M	Oscillating disc (23,24) (0.1-0.3%; 300-900K) Capillary flow (29) (1.5%:1000-1600K)	Chapman-Enskog theory and extended law of corresponding states (3,4,10) (0.3%)	Chapman-Enskog theory and Lennard-Jones (12-6) potential parameters by estimation (40) (5-20%)	———	———
	NP				———	———
	P		———	Mason and Monchick (15) (5%)	———	———
MODERATE DENSITY	M	Oscillating disc (23,24) Capillary flow (25) same accuracy as for low density	———	Enskog theory for dense hard sphere fluids (27,28) (2-3%)	Extended law of corresponding states (29) (0.5%)	Method of Jossi et al (30) (2-10%)
	NP		———			
	P				———	Method of Stiel and Thodos (31)
HIGH DENSITY	M	Capillary flow (26) (2%)	———	———	———	(2-10%)
	NP					
	P					

TABLE I (Cont'd)

Sources of viscosity data for the gaseous phase (Typical claimed accuracy quoted in parenthesis)

GASEOUS MIXTURES		EXPERIMENTAL	PREDICTION CLASS I	ESTIMATION		
				Semi-empirical CLASS II	Semi-empirical CLASS III	Empirical CLASS IV
LOW DENSITY	M-M M-NP NP-NP	Oscillating disc (5,23) (0.1-0.3%; 300-800K) Capillary flow (25) (1.5%:1000-1600K)	Chapman-Enskog theory with extended law of corresponding states (3,5,10) (0.3%)	—	Sutherland equation (32) with coefficients given by Wilke (33) (2-3%)	—
	P-P		—	Mason and Monchick (15 (5%)	Sutherland equation coefficients given by Brokaw (34) (3-4%)	—
MODERATE DENSITY	M-M M-NP NP-NP	Oscillating disc (23)	—	Enskog theory for dense hard sphere fluids (27,48) (2-4%)	Hanley (37 (3%-?) Extended law of corresponding states (29,35) (1%)	Method of Dean & Stiel (36) (3-4%)
	P-P		—	—	—	—
HIGH DENSITY	M-NP-P	Capillary flow (26) (2%)	—	—	—	Method of Dean & Stiel (36) (3-4%) (not for P-P)

TABLE II

Sources of thermal conductivity data for the gaseous phase (typical claimed accuracy quoted in parenthesis)

M = Monatomic, NP = Non Polar Polyatomic, P = Polar Polyatomic

PURE GAS		EXPERIMENTAL	PREDICTION CLASS I	ESTIMATION		
				Semi-empirical CLASS II	Semi-empirical CLASS III	Empirical CLASS IV
LOW DENSITY	M	Transient hot-wire technique (9,38) (0.2%)	Chapman-Enskog theory with empirical law of corresponding states (3,10) (0.3%)	—	—	—
	NP		—	Mason and Monchick (15,32,40) (3%)	—	—
	P		—		—	—
MODERATE DENSITY	M	Transient hot-wire technique (9,38) (0.2%) Parallel plates (39) (1-2%)	—	Enskog theory for dense hard spheres fluid (27) (1%)	Extended law of corresponding states (29,35) (1%) Hanley (42) (3%)	—
	NP		—	—		—
	P		—	—	—	—
HIGH DENSITY	M	Transient hot-wire technique (9,38) (0.2%) Parallel plates (39) (2%)	—	Enskog theory for dense hard spheres (27) (5% until $0.7\rho_c$)	—	Stiel and Thodos method (43) (10-20%)
	NP		—	—	—	
	P		—	—	—	—

TABLE II (Cont'd)

Sources of thermal conductivity data for the gaseous phase (typical claimed accuracy in parenthesis)

GASEOUS MIXTURES		EXPERIMENTAL	PREDICTION CLASS I	ESTIMATION		
				Semi-empirical CLASS II	Semi-empirical CLASS III	Empirical CLASS IV
LOW DENSITY	M-M	Transient hot-wire method (44) (0.29%)	Chapman-Enskog theory with empirical law of corresponding states (6) (10%)		Wassiljewa equation with coefficients given by Mason and Saxena (46) 1% or by Lindsay and Bromley (47) (1-3%)	——
	M-NP	Steady state Concentric cylinders (45)	——	Mason and Monchick (15,17) (5%)		——
	NP-NP		——			
	P-P		——		Lindsay and Bromley (47) (5-10%)	——
MODERATE DENSITY	M-M	Transient hot-wire method (44) (0.2%)	——	Enskog theory for dense hard spheres fluids (27,48) (2-5%)	Extended law of corresponding states (29,35) (1%) Hanley (42) (3%)	Stiel and Thodos (5-20%)
	M-NP		——	——		
	NP-NP					
	P-P		——	——	——	——
HIGH DENSITY	M-NP-P	Transient hot-wire method (44) (0.2%)	——	——	——	Stiel and Thodos (43) (10-20%) (not for P-P)

TABLE III

Sources of viscosity data for the liquid phase (typical claimed accuracy quoted in parenthesis)

T_c represents the critical temperature, ρ_c the critical density.

	CONDITIONS	EXPERIMENTAL	ESTIMATION	
			Semi-empirical CLASS III	Semi-empirical CLASS IV
PURE LIQUID	Saturated liquids at low temperature ($T/T_c < 0.80$)	Capillary flow (55) (0.1%)	Rough hard spheres theory (20,49,50) (2%)	Van Velzen et al (52) (5-15%)
	Saturated liquids at high temperature ($T/T_c > 0.80$)		Rough hard spheres theory (20,49) (2-3%) ($\rho > 2\rho_c$)	Letsou and Stiel (53) (3% until $T_r \simeq 0.92$)
	High pressure Low temperature	Falling body viscometer (56)(2%) Quartz crystal Viscometer (65)(2%)	Rough hard spheres theory (20,49,51) (3%)	—
MIXTURES	Low pressure Low temperature	—	Hanley (37) (3%)	McAllister (54) (≥ 20%)

TABLE IV

Sources of thermal conductivity data for the liquid phase (typical claimed accuracy quoted in parenthesis)

T_c represents the critical temperature.

	CONDITIONS	EXPERIMENTAL	ESTIMATION	
			Semi-empirical CLASS III	Semi-empirical CLASS IV
PURE LIQUID	Saturated liquids $(T/T_c) < 0.80$	Transient hot-wire Technique (49, 57, 58) (0.6%)	Rough-hard sphere theory (20,59) - only monatomic liquids (2%)	Robbins & Kingsea (60) - organic liquids only (≤ 5%)
	Saturated liquids at high temperature $(T/T_c) > 0.80$		Rough-hard sphere theory (20, 59) - only for monatomic liquids ($\rho > 2\rho_c$) (≥ 3%)	High pressure gas phase estimation techniques (see Table II) (20%)
	High pressure Low temperature	Transient hot-wire Technique (56) (0.6-1%)	Rough-hard spheres theory - only monatomic (20-59) (unknown)	Missenard (61) (> 5%)
MIXTURES	Any	Extention possible of same technique	Murad and Gubbins (62) (2-3%) (n-alkane mixtures only)	NEL equation (63) Binary mixtures only (49%) Li method (64) (3-4%)

Figure 1 - Algorithm for the prediction or estimation of the viscosity of pure gases

Figure 2 - Algorithm for the prediction or estimation of the thermal conductivity of pure gases

Figure 3 - Algorithm for the prediction or estimation of the viscosity of gaseous mixtures

Figure 4 - Algorithm for the prediction or estimation of the thermal conductivity of gaseous mixtures

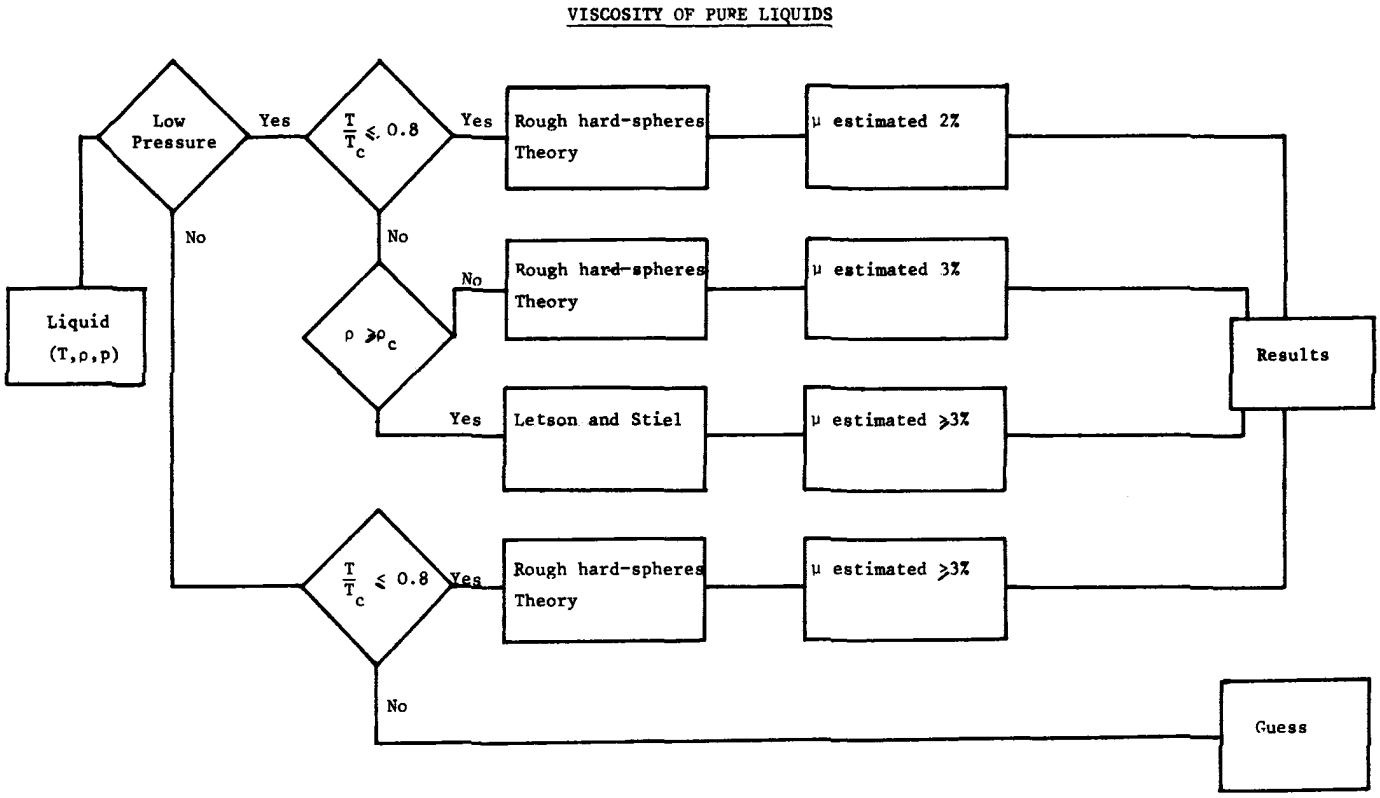

Figure 5 - Algorithm for the estimation of viscosity of pure liquids

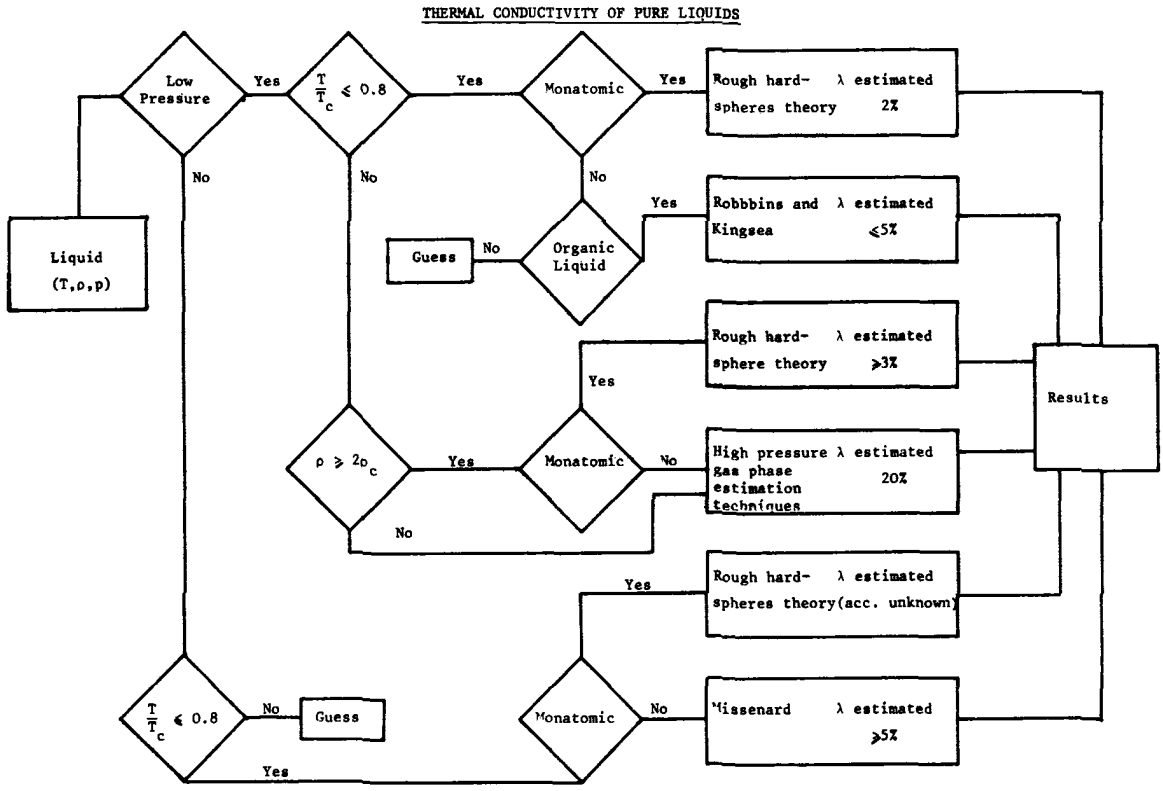

Figure 6 - Algorithm for the estimation of thermal conductivity of pure liquids

VISCOSITY OF LIQUID MIXTURES

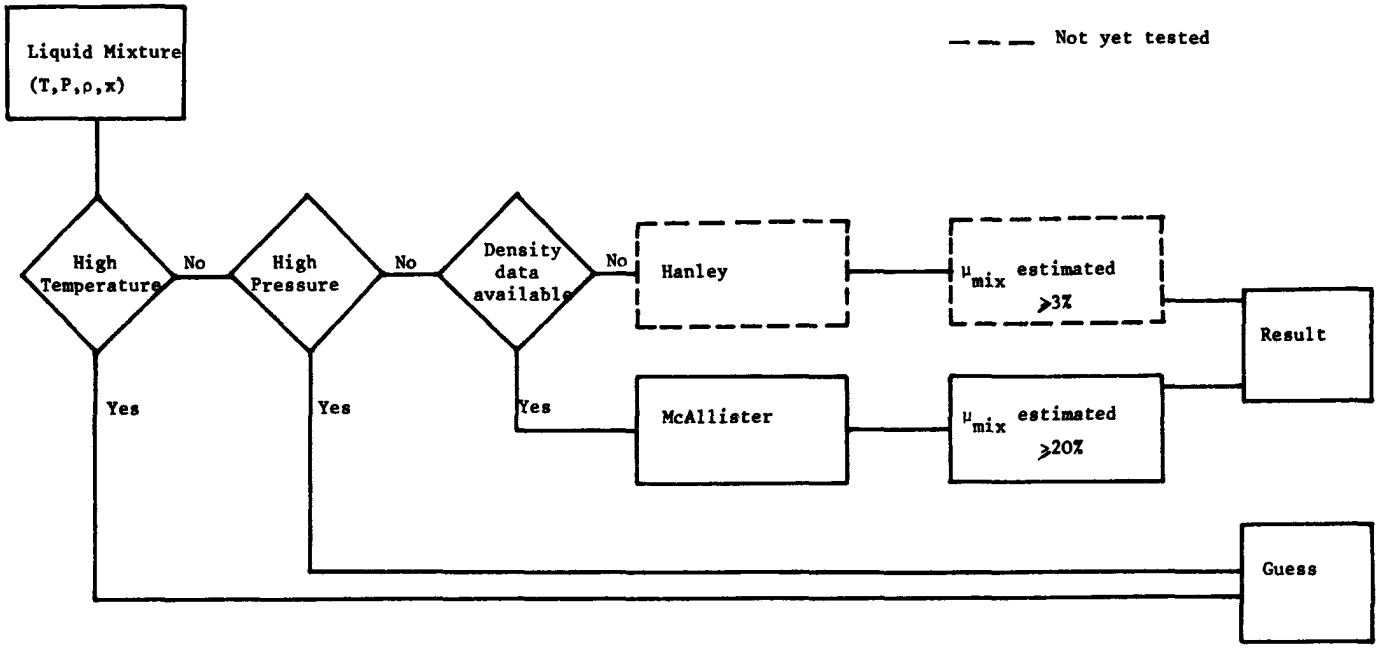

Figure 7 - Algorithm for the estimation of viscosity of liquid mixtures

THERMAL CONDUCTIVITY OF LIQUID MIXTURES

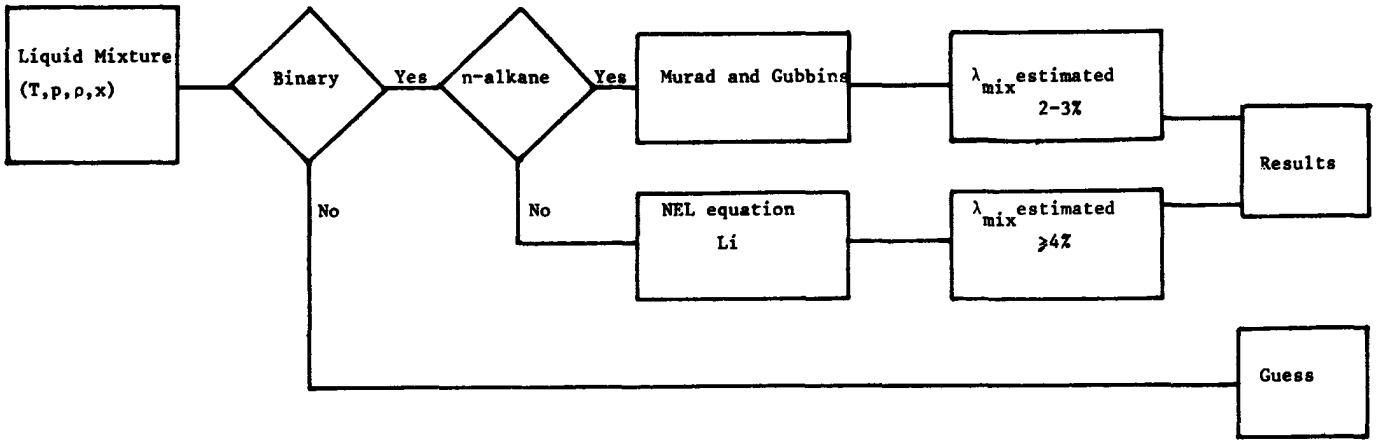

Figure 8 - Algorithm for the estimation of thermal conductivity of liquid mixtures

6. REFERENCES

1. Assael, M.J., Nieto De Castro, C.A., Wakeham, W.A., Proceedings of the CHEMPOR '78, Braga, Portugal 1978 - following paper
2. Boltzmann, L. Wien. Sitz., 66, 275 (1872)
3. Chapman, S., Cowling, J.G., "The Mathematical Theory of Non-Uniform Gases", 3rd ed., Cambridge University Press (1970)
4. Kestin, J., Ro, S.T., Wakeham, W.A., J. Chem. Phys., 56, 4114 (1972)
5. Kestin, J., Kalifa, H.E., Ro, S.T., Wakeham, W. A., Physica 88A, 242 (1977)
6. Maitland, G.C., Smith, E.B., J. Chem. Eng. Data, 17, 150 (1972)
7. Maitland, G.C., Wakeham, W.A., Mol. Phys. (in press) (1978)
8. Maitland, G.C., Wakeham, W.A., Mol. Phys. (in press) (1978)
9. Groot, J.J. de, Kestin, J., Sookiazian, H., Physica 75, 454 (1974)
10. Kestin, J., Ro, S.T., Wakeham, W.A., Physica 58, 165 (1972)
11. Kestin, J., Khalifa, H.E., Wakeham, W.A., J. Chem. Phys. 65, 5186, (1976)
12. Kestin, J., Khalifa, H.E., Wakeham, W.A., J. Chem. Phys. 66, 1132 (1977)
13. Kestin, J., Khalifa, H.E., Wakeham, W.A., J. Chem. Eng. Data, 23, 80, (1978)
14. Wang-Chang, C.S., Uhlenbeck, G.E., Univ. Michigan Report CM68 (1951)
15. Mason, E.A., Monchick, L., J. Chem. Phys. 36 1622 (1962)
16. Monchick, L., Pereira, A.N.G., Mason, E.A., J.Chem. Phys. 42, 3241 (1965)
17. Monchick, L., Mason, E.A., J. Chem. Phys. 35 1676 (1961)
18. Bearman, R.J., Kirkwood, J.G., J. Chem. Phys. 28, 136 (1958)
19. Eyring, H., Jhon, M.S., "Significant Liquid Structures", Wiley, New York (1969)
20. Dymond, J.H., Physica 75, 100 (1974)
21. Rice, S.A., Alnatt, A.R., J. Chem. Phys. 34, 2144 (1961); ib. 2156 (1961)
22. Hildebrand, J.H., Science 174, 490 (1971)
23. Dippipo, R., Kestin, J., Withelaw, J.H. Physica 32, 2064 (1966)
24. Kestin, J., LeidenFrost, W.,Physica 25, 1033 (1959)
25. Dawe, R.A., Smith, E.B., J. Chem. Phys. 52, 693 (1970)
26. Michels, A., Schipper, A.C.J., Rintoul, W.H., Physica 19, 1011 (1953)
27. Reed, T.M., Gubbins, K.E., "Applied Statistical Mechanics" McGraw-Hill, New York (1973)
28. Frich, H.l., McLaughlin, E., J. Chem. Phys. 55, 3706 (1971)
29. Kestin, J., Mason, E.A., AIP Conference Proceedings, 11, 137 (1973)
30. Jossi, J.A., Stiel, L.I., Thodos, G., AIChE J. 8, 59 (1962)
31. Stiel, L.I., Thodos, G., AIChE J. 10, 275 (1964)
32. Reid, R.C., Prausnitz, J.M., Sherwood, T.K., "The Properties of Gases and Liquids", McGraw-Hill, New York (1977)
33. Wilke, C.R., J. Chem. Phys. 18, 517 (1950)
34. Brokaw, R.S., Ind. Eng. Chem. Process. Des. Dev. 8, 240 (1969)
35. Wakeham, W.A., Kestin, J., Mason, E.A., Sandler, S.I., J. Chem. Phys. 57, 295 (1972)
36. Dean, D.E. Stiel, L.I., AIChE J. 11, 526 (1965)
37. Hanley, H.J.N., Cryogenics 16, 643 (1976)
38. Groot, J.J. de, Kestin, J., Sookiazian, H., Wakeham, W.A., Physica (in press) (1978)
39. Michels, A., Sengers, J.V., Van Der Gulik, P.S., Physica 28, 120 (1962)
40. Silva Joao, A.F., Melo Arruda, A.M., Nieto De Castro, C.A., Tecnica (AEIST) - Lisbon (in press)
41. Roy, D., Thodos, G., Ind. Eng. Chem. Fund. 7, 529 (1968) ib. 9, 71 (1970)
42. Hanley, H.J.H., Proceedings of the 7th Symposium on the use of Physical Properties, NBS., Washington (1977)
43. Stiel, L.I., Thodos, G. AIChE J. 10, 26 (1964)
44. Sookiazian, H., PhD Thesis, Brown University, Providence (1977)
45. Saxena, S.C., Gupta, G.P., Proc. 5th Symposium on thermo-physical Properties, Newton, Massa. (1970)
46. Mason, E.A., Saxena, S.C., Phys. Fluids. 1, 361 (1958)
47. Lindsay, A.L., Bromley, L.A., Ind. Eng. Chem. Fund. 42, 1508 (1950)
48. Kandiyoti, R. McLaughlin, E., Mol. Phys. 17, 643 (1969)
49. Dymond, J.H., Chem. Phys. 17, 101 (1976)
50. Nieto De Castro, C.A., PhD Thesis I.S.T., Lisbon (1977)
51. Parkhurst Jr. H.J., Jonas, J., J. Chem. Phys. 63, 2705 (1975)
52. Van Velzen, D., Cardozo, R.L., Langenkamp, H., Ind. Eng. Chem. Fund. 11, 20 (1972)
53. Letsou, A., Stiel, L.I., AIChE J. 19, 409 (1973)
54. McAllister, R.A., AIChE J. 6, 427 (1960)
55. Goncalves, F.A., PhD Thesis, Fac. Ciencias Lisbon (1977)
56. Dickinson, E., J. Phys. Chem. 81, 2108 (1977)
57. Nieto De Castro, C.A., Calado, J.C.G., Wakeham, W.A., Dix, M., J. Phys. E, Scientific Inst. 9, 1073 (1976)
58. Nieto De Castro, C.A., Calado, J.C.G., Wakeham, W.A., Proc. 7th Symposium on Thermophysical Properties, NBS Washington (1977)
59. Dymond, J.H., Proceedings of the 6th Symposium on Thermophysical Properties, Georgia (1973)
60. Robbins, L.A., Kingrea, C.L., Hydroc. Proc. Pet. Ref. 41, 133 (1962)
61. Missenard, A. Rev. Gen. Termique, 101, 649 (1970)
62. Murad, S., Gubbins, K.E., Chem. Eng. Sci. 32, 499 (1977)
63. Jamieson, D.T., Irving, J.B., 13th International Thermal Conductivity Conference, Missouri (1973)
64. Li, C.C., AIChE J. 22, 927 (1976)
65. Haynes, W.M., Physica 67, 440 (1973)

THE ESTIMATION OF PHYSICAL PROPERTIES OF FLUIDS
PART II. THE ECONOMIC ADVANTAGES OF ACCURATE TRANSPORT PROPERTY DATA

M. J. Assael
C. A. Nieto De Castro
W. A. Wakeham

Imperial College, London, England

ABSTRACT

In a companion paper a hierarchy of procedures for the estimation of the transport properties of fluids was established. It was shown that at present, for many fluids, the transport properties must be estimated by methods which depart considerably from the ideal and that therefore the data generated are burdened with large uncertainties. In this paper the technical and economic consequences of these uncertainties to process plant design and operation are assessed. This assignment is carried out by means of specific examples of heat exchanger design frequently encountered.

It is shown that the uncertainties in the transport coefficients which result from commonly used estimation procedures have a significant effect upon the overall technical design of heat exchange equipment. In turn these effects contribute to the necessary capital expenditure on the items of plant. It is demonstrated that such expenditure would be considerably reduced by more reliable estimation procedures based upon accurate experimental data for the transport coefficients of fluids. This improvement could be achieved by an expenditure amounting to only a fraction of the current wastage of resources.

1. INTRODUCTION

In a companion paper (1) the techniques available for the estimation of fluid properties were discussed, and a means for selecting the best procedure for a particular fluid system described. It was then shown that at one extreme the viscosity of multicomponent mixtures of dilute non-polar gases could be predicted until an uncertainty of ±0.5%, whereas at the other extreme the thermal conductivity of a liquid mixture could be estimated to at best ±20%. This range of accuracy corresponds to the extent to which the estimation procedures rely on rigorous theory and accurate experiment.

It has frequently been noted by workers in the field of transport properties of fluids that a knowledge of these properties is significant for process plant design. However, there seems to have been no discussion of how significant accurate values of these properties are in quantitative technical and economic terms. This paper is devoted to a study of this type in order to illustrate the need for improved estimation techniques and more accurate experimental measurements.

In order to carry out this programme we have chosen to study the effect of fluid transport property uncertainties upon the design of heat exchange equipment. This is because on the one hand such equipment is present in nearly every installation in the Chemical Industry and on the other hand because its design is largely determined by the fluid transport properties. Two types of heat exchanger have been selected for study, first a shell and tube exchanger and secondly a simple double pipe exchanger. To encompass the full range of fluid states in our discussion we have also considered three types of fluid system: those involving liquid-liquid, liquid-gas and gas-gas heat exchange.

2.1 THE METHODOLOGY

As the introduction has indicated our purpose in this paper is to examine the consequences of uncertainties in fluid transport properties for heat exchanger design. Thus, the aim of our calculations will be to evaluate the changes in the design parameters of a heat exchanger which results solely from changes made in the transport coefficients of the fluids involved in the process. Evidently, the complete design of heat exchangers to suit every possible circumstance is beyond the scope of this work. Furthermore, such a series of calculations is not necessary in order to establish the importance of an accurate knowledge of the transport coefficients of fluids. Consequently, we prefer to adopt a simpler approach which retains the essentials of the argument while providing great simplification.

We begin by reducing the number of parameters necessary to define the design of the heat exchanger, to one. This is made possible by the selection of a particular type of exchanger, with a prescribed number of tubes of fixed radial dimensions and geometrical arrangement within a shell of known geometry. If the duty of the exchanger is then fixed by the external constraints of a particular process the remaining variables which characterize the exchanger are its heat transfer area (or equi-

valently its length) and the pressure drop across the fluid ducts. Because the pressure drop across the exchanger is usually not a major factor in its design we see that in these circumstances the heat transfer area becomes the sole charateristic of the exchanger and that it is this variable alone which will reflect changes in the design arising from changes in the transport coefficients of the process streams. The reduction of the number of parameters necessary to define the design in this way has the added advantage that the economic consequences of changes in the design can be readily estimated.

A second simplification is afforded by the adoption of a standard methodology for the evaluation of the heat exchange area. Since any reasonable design technique incorporates the physical properties of the fluid streams into correlations for heat transfer coefficients we are free to use any one of then. In accord with the aims of this paper we adopt one of the simplest.

Thus, for the heat transfer coefficient on the inside of heat exchanger tubes, referred to as the inside tube area, h_i, we employ the correlation due to Sieder and Tate (2)

$$\frac{h_i D_i}{\lambda} = 0.027 Re^{0.8} Pr^{1/3} \left(\frac{\mu}{\mu_w}\right)^{0.14} \qquad (1)$$

where the Reynolds Number (2)

$$Re = \frac{D_i G}{\eta}$$

and the Prandtl number (3)

$$Pr = C_p \eta / \lambda$$

Here, D_i is the internal diameter of the tubes λ the thermal conductivity of the fluid, μ its viscosity and C_p its heat capacity, all evaluated at the mean bulk temperature of the fluid. G represents the mass flux in the heat exchange tubes and μ_w the viscosity at the temperature of the wall. The correlation of equation 1 is applicable to the turbulent flow regime only (Re > 2100) which corresponds to the conditions of our studies.

The heat transfer coefficient on the steel side of the heat exchanger tubes referred to the outside tube area, h_o, is given by the correlation (3).

$$\frac{h_o D_e}{\lambda} = 0.36 \; Re^{0.55} \; Pr^{1/3} \left(\frac{\mu}{\mu_w}\right)^{0.14} \qquad (4)$$

which is again valid for Re > 2100.
Here, D_e is the equivalent diameter for the shell (3) and the remaining quantities have already been defined.

The overall heat transfer coefficient, U_o, referred to the outside tube area is then calculated from the equation

$$\frac{1}{U_o} = \frac{D_o}{h_i D_i} + \frac{1}{h_o} + R$$

where D_o is the outside tube diameter and R represents the combined resistance of the tube wall and any scale.

Finally, the heat transfer are, A_o, based on the external surface area of the tubes is obtained from the prescribed dury of the exchanger, Q, according to the equation

$$Q = U_o A_o (\Delta T)_{\ell m} \qquad (6)$$

where $(\Delta T)_{\ell m}$ is the corrected logarithm mean temperature difference for the precess streams (3).

Equation 1 to 6 demonstrate how the transport properties of the fluids in the heat exchanger will influence the calculated heat transfer area and so the length of the heat exchanger. Each film heat transfer coefficient depends upon the transport properties raised to fractional powers. It is clear that it is the themal conductivity of the fluids which provides the major factor in the determination of the heat transfer area. It is noteworthy our previous paper (1) has demonstrated that it is the transport property which is the more difficult to estimate accurately.

2.2 THE HEAT EXCHANGERS

In order to provide meaningful data for the effect of fluid property uncertainties on heat exchanger design we have chosen to study four practical examples. Although the study is therefore not exhaustive the results may be regarded as typical of those which would be obtained for other heat exchangers of the same type. Sufficient detail of each exchanger is given below to identify the nature of the problem. A complete specification of each problem is unnecessary for the purposes of this paper.

Case 1

In the first case an exchanger is designed to cool an efficient fraction resulting from a crude oil distillation column by means of fresh feed of crude oil from storage. The fluid flow rates and temperatures and thereby the duty of the exchanger have been fixed with reference to a practical solution. The heat exchanger is prescribed to be of the baffled shell and tube type having one shell pass and four tube passes and containing 158 tubes of external diameter 25 mm and wall thickness 2.4 mm arranged in a square configuration. This heat exchanger therefore represents an example of one applied to liquid-liquid heat exchange.

Case 2

The second exchanger exemplifies a situation involving gas-liquid heat exchange. Dry ammonia from a compressor is cooled with water before passage to a reactor. Again the fluid flow rates, temperatures and the duty have been determined from industrial practice. The exchanger chosen is of the baffled shell and tube type involving one shell pass and eight tube passes. The exchanger contains 364 tubes

of 19 mm external wall thickness 1.6 mm mounted in a triangular arrangement.

Case 3

The third exchanger is designed for gas-gas heat transfer. The product stream from a methanol reactor is to be cooled by incoming fresh feed to the reactor, and the duty of the exchanger has again been fixed with reference to a practical application. In this case a shell and tube exchanger involving three shell passes and six tube passes is to be used. The exchanger contains 688 tubes of 25 mm external diameter, wall thickness 2.5 mm mounted in a triangular arrangement.

Case 4

The final example returns again to the situation of liquid-liquid heat exchange but employs instead of a shell tube exchanger a simple double pipe system. Benzene is heated from ambient temperature by a stream of toluene. The duty of the exchanger is fixed by the flow rates and temperatures of the two streams either side of the exchanger. It is presumed that standard single hairpin double pipe units are available of length 6 m with an internal pipe diameter of 35 mm and an external pipe diameter of 87 mm. In this case the design effectively reduces to the determination of the number of such units required to fulfil the desired function.

2.3 THE CALCULATIONS

For each of these four heat exchangers the transport properties of the two fluid streams have first been assigned reasonable reference values obtained from the literature or by extimation. Subsequently the heat transfer area for each exchanger has been evaluated using the methods of section 2.1. To fix our ideas the results are given below:

Case 1 Reference heat transfer area, $(A_o)_r = 63.1 m^2$
Tube length, L = 5 m

Case 2 Reference heat transfer area, $(A_o)_r = 53.5 m^2$
Tube length, L = 2.4 m

Case 3 Reference heat transfer area, $(A_o)_r = 460 m^2$
Tube length, L = 8.4 m

Case 4 Reference heat transfer area, $(A_o)_r = 4.7 m^2$
No. of hairpin units required, N = 3.

It should be emphasized that these values constitute an arbitrary reference for our subsequent calculations, rather than any optimized design.

The next stage in our calculations involves the perturbation of the assumed values for the transport coefficients of the two fluids about the assigned reference values. For each perturbation of either viscosity or the thermal conductivity value of a particular stream the resulting heat transfer area has been evaluated by the methods of section 2.1. The perturbation of each transport property has been carried out within the range corresponding to the likely uncertainty in the data were it generated by the estimation schemes described in our earlier paper (1). The changes in the calculated heat transfer area from the corresponding reference area have then been determined as functions of the changes in the transport coefficients, for each of the exchangers described above. Such calculations therefore lead to a determination of the extent to which each heat exchanger may be over or under - designed as a result of uncertainties in the appropriate transport coefficients.

For the purposes of these calculations values of the wall resistance to heat transfer have been obtained from standard sources (3) and maintained constant throughout.

3. THE RESULTS

Since the gross features of the results of our calculations are the same among the four heat exchangers we shall discuss only one in detail. The graphical presentation of the results for the other three examples can then be interpreted in a similar way.

Figure 1 contains plots of the deviation of the calculated heat transfer coefficients, $(h)_c$ from that of the reference conditions, $(h)_r$ for both sides of the shell and tube heat exchanger of case 1. In these diagrams the change in the thermal conductivity of the appropriate fluid is plotted along the abscissa, whereas the change in the viscosity is shown as a parameter of the curves. The changes in the properties are expressed as a percentage of the reference value. We note from these diagrams first that the inside film heat transfer coefficient is much more markedly affected by changes in the thermal conductivity of the fluid than is the outside film heat transfer coefficient. Furthermore, for both inside and outside heat transfer coefficients it can be seen that the effect of changes in the viscosity of the fluid have smaller effect than the changes in its thermal conductivity as is to be expected from the analysis of section 2.1.

Figure 2 contains a plot of the deviations of the calculated area of the heat exchanger, $(A_o)_c$ from that of the reference conditions $(A_o)_r$ for the exchanger of Case 1 as functions of the changes in the two film heat transfer coefficients. In this figure the change in the inside film heat transfer coefficient from the reference conditions is plotted along the abscissa and the change in the outside film heat transfer coefficient is given as a parameter to the curves.

Figures 1 and 2 together then allow us to determine the variation in the design area of the heat exchanger as a result of variation in the transport properties of the two fluids. As an example of the use of these figures we take the situation when the viscosity of the fluid in the shell side of the exchanger exceeds the reference value by 10%, the thermal conductivity is 15% below its reference value and there are identical changes for the transport properties of the fluid in the tubes of the exchanger. Then it follows from figure 1 that the changes in the inside and outside film transfer coefficients are -16% and -13% respectively with regard to the reference

conditions. Figure 2 then shows that the corresponding change in the design heat exchange area amounts to an increase above the reference value of 15%.

We may now relate these calculations directly to the consequences for design of uncertainties in the fluid transport properties. If we suppose that the reference values we have assigned to the transport properties of the fluids represent their true values and that their perturbed values correspond to data generated by an estimation scheme, then the reference heat exchange area corresponds to that which would be adequate to perform the desired function and the values obtained with the perturbed transport properties correspond to the areas deduced from a design study. Thus, for the example considered above we see that owing to the uncertainties in the transport properties of the fluid we have overestimated the heat exchanger area by 15%. It may be seen from the combination of figures 1 and 2 that it is also possible to overestimate the area of the exchanger by as much as 30%.

The presentation of our results for the heat exchanger of Case 2 is contained in Figures 3 and 4. In order to simulate one situation where the properties of one fluid are known with far greater accuracy than these of the second fluid we have considered here that the uncertainty in the transport properties of water is negligible. Thus the only changes in the design heat exchange area arises from the perturbations in the properties of the second fluid, gaseous ammonia. Even in this case the possible uncertainties in the design heat exchange area can range from -15 to +30% around the reference area.

For Case 3 the results of our calculations are displayed in figures 5 and 6 whereas for the simple double pipe exchanger of Case 4, figures 7 and 8 contain the data. For each situation the results are similar. It is evident, therefore, that the errors in the evaluated heat exchange area arising from typical uncertainties in the transport coefficients can amount to as much as ±25% in all four heat exchangers studies.

DISCUSSION

In our earlier paper (1) it was shown that for many fluids or fluid mixtures it is at present impossible to extimate their transport properties with an error less than 20%. In the preceeding section we have shown that because of such uncertainties alone it is possible to over or underestimate the heat transfer area for a heat exchanger to fulfil a particular need by as much as 25%. Of course, it must also be recognised that any methodology for heat exchanger design such as that given in section 2.1 has an inherent uncertainty, by virtue of its empirical nature. Generally, this latter uncertainty is accommodated into a practical design by increasing the design heat transfer area by a multiplicative safety factor. The results of our calculations could be interpreted as a demonstration that the safety factor should be increased to allow for the effect of the uncertainty in the fluid transport properties.

If this argument is pursued then merely because of the uncertainty in fluid transport properties heat exchangers should be manufactured an additional 25% larger than may be necessary in order to ensure that they fulfil their designated function. Table 1 illustrates the economic consequences of this over-design for heat exchangers corresponding to types 1, 2 and 3 of section 2.2. In this table we quote current approximate capital costs for an exchanger of each type and the incremental cost resulting from an over-design of 30%. The figures indicate that as a fraction of the total capital expenditure on a particular chemical plant the incremental cost is small. However, if the total extra expenditure is taken over a series of plants and a number of years it represents a considerable extra investment.

An alternative interpretation of the results of our calculations is however possible. If the uncertainties in the estimation of the transport coefficients of fluids could be reduced to a few percent from their present much higher values, then the additional over-design of heat exchange equipment could be similarly reduced. Such a reduction in the uncertainties could be achieved by a series of accurate measurements on carefully chosen systems, supported by the development of fundamental theories and subsequently estimation schemes (1). The incremental costs detailed in Table 1 which result from over-design of only three items of plant equipment would provide a significant contribution to such a research effort. Furthermore, the savings effected as a result of such a research programme would rapidly justify the initial expenditure.

In summary, research effort in the field of the transport properties of fluids has been shown to have a quantatively important technical and economic role in the optimum design of at least some items of chemical process plant.

Thus, accurate measurements of these properties will be of value not only to the understanding of the fundamental theories of fluids but also for industrial purposes.

ACKNOWLEDGEMENTS

One of us (C.A.N.C.) acknowledges the leave of absence from Instituto Superior Tecnico, Lisbon, and the financial support from INVOTAN, Lisbon, Portugal.

TABLE I

Reference, and incremental costs for heat exchangers.

Heat Exchanger	Approximate, current capital cost for reference conditions, £	Approximate, incremental capital cost for 30% increase in heat exchanger area, £
Case 1	10,000	2,800
Case 2	7,500	2,100
Case 3	60,000	16,800

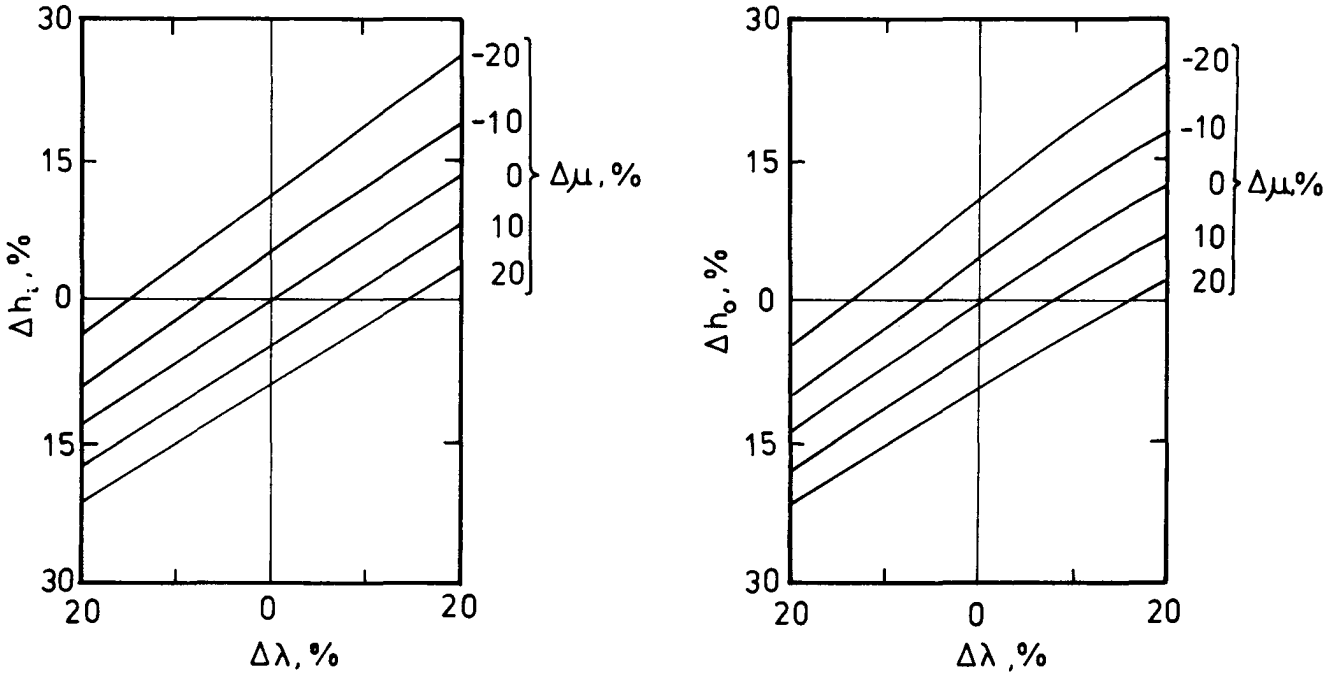

Figure 1 - The influence of the fluid transport properties upon the film heat transfer coefficients for Heat Exchanger 1.

a) The inside heat transfer coefficient.
b) The inside heat transfer coefficient.

$$\Delta h_i = \left\{ \frac{\{(h_i)_c - (h_i)_r\}}{(h_i)_r} \right\} \times 100$$

$$\Delta h_o = \left\{ \frac{\{(h_o)_c - (h_o)_r\}}{(h_o)_r} \right\} \times 100$$

$$\Delta \mu = \left\{ \frac{\mu - \mu_r}{\mu_r} \right\} \times 100$$

$$\Delta \lambda = \left\{ \frac{\lambda - \lambda_r}{\lambda_r} \right\} \times 100$$

The subscript r denotes reference conditions.

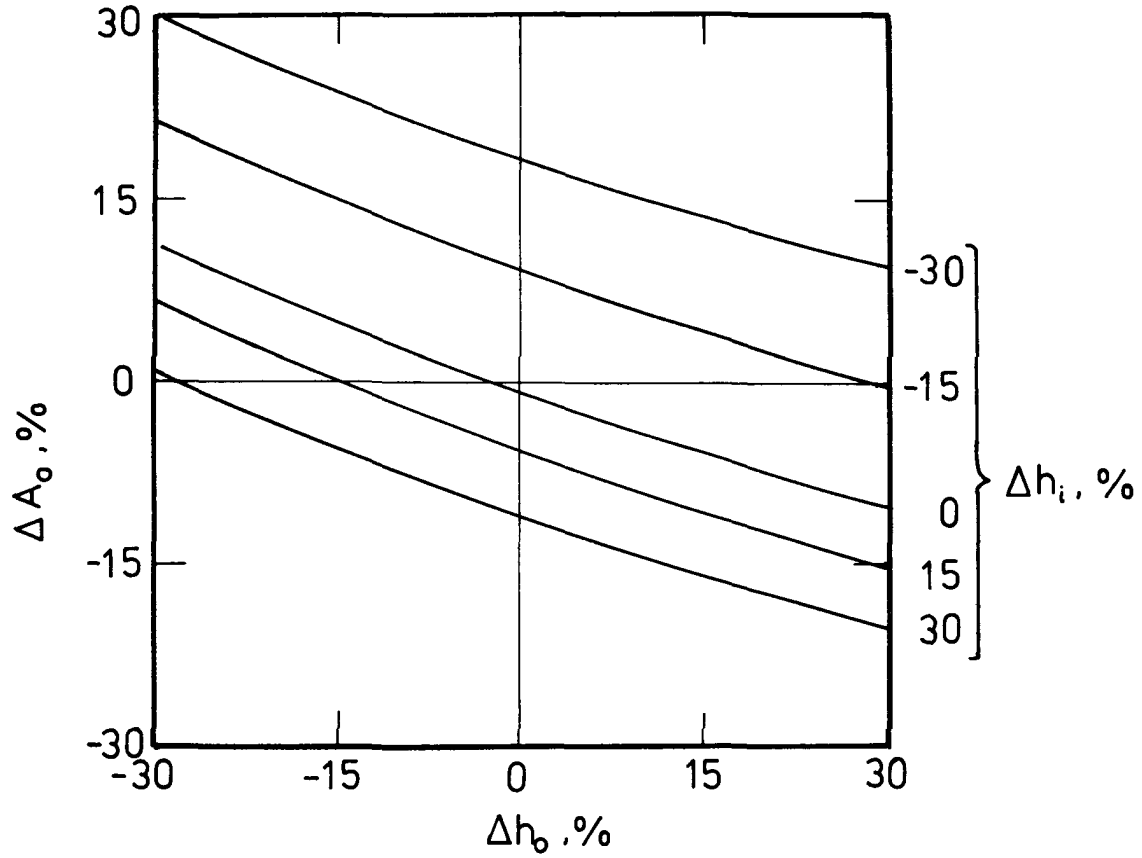

Figure 2 - The influence of the film heat transfer coefficients upon the heat exchange area for heat exchanger 1.

$$\Delta A_o = \left\{ \frac{\{A_o - (A_o)_r\}}{(A_o)_r} \right\} \times 100$$

The remainder of the legend is the same as for Figure 1.

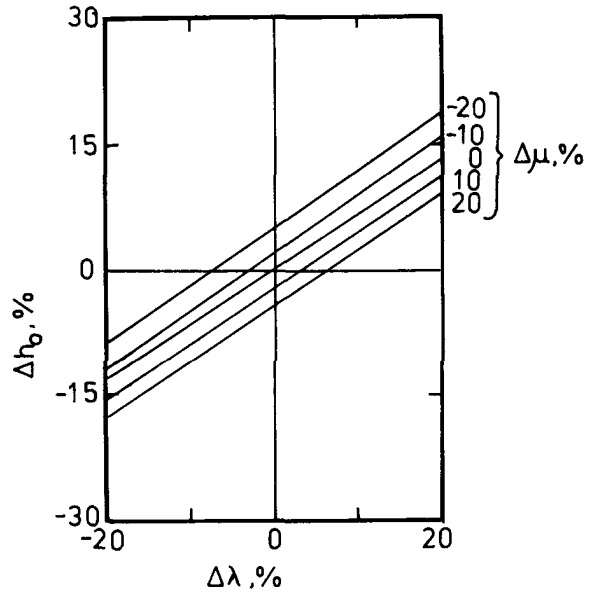

Figure 3 - The influence of the fluid transport coefficients upon the inside film heat transfer coefficient, for heat exchanger 2. The legend is the same as for Figure 1.

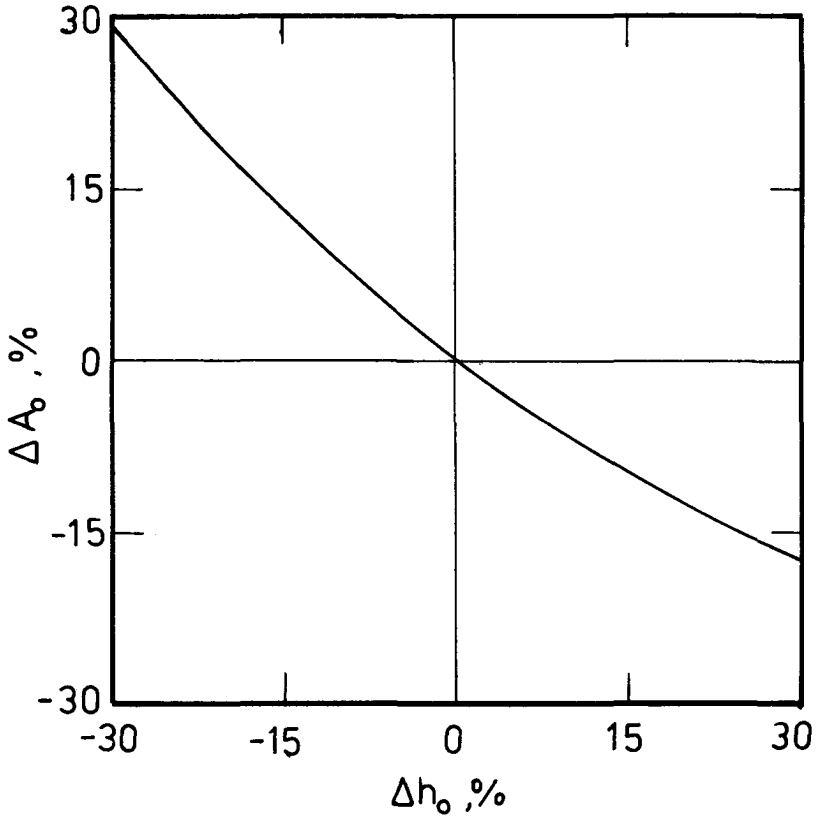

Figure 4 - The influence of the inside film heat transfer coefficient upon the heat exchange area for heat exchanger 2.
The legend is the same as for Figure 2.

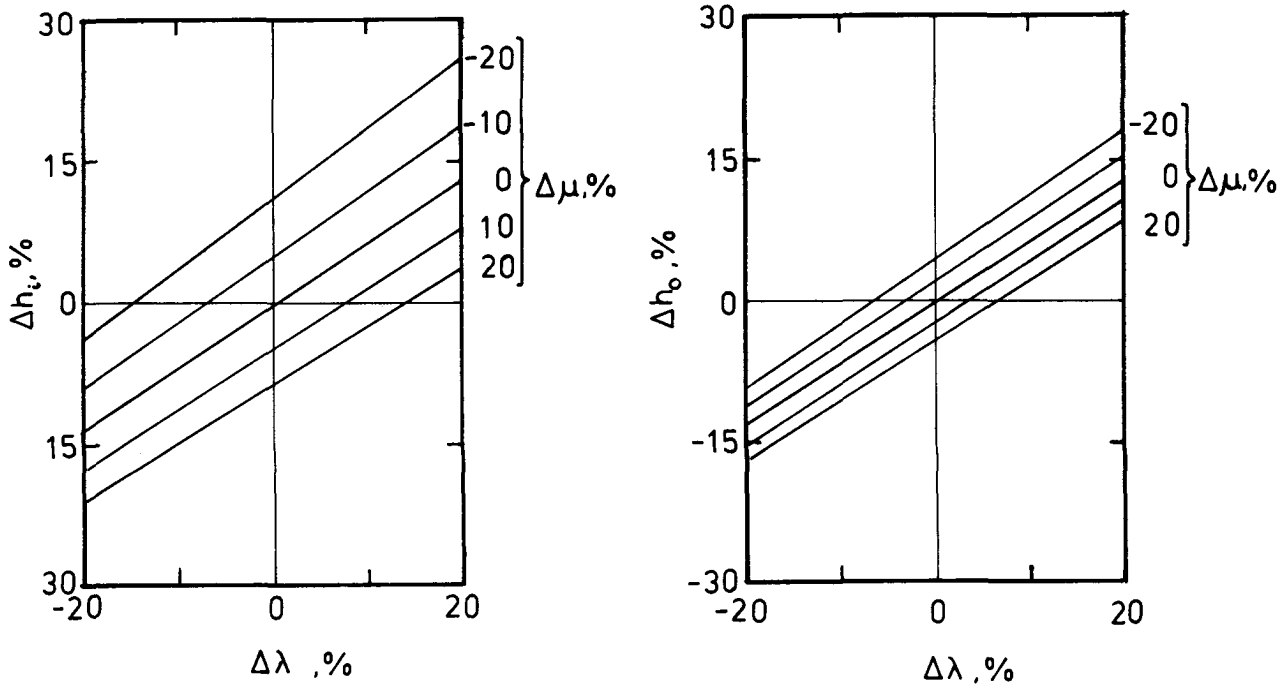

Figure 5 - The influence of the fluid transport coefficients upon the film heat transfer coefficients for heat exchanger 3. The legend is the same as for Figure 1.

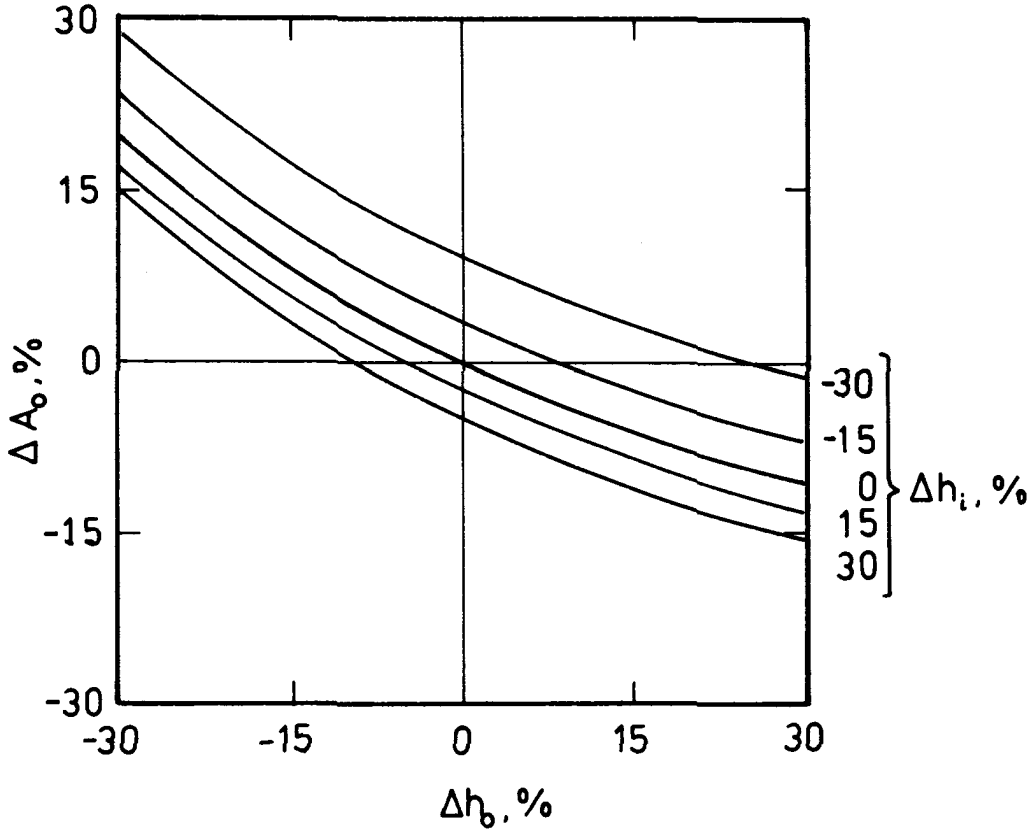

Figure 6 - The influence of the film heat transfer coefficients upon the heat exchange area for heat exchanger 3.
The legend is the same as for Figure 2.

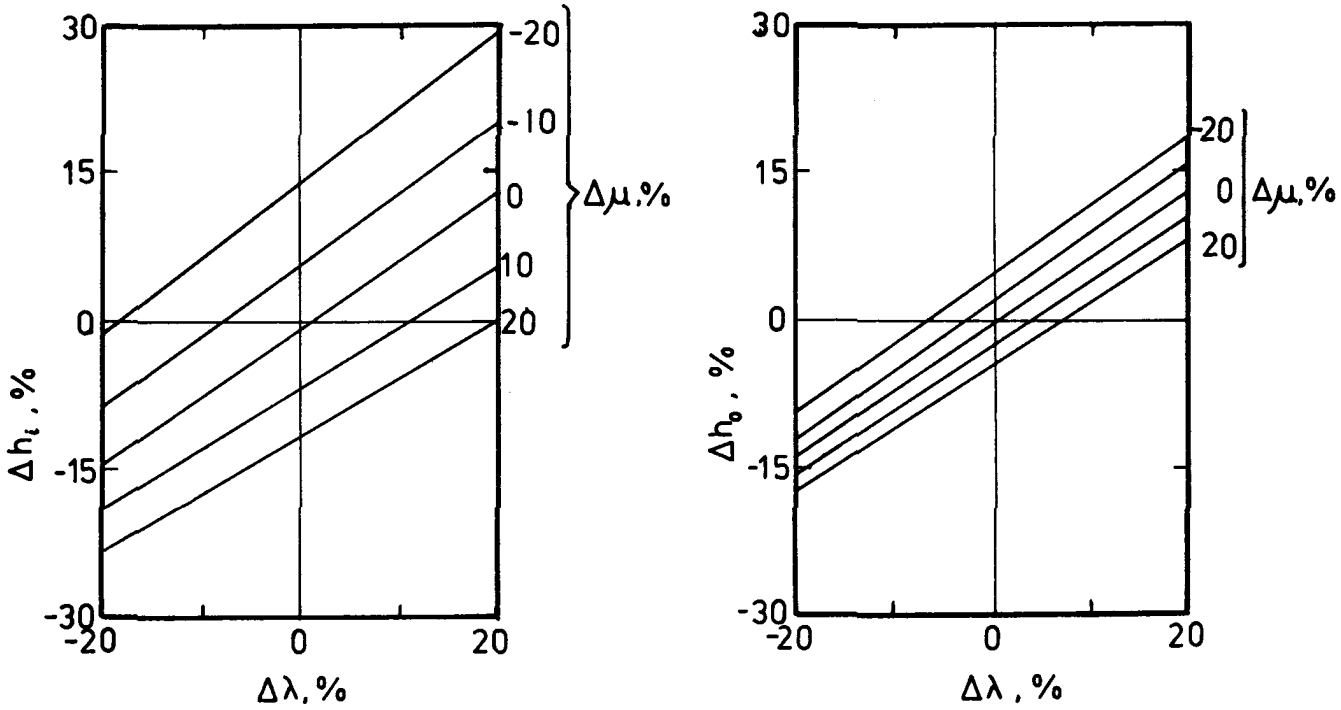

Figure 7 - The influence of the fluid transport coefficients upon the film heat transfer coefficients for heat exchanger 4.
The legend is the same as for Figure 1.

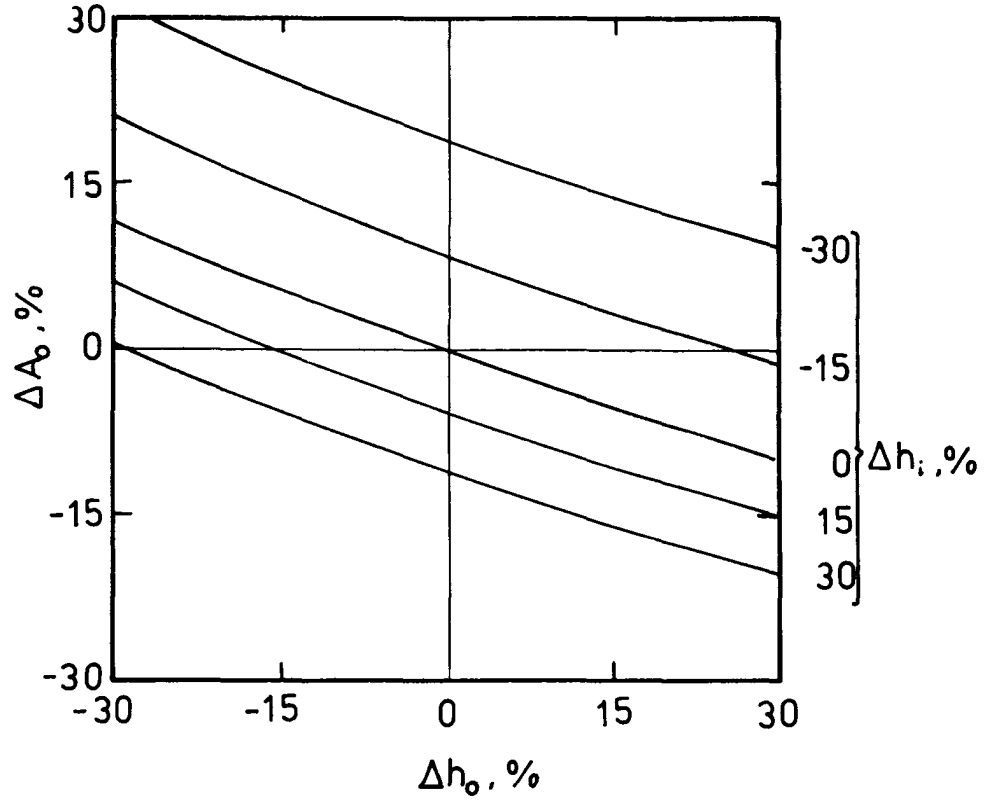

Figure 8 - The influence of the film heat transfer coefficients upon the heat exchange area for heat exchanger 4.
The legend is the same as for Figure 2.

REFERENCES

1. Castro, C.A.N. and Wakeham, W.A., (Proceedings of the CHEMPOR '78, Braga, Portugal 1978 - Preceeding paper)
2. Sieder, E.N. and Tate, G.E., Ind. Eng. Chem. 28, 1429 (1936)
3. Kern, D.Q., Process Heat Transfer, McGraw-Hill New York (1950)

A COMPARISON OF PREDICTED AND MEASURED DISPERSION CHARACTERISTICS IN FIXED AND FLUIDISED BED REACTORS

J. P. Cardoso [1]
A. N. Emery [2]

1 Instituto Superior Técnico, Lisboa
2 University of Birmingham, Birmingham, England

ABSTRACT

A comparison is made between experimental and predicted dispersion characteristics for a pilot plant reactor operating both as a fixed and fluidised bed. Solid lead glass beads are used as support for an enzime catalyst.
Correlations of velocity versus bed voidage for the fluidised bed mode are established and the minimum fluidisation velocity U_{mf} determined.
This study suggests that until more widely applicable correlations are proven the only reliable course is for the investigator to determine dispersion characteristics for himself.

INTRODUCTION

In connection with the modelling of the fixed and fluidised bed modes of a pilot plant reactor we have been considering the applicability of a dispersed plug flow (DPF) model to describe the conversion in the system starch - glucose using immobilised amyloglucosidase.
The DPF model is based on the concept of mixing in an analogous manner to molecular diffusion governed by Fick's law. According to Levenspiel (1) such model may be written as in equation (1) for a first order reaction.

$$\frac{D_v}{vL}\frac{d^2C_S}{dZ^2} - \frac{dC_S}{dZ} - \frac{\chi}{Q}C_S = 0 \qquad (1)$$

The solution of this equation implies the use of a suitable correlation for the dispersion number D_v/vL with flow rate or if such correlation is not available its experimental determination.

In the work here reported experimental determinations of D_v/vL are compared with the D_v/vL values predicted from some correlations available in the literature. Since the solution of these correlations implies, for the fluidised bed mode, the use of fluidisation characteristics, namely U_{mf} and $U = U(\varepsilon)$ relations , the work here reported also deals with their determination.

THEORY

1-Correlations for the dispersion number

The dispersion number $D_v/vL = D_U/UL$ may be used to describe quantitatively the mixing effect in the reactor. The Peclet number $-N_{Pe} = vd_p/D_v$ - is related with the dispersion number by equation (2),

$$D_v/vL = 1/N_{Pe} \cdot d_p/L \qquad (2)$$

Chung and Wen (2) developed a correlation (Equation (3)) for the Peclet number for fixed and fluidised beds

$$\varepsilon N_{Pe}/\chi = 0.20 + 0.011\, N_{Re}^{0.48} \qquad (3)$$

covering the range $0.4 < \varepsilon < 0.8$ and a particle density range up to 8 g/cm^3 .
Hence can be written

$$\frac{D_v}{vL} = \frac{D_U}{UL} = \frac{d_p}{L}\left[\frac{\varepsilon}{(0.20 + 0.011 N_{Re}^{0.48})\chi}\right] \qquad (4)$$

Bruinzel et al (3) propose equation (5) for the dispersion number in fluidised beds.

$$\frac{D_v}{vL} = \frac{D_U}{UL} = \frac{d_p}{L}\,\frac{10^3}{4.3\, N_{Re}^{0.18}\,\varepsilon^{0.82}} \qquad (5)$$

It may be seen that while D_v/vL increases as ε increases in equation (4) it decreases with ε in equation (5). Moreover it may be shown that equation (5) predicts D_v/vL values higher than those given by equation (4) by a factor varying from 300 to 1 when the voidage ε varies from ε_{mf} to 1. This emphasised the need to determine values of D_v/vL in both fixed and fluidised beds to test the DPF model properly.

2-Fluidisation

The phenomenon of fluidisation can be visualised in the ideal dependence of pressure drop on velocity presented in Figure 1 for a bed of solids, though this ideal behaviour is virtually never achieved in practice.

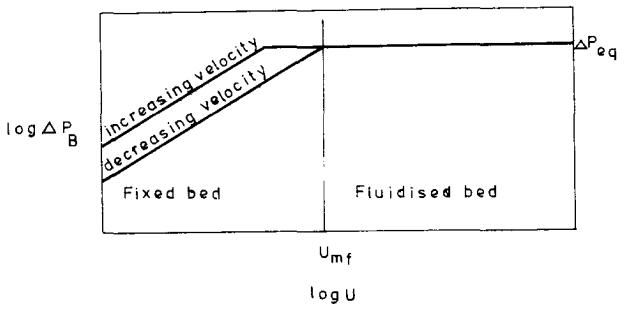

FIGURE 1 -Pressure drop velocity relationship over a fixed and fluidised bed.

The value of U_{mf} is not an absolute one and therefore its determination must be standardised.

There are several procedures to determine U_{mf} . One of them makes use of the experimental curve corresponding to Figure 1. The determination must be made for decreasing flow rates and the precautions that must be taken are referred to by Richardson (4). U_{mf} may alternatively be calculated from the physical properties of the system under study.

Richardson and Zaki (5) and others have suggested that the most convenient way of showing the variation of fluidisation velocity with voidage is by means of a log-log plot of velocity against voidage since this plot normally gives a linear relationship showing that

$$U/U_i = \varepsilon^n \qquad (6)$$

Equation (6) has no theoretical basis but is widely used because it is simple in form and can therefore be readily applied. Furthermore it more accurately represents the experimental results than any other equation which has been used.

The value of U_i for fluidisation is such that

$$\log U_i = \log U_o - d_p/D \qquad (7)$$

while the value of n can be computed by

$$n = (4.4 + 18\, d_p/D)\, N_{Re_o}^{-0.1} \qquad (8)$$

$$\text{for } 1 < N_{Re_o} < 200 \qquad (9)$$

and by similar equations for other N_{Re_o} values. U_o in its turn, in this range of N_{Re_o} values, can be computed according to an iterative process by using equations (10) and (11).

$$U_o = \left[\frac{4(\varrho_s - \varrho_f)\, d_p g}{3\, C_d\, \varrho_f} \right]^{1/2} \qquad (10)$$

$$C_d = \frac{24}{N_{Re}} \left(1 + 0.15\, N_{Re}^{0.687} \right) \qquad (11)$$

However since some deviations may occur in relation to the calculated values it is better to use the experimental values to obtain the constants of equation (6). If the system under study obeys equation (6) then a plot of logU vs. logε will be as presented in Figure 2 and so the constants n, U_i and U_{mf} can be obtained.

The relation $U = U(\varepsilon)$ is readily obtained by measuring the values of bed height for the corresponding velocity, the voidage of the bed being computed by equation (12)

$$\varepsilon = 1 - \frac{L_o}{L} (1 - \varepsilon_o) \qquad (12)$$

The experimental constants can then be compared with the predicted ones using

equations (7) to (11) .

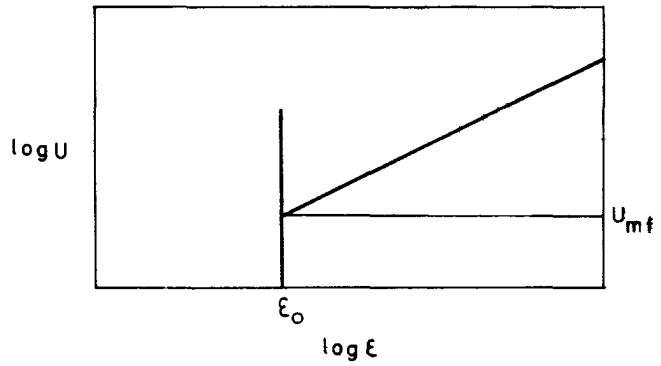

FIGURE 2 - Relationship between fluid velocity and bed voidage for a system obeying equation (6)

MATERIALS AND METHODS

Lead glass beads (ballotini) from Jencons Glass Co. of two sizes-No. 10 $\bar{d}_p$ =0.258 mm, ρ_s =2.905 g/cm^3;No. 8 $\bar{d}_p$ = 0.524 mm, ρ_s= 2.929 g/cm^3 - were used.Particle sizes were determined by cumulative screen analysis.
Stactic bed voidage (ε_o) in the conditions achieved in the reactor were calculated by measuring the volume in the reactor of a known volume of glass particles,calculated from its weight and density.
The voidage ε for each flow rate across the reactor was calculated by means of equation (12) using the L_o and ε_o values and the recorded values of L at each flow rate.

EQUIPMENT

A flow diagram of the pilot plant reactor used is shown in Figure 3 . The reactor itself is made of a cylindrical QVF precision glass column 100x4.78 cm surrounded by a jacket.The liquid is pumped through the reactor by a monopump and the flow rate measured by means of rotameters.Additionally a peristaltic Watson Marlow pump can also be used.The liquid distributor system comprises a series of discs and the bed of particles is retained in the reactor by a stainless steel wire mesh 80/39.
The height of the bed was measured on a scale on the front of the reactor.The temperature of the liquid in the reactor is controlled by means of immersion heaters acting both on the liquid itself and on the jacket surrounding the reactor.

EXPERIMENTAL

1-Measurement of dispersion in the reactor

The dispersion characteristics during fixed and fluidised bed operation were calculated from the results of tracer experiments using a 60 mg/ml solution of glucose.
Figure 4 shows the arrangement of the reactor as used to perform these experiments.Figures 5a an 5b present the C curves for the fixed and fluidised beds respectively,together with the experimental conditions prevailing.
To calculate the dispersion number in the region tested the closed vessel situation was considered.
For this case the value of D_v/vL can be calculated using equation (13).

$$\sigma_\theta^2 = \frac{\Delta\sigma^2}{\Delta\mu^2} = 2\frac{D_v}{vL} - 2\left(\frac{D_v}{vL}\right)^2\left(1 - e^{-vL/D_v}\right) \quad (13)$$

where $\Delta\sigma^2 = \sigma^2_{out} - \sigma^2_{in}$

$$\Delta\mu = \mu_{out} - \mu_{in}$$

σ^2_{out} and μ_{out} are calculated from the C curves presented in Figure 5 whereas σ^2_{in} and μ_{in} are calculated from the input function,equation (14)

$$C_g = C_{go}\, e^{-t/\bar{c}} \quad (14)$$

as $\mu_{in} = \bar{c}$ and $\sigma^2_{in} = \mu^2_{in} = \bar{c}^2$

Since we were unable to take samples immediately at the boundary of the bed of particles correction was made for the column volume above the bed by considering it as an ideal stirred reactor as outlined by Levenspiel (1).
The Peclet numbers obtained for fixed and fluidised bed operation are presented in Figure 6.

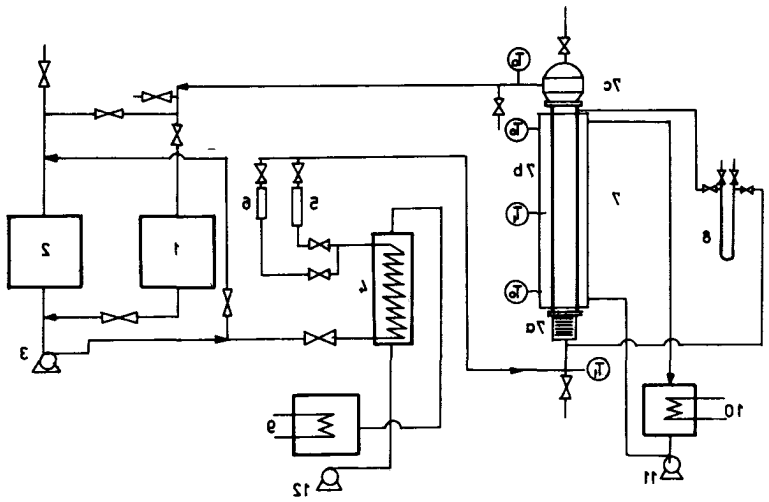

FIGURE 3 -Flow diagram of the pilot plant reactor:1÷2 feeding tanks,3 monopump, 4 heat exchanger,5÷6 rotameters,7 column,8 manometer,9÷10 immersion heaters,11÷12 centrifugal pumps,T_o thermometers,T_1 thermisters

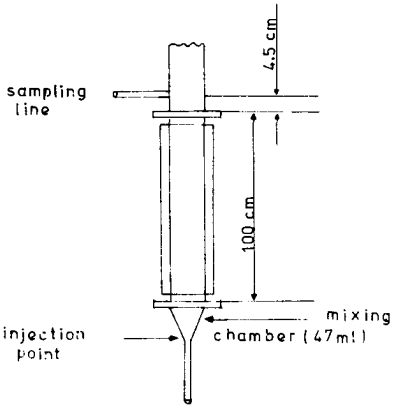

FIGURE 4-Arrangement of the pilot plant reactor to perform the tracer studies

In the range of flow rates tested the Peclet number for each bed could be expressed as:

Fixed bed $N_{Pe}=10^{-5}(160.69Q - 3.53Q^2)$ (15)

Fluidised bed $\log N_{Pe} = -1.172 -0.0621Q$ (16)

2 - Fluidisation characteristics

a) Determination of stactic bed voidages

Stactic bed voidages-ε_o- in the conditions achieved within the reactor were calculated as follows:

No. 10 glass

Reactor height for 1000g of glass=30.2 cm

Density of glass ρ_s = 2.905 g/cm^3

Reactor's internal diameter D=4.78 cm

Thus $\varepsilon_o = \frac{V_R - V_G}{V_R} = 0.365$

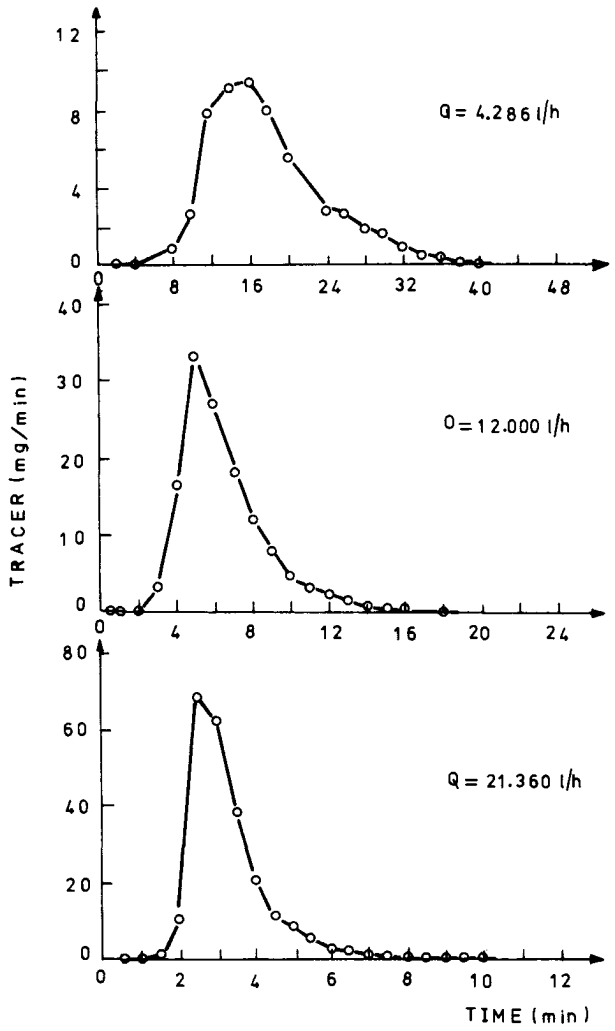

FIGURE 5a-Fixed bed C curves:Pulse input 120 mg glucose,L = 78.5 cm, temperature 45ºC,$\bar{d}_p$=0.0258 cm

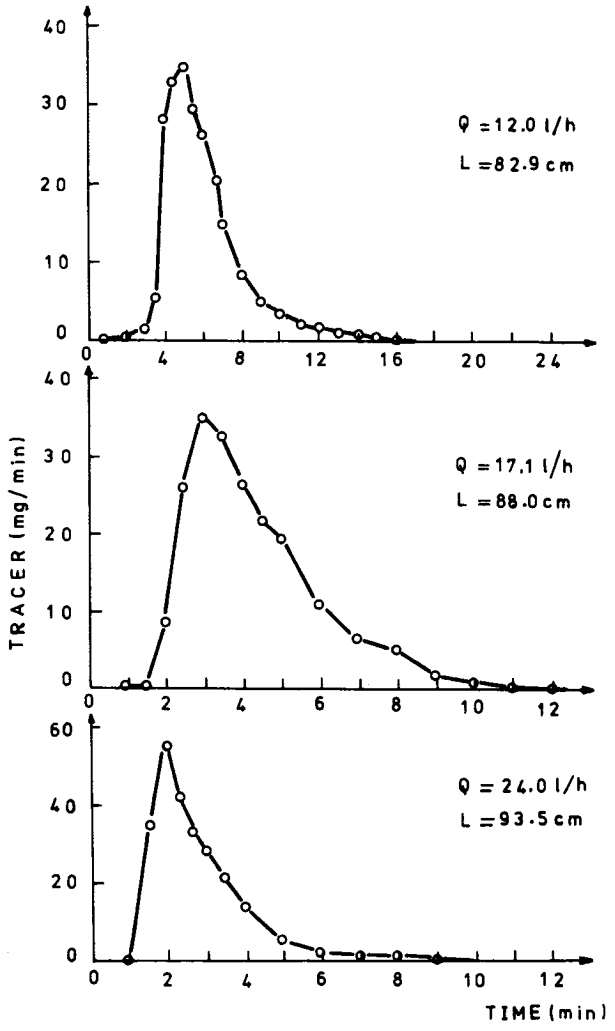

FIGURE 5b -Fluidised bed C curves:Pulse input 120 mg glucose, temperature 45ºC, $\bar{d}_p$ =0.0258 cm.

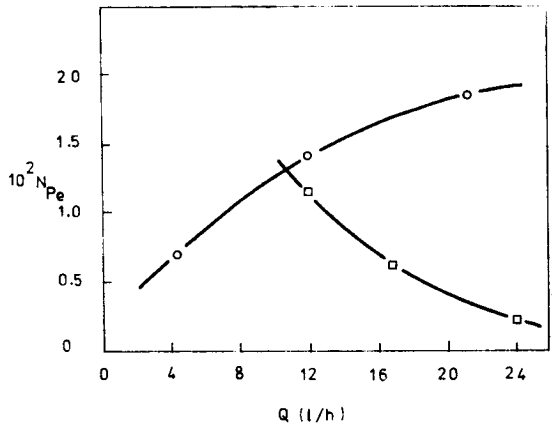

FIGURE 6 -Peclet number as a function of flow rate
—o—o— fixed bed mod
—□—□— fluidised bed mode

No. 8 glass

Reactor's height for 1000g of glass=31.0 cm

$\rho_s = 2.929\ g/cm^3$

$\varepsilon_o = \frac{V_R - V_G}{V_R} = 0.386$

The different values of ε_o for No. 10 and No. 8 glass reflect probably the fact that different spectra for the two sizes of glass were present in the samples

b)Determination of U_{mf} and $U = U(\varepsilon)$ relationships

The bed voidage ε may be calculated from equation (12) knowing $\varepsilon_o \propto L_o$ and the bed height L at different flows of water across the reactor.

A log-log plot (U vs. ε) was made and the least squares method used do obtain the values of n, U_i, and U_{mf} from the non-vertical portion of the plot.For both sizes of glass three temperatures- 35, 45 and 55 ºC - were used.

For No. 10 glass the effect of the sample size was investigated at 45ºC by using samples of 400,600,800 and 1000 g,and at 55ºC by using samples of 400 and 600g. The U =U (ε) curves for No. 10 glass are presented in Figures 7a,7b, and 7c, respectively for 35,45 and 55 ºC.In Figures 7b and 7c it is apparent that there is no influence of the sample size on the constants of equation (6).There have been reports of systems where for high solid loads equation (6) no longer applies (Richardson (4)).

The predicted constants of equation (6) may be calculated from fundamental physical properties of the system and correlations (7) to (11)

The comparison between the experimental and predicted constants of equation (6) for No. 10 glass is presented in Table 1.

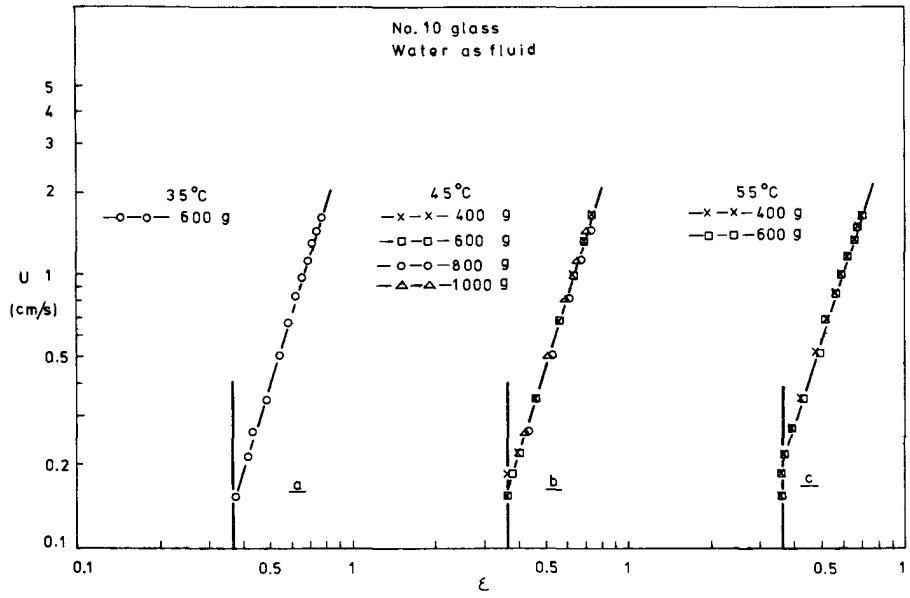

FIGURE 7 -Experimental U=U(ε) correlations for No. 10 glass

TABLE 1 -Comparison between experimental and predicted constants of equation (6) for No. 10 glass

Parameters \ Temp ºC	35	45	55
n_{exp}	3.325	3.374	3.187
n_{pred}	3.294	3.302	3.224
$U_{i\ exp}$	4.165	4.639	5.112
$U_{i\ pred}$	4.648	5.088	5.482
$U_{mf\ exp}$	0.146	0.155	0.206
$U_{mf\ pred}$	0.152	0.183	0.212

TABLE 2- Comparison between experimental and predicted constants of equation (6) for No. 8 glass

Parameters \ Temp ºC	35	45	55
n_{exp}	3.439	3.299	3.182
n_{pred}	2.989	2.916	2.853
$U_{i\ exp}$	11.881	12.227	12.569
$U_{i\ pred}$	10.035	10.671	11.252
$U_{mf\ exp}$	0.450	0.528	0.608
$U_{mf\ pred}$	0.583	0.665	0.744

For No. 8 glass, since the sample size had no effect on the hydrodinamic conditions of fluidisation, samples of 1000g were used at all temperatures.

The U = U (ε) curves for No. 8 glass are presented in Figures 8a, 8b and 8c respectively for 35, 45 and 55ºC.

The comparison between the experimental and predicted constants of equation (6) for No. 8 glass is presented in Table 2.

3-Comparison between measured and correlated dispersion numbers.

To compare the experimental and predicted values of the dispersion number using equations (4) and (5) a correlation of U = U(ε) for the fluidised bed is needed.

From Table 1, at 45 ºC , one can write that $U = 4.639\ \varepsilon^{3.374}$. Additionally to solve equation (4) in the fluidised bed mode one needs to use U_{mf}. This value can also be obtained from Table 1 as 0.155 cm/sec.

Table 3 presents the comparison between experimental and predicted D_v/vL values in both fixed and fluidised beds.

From this Table it may be seen that the direction of change with flow rate of the D_v/vL values we determined is the same as

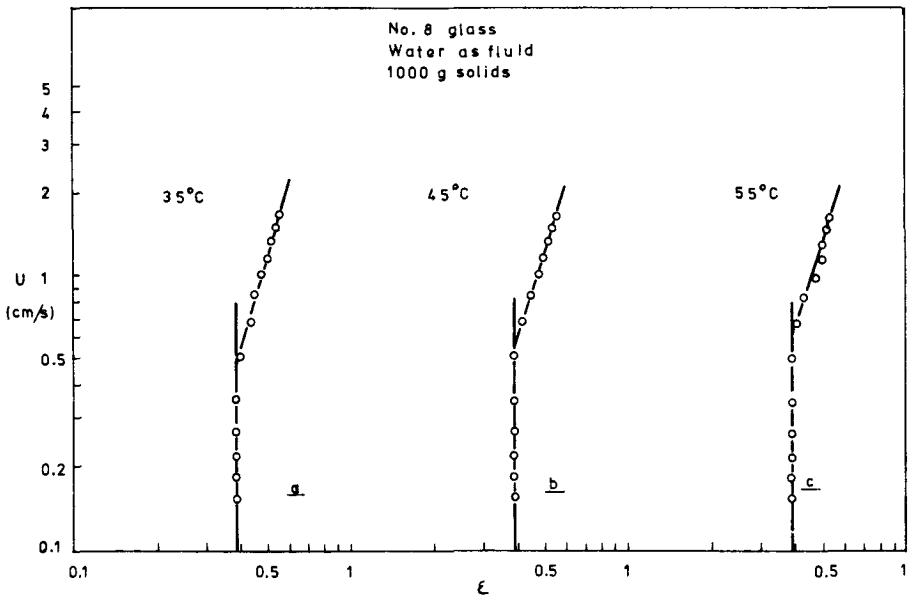

FIGURE 8 - Experimental U = U (ε) correlations for No. 8 glass

TABLE 3 - Comparison between measured and correlated D_v/vL values

	Flow rate (l/h)	Chung and Wen correlation	Bruinzel et al correlation	Levenspiel correlation	This work
Fixed bed	4.286	0.000582		0.000977	0.0480
	12.000	0.000572		0.000981	0.0232
	21.360	0.000563		0.001013	0.0179
Fluid. bed	12.000	0.000686	0.160		0.0268
	17.400	0.001013	0.132		0.0469
	24.000	0.001465	0.110		0.131

that predicted by the correlation of Chung and Wen (2) but our own values are much higher.

Comparison of the measured D_v/vL values for the fluidised bed mode with those predicted by the correlation of Bruinzel et al (3) indicates values of a similar order of magnitude but a different change with flow rate. For the fixed bed mode our own D_v/vL values are much higher than those given by Levenspiel (1). The direction of change cannot be compared since this latter correlation is expressed graphically by a range of D_v/vL values rather than by an equation.

CONCLUSIONS

As Table 3 indicates, widely varying values for D_v/vL are predicted by the correlation of Chung and Wen (2) and Bruinzel et al (3) for a fluidised bed . Moreover, none of these correlations are able to predicted the values we determined in the fluidised bed mode . The same situation is true when considering the D_v/vL values for fixed bed operation, for which in addition Levenspiel (1) predicts D_v/vL values lower than those we determined. Our D_v/vL values for the fixed bed mode are more closely comparable with those

determined by Marsh and Tsao (6).

Both correlations quoted above for fluidised beds have been advocated for the calculation of D_v/vL values: Kobayashi and Moo-Young (7) used the correlation of Bruinzel et al (3), while Liberman and Ollis (8) suggest that of Chung ant Wen (2).

It may however be suggested that until more widely applicable correlations are proven, the only reliable course is for the investigator to determine dispersion characteristics for himself.

Concerning the $U = U(\varepsilon)$ correlations it may be concluded that the system under study is well described by equation (6).

The experimental and predicted values of the constants in equation (6) for No. 10 glass are in reasonable agreement but for No. 8 glass the experimental values for n and U_i are underestimated by prediction leading to overestimates of U_{mf} by as much as 30 %.

The sample size had practically no influence on the correlations determined.

The data here derived has proved to be suitable for the successful modelling of a fluidised bed immobilised enzime reactor. (Cardoso (9)).

NOMENCLATURE

C_d	Drag coefficient, (dimensionless)
C_g/C_S	Glucose/Starch concentration, (ML^{-3})
C_{go}	Initial glucose concentration, (ML^{-3})
D	Reactor diameter (L)
d_p	Particle diameter, (L)
D_U/D_v	Effective longitudinal dispersion coefficient based on superficial and interstitial velocity, respectively, (Lt^{-2})
g	Acceleration due to gravity, (Lt^{-2})
l	Distance along the bed or reactor, (L)
L	Length of expanded bed or reactor, (L)
L_o	Length of fixed bed or reactor, (L)
n	Exponent in Richardson and Zaki equation, (dimensionless)
N_{Pe}	Particle Peclet number, $(Ud_p/D_U = vd_p/D_v)$
N_{Re}	Particle Reynolds number, $(Ud_p\rho_f/\mu_f)$, dimensionless
N_{Remf}	Particle Reynolds number at minimum fluidisation velocity $(U_{mf}d_p\rho_f/\mu_f)$, dimensionless
N_{Re_o}	Particle Reynolds number based on the terminal velocity of the particle, $(U_o d_p \rho_f/\mu_f)$, dimensionless
ΔP_B	Pressure drop, $(ML^{-1}t^{-2})$
ΔP_{eq}	Weight per unit area of the bed, $(ML^{-1}t^{-2})$
Q	Liquid flow rate (L^3t^{-1}), (l/h)
U	Superficial liquid velocity, (Lt^{-1})
U_i	Constant in Richardson and Zaki equation, (Lt^{-1})
U_{mf}	Superficial minimum fluidisation velocity, (Lt^{-1})
U_o	Terminal free falling velocity of particle, (Lt^{-1})
v	Interstitial liquid velocity, (U/ε) (Lt^{-1})
V_R	Volume of reactor (L^3)
V_G	Volume of solids in reactor (L^3)
Z	Dimensionless distance along the reactor (l/L)

Greek letters

γ	Kinetic parameter for the first order reaction (L^3t^{-1})
ε	Bed voidage of fluidised bed, dimensionless
ε_{mf}	Bed voidage at incipient fluidisation, dimensionless
ε_o	Bed voidage of fixed bed, dimensionless
μ	Mean of the C curves (t)
μ_f	Dinamic viscosity, $(ML^{-1}t^{-1})$
ρ_f	Fluid density, (ML^{-3})
ρ_s	Solid density, (ML^{-3})
σ^2	Variance of the C curves, (t^2)
$\bar{t}$	Mean residence time (t)
χ	1 for fixed bed, N_{Remf}/N_{Re} for fluidised beds, dimensionless

ACKNOWLEDGEMENT

One of us (J.P.Cardoso) was supported

by a grant from the Instituto Nacional de Investigação Científica,Lisboa.

REFERENCES

1. Levenspiel,O.,"Chemical Reaction Engineering",John Wiley and Sons Inc.,New York,1972
2. Chung,S.F. and Wen,C.Y.,A.I.Ch.E. J., 1968,14,(6), 857
3. Bruinzel,C.,Reman,G.H. and Van Der Laan, E.Th.,Proc. Symp.Interaction between Fluids and Particles,Inst. Chem. Engrs., 1962,B7
4. Richardson,J.F.,in Davidson and Harrison, "Fluidisation",Academic Press,London, 1971
5. Richardson,J.F. and Zaki,W.N.,Trans. Inst.Chem. Engrs.,1954,32,35
6 Marsh,D.R.,and Tsao,G.T.,Biotechnol. Bioeng.,1976,18,349
7 Kobayashi,T. and Moo-Young,M.,Biotechnol. Bioeng.,1971,13,893
8 Lieberman,R.B. and Ollis,D.F.,Biotechnol. Bioeng.,1975,17,1401
9 Cardoso,J.P.,Ph.D. Thesis,University of Birmingham,1977

A TECHNIQUE FOR THE DETERMINATION OF THE SHAPE OF A FLUID FRONT PROGRESSING THROUGH A PACKED BED

A. V. BRIDGWATER
G. A. IRLAM

Department of Chemical Engineering
University of Aston in Birmingham,
United Kingdom.

ABSTRACT

In certain operations it is necessary to be able to predict the shape of a liquid front flowing through a packed bed. A survey of possible methods is given. This is followed by details of a technique that has been developed to show how the shape of the liquid front develops as flow proceeds through the bed. This is related to the system characteristics, and ways of overcoming problems due to the shape of the liquid front are suggested.

INTRODUCTION

Many manufacturing processes involve the flow of liquid through a packed bed of solid particles. The objective of this work was to study the initial contact between liquid and solid by measuring the shape of the liquid front as it passes through the bed. Theory suggested and preliminary experimentation demonstrated that with liquid flowing upwards, an essentially flat profile was obtained from wall to wall under all conditions. This was not true of downward flowing liquid and all the experimental work was carried out in this mode.

MATERIALS AND EQUIPMENT

Right circular cylinders of cellulose acetate were employed for the solid phase, and glycerol/water for the liquid base. A procedure was developed to obtain reproducible packing densities with minimum wall effects in a 50mm diameter sectioned glass column with a fixed perforated plastic support at the bottom. Liquid was introduced over a range of constant back pressures and measurements of the shape were made at three distances from the top of the bed.

DETECTION DEVICE

A range of methods of detecting the liquid front were considered. As a three dimensional system was involved, any device external to the bed and container would be unlikely to give sufficiently positive results. An external technique would probably rely on transmitted or reflected elec tromagnetic radiation which would raise a number of problems such as interference by the solid particles, safety factors, and the three dimensional location necessary. An alternative method would be to monitor the timing of liquid leaving the bottom of a packed column through concentric rings. This was employed in early experimentation to obtain qualitative information. Internal devices need to be sufficiently small and sensitive to detect the liquid front without interfering with the flow pattern, and generally fall into the three categories of ultrasonics, radiation and electrical.

Ultrasonic detection is satisfactory from a practical viewpoint as the signal generactor or transmitter may be placed in the liquid bulk, and the receiving crystals mounted suitably in the bed. These receiving devices may be made sufficiently small to avoid interference but are expensive with the necessary ancillary equipment.

Radiation devices require a transmitter and receiver to detect the arrival of the liquid front. The degree of miniaturisation necessary would be difficult and costly.

Electrical measurement includes measuing capacitance, resistance, voltage or current. The measurement of changes in capacitance is theoretically possible but a suitably small capacitor would impose almost impossible sensitivity requirements on the detection equipment. Resistance measurement has been found in anemometers for example, for measuring velocity profiles, but these are unnecessarily sophisticated and fragile. The completion of an electrical circuit, i.e. resistance, voltage of current change is attractive, as very small electrodes can be easily and cheaply manufactured, and any of the three variables may be directly measured or recorded on conventional instruments. This alternative was chosen for the experimentation due to the ease and cheapness of manufacture and operation.

APPARATUS AND PROCEDURE

Initially one electrode was placed in the bulk liquid and the detecting electrodes mounted in the bed. Due to poor control and lack of sensitivity this was modified

to a double electrode assembly (Figure 1 and Plate 1) which gave much improved results.

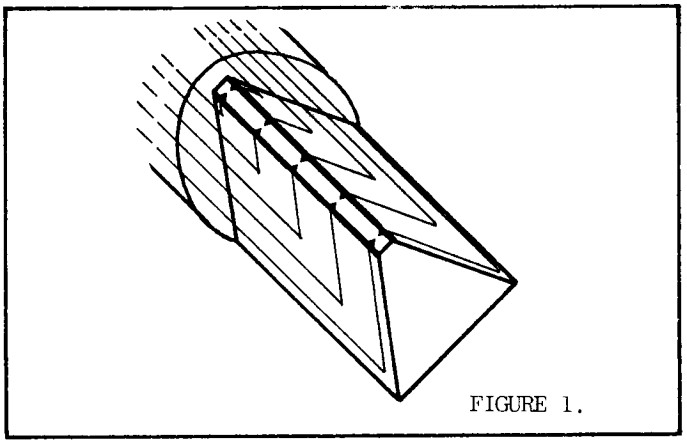

FIGURE 1.

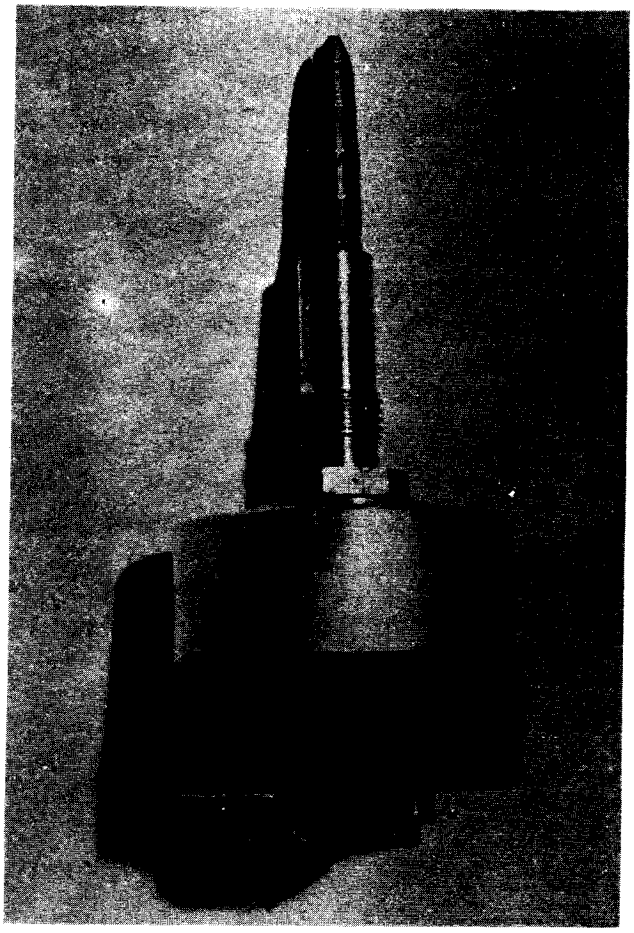

The device was manufactured by positioning platinum wires in an inert support to an accuracy of 0.3 mm. The base of the platinum electrodes, connecting leads, and inert support were embedded in epoxy resin. This was attached to the end of a threaded pipe which fitted into the spacer shown in Figure 2.

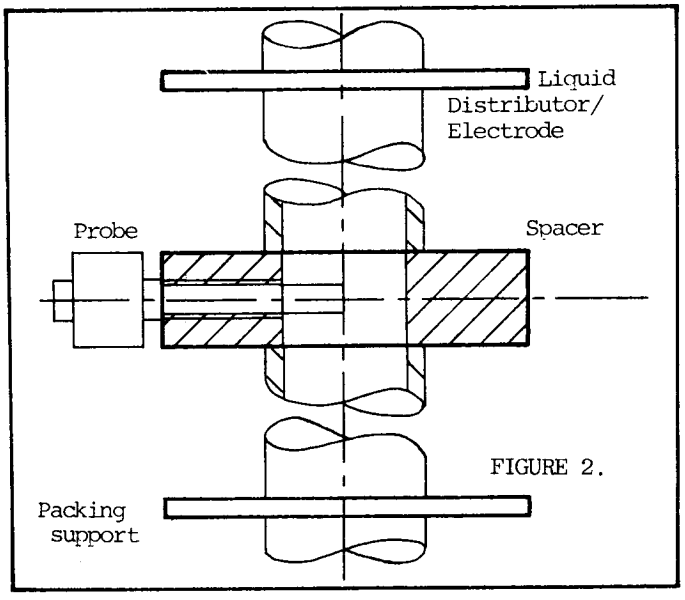

FIGURE 2.

A multipin plug completed the device and this is shown in Plate 2.

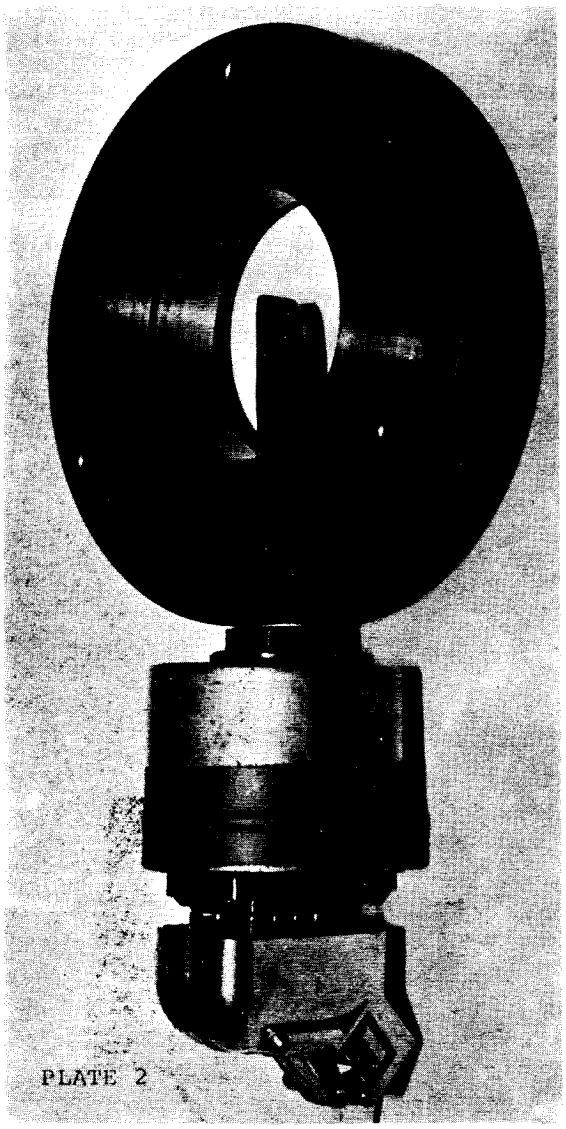

PLATE 2

The degree of accuracy was controlled by the position of the platinum wires which was held to 0.3 mm in 25 mm or $\pm$ 0.6%. Interference with the liquid flow pattern was minimised by having a triangular cross section (Figure 1) with the space between individual electrodes cut down.
Five points which were positioned across the radius of the tube were used on the device, (Figure 3).

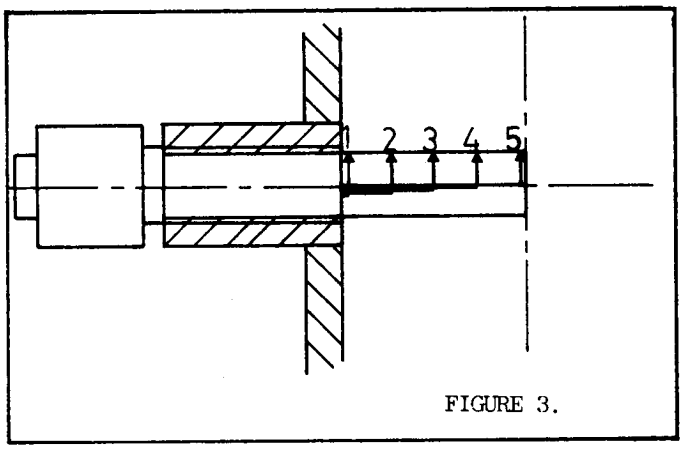

FIGURE 3.

Each electrode assembly was connected to separate channel on a multichannel continuous recorder, which was arranged to give adequate separation between each trace (see Figure 4).

FIGURE 4.

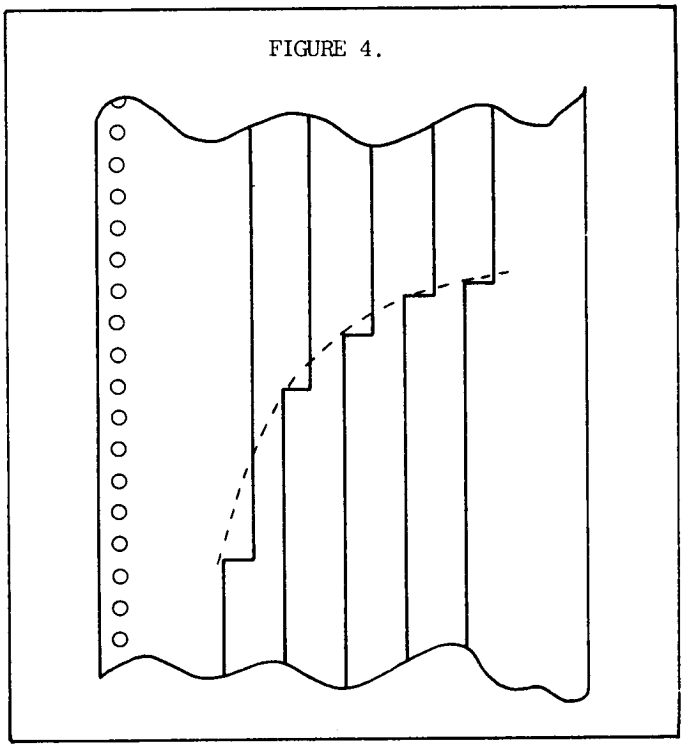

The electrical circuit for one channel is shown in Figure 5.

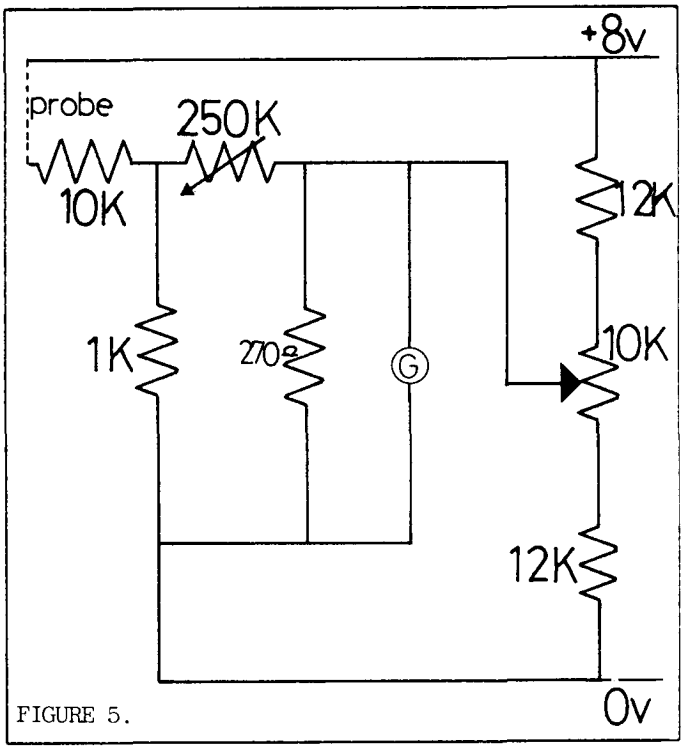

FIGURE 5.

The overall apparatus is shown in Plate 3. A 50 mm. diameter glass column was employed with a perforated plastic bottom plate to support the bed. The detecting device was fitted at the desired distance from the top by screwing into a special spacer at a join. This is shown in Figure 3. The column was filled with solid particles using a standard gravity filling procedure that had been demonstrated to give good reproducibility of packing. A distributor was then fitted to the top which consisted of either a gauze or a perforated plate. Liquid (glycerol-water and some salt for improved conductivity) was added at constant back pressure using a constant head device or pressurised tank.

PLATE 3

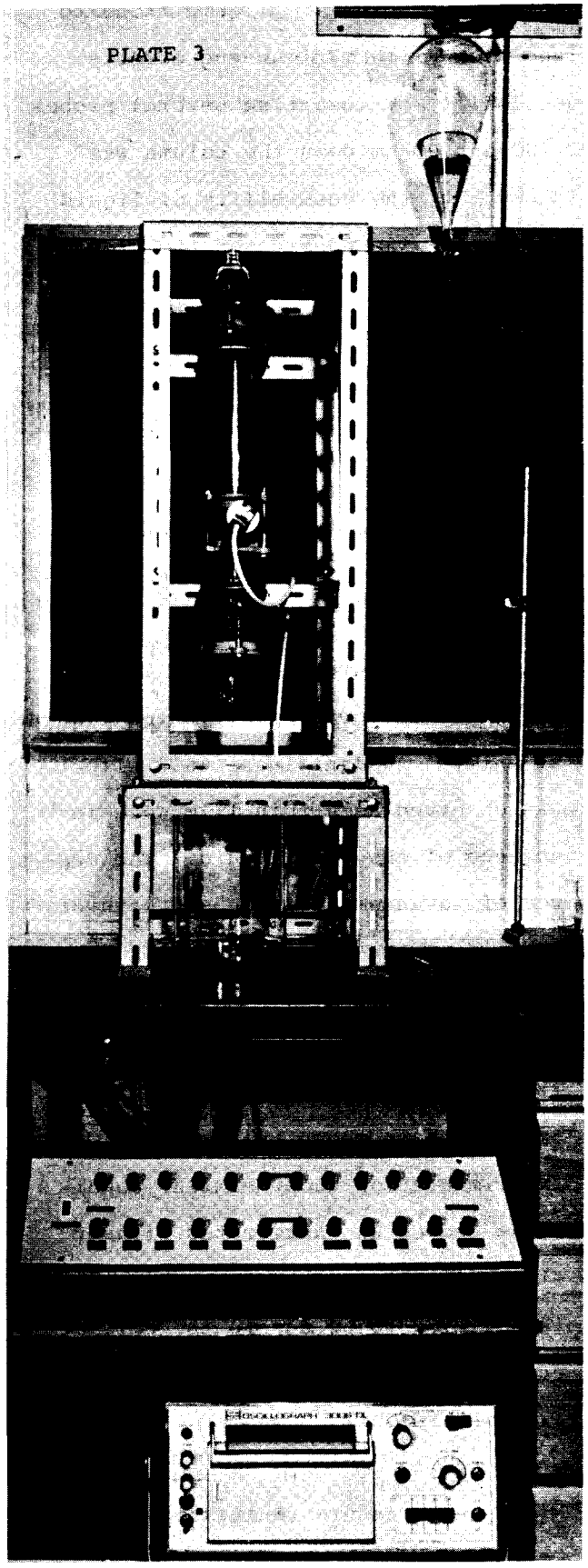

It was considered important to continue the packed bed to a significant depth below the probe to allow the entire liquid front to pass the probe with minimum end effects. The possibility of inserting several probes at 30, 60 and 90 cm down the column was considered, but the possibility of liquid maldistribution was considered too great.

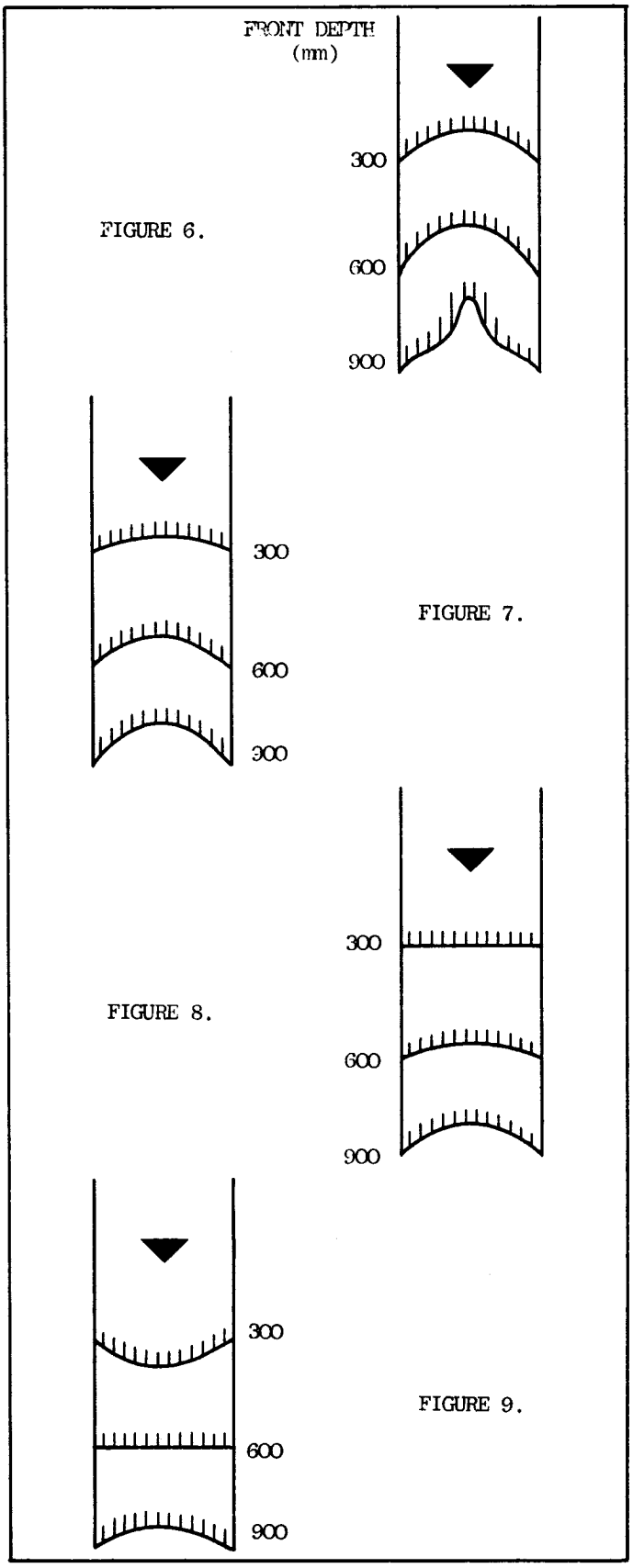

FIGURE 6.

FIGURE 7.

FIGURE 8.

FIGURE 9.

RESULTS

The complete programme of experimentation is not yet complete, but the following results have been obtained:

1) Low back pressure (initially 2 x 10^3 Nm^{-2}) and uniformly distributed liquid at entry. A significant wall effect was observed as a thin film well in advance of the bulk liquid. The degree of advancement increased with distance down the column which might be expected with the increased voidage at the wall and low flow rate. The profile developed most rapidly in this case which is shown in Figure 6. Other experimentation under similar conditions showed an exaggerated "finger" effect in the centre of the bed. This is believed to be due to the wall effect described above enhancing radial flow inwards.

2) High back pressure (initially 20 x 10^3

2) contd.

Nm^{-2}) and uniformly distributed liquid at entry. The wall effect was not clearly defined initially but slowly developed as the flow rate dropped. The shape of the liquid front developed more slowly. Figure 7.

3) Low back pressure (initially 2 x 10^3 Nm^{-2}) and distributing liquid to the centre of the bed. No wall effect was observed. The shape of the liquid front developed from convex initially to concave whence it would be expected to develop as for uniformly distributed liquid. Figure 8.

4) High back pressure (initially 20 x 10^3 Nm^{-2}) and distributing liquid to the centre of the bed. The profile adjusts to the horizontal position more slowly, and would be expected eventually to follow the same pattern of developing a concave liquid front. Figure 9.

The shape of liquid front at any given point seems to be dependant on flow rate and initial distribution, although a very long column is likely to always give a con cave shape. When more quantitative results are available, it is hoped to obtain a model to predict the shape of front. It is likely that the following terms will be involved :

a) ratio of maximum deviation of liquid front from horizontal to column diameter - positive for concavity and negative for convexity.

b) rate of descent of liquid front or volumetric flow rate.

c) ratio and location of entry area to area available for flow.

CONCLUSIONS

The shape of the descending fluid front is particularly dependant on flow rate and initial distribution. Careful control of flow rate and distributor design should give a flat, convex or concave front as required for a given column length. It is likely that other cross sectional geometries could be similarly analysed, such as the effect of discontinuities within the column. For very long columns, it is probable that the concave front as indicated in Figure 7, cannot be avoided.

ACKNOWLEDGEMENT

This work has been carried out with the support of Procurement Executive, Ministry

of Defence.

REFERENCES

1. Steinberger and Drechsel - Advances in Chemistry Series 88 "Propellants Manufacture, Hazards and Testing" ACS 1969 pp 1 - 28.

2. Irlam, G.A., 1978, "An investigation into the manufacturing variables of cast double base propellant". Ph.D. Thesis, University of Aston.

MASS TRANSFER IN FLUIDISED BED ELECTROCHEMICAL REACTORS

A.A. Wragg[1]
A.T.S. Walker[2]

1. Department of Chemical Engineering, University of Exeter
2. United Kingdom Atomic Energy Authority, AEE Winfrith, Dorchester, Dorset, England

ABSTRACT

Electrochemical mass transfer experiments have been carried out involving the cathodic deposition of copper from aqueous solutions containing H_2SO_4 for two distinct cases.

a) Determination of mass transfer rates at a plane wall electrode in the presence of a fluidised bed of inert particles (glass beads). In this work bed height, bead size and fluidisation conditions have been varied and a correlating equation

$$j_{D\varepsilon} = 0{\cdot}138\left[\frac{Re_{dp}}{(1-\varepsilon)}\right]^{-0.39}\left[\frac{d_p}{d_e}\right]^{-0.39}$$

is suggested as applying over the range $0{\cdot}936 < \frac{Re_{dp}}{(1-\varepsilon)} < 67$. Comparison with mass transfer data of several other authors is made which reveals considerable variance.

b) Determination of mass transfer rates between electrolyte and particles within an active bed of fluidised conducting copper particles. Two techniques have been used:

1. Once through steady state experiments in which the depletion of solution copper content is measured.
2. Batch recirculation experiments in which the mass transfer rate is indicated by continuous monitoring of the electrolyte Cu^{++} concentration.

Analysis of the data yields a correlating equation

$$j_D = \frac{k}{u} Sc^{2/3} = 1{\cdot}55\left[\frac{Re_{dp}}{(1-\varepsilon)}\right]^{-0.49}$$

in the range $2{\cdot}6 < \frac{Re}{(1-\varepsilon)} < 30$. This compares very well with another source for electrolytic fluidised bed mass transfer, but is somewhat lower than other equations for particle to fluid non-electrolytic mass transfer. This work is of importance in the design of electrochemical fluidised bed reactors for metal extraction and effluent clean-up processes.

INTRODUCTION

The past decade has seen a considerable effort in research and development of fluidised bed electrochemical reactors. The attractions of high specific surface, good mass transfer rates and other properties has led many workers to believe that fluidised beds possess many advantages over conventional plate cells in areas such as organic electrosynthesis, metal recovery and pollution abatement from metal-containing effluent and even primary metal winning from ore leach liquors. Pioneering work was undertaken by Backhurst [1,2], and further experimental and theoretical development was due to Fleischmann et al [3-6] and Goodridge [7,8]. Larger units were demonstrated for cathodic copper extraction by Wilkinson and Haines [9] and later in further work by Germain and Goodridge [10]. Among other contributors in this field are Kreysa, Pionteck and Heitz [11]

who worked with non-conducting and conducting beds, and Sabacky and Evans [12] who have discussed metal phase conductivity and presented a more refined model. The properties of bipolar fluidised beds have also been investigated [13].

Whereas the foregoing work deals with fluidised electrode applications, i.e. cells in which the fluidised particles are conducting so that the bed is electrochemically active throughout, a simpler type of cell has also received attention wherein the fluidised particles are electrochemically inert and simply serve to enhance mass transfer and modify the electrodeposit at a conventional plate or grid electrode immersed in the bed. This is the basis of the 'Chemelec' cell developed at the Electricity Council Research Station, Capenhurst, England, and described by Lopez-Cacicedo [14].

An important property of such cells (of both types) in their design and scale up is their mass transfer performance. In many applications where supporting electrolyte is present, the problem reduces to a diffusion-convection situation similar to that obtaining in non-electrochemical mass transfer such as in particle dissolution or crystallisation. The designer needs information on how the rate of electrochemical mass transfer to a surface in a fluidised electrolyte or between the particles and fluid in a fluidised electrode, vary with such operating parameters as particle size flow rate and bed expansion. Some variable data exists for fluidised electrolytes [15-19] but very little for particle to fluid transfer in active beds. Pickett [20] in analysing results for dissolved oxygen reduction on silver by Fleischmann et al [5] presents the equation

$$\frac{K}{u}\,\varepsilon\,Sc^{2/3} = 1.52\left[\frac{Re_{dp}}{(1-\varepsilon)}\right]^{-0.5} \qquad (1)$$

which he shows to lie close to an earlier equation for non-electrolytic mass transfer given by Chu et al [21].

EXPERIMENTAL

The present work made use of a side-by-side electrode configuration consisting of parallel 1 cm × 5 cm flow channels (Fig. 1).

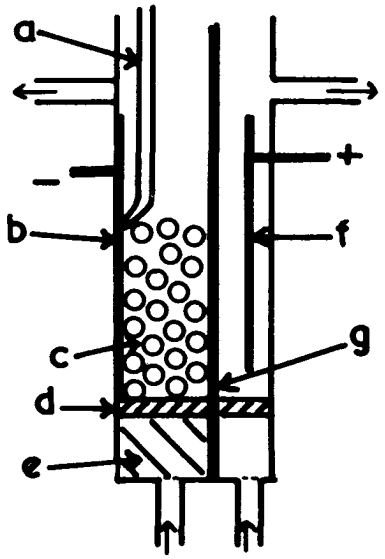

Figure 1. The fluidised bed cell.

a - reference electrode
b - cathode feeder
c - fluidised particles
d - glass sinter
e - calming section
f - anode
g - diaphragm

A supported ion exchange membrane (Ionac) separated the catholyte and anolyte channels and the particles were supported on glass sinter inserts. A plane copper sheet acted as cathode feeder electrode and presented a 5 cm x 20 cm surface to the electrolyte. Four distinct types of experiment were carried out:

a) Investigation of mass transfer of Cu^{++} ions to the plane copper feeder cathode from plain electrolyte and electrolyte containing glass ballotini particles. The use of a copper anode with recirculating electrolyte ensured a fairly constant Cu^{++} concentration.

b) Investigation of current-potential characteristics and of mass transfer of Cu^{++} ions to active cathode beds of copper particles, the anode being a similar copper particle bed so that again the recirculating mixed electrolyte composition remained constant.

c) As b) but using an inert Pb anode (O_2 evolution) so that a progressive depletion of Cu^{++} took place over a period of several hours as the 10 dm^3 electrolyte batch was continuously recirculated.

d) As c) but using a once through catholyte flow system so that a batch of Cu^{++}-weak producted was collected from a Cu^{++}-strong feed.

Cu^{++} concentration was continuously monitored, using for relatively strong solutions, a linear readout U.V. spectrophotometer at wavelength 810 nm and, for dilute solutions as achieved especially in the c) series experiments, an Atomic Absorption spectrophotometer at a wavelength of 324·8 nm. (Some terminal concentrations achieved were as low as 0·12 ppm from a starting concentration of ≈ 100 ppm thus illustrating the potential application in heavy metal effluent clean up.)

Cathode potential was controlled using a Chemical Electronics 20/20A potentiostat. A saturated calomel electrode was used as reference electrode the luggin salt bridge tip being normally positioned at the bed surface pointing toward the feeder electrode though other positions were also investigated. The electrical circuit is depicted in Fig. 2 and further detail of apparatus and experimental techniques used may be found elsewhere [22].

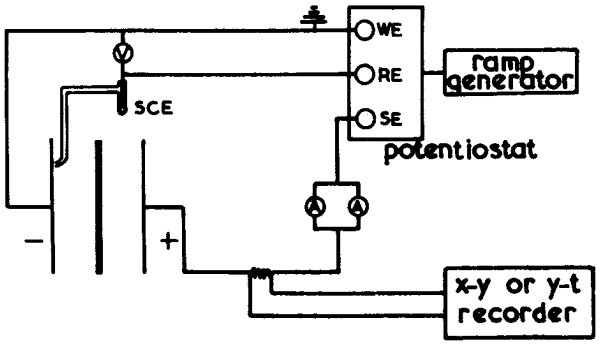

FIGURE 2. The electrical circuit.

SCE - saturated calomel electrode
WE - working electrode
RE - reference electrode
SE - secondary electrode

The experimental approach to the determination of wall mass transfer coefficients was a straightforward application of the Limiting Diffusion Current Technique (LDCT). The use of the LDCT in chemical

engineering is well documented [23,24] and will not be described in detail here. The approach is to determine the limiting electrolysis current for a diffusion controlled process by identifying the plateau region on a current-potential plot and then using the simple equation

$$K = \frac{I_{Lim}}{zFAc_{\infty}} \qquad (2)$$

to calculate the mass transfer coefficient, since the interface concentration of the consumed species approaches zero. However, due to the problem of non-uniform potential distribution in the case of conducting beds, the problem is much more complex and it cannot be assumed that all parts of the bed are operating near or on the limiting plateau. This problem is discussed more fully later and especially in [23].

In the ensuing data treatment, the electrolyte viscosity and density have been taken from Eisenberg et al [25] and the diffusivity from Arvia et al [26] as interpreted by Wragg and Ross [27].

RESULTS AND DISCUSSION

a. Electrolyte to wall mass transfer (No-fluidisation)

Typical current-potential curves in the absence of particles are indicated in Fig. 3 and values of i_{Lim} so determined were correlated in terms of Sh_{de} against Re_{de} as shown in Fig. 4. The equation of the solid line through the data points is

$$Sh_{de} = 8{\cdot}15\ Re_{de}^{0{\cdot}54} \qquad (3)$$

which, since the Schmidt number has a value of 2674 can, by using a $^1/_3$ exponent, be written as

$$Sh_{de} = 0{\cdot}602\ Re_{de}^{0{\cdot}54}\ Sc^{0{\cdot}33} \qquad (4)$$

It is notable from Fig. 4 that there is a

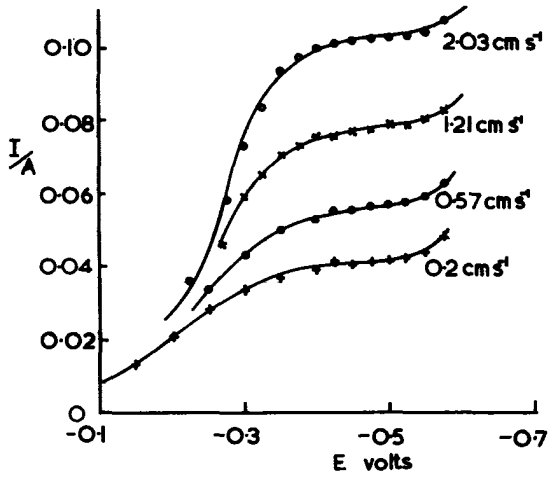

FIGURE 3. I/A against E curves for wall electrode with no fluidisation.
c = 0·0114 M

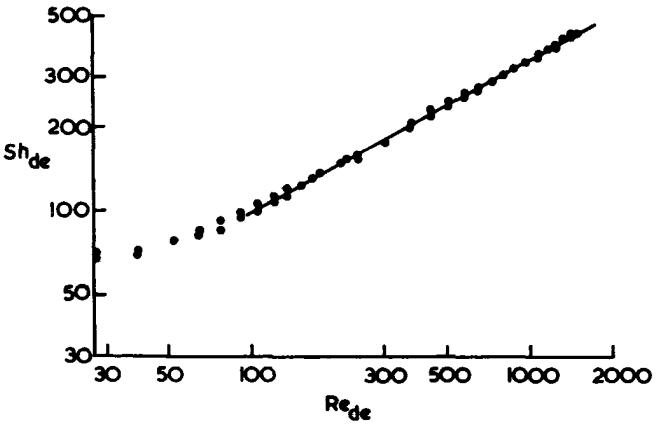

FIGURE 4. Sh_{de} against Re_{de} for mass transfer to the wall electrode.

deviation from equations (3) and (4) at low Re due to the significant contribution of free convection effects. The results indicated by equation (4) lie higher than the predictions of the

Blasius-Pohlhausen equation for developing laminar flow by a factor of 3. This difference is due both to the disturbance of the flow by its passage through the interstices of the distributor and also to the well known effect of secondary flows enhancing transfer processes in the corners of rectangular channels. The above equations are not of particular significance in themselves but were used in order to estimate the mass transfer rates from the electrolyte to the wall in the region above the level of the bed during the fluidisation experiments. The current value so calculated was then subtracted from the total observed current to yield that for the fluidised section of the wall alone.

b. Electrolyte to wall mass transfer with an inert fluidised bed

Figure 5 details typical total current-potential curves obtained with glass ballotini fluidised beds, fairly well-defined limiting plateaux being observed. All subsequent data discussed have been corrected for the effect of the convective transfer to the wall electrode (feeder) alone in the open channel above the bed via the use of equation (3). Three bed weights of 30g, 50g and 70g were used for each of the three mean particle sizes d_p = 274 μm, 386 μm and 548 μm giving, with each experiment repeated, a total of 446 data points for this part of the work. The enhanced mass transfer due to the presence of the fluidised bed as compared to that for electrolyte flow alone is illustrated for a 50g bed for the three separate particle sizes in Fig. 6.

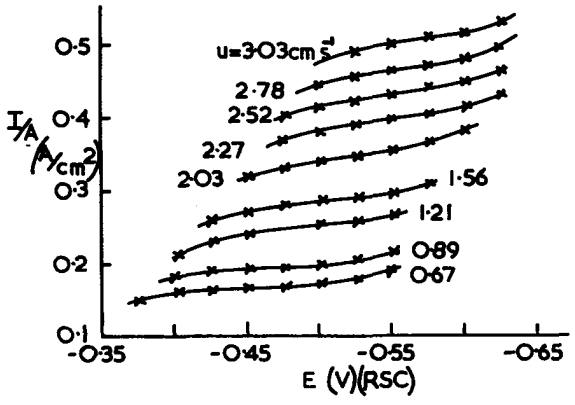

FIGURE 5. I/A against E curves for wall electrode with fluidised electrolyte d_p = 548 μm; c = 0·012 M, 50 g bed.

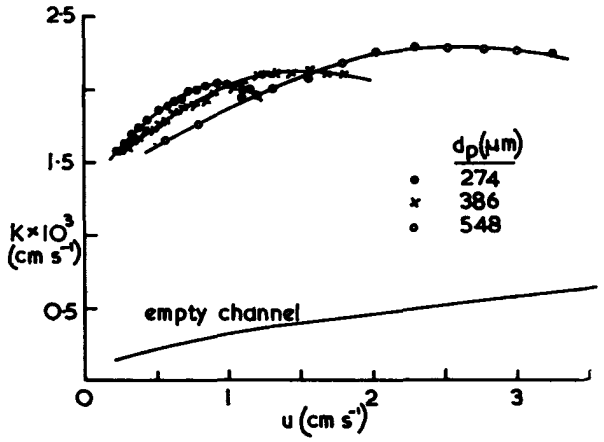

FIGURE 6. Comparative effect of fluidised bed on wall mass transfer.

The increase in K is seen to vary between about 8 and 4·5 which is a similar range to that observed by workers such as Carbin and Gabe [16] who used a small vertical solid copper cylinder immersed in a cylindrical ballotini bed, Jottrand and Grunchard [17] who used a planar electrode in a cylindrical bed, Couret et al [18]

who used small cylindrical probes and King and Smith [28] who used a cylindrical wall test electrode.

Figure 7 shows a plot of K against ε as

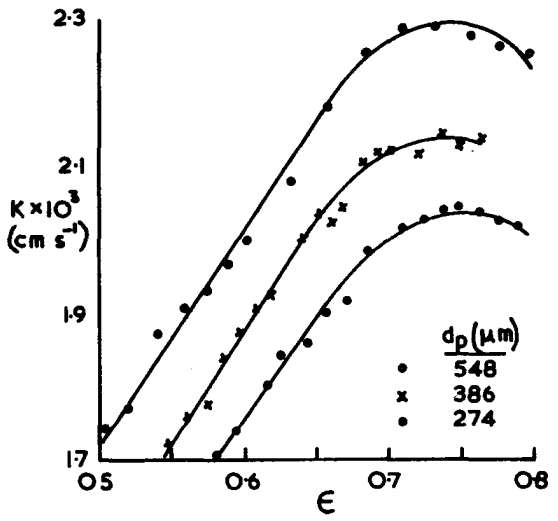

FIGURE 7. Plot of mass transfer coefficient against fluidised bed voidage.

a function of particle size and distinct maxima are observed in the graphs at a value of $\varepsilon \approx 0{\cdot}7$ to $0{\cdot}75$. The data of Smith and King [15] exhibited a similar trend giving a fairly broad peak comparable with those of Fig. 7 at $\varepsilon \approx 0{\cdot}7$. The maxima values $\varepsilon \approx 0{\cdot}65$ of King and Smith [23] and $\varepsilon \approx 0{\cdot}7$ of Jagannadharaju and Venkata Rao [19] also show close agreement with the present work. On the other hand the work of Carbin and Gabe [16], Jottrand and Grunchard [17] and Coeuret [18] suggest a much sharper peak K in the range $0{\cdot}55 < \varepsilon < 0{\cdot}6$. Bordet et al [29] have measured the kinetic energy of fluidised ballotini using a membrane probe linked to a piezo-electric crystal. They found that the kinetic energy passed through maximum at $\varepsilon \approx 0{\cdot}58$ and concluded that the phenomena of maximum kinetic energy and maximum mass transfer rate are closely related.

It is difficult to account for the two relatively clearly defined ranges of ε over which peak mass transfer coefficient values have been observed. But those in the range $0{\cdot}65 < \varepsilon < 0{\cdot}75$ are from work, including the present, involving fluid to wall mass transfer [15, 28, 19], whereas those in the range $0{\cdot}55 < \varepsilon < 0{\cdot}6$ have all been concerned [16, 17, 18] with mass transfer to a small test electrode immersed in the bed. It appears therefore that results from a small probe test surface are not thoroughly representative of wall processes, especially for low d_e/d_p ratios where the local wall voidage is higherthan the overall value for the bed.

Figure 8 shows a good correlation for the mean of each pair of data points, the straight line through the results having the equation

$$j_D\varepsilon = \frac{K}{u}.\varepsilon.Sc^{0{\cdot}67} = 0{\cdot}138\left[\frac{Re_{dp}}{(1-\varepsilon)}\right]^{-0{\cdot}39}\left[\frac{dp}{de}\right]^{0{\cdot}39} \quad (5)$$

over the range $0{\cdot}936 < Re_{dp}/(1-\varepsilon) < 67$.

It is not possible to compare (5) directly with equations of other authors, only Smith and King [15] having found a particle size effect which they attributed to wall and agglomeration effects, producing two separate equations for different ranges of d_e/d_p. However it is

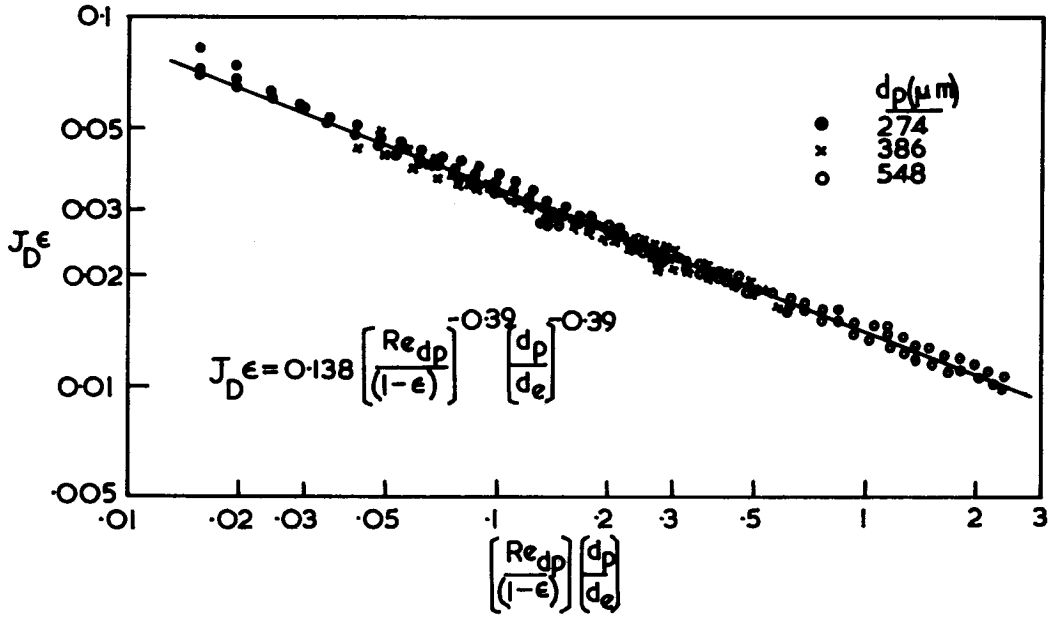

FIGURE 8. Plot of $j_D\varepsilon$ against $\left[\frac{Re_{dp}}{(1-\varepsilon)}\right]\left[\frac{d_p}{d_e}\right]$ for wall mass transfer in the presence of a fluidised bed.

possible to deduce a general equation for comparison purposes by evaluating (5) for the intermediate particle size used, i.e. d_p = 386 μm, the geometric mean of the three sizes used. Thus equation (5) becomes

$$j_D\varepsilon = 0{\cdot}60\left[\frac{Re_{dp}}{(1-\varepsilon)}\right]^{-0.39} \qquad (6)$$

Figure 9 compares this equation with those

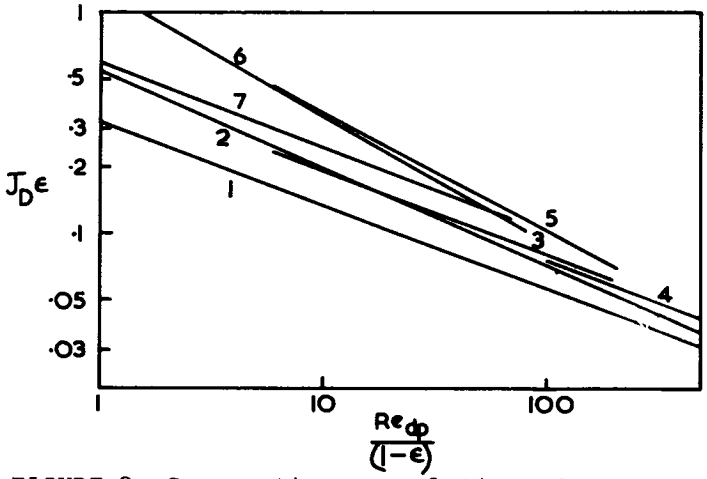

FIGURE 9. Comparative correlations from various sources (see Table 1).

of other authors as detailed in Table 1. It can be seen that the present results lie squarely among the others and also that there is considerable variance among proposed correlations.

c. Particle to fluid mass transfer in an active bed with time-steady concentration (Operating mode 2)

For experiments with an active conducting bed the problem of non-uniform potential distribution and hence the loss of well-defined limiting plateaux on the i-E curves is encountered. A typical set of polarisation curves for an inlet Cu^{++} concentration of ≈ 1·3 × 10^{-4} M is shown in Fig. 10. A current wave at low E is obtained and a near linear portion at high E. Walker [22] has termed these "the

TABLE 1

Author(s)	Curve on Fig.9	Constants in equation $J_D\varepsilon = a\left[\frac{Re_{dp}}{(1-\varepsilon)}\right]^x$ a	x	d_e/d_p	System	$\frac{Re_{dp}}{(1-\varepsilon)}$	Sc
Smith and King (15)	1 2	0·32 0·54	0·38 0·44	41-105 17-27	Cylindrical wall mass transfer	·7-1067 34-2334	580-2100
Jottrand and Grunchard (17)	3	0·45	0·375	93-360	Plannar test electrode in cylindrical bed	6-200	1250
Jagannadharaju and Venkata Rao (19)	4	0·43	0·38	8-27	Inner anode of annular bed	200-23800	1300
Coeuret et al (18)	5	1·2	0·52	93-290	Various cylindrical probes	6-200	1250
Carbin and Gabe (16)	6	1·24	0·57	80-150	Cylindrical test electrode in cylindrical bed	0·1-70	787-1777
Present work	7	0·6	0·39	43	Rectangular channel wall mass transfer	·936-67	≈ 2675

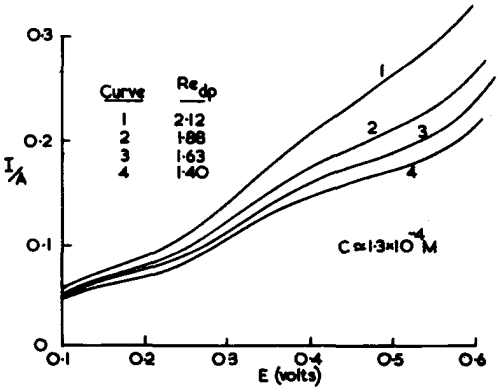

FIGURE 10. Typical current-potential curves for a conducting bed.

50g bed; d_p = 274 μm.

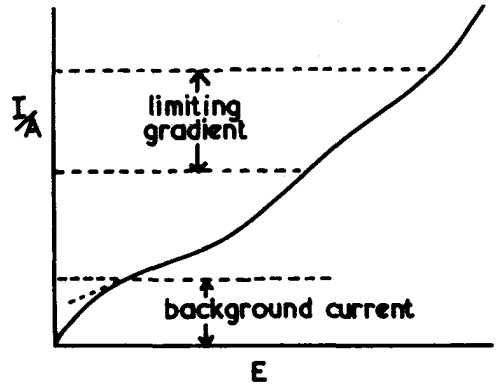

FIGURE 11. Illustration of terms "limiting gradient" and "background current".

background current" and "the limiting gradient" as depicted in Figure 11. The low E wave is probably due to the lower regions of the bed operating outside the region of cathodicity so that a local anodic dissolution occurs with redeposition in the upper regions, a phenomenon first recognised by Flett [30]. In the limiting gradient region the upper part of the curve is in the cathodic H_2 evolution region. A true estimation of a limiting current is thus impossible. Walker [22] has commented on the conflicting reports in the literature concerning the obtainability of limiting currents in fluidised bed cells. By measurement of both inlet and outlet catholyte Cu^{++} concentration, current efficiency for Cu^{++} deposition was calculated and due to the anodic dissolution effect at one extreme and the

co-evolution of H_2 at the other, these showed a marked deviation from 100% as illustrated in Fig. 12 for a bed of 274 μm particles with an inlet concentration of approximately $2{\cdot}6 \times 10^{-3}$ M. Efficiencies of 75 to 80% are obtained over much of the potential range.

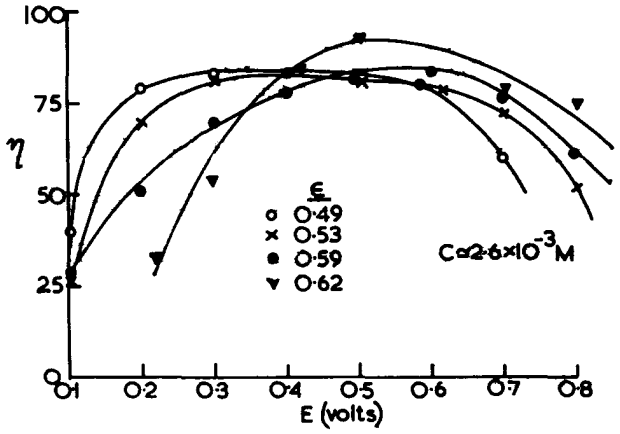

FIGURE 12. Current efficiencies for a 274 μm conducting bed as a function of E.

For the purpose of mass transfer coefficient calculation the diffusion limiting condition was taken to be that where maximum degree of copper extraction took place, and a log-mean concentration difference was used. Data were correlated by the expression

$$j_D = 2{\cdot}0\left[\frac{Re_{dp}}{(1-\varepsilon)}\right]^{-0.51} \qquad (7)$$

though as can be seen from Fig. 13 the results exhibited considerable scatter Also included on this plot are the equations due to Chu et al [21] and Upadhyan and Tripathi [31] and an indication of the data spread of the latter authors from which it can be seen that the present

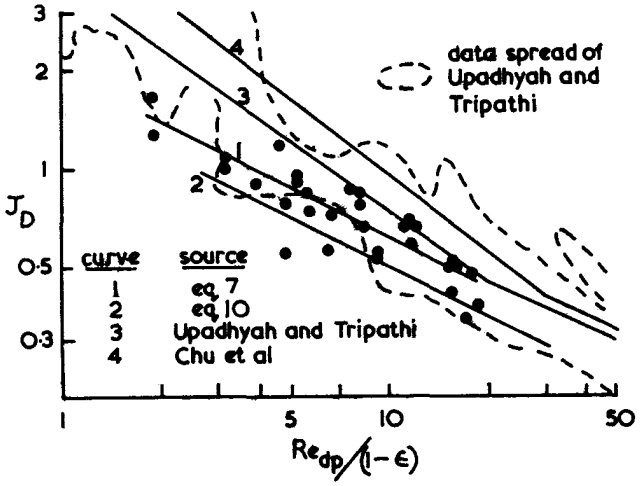

FIGURE 13. Comparison of mass transfer data with other correlations for fluidised beds

electro-chemical results lie toward the lower extreme of this spread.

In order to clearly compare the performance of a conducting bed with a planar electrode or a non-conducting bed, current density factors similar to those proposed by Kreysa [11] et al are helpful. The factor f_c' is defined here as

$$f_c' = \frac{I-I_f'}{A'i_{pl}} \qquad \ldots \qquad (8)$$

and Figure 14 shows values of this parameter as a function of bed potential and illustrates the enormous increase in the current supported by an active bed as compared to that of a plane electrode.

d. Mass transfer for an active bed with batch recycle of electrolyte (Operating mode 3).

These experiments were conducted with a recirculating batch of electrolyte of

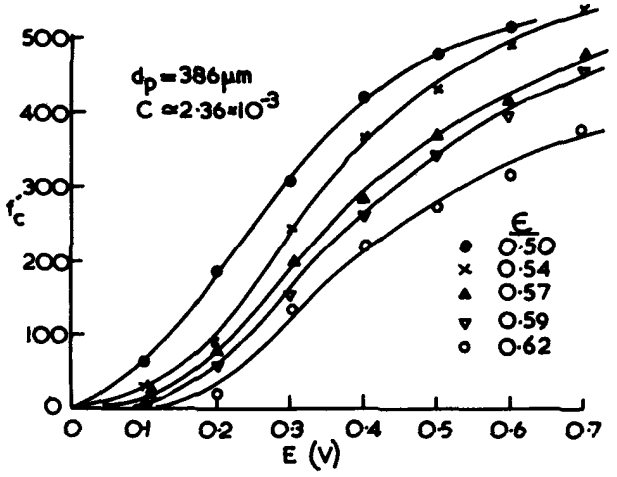

FIGURE 14. Variation of the current enhancement factor, f_c' with potential

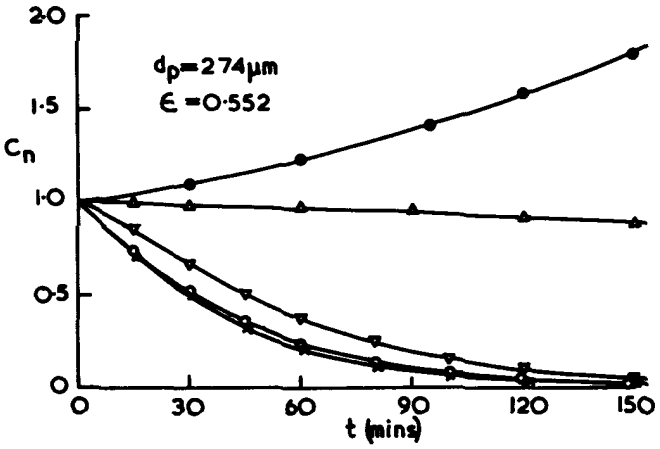

FIGURE 15. Change of normalised concentration with time in batch recirculation

Potential -E (volts) (rel. sat. cal.)

●	Open circuit	○	0·400
△	0·100	X	0·550
▽	0·250		

nominally 10^{-3} M Cu^{++} with an inert anode (Pb grid) at which O_2 evolution took place so that due to the net deposition of Cu^{++} a progressive depletion of the Cu^{++} content of the batch took place. This situation has recently been modelled by Walker and Wragg [32], the equation for the Cu^{++} concentration change with time for diffusion limiting electrolysis with plug flow in the cell being

$$C_i(t) = C_i^o \exp\left(-\frac{t}{\tau}\left[1-\exp\left(\frac{-kAaL}{Q}\right)\right]\right) \quad \ldots \quad (9)$$

More recently, Mustoe and Wragg [33] have shown that the plug flow assumption is reasonable in beds of this type, dispersion effects being small.

The effect of varying cathode potential on the normalised concentration change with time is shown in Fig. 15 where the fact that little change in the rate of depletion occurs as the potential changes from -0·4 to -·55 volts suggests that limiting conditions are approached at the latter potential. (With no applied potential the concentration is seen to rise with time due to spontaneous dissolution.)

The normalised current histories corresponding to the conditions of Fig. 15 are shown in Fig. 16 where it is apparent

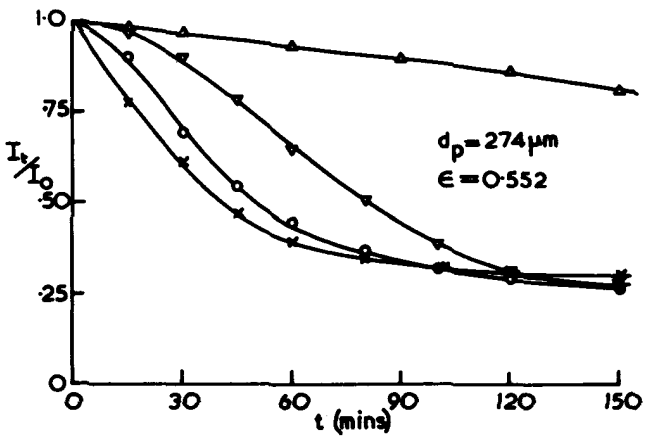

FIGURE 16. Normalised current-time plots for batch recirculation.

	-E(SCE) (volts)		-E(SCE) (volts)
△	0·100	▽	0·250
○	0·400	X	0·550

that a limit is reached at long times where no further fall in I_t occurs. This unproductive (H_2 evolving) current is termed the residual current and in order to take its effect into account further plots were made [22] in terms of the residual corrected and normalised current I_n (i.e. $(I_t-I_r)/(I_o-I_r)$. Since limiting conditions were approached at potentials of E = -·55v a series of experiments were performed at this potential in which the effect of various parameters were investigated. These results will be published in full elsewhere [34] but an example of the c-t behaviour is given as Fig. 17 for a constant voidage of 0·552. From such results and by application of equation (9), the mass transfer coefficient K was evaluated for a number of conditions, results being plotted on Fig. 18 and compared with

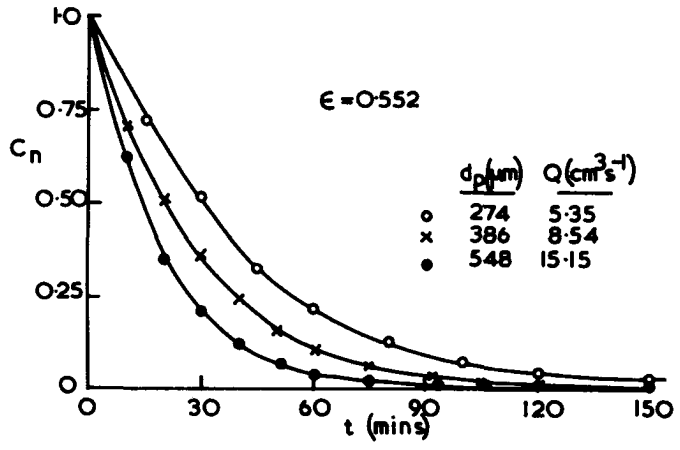

FIGURE 17. Normalised concentration-time curve for batch recirculation at constant voidage.

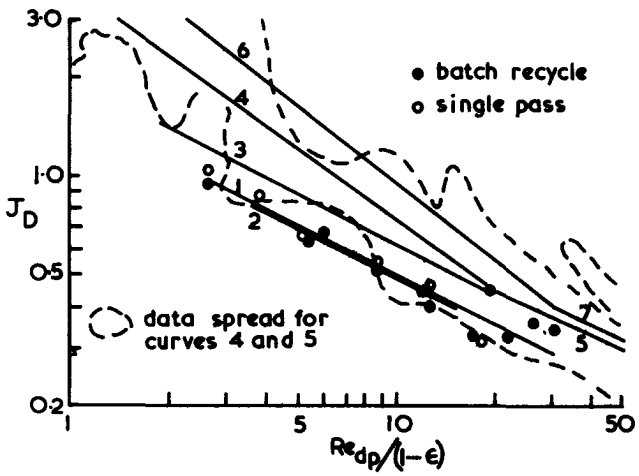

FIGURE 18. Plot of j_D against modified particle Reynolds number for batch recycle and single pass mass transfer results

Curve	Source
1	Equation 10 (present)
2	Equation 11 (Pickett)
3	Equation 7 (present)
4,5	Upadhyay and Tripathi
6,7	Chu et al

the results from the previous section and with the other sources of data discussed earlier [21, 31]. The present data are well described by the equation

$$j_D = 1{\cdot}55\left[\frac{Re_{dp}}{(1-\epsilon)}\right]^{-0.49} \qquad (10)$$

which agrees very closely with the corrected form of an equation due to Pickett [20] which is based on an analysis of the O_2 reduction data of Fleischmann et al [5]

$$j_D = 1{\cdot}52\left[\frac{Re_{dp}}{(1-\epsilon)}\right]^{-0.5} \qquad (11)$$

(Pickett's equation [20] contains an erroneous ϵ deriving from a mis-stated mass balance in the analysis of Fleischmann

and Oldfield [3]). It is apparent that equation (10)indicates lower mass transfer performance than that given by the results of the work in the previous section (equation (7)) where some particle agglomeration may have improved the metal phase conduction.

e. Mass transfer for operation in the once through mode (Operation mode 4)

By operating the cell with once-through flow of catholyte and collecting the Cu^{++}-depleted product, mass transfer coefficients were calculated via the equation (for plug flow)

$$C_o = C_i^o \exp\left(\frac{-kAaL}{Q}\right) \qquad (11)$$

and such values are also included on Fig. 18 where they are seen to agree very well with the results of the previous section. Table 2 shows the percentage extraction achieved during the straight through runs and also includes a projected process time to treat 10 dm^3 of electrolyte so that comparison can be made with the process time necessary to achieve an identical final concentration via batch recirculation. The straight-through mode is seen to give much more favourable process times under the conditions investigated.

ACKNOWLEDGEMENT

One of us, ATSW, wishes to acknowledge the receipt of a grant from the Science Research Council for the duration of much of the work reported here.

NOMENCLATURE

a	Electrode specific surface
A	Electrode area
A'	Active area in direction of current flow
C	Concentration
C_o	Outlet concentration
C_i^o	Initial inlet concentration
C_t	Concentration at time t
C_n	Normalised concentration c_t/c_i^o
d_e	Channel equivalent diameter
d_p	Particle diameter
D	Diffusion coefficient
ε	Bed voidage

Table 2

Comparison of single pass and batch recycle modes

Voidage	% extraction	Single pass mode process time (mins)	Batch recycle mode process time (mins)
0·49	92·9	55	140
0·552	81·4	31	66
0·6	73·2	21	36
0·638	63·8	17	24
0·67	55·8	13	16

E	Electrode potential
F	Faraday number
i	Current density
i_{pl}	current density at feeder electrode alone
I	current
I_f'	feeder limiting current with fluidised electrolyte
I_r	residual current
I_n	normalised modified current $= (I_t - I_r)/I_o - I_r)$
I_t	Current at time t
I_o	Current at time zero
j_D	Mass transfer j-factor
K	Mass transfer coefficient
L	Electrode length
RSC	Potential measured Relative to Saturated Calomel Electrode
Q	Flow rate (volumetric)
Re_{dp}	Particle Reynolds number $(d_p u \rho/\mu)$
Sc	Schmidt number $(\mu/\rho D)$
Sh_{de}	Sherwood number (Kd_e/D)
u	fluid velocity
z	number of electrons exchanged
μ	fluid viscosity
ρ	fluid density
η	current efficiency

REFERENCES

1. Backhurst, J.R., Ph.D. Thesis, University of Newcastle (1967)
2. Backhurst, J.R., Coulson, J.M., Goodridge, F., Plimley, R.E. and Fleischmann, M., J. Electrochem. Soc. 116 (1969), 1600.
3. Fleischmann, M. and Oldfield, J.W. J. Electroanal. Chem. 29, (1971) 211.
4. Fleischmann, M. and Oldfield, J.W. J. Electroanal. Chem. 29, (1971) 231.
5. Fleischmann, M., Oldfield, J.W. and Porter, D.F., J. Electroanal. Chem. 29, (1971), 241.
6. Fleischmann, M., Oldfield, J W. and Tennakoon, L., J. Applied Electrochem. 1, (1971), 103.
7. Goodridge, F., Holden, D.I., Murray, H.D., and Plimley, R.F., Trans. Instn. Chem. Engnrs. 49, (1971), 128.
8. Goodridge, F., Holden, D.I., Murray, H.D. and Plimley, R.F., Trans. Instn. Chem. Engnrs., 49, (1971), 137.
9. Wilkinson, J.A.E. and Haines, K.P., Trans. Instn. Mining and Metallurgy, 81, (1972), 157.
10. Germain, S. and Goodridge, F., Electrochim. Acta, 21, (1976), 545.
11. Kreysa, G., Pionteck, S. and Heitz, E.A. J. Applied Electrochem. 5, (1975), 305.
12. Sabacky, B.J. and Evans, J.W., Metallurgical Transactions B, 8B (1977), 5.
13. Goodridge, F., King, C.H.J. and Wright, A.R., Electrochim Acta, 22, (1977), 1087.
14. Lopez-Cacicedo, C.L., Trans. Instn. Metal Finishing., 53, (1975), 74.
15. Smith, J.W. and King, D.H., Can. J. Chem. Eng., 53, (1975), 41.

16. Carbin, D.C. and Gabe, D.R., Electrochim Acta, 19, (1974), 645.
17. Jottrand, P.R. and Grunchard, F., Symposium on Interaction between Fluids and Particles, Instn. Chem. Engnrs, London (1962).
18. Couret, F., Le Goff, P. and Vergnes, F., in Proceedings Int. Symp. on Fluidisation, Netherlands, Universities Press, (1967).
19. Jagannadharaju, G.J.V. and Venkata Rao, C., Ind. J. Technol. 3, (1965), 201.
20. Pickett, D.J., J. Applied Electrochem. 5 (1975), 101.
21. Chu, J.C., Kalil, J. and Wetteroth, W.A., Chem. Eng. Progress, 49 (1953), 141.
22. Walker, A.T.S., Ph.D. Thesis, University of Exeter, 1977.
23. Mizushina, T., in Advances in Heat Transfer, Vol. 7, (1971), 87.
24. Wragg, A.A., The Chemical Engineer, No. 316, (January, 1977), 39.
25. Eisenberg, M., Tobias, C.W. and Wilke, C.R., J. Electrochem. Soc. 103, (1956), 7.
26. Arvia, A.J., Bazan, J.C and Carrozza, J.S.W., Electrochim Acta, 11, (1966), 881.
27. Wragg, A.A. and Ross, T.K., Electrochim Acta, 13, (1968), 2192.
28. King, D.H. and Smith, J.W., Can. J. Chem. Eng., 45, (1967), 329.
29. Bordet, J., Borlai, O., Vergnes, F. and Le Goff, P., Instn. Chem. Engnrs. Symp. Series 30, (1968), 165.
30. Flett, D.S., Chemistry and Industry. March 13 (1971).
31. Upadhyay, S.N. and Tripathi, G., J. Chem. Eng. Data 20, (1975), 20.
32. Walker, A.T.S. and Wragg, A.A. Electrochim Acta. 22 (1977), 1129.
33. Mustoe, L.H. and Wragg, A.A. J. Applied Electrochem., in press (1978).
34. Walker, A.T.S. and Wragg, A.A. Paper in preparation for J. Applied Electrochem.

THE REMOVAL OF ORGANIC LEAD COMPOUNDS FROM AQUEOUS EFFLUENTS BY ACTIVATED CARBONS IN A FIXED BED COLUMN

A. J. Barker[1]
A. J. Matchett[2]

1. University of Birmingham, Birmingham, England.
2. Burrel Colours Ltd., Stockport, Cheshire, England.

ABSTRACT

Low concentrations of ethyl lead salts can be removed from aqueous solutions containing a high chloride ion concentration by adsorption onto activated carbon. The limiting factor in their removal from aqueous solution is the extent of oxidation of the triethyl lead species to the diethyl lead species in the presence of activated carbon. Supression of the oxidation reaction by pretreatment of the activated carbon by reducing agents such as sodium thiosulphate or sodium borohydride, greatly improves the loading of lead on carbon. Fixed bed column work indicates that by using the pretreatment technique, hundreds of bed volumes of effluent may be treated giving loads of lead on carbon of approximately 1.0% w/w before break-through is reached. The eventual viability of the process for the treatment of large flows of effluent is dependent upon the successful regeneration of the carbon bed.

INTRODUCTION

During the manufacture of tetra-alkyl lead antiknock compounds, an aqueous effluent is produced which contains trace quantities of organic lead salts in an aqueous solution of high chloride ion concentration. Organic lead salts are soluble in the aqueous phase and cannot be removed from solution by pH adjustment followed by precipitation and filtration.

Methods of treatment have been developed which can reduce lead levels in the effluent to less than 5mg/l. For instance, the organic lead salts can be complexed by sodium diethyl dithiocarbamate and removed into the organic phase by solvent extraction (1). Alternatively, they can be reduced by sodium borohydride to the tetra-alkyl and hexa-alkyl dilead products which can then be removed by settlement (2). Both these treatment techniques suffer from the disadvantage that a reagent which itself may be a potential polluant must be added to the aqueous phase to remove the organic lead species.

There is therefore a need to develop a process which avoids this problem and is capable of reducing the organic lead species in aqueous solution to any value which may be required to comply with future discharge limits.

A possible method of achieving this aim is to absorb the organic lead species onto activated carbon in a fixed bed adsorption column. Activated carbons have been used extensively in water purification processes for removing a wide variety of metal ions and organic species at low concentration in solution. They would therefore appear to offer a potentially effective, low cost technique for treating the aqueous effluents containing organic lead alkyls.

SELECTION OF THE ADSORBENT

The activated carbon used in the experimental work was selected from a number of carbons after an extensive series of screening tests. In these tests isotherm data for the activated carbon/triethyl lead chloride system were determined. The adsorption experiments were carried out at 25°C using a neutral solution containing 25mg/l Pb as the triethyl lead salt and 0.083M sodium chloride. During the course of this work it was observed that the isotherm characteristic was dependent upon the extent to which the triethyl lead species were oxidised to the diethyl lead species (3). It was found that the presence of carbon itself catalysed the oxidation reaction to form the diethyl lead ions. This effect was detrimental to the overall loading of triethyl lead on carbon as the diethyl lead species was less readily absorped onto the carbon than the triethyl lead species. When the oxidation of the species was suppressed by adding 0.05M concentration of sodium thiosulphate to the solution, a Langmuir isotherm characteristic was obtained, Fig 1.

When the oxidation reaction was not suppressed, then the isotherm characteristic was unfavourable.

A number of neutral and basic carbons were investigated and from them activated carbon A3/8 was chosen for the packed column work. The properties of this carbon are summarised in Table 1. The specific surface area of the carbon was determined from pressure drop data using the Carman-Kozeny equation.

EXPERIMENTAL

The major aim in the experimental work was to determine the mode of operation of a fixed bed column packed with activated carbon so that its merits as a process for treating the industrial effluent could be established. Hence, in the experimental work particular emphasis was placed upon accumulating data on the break-through times and loading of lead on the carbon. In addition, with a view to scale up, it was anticipated that analysis of the performance data should yield information on the mass transfer and oxidation rates of the ethyl lead species in the column.

Preparation of the column

Before the activated carbon was packed in the column, it was ground and sieved to give material of a suitable particle size, typically 2.5mm. It was then degassed by placing it under water in a vacuum for 24 hours prior to use. This procedure removed air from the pores and prevented the collection of air bubbles in the column. Finally, the carbon was packed into the column under water in order to prevent air inclusion in the bed.

Fixed bed apparatus

The equipment for providing a steady flow of effluent to the adsorption column at a constant temperature is shown in Fig. 2.

The dimensions of the packed section of the column were 23mm diameter x 520mm long and hence when fully packed it contained about 56gm of carbon. The column was surrounded by a water jacket through which effluent was pumped before entering the column so ensuring that isothermal conditions in the column were maintained. There were five sample points down the length of the column through which effluent could be collected periodically for analysis. The column was fitted with quick acting valves so that a step input flow of effluent to the column could be achieved.

Procedure

When the packed column had been fitted to the apparatus it was back flushed to remove any residual air in it. Effluent was circulated from the bulk tank, through the heating coil and column water jacket and back to the tank until thermal equilibrium had been achieved. A step input of effluent was then introduced to the column and samples collected periodically until break-through was reached. These samples were analysed for diethyl lead ions and diethyl plus triethyl lead ions in a solution as the complex diethyl lead 4(2-pyridylazo) resorcinol (PAR) at pH 9 using a Pye-Unicam Sp 8000 spectrophotometer (4).

Three effluent flowrates through the column were selected for study; a laminar flow (Re = 1), flow approaching the transition region (Re = 5), and a turbulent flow (Re = 20). The corresponding volume flows through the packed bed ranged from 0.2ml/s to 4.0 ml/s.

The effects of temperature on the adsorption process were evaluated by carrying out runs at 25°C and 35°C.

Two groups of experiments were conducted. In the first group break-through curves were determined in the absence of reducing agent either in solution or on the carbon. In the second group, the break-through curves were determined when the oxidation reaction for the conversion of triethyl lead ions to diethyl lead ions in the presence of carbon had been suppressed by the use of reducing agents adsorbed directly onto the carbon prior to its use in the column.

In the first group of experiments a standard effluent solution was used containing 10mg/l Pb as triethyl lead chloride and 0.83M NaCl. In the second group of experiments the same standard effluent was used but in addition it also contained 500mg/l of $Na_2S_2O_3$. This latter constituent is usually contained in the industrial effluent at a similar concentration.

RESULTS AND DISCUSSION

Column performance in the absence of pre-treatment of the carbon

A typical set of column break-through curves are shown in Fig. 3 for an effluent containing no reducing agent in solution. The overall shape of the break-through curves were maintained at the high flow-rates but the triethyl lead ion

concentration increased more rapidly and the diethyl lead ion concentration decreased relative to that obtained at the lower flowrates.

The unusual feature about these break-through curves is the concentration plateau that the triethyl lead ions remain at for sometime before tending to a value such that the total organic lead in solution is equal to that at inlet. This plateau concentration represents a temporary steady state between the rate of bulk transport of triethyl lead ions to a point in the column and their rate of removal from solution, by the carbon.

The results from a number of runs were analysed in order to establish the rate controlling process for plateau conditions. For a first order mass transfer mechanism, a plot of log Cp, plateau concentration, against the column length should give a straight line relationship. A good correlation was obtained, but the correlation was equally satisfactory when the results were analysed in terms of a zero order mechanism so this approach did not uniquely define the rate process.

A useful test of the rate controlling mechanism is to plot the plateau concentration against the residence time of fluid in the column. For both zero order and first order models, at equal residence time, equal plateau conditions were not obtained for different flowrates in the column. This is typical of a situation in which liquid phase mass transfer conditions are controlling.

Analysis also demonstrated that the first order reaction rate constant showed little variation with temperature and therefore the conversion of triethyl lead ions to diethyl lead ions by an oxidation reaction was not a rate controlling mechanism at plateau conditions.

Finally, if a mass transfer controlled mechanism exists, there should be a relationship between the apparent mass transfer coefficient calculated from the log/linear plateau gradient and Reynolds number. When the apparent mass transfer coefficient, which is expressed as $\frac{K\,dp}{\alpha\,v}$, was plotted against Re, Fig. 4, a good correlation was obtained.

From the foregoing evidence it was concluded that at plateau conditions, the triethyl lead ions were removed from solution by a first order liquid phase mass transfer mechanism, at a rate proportional to the rate of bulk flow at a particular point in the column.

A similar analysis of the data established that the oxidation of triethyl lead ions to diethyl lead ions conformed to a zero order reaction model. For a zero order reaction, the reaction rate should be independent of the flowrate for similar effluent inlet conditions. Within the limits of experimental error this was found to be the case, Table 2. On the other hand, for a chemical reaction the effects of temperature should be apparent. As seen in Table 2 the reaction rate has almost doubled for a temperature rise from 25°C to 35°C.

The performance of the fixed bed adsorption system under these non reducing conditions was assessed in terms of the bed volumes of solution treated at break-through, load of lead on carbon at break-through, and final load of lead on carbon at exhaustion of the bed. A break-through level of 1mg/l of Pb as organic lead was considered to represent a realistic degree of reduction in concentration for practical purposes. A summary of this performance data for samples taken from the bottom of the column is set out in Table 3. Consistent results from other sample points up the column were also obtained but for the sake of brevity are not included in the table.

The main features of these results is that at break-through, both the loading of the lead on carbon, and volumes of effluent treated are critically dependent upon the flowrate, and hence the residence time of the effluent in the column. The correlation between bed, volumes treated before break-through against residence time is shown in Fig.5. The inference of this plot is that column performance could be improved by increasing the length of the column.

After two of the runs had been completed, samples of carbon were taken from the column well mixed and analysed for total lead. The lead on the carbon was mainly in a form that could be extracted into an acid solution as inorganic lead. Only a small amount of lead was removed into a non-polar solvent. The lead would therefore, seem to exist on the carbon mainly in an ionic form.

From a practical point of view the operating time of the column before break-through was relatively short and the result and loads of lead on the carbon were small. Great advantages could be gained if the column could be operated in the plateau region, including longer run times to break-through, higher lead loads on the carbon and a very stable effluent concentration. None of the runs performed managed to achieve a plateau below the desired break-through level of 1mg/l Pb as organic lead. As

shown in Fig. 6 plateau concentration of trialkyl lead ions in solution decreases in a first order manner with column length and hence residence time of effluent in the column. It should be possible, by increasing column length, to obtain a plateau below 1mg/l Pb as the triethyl lead ion in solution. Unfortunately, the diethyl lead ion concentration in solution increases in a zero order manner with column length such that as the plateau concentration decreases, the diethyl lead ion concentration increases. The net result is that the total organic lead in solution passes through a minimum with column length as illustrated in Fig. 7. It can be shown that at reasonable flowrates for practical column sizing and operation, this minimum is above 1mg/l Pb as total organic lead in solution. Therefore, operation of the column at a break-through of 1mg/l in the plateau region is prevented by the formation of diethyl lead ions in solution.

For the process to be an economic proposition on an industrial scale, improvements in both operating time and *load of lead on the carbon were required.* The most direct way of improving column performance was to eliminate the oxidation reaction which lead to the presence of diethyl lead ions in solution. Comparison of column loads with batch isotherm data, particularly that obtained under reducing conditions suggested that such improvements were possible, (3).

Column performance using activated carbon pretreated with a reducing agent

The pretreatment agents were 1.0M sodium *thiosulphate and 0.1M sodium borohydride* in alkaline solution. Carbon was pretreated by soaking it in a know weight of a standardised solution of the required reducing agent and maintaining the mixture under a vacuum for 48 hours. The uptake of reducing agent on the carbon was then calculated by back titration to determine the residual amount of reducing agent left in the filtrate after the carbon had been separated.

A series of runs were performed at 25°C using a flowrate giving a Reynolds No. of about 1.45. The standard effluent solution was used but in addition to sodium chloride in solution, it also contained 500 mg/l of $Na_2S_2O_3$.

For the purposes of comparison a series of runs were performed using this same effluent in a column packed with carbon which had not been pretreated.

Break-through curves for three sets of conditions are shown in Fig. 8, 9 and 10 and the performance data for the column based on samples taken from the last sample point in the column are given in Table 4.

It is seen by comparing the data in Table 4 with that in Table 3, that by suppressing the oxidation reaction there is an appreciable improvement in the column performance. This point is supported by the break-through data plotted in Fig. 11 when compared to that in Fig. 5. The change in tri- and diethyl lead ion concentrations in solution is shown in Fig. 12 for the three systems investigated. It can be seen that for sodium thiosulphate pretreatment of the carbon, both diethyl and triethyl lead ions in solution are maintained at a low level for a prolonged period of time compared with that which is achieved when untreated carbon is used in the column. Once the level of lead in solution begins to rise subsequent performance of the column tends to that of untreated carbon. The rate of formation of diethyl lead ions in solution and plateau concentrations are then similar to that obtained when *using untreated carbon in the column.*

In the case of column performance using sodium borohydride pretreated carbons, the di and triethyl lead ions are maintained at a very low level for a substantial period from the start of the run. Subsequently, the break-through curves conform to the pattern that is obtained using untreated carbons in the column. This suggests that pretreatment has little effect on column hydrodynamics, but rather it interacts chemically or physico-chemically with the ethyl lead ions and the carbon.

It was found that much less sodium thiosulphate was adsorbed during pretreatment than borohydride inspite of the higher concentration of thiosulphate ions in the pretreatment solutions. The experimental data suggests that the sodium thiosulphate interacts with the carbon surface in such a manner as to enhance its capacity to adsorb triethyl lead ions from solution. The concentration of diethyl lead ions in solution was hardly influenced at all by the presence of this reducing agent and they *eventually became the limiting factor* for break-through.

The action of sodium borohydride on the system appears to be somewhat different to that of sodium thiosulphate. Its action could be interpreted in terms of either a surface based, or solution based mechanism. For a solution based mechanism to be effective the borohydride would have to react with the triethyl lead ions in bulk solution according to

the following stoichiometric equations.

$$8R_3Pb^+ + BH_4^- + 8OH^- \longrightarrow 4H_2O + B(OH)_4 + 4R_3Pb.PbR_3$$

or

$$R_3Pb^+ + BH_4^- \longrightarrow R_3P_b.BH_4 \longrightarrow R_3PbH + BH_3$$

$$R_3PbH + 2H_2O \longrightarrow Pb + 3RH + 2OH^-$$

The fixed bed would simply act as a filter and adsorption medium for the tetraethyl lead and hexaethyl di-lead thus formed. Reduction would cease when all the sodium borohydride had been consumed.

A surface base mechanism would require that the sodium borohydride interacted with the solid surface of the carbon to modify its properties of adsorption and oxidation. There is not conclusive evidence available to differentiate between either of these mechanisms. It is possible that both types of mechanism are operative in the column.

CONCLUSIONS

The work has shown that it is possible to remove ethyl lead salts from an aqueous effluent by adsorption onto activated carbon in a fixed bed column. The economic viability of the process is more difficult to evaluate as it depends upon many external factors as well.

A fixed bed column working with synthetic effluent will give treatment of approximately forty bed volumes before a break-through of 1mg/l Pb for a 10mg/l feed solution. This will give a load of approximately 0.1% w/w lead on carbon. This loading is too low to consider a one cycle use of the carbon, and so regeneration of the carbon must be considered.

Pretreatment of the carbon with reducing agents such as sodium thiosulphate or sodium borohydride, greatly improves column performance. Hundreds of bed volumes may be treated giving loads of 1.0% w/w lead on carbon. Thus, pre-treated carbons offer an effective method of effluent treatment for one cycle but regeneration of the carbon must be sought as the loading of lead on carbon is still too low to consider its disposal. Regeneration of the carbon is crucial to the success of the process. Unless a practical, economic method of regenerating the carbon can be found, then the only potential this process has, is its use for giving a final polish to effluents treated by alternative means.

NOMENCLATURE

K	- 1st order rate const.	s^{-1}
d_p	- particle diameter	m
ρ	- effluent density	kg/m^3
μ	- effluent viscosity	kg/ms
v	- effluent velocity	m/s
α	- bed voidage	
Cp	- plateau concentration	mg/l Pb

ACKNOWLEDGEMENTS

The authors would like to thank the Associated Octel Company for the provision of a research grant and analytical equipment. In particular, we would like to express our thanks to Professor Ellis (Chemical Engineering Department, Birmingham University) and Dr. J.R. Grove and Mr. T. Edmondson (A.O.C.) for their sustained interest in the work.

REFERENCES

1. Barker, A.J., Clarke, A.B. and Ellis, S.R.M., 'The Removal of Organic Lead from Aqueous Effluents by a Combined Chemical Complexing - Solvent Extraction Technique', Advances in Chemistry Series No. 155, 1976, pp.381-395.

2. Lores, C. and Moore, R.B., U.S. Pat. 3,770, 423 Nov. 1973.

3. Matchett, A.J., Ph.D. Thesis, University of Birmingham, 1976.

4. Pollard, F.M., Hasson, P. and Geary, W.J., Anal. Chim. Acta, 20, 26, 1959.

TABLE 1

Properties of the activated carbon adsorbent

Activated carbon	A3/8 Shirley-Aldred Co. Ltd.
Bulk density	0.231 ± 0.042 g/ml
Material density	1.758 ± 0.062 g/ml
Specific surface area	1.57 m^2/g
Size range	3.01 - 1.98 mm

TABLE 2

Rates of oxidation of triethyl lead ions to diethyl lead ions

Run No.	Re. No.	Temperature °C	Zero order reaction rate mg/l.s x 10^{-3}
1	1.5	25	2.21
2	5.5	25	2.92
4	6.7	35	5.33

TABLE 3

Performance data calculated from the break-through curves

Re.No.	Temp. °C	Break through time min	Bed volumes at break-through	Lead removed by carbon mg Pb	Lead removed by carbon at end of run mg Pb	Lead on carbon at end of run % w/w	Analytical estimate of final lead on carbon
1.5	25	1060	79	123	1018	2.15	
5.5	25	22	6	10	683	1.44	
17.5	25	5	4	7	446	.98	0.88
6.7	35	64	17	31	887	1.57	
21.5	35	6	5	8	599	1.26	0.98

TABLE 4

Performance data calculated from the break-through curves

Temp. °C	Re.No.	Break through time min	Bed volume at break-through	Lead removed by carbon mg Pb	Lead on carbon at break through % w/w	Carbon pretreat-ment
25	1.50	723	53	80	0.16	NONE
25	1.4	2659	177	253	0.53	1.0M$Na_2S_2O_3$
25	1.4	3666	264	411	0.87	0.1M$NaBH_4$ in 0.5MNaOH

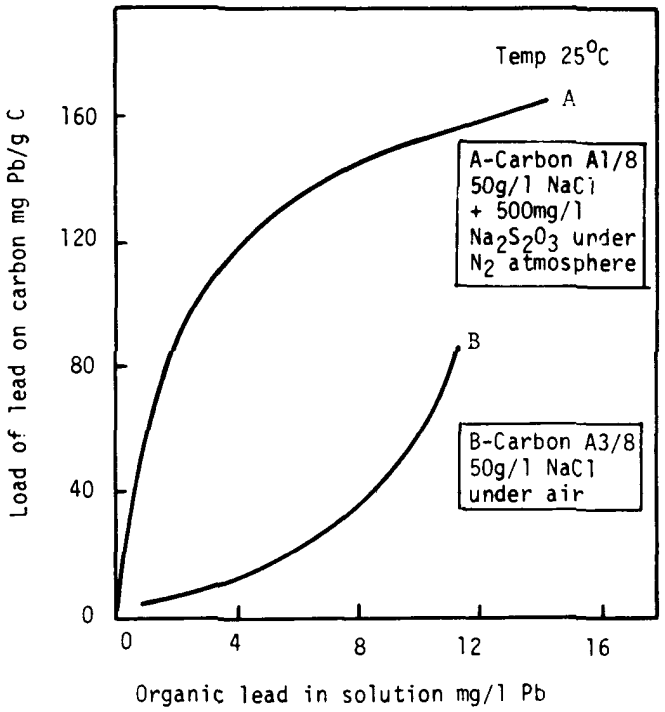

Figure 1 ADSORPTION ISOTHERMS OF TRIETHYL LEAD CHLORIDE ON CARBON

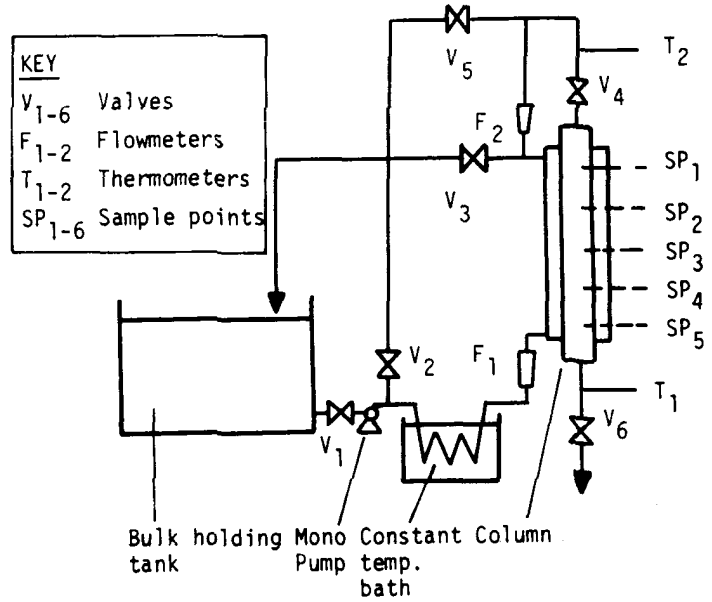

Figure 2 FIXED BED ADSORPTION APPARATUS

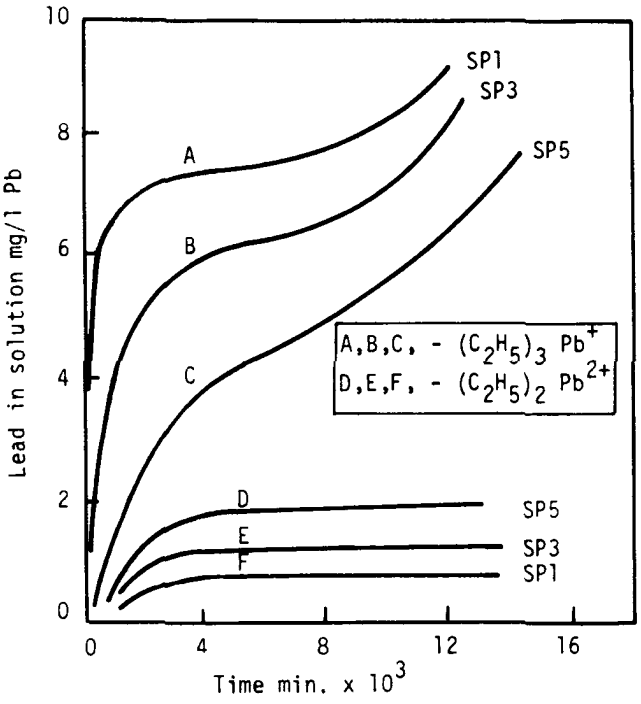

Figure 3 BREAK-THROUGH CURVES FOR THE PACKED COLUMN

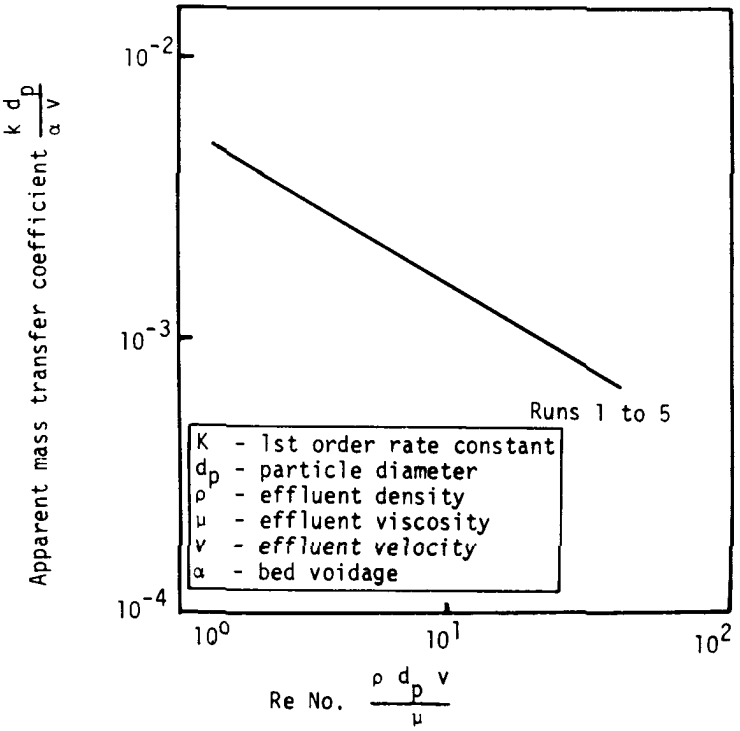

Figure 4 CHANGE IN APPARENT MASS TRANSFER COEFFICIENT WITH REYNOLDS NUMBER

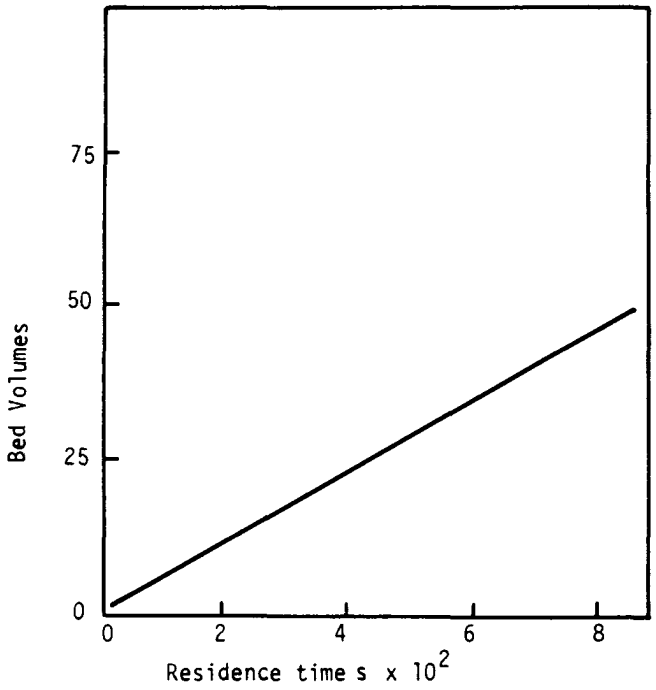

Figure 5 BED VOLUMES TREATED BEFORE BREAK-THROUGH

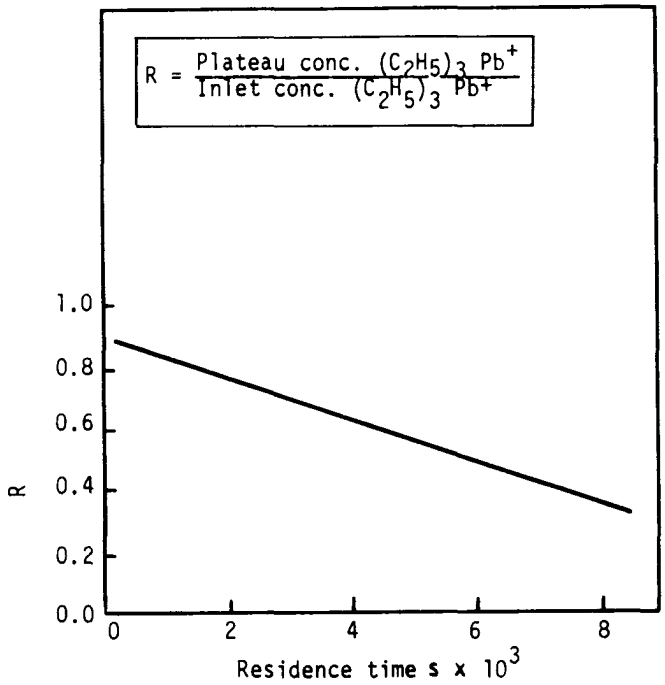

Figure 6 CHANGE IN CONCENTRATION OF TRIETHYL LEAD IONS IN THE COLUMN WITH RESIDENCE TIME

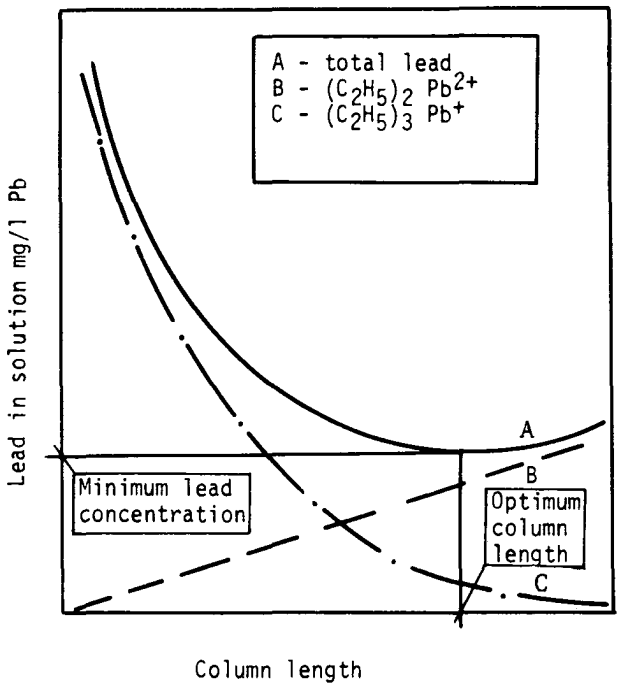

Figure 7 VARIATION OF LEAD CONCENTRATION WITH COLUMN LENGTH AT PLATEAU CONDITIONS

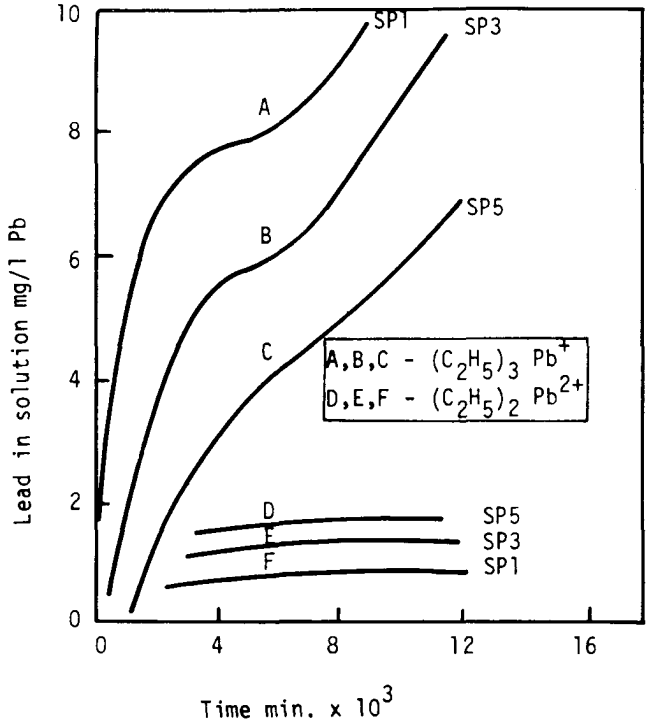

Figure 8 BREAK-THROUGH CURVES FOR THE PACKED COLUMN - NO PRETREATMENT OF THE CARBON

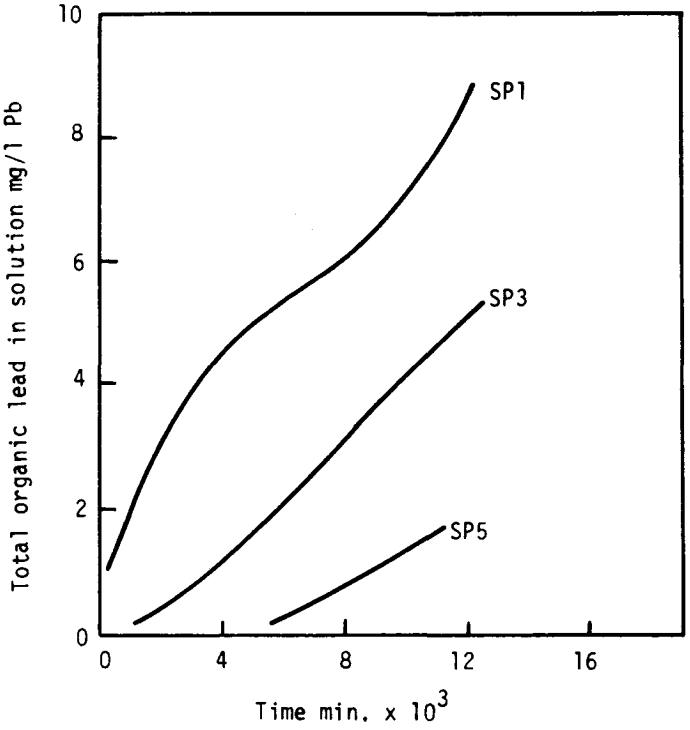

Figure 9 BREAK-THROUGH CURVES FOR THE PACKED COLUMN. CARBON PRETREATED WITH $Na_2S_2O_3$

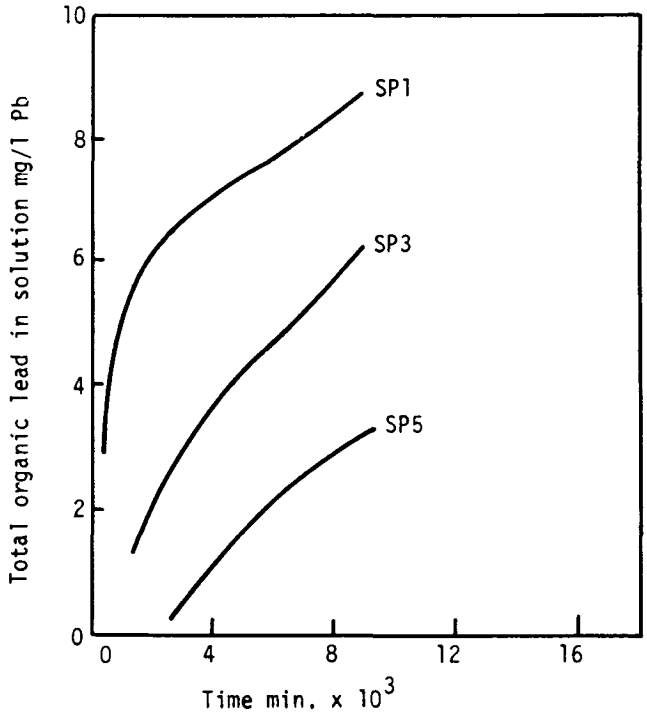

Figure 10 BREAK-THROUGH CURVES FOR THE PACKED COLUMN CARBON PRETREATED WITH $NaB\ H_4$

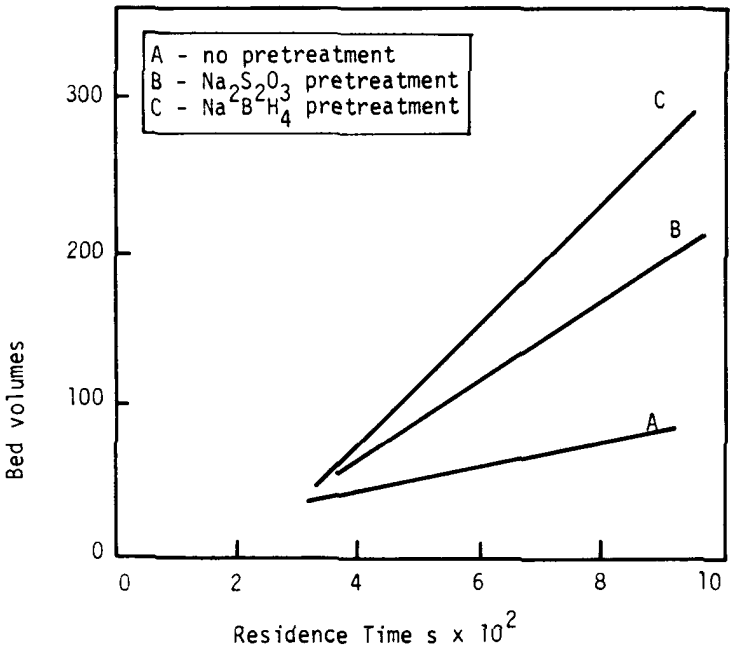

Figure 11 BED VOLUME TREATED BEFORE BREAK-THROUGH

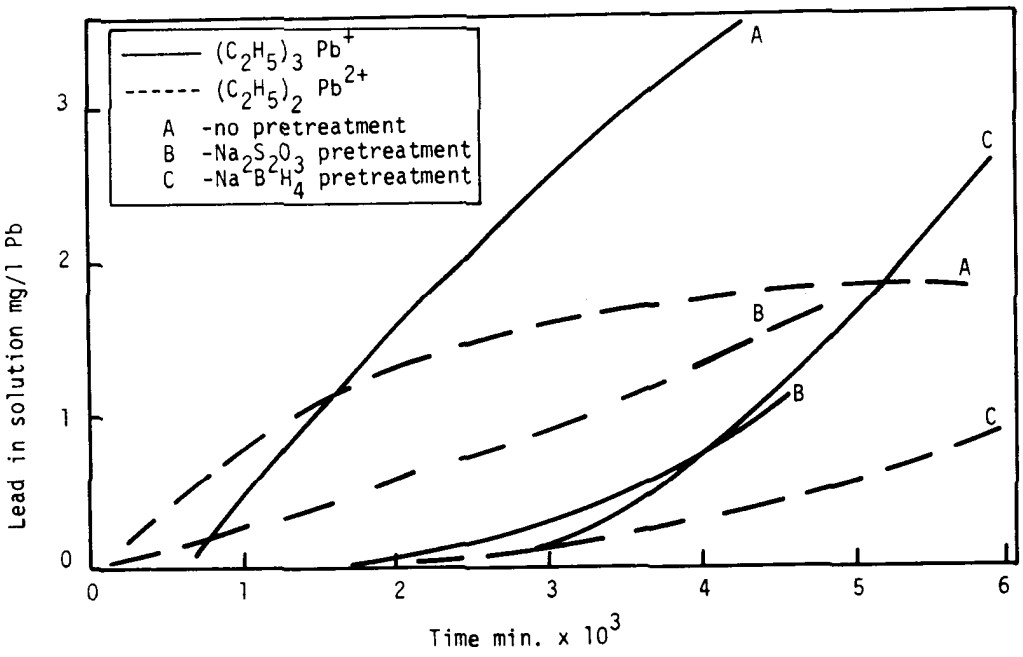

Figure 12 INITIAL PARTS OF THE BREAK-THROUGH CURVES FOR THE PACKED COLUMN SHOWING A COMPARISON IN PERFORMANCE OF TREATED CARBONS WITH UNTREATED CARBONS

FACTORS AFFECTING THE FOULING OF HEAT EXCHANGER SURFACES

T. R. Bott

University of Birmingham, Birmingham, England

ABSTRACT

The fouling of heat exchangers is one of the least understood industrial problems. A number of factors affect the laying down and accumulation of dirt or scale on a surface including time, fluid velocity, character of the surface and foulant concentration. In some instances the effects of certain variables such as velocity, may be contradictory. Further work on the effects of these factors needs to be done before a proper appreciation of their significance can be established.

1. INTRODUCTION

Fouling of heat exchanger surfaces remains one of the least understood phenomena in the process industries in spite of its wide occurrance, largely on account of its complexity. In recent years however, fouling has attracted the attention of a number of research workers who are attempting to analyse fouling with the object of being able to make a more realistic approach to prediction for design purposes.

Furthermore, quite apart from the costs involved, the energy crisis facing the world makes it imperative that the maximum use is made of the fuel available. The fouling process represents an inefficiency in the utilisation of energy.

2. THE CLASSIFICATION OF FOULING

It is useful to classify fouling as a basis for discussion; five broad areas of fouling are generally recognised.

1. Deposition from solution may occur during heating or cooling of saturated solutions. Normal solubility, i.e. deposition on reducing the temperature of a saturated solution or inverse solubility, i.e. deposition on raising the temperature of the solution may be involved.

2. Corrosion of the surface is possible in many situations ranging from mild attack to aggressive conditions between process fluid and transfer surface. The subject is as wide as corrosion technology itself.

3. Fouling involving a chemical reaction is possible where suitable conditions are present e.g. in organic liquid vaporisers working at high temperature when cracking and subsequent coking could occur. In processes involving molecules capable of polymerisation, conditions at the heat transfer surface may cause a polymer layer to be formed.

4. Particulate deposition is likely where solid particles are present or formed in process fluid streams e.g. particles of rust circulating in a boiler system.

5. Biological fouling involves the deposition and usually growth,of living organisms on a heat transfer surface.

One or more of these arbitary definitions may be involved in a single fouling occurrance although in many instances one mechanism will be dominant.

In basic terms the fouling process involves the movement to and from the heat transfer surface of a substance which may or may not constitute the actual deposit. For instance the growth of a biological film may depend upon the movement of nutrients to the organisms on the transfer surface and the removal of waste products rather than the transfer of the biological material itself. In fouling from corrosion, the development of the corrosion layer will depend upon the transfer of the corrosion agent to the surface and the subsequent removal of possible products of reaction to leave behind the corrosion deposit.

3. FACTORS AFFECTING THE FOULING PROCESS

A number of factors which affect the fouling process can be identified.

3.1 Time

The effect of time on the fouling process is rather obvious; in general terms the longer the time the greater the exent of the fouling. Figure 1 shows two idealised curves.

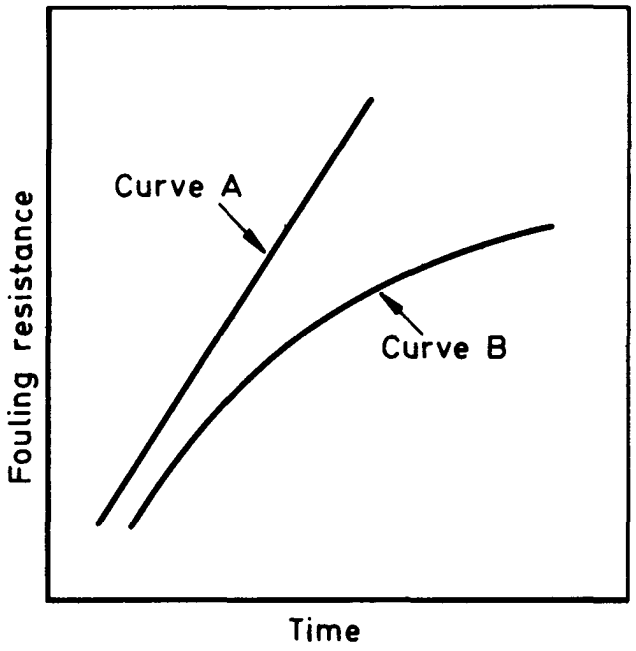

Fig. 1 Two idealised fouling curves.

In curve A the fouling resistance is proportional to time; this type of fouling is often associated with deposits occuring in evaporators and boilers. In general the fluid from which the deposition occurs is relatively slow moving.

Curve B is an idealised curve for many situations. As the deposit thickness increases, the flow area becomes restricted so that for a given mass velocity, the flow velocity increases. In the case of heavy deposition the increase in velocity can be considerable. Under these conditions the fluid shearing force acting on the deposit increases. For many deposits, other than hard tenacious deposits (those possibly associated with curve A for instance), the increased shearing force removes deposit until an equilibrium is reached when:-

The deposition rate = The removal rate

Under these circumstances there is no further increase in deposit thickness with time and the fouling resistance remains constant.

The equation describing the fouling process has an asymptotic form (1).

$$R_{f\theta} = R_{f\infty} (1 - e^{\beta\theta}) \quad \ldots\ldots (1)$$

and represents a simplified model of the fouling process

where $R_{f\theta}$ = fouling resistance at time θ

$R_{f\theta}$ = resistance at time = ∞ (ie. when equilibrium has been reached)

θ = time

β is a constant depending upon the system.

It should be emphasised that although equilibrium is established, and theoretically the heat exchanger can operate in this condition, two important consequences obtain.

1. The capacity of the equipment to transfer heat is reduced and it may not fulfill its required function,

and probably much more important,

2. The pressure drop through the exchanger due to the increased velocity may become intolerable due to high pumping costs and operating problems.

3.2 Velocity

Some aspects of velocity have already been discussed in connection with the long term properties of fouling, but velocity has an important effect in the short term due to the effects of the laminar layer and mass transfer. High velocity may not always result in lower deposition rate since under these conditions the laminar layer is relatively thin which represents a reduced resistance to mass transfer. Any deposition which depends upon diffusion to the surface therefore, is increased with increased velocity.

In some respects the effects of velocity are contradictory - high velocity increases the shear forces and the removal rate whereas high velocity can also represent a greater deposition rate with increased mass transfer

3.3 Concentration of foulant or deposit precurser

In general higher concentrations of foulant in the fluid stream lead to higher rates of deposition. In other systems, such as biological fouling the concentration of nutrients is important.

In certain situations the concentration of impurities in a process stream, which react at the transfer surface to produce a heat resistant layer, will be important.

3.4 Temperature

The temperature, particularly at the transfer surface, may be an extremely important parameter in particular systems. At one temperature fouling may not be a problem, but the same process fluid at a higher temperature can give rise to substantial fouling. A number of different effects can be noted:-

1. The effect on solubility. Under normal solubility conditions where the process fluid is being cooled deposition is likely if the temperature is lowered below the saturation temperature. The exact location of the saturation temperature eg. in the bulk fluid, in the laminar layer or at the heat transfer surface, will influence the mechanism of deposition. If saturation occurs outside the laminar layer the deposition is likely to involve particle diffusion to the surface. If the layers near the surface in contact with the fluid are cooled to saturation, crystallisation may actually occur on or near the surface.

Deposition from solutions containing salts with inverse solubility is highly probable when such solutions are being heated, as may happen in evaporators. The layers of fluid near the fluid/solid interface will be the hottest and will give rise to deposition if the saturation temperature is reached or exceeded.

2. The effect on chemical reaction. Some fouling problems are the direct result of a chemical reaction eg. Polymerisation or cracking. In certain situations the transfer surface may act as the catalyst. It is well known that many chemical reactions are sensitive to temperature and therefore the fouling rate is likely to be dependent on temperature. An organic vapouriser using steam as the heating medium may operate without fouling problems. If, however, for heat conservation reasons, the varpouriser is placed in a hot flue gas stream the resulting high surface temperature may give rise to cracking reactions and soot formation on the transfer surface. Similarly a stream containing a polymerisable material, even if only in small quantities, may give rise to little difficulty at low temperature but at higher operating temperatures a hard polymeric deposit may form on the heat transfer surface.

3. The effect on biological systems. Biological systems are sensitive to temperature and therefore the rate of growth on a heat transfer surface will be very dependent upon temperature. At low temperature biological activity is supressed and at high temperature (say in excess of 100°C) the cells are killed. Between the extremes there is an optimum for maximum biological growth (often around 40°C). Provided that other conditions are maintained, such as nutrient or dissolved oxygen concentration, high rates of growth are likely if the heat transfer surface is near to the optimum; unfortunately these are the conditions likely to be encountered in cooling water systems.

4. It is generally not appreciated that temperature can have a profound effect on the nature of the deposit. A deposit which is loose and open structured, easily removed by low velocity, can become hard and difficult to remove at high temperature. Problems of this kind can produce operating difficulties in process plant subject to temperature fluctuations. In other situations long exposure to the effects of temperature results in a deposit which is difficult to remove.

3.5 Physical properties of the process fluid

The physical properties of the process fluid are important in so far as they contribute to the level of turbulence and mass transfer processes, according to the usual relationships.

3.6 The condition of the transfer surface

The initial state of the heat transfer surface onto which the foulant deposits may have an effect on the deposition rate, at least until the surface becomes fully coated with changed properties. A highly polished or smooth surface may be inhospitable to the scale or deposit but a rough surface may assist the deposition process. A rough surface may help to create turbulence which influences the laying down of a deposit; disturbance of the laminar layer may provide increased opportunity for diffusion to the surface to take place. In addition the roughness may provide sites suitable for deposition and growth and may help to key the deposit to the surface thereby making the deposit difficult to remove.

As a deposit becomes established on the surface the nature of the surface in contact with the process fluid is likely to change. It is possible

for instance, to obtain increased roughness in comparison with the original transfer surface which in turn influences the level of turbulence with secondary effects such as higher rates of deposition and possibly heat transfer.

3.7 The design of heat exchangers

Good mechanical design can to some extent at least, reduce the incidence of fouling. Good design is often a matter of experience in particular heat transfer situations and generally calls for a "well swept" transfer surface avoiding problems of sedimentation qualified by the points already discussed in relation to velocity. In addition the foregoing points regarding temperature of operation can be considered although the designer generally has little opportunity to make changes as with many of the other factors affecting deposition, such as concentration of foulant and physical properties of the fluid.

3.8 The operation of heat exchangers

The way in which a heat exchanger is operated in service can influence to a large degree, the extent of fouling. Even a well designed heat exchanger can lead to deposition problems if it is not operated as the designer intended. It is clear that substantial changes in velocity or temperature of operation could well lead to accelerated fouling. Even short periods at changed conditions can produce high accummulations of deposit which are not easily removed when normal operating conditions are resumed. Interruptions in flow can be particularly difficult where relatively high temperatures are involved; the deposit may change its form and become hard and difficult to remove or fouling may be apparent due to cracking or some other chemical reaction, when it is not generally present.

4. THE EFFECT OF FOULING ON HEAT TRANSFER AND ITS PREDICTION

It is generally appreciated that the result of fouling is to reduce the value of the overall heat transfer coefficient for a given set of conditions. The overall effect may be summarised (2) by the following.

Change in heat transfer coefficient = change due to the conductivity of the foulant
+ change due to the roughness of the foulant
+ change due to the change in Reynolds No.

Although this statement is a true description of the effects of deposits and the fouling process, the real problem is determining the individual effects.

A number of mathematical models to explain the fouling process and its effect on heat transfer have been devised (3) but except in very special situations they are not universally applicable. A great deal more research needs to be carried out on the fundamentals of the fouling process before satisfactory models can be established. A reliable model would of course, be invaluable in predicting the effects of fouling in particular designs, and may provide the opportunity to design heat exchangers which would operate satisfactorily without cleaning, provided the attendent pressure drop could be tolerated.

5. THE RESULTS OF SOME FOULING STUDIES

The following results of fouling studies have been selected to demonstrate the wide range of different effects possible.

5.1 Deposition of wax from waxy hydrocarbons

One of the common problems in the oil industry is the deposition of wax from solution in hydrocarbons onto cooled surfaces. Experiments to investigate the problem have been made using paraffin wax/kerosene mixtures (4,5): In general the fouling process is rapid resulting in fluctuating heat transfer resistance about an equilibrium value. The fluctuations are considered to be the result of alternate partial shedding of the deposit followed by its re-establishment.

Figure 2 shows that increasing the wax concentration increases the level of deposition.

5.2 Deposition of silica from geothermal water

With increasing interest in alternative energy sources the utilisation of energy derived from geothermal sources is becoming important. One of the attendant problems is the deposition of dissolved solids onto heat transfer surfaces. At the high temperature and pressure associated with deep geothermal wells the hot brine is supersaturated when it is brought to the surface, the pressure reduced and heat extracted. The changed conditions can give rise to excessive deposition in the heat extraction equipment.

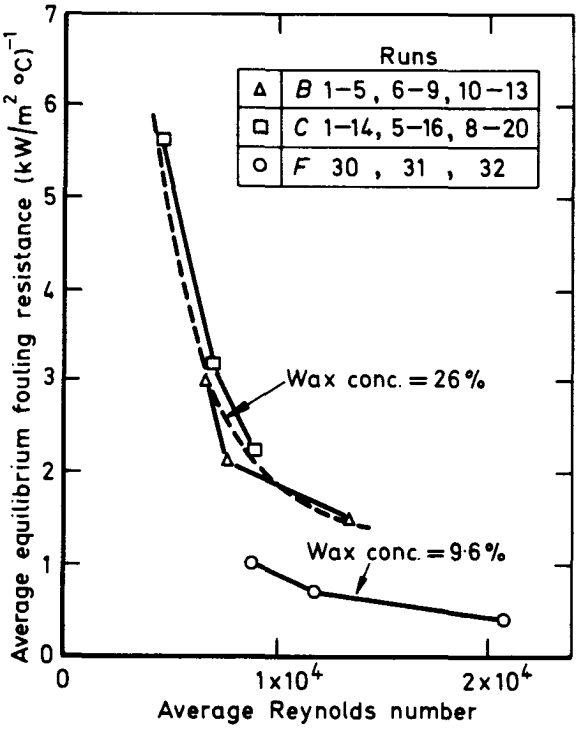

Fig. 2. The effects on wax deposition on a cooled surface with concentration (6).

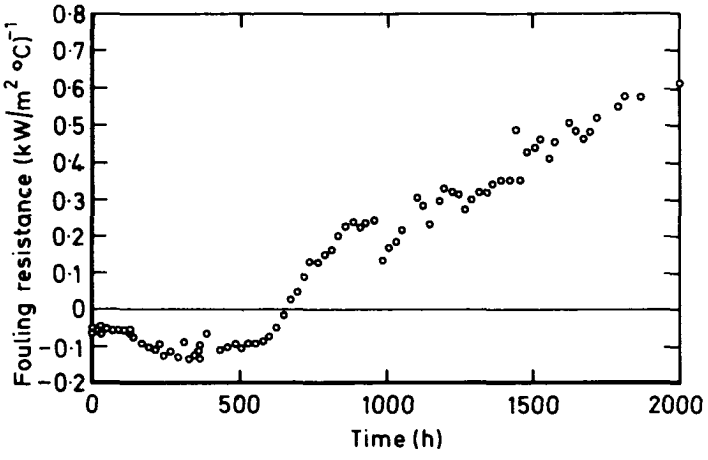

Fig. 3. The change in heat transfer resistance with time in a geothermal system (7).

Figure 3 shows the effects of silica deposition on a cooled simulated heat exchanger tube on field trials in Iceland (7). Initially the heat transfer resistance falls due to the enhancement of heat transfer resulting from increased turbulence within the flowing brine solution. The increase in turbulence is the direct result of the increased roughness of the deposit in comparison with the original heat transfer tube. After a period of time the beneficial effects of the turbulence are overtaken by the increasing thickness of the deposit and the heat transfer resistance increases with time. Even after 2000 hours there is no evidence that the resistance has reached an equilibrium value.

5.3 The deposition of magnetite in simulated boiler water systems

Particulate deposition has been studied using magnetite particles suspended in water passing through simulated heat exchanger tubes (5). An x-ray technique to examine the thickness of the deposit in situ has been devised. The preliminary results show a gradual build up of the deposit thickness with time with an apparent approach to a steady state condition, (see Fig. 1). The particle size was in the range 1-10 μm and the mean water velocity was of the order of 5 m/s.

5.4 The deposition and growth of biological films

Experiments have been conducted to investigate the growth of *E. Coli* on heat transfer surfaces (8). The results obtained at different velocities in the turbulent regime are shown in Figure 4.

The data show that an increase in the Reynolds number by a factor of 2.5 promoted a decrease in slime thickness by almost a similar factor (245-100μm).

Figure 5 shows the remarkable effect of temperature on the thickness of slime developed. A temperature difference of 5°C (30°C to 35°C) promotes an increase of almost 70% on slime thickness. It is to be noted that the optimum growth for the *E. Coli* is near 37°C (10).

CONCLUSIONS

Many factors contribute to the development of a foulant layer. Although certain trends can be observed and appreciated, a great deal more fundamental work needs to be carried out in order to establish the true mechanism of

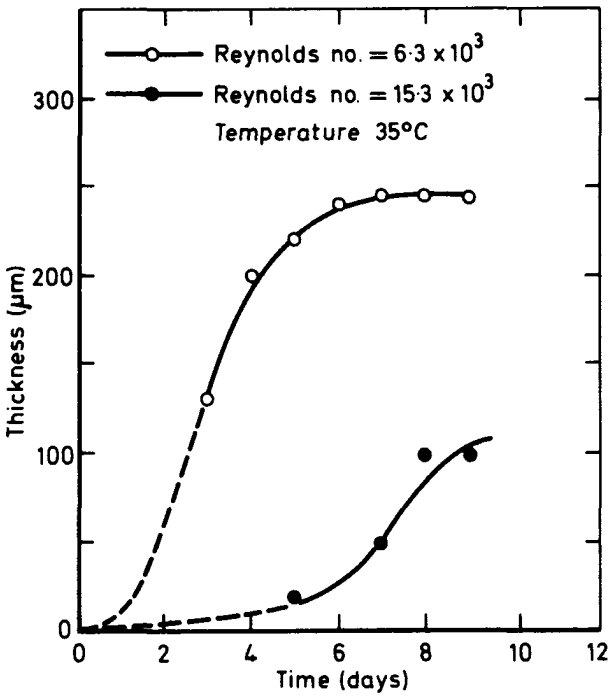

Figure 4. The effect of velocity on slime thickness (9)

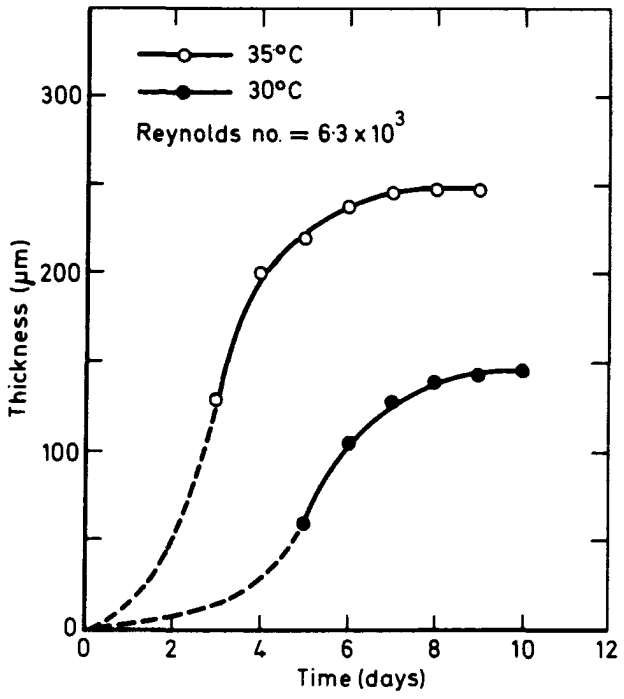

Figure 5. The effect of temperature on slime development (9)

the fouling processes before substantial improvements in heat exchanger design and efficiency can be obtained. In addition improved knowledge will suggest ways in which the fouling process can be reduced or eliminated.

NOMENCLATURE

$R_{f\theta}$ = fouling resistance at time θ.
$R_{f\infty}$ = resistance at time = ∞ (ie. when equilibrium has been reached).
θ = time.
β is a constant depending upon the system.

ACKNOWLEDGEMENT

The author would like to record his appreciation of the work of his colleagues Manella Pinheiro, Rob Walker, Jon Gudmundsson and Derek Harty, and for many interesting discussions.

REFERENCES

1. Kern, D.Q., and Secton, R.E. Brit. Chem. Eng. 4, 258, 1959.
2. Bott, T.R., and Walker, R.A., Chem. Engr. No. 255, 391, 1971.
3. Taborek, J., et al, Chem. Eng. Prog. 68, No. 2, 59, 1972.
4. Walker, R.A., Ph.D. thesis, Birmingham University, 1973.
5. Gudmundsson J.S., Ph.D. thesis, Birmingham University, 1977.
6. Bott., T.R., and Gudmundsson, J.S., Can. J. Chem. Eng. 55, 381, 1977.
7. Gudmundsson, J.S., and Bott, T.R., Inst. Chem. Engrs. Symposium Series No.48 Energy in the 80's, 1977.
8. Pinheiro, M.M.V.P.S., M.Sc. thesis, Birmingham University, 1976.
9. Bott T.R., and Pinheiro M.M.V.P.S., Can. J. Chem. Eng. 55, 473, 1977.
10. Butlin K.R., Blakebrough, N., Ed. "Biochemical and Biological Engineering Science". Academic Press London, 1967.

MANAGING ENERGY AND WATER WITH EVAPORATIVE RECYCLING COOLING SYSTEMS

G.A. BIRCHALL

DEARBORN CHEMICALS LIMITED

Most industrial manufacturing processes consist of a series of interlinked stages, each of which demands either energy input or energy removal, in order to progress to the succeeding stage.

If a process does not obtain energy input or removal at the designated rate the efficiency of the stage, and consequently of the whole process, is inevitably impaired.

Ideally all points of energy excess should be linked to points of energy requirement, and this principle is used very effectively in such plant as boiler feed-water economisers, waste heat boilers and certain types of district heating schemes.

For most industrial processes however it is not at present a realistic proposition to utilise process energy excess in this way, and the most widespread practical solution to the need is to divert such excesses to a cooling-water system.

Cooling Water Systems therefore provide industry with a convenient method of managing energy, by extracting surplus heat at the selected stage of the manufacturing process.

Large volumes of cooling water are utilised throughout industry, notably by those processes which require close energy control after individual stages of manufacture, especially where large throughputs are involved. Examples are the steel and chemical industries, and of course electricity generation.

As water-costs have risen (See Figure 1) so has the trend towards water-conservation, by the re-cycling of cooling water over cooling towers.

The evaporative cooling water system is, therefore the key to the efficient management of energy and water. Consequently their design, and the manner in which they are operated, can have a very significant bearing on production and water costs.

Early designs of such systems tended to employ oversized towers and heat-exchangers, which were wasteful of materials, energy and water. In recent years however, a growing awareness of the need to conserve resources has led not only to more widespread use of cooling towers, but also to improvements in their design. Modern compact high-performance units use the cooling medium more efficiently, and feature smaller water volumes, narrower waterways and higher temperatures.

Unfortunately, many cooling systems are still subjected to outmoded and frequently haphazard methods of operation and water-treatment.

There is a failure to recognise on the part of many operators, that modern cooling plant demands improved control standards, not only to fully realise its high-efficiency potential, but to avoid thermal and mechanical troubles, which can have serious disruptive effects on production.

Adequate control of these systems need not involve high capital expenditure but usually simply requires an awareness of, and willingness to employ, up-to-date water-treatment and control procedures.

Mis-management of these systems means no less than the squandering of energy and water resources.

(1) ENERGY WASTAGE

Energy wastage can be considered from two aspects:-

(a) Wastage of the primary energy used to fuel the industrial process. This occurs when heat contained in the process medium is inadequately removed by the cooling medium. When this happens the process medium is unprepared for the next stage in the production process, which usually means that there is loss of product throughput. The process of distillation is perhaps easiest to visualise in this way, although it is in fact true of any industrial process which requires but does

not get, effective energy removal at a particular stage.

(b) Wastage of the power used to operate the cooling system. A cooling system which is not operating efficiently is wasting the power used to operate the water circulation pumps and tower fans (where these are fitted).

Indeed under certain circumstances (to be discussed later) power costs can actually rise sharply when cooling is ineffective.

Causes of Energy Wastage

Given a correctly designed system, the basic cause of energy wastage by evaporative cooling water systems is the presence of fouling deposits. These arise from several sources, which will be considered later, as first we should look at the effect of these deposits at various stages in the cooling process.

(a) The Effect of Fouling at the Cooling Tower

Cooling Towers are designed to dissipate the heat which has been taken up by the circulating water at the heat exchangers. It can be seen therefore that cooling towers are themselves a specialised form of heat-exchanger.

Warm water returning from the heat exchangers is cascaded down the cooling tower, meeting a stream of air travelling in the opposite direction.

Since most of the heat loss takes place by the evaporation of water at the air/water interface, towers are designed so as to maximise the water surface area presented to the air stream. The rated cooling efficiency of a particular cooling tower is based therefore on the maintenance of an optimum water surface area/air ratio.

Towers incorporate distribution troughs to spread the incoming water evenly across the packing, the latter being designed to induce the cascading water to form either thin films or small water droplets, which continuously break up and re-form.

The presence of fouling debris in the distribution troughs and on the tower packing interferes with the formation of these water films or droplets, thereby reducing the water surface area presented to the air stream.

Fouling on the tower packing increases resistance to the passage of air through the tower. Air throughput is thereby reduced and this again adversely affects the water/air ratio.

A badly-fouled cooling tower, therefore, will operate at a reduced thermal efficiency, with the result that over-warm water will be discharged from the tower sump to the heat exchangers.

(b) The Effects of Fouling At the Heat Exchanger

Heat exchangers are usually either 'shell-and-tube' or 'plate' type, designed to transfer heat from the process medium to the circulating water.

The principal factors which govern the effectiveness of this transfer of heat are:

(1) The degree of resistance to the passage of heat by:

(a) The process medium.
(b) The material of construction of the heat exchanger.
(c) The cooling medium.

(2) The area available for the transfer of the heat - this is normally termed the heat-transfer surface area.

(3) The difference in temperature between the process medium and the cooling medium.

Fourier expressed this in the form of the classical equation:-

$$Q = U. A. \triangle T$$

Where: Q = The Total Heat Flow.
U = The Overall Heat-Transfer Co-efficient.
A = The Heat Transfer Surface Area.
$\triangle T$ = The Temperature Differential between Process and Cooling Medium.

It can thus be readily seen that if over-warm water is circulated through the heat exchanger the value of $\triangle T$ will decrease and hence so will the value of Q, thus the design heat flow from process medium to cooling water will not be achieved.

The Overall Heat Transfer Co-efficient (U)

U is defined as the reciprocal of resistance to heat-transfer, so:

$$U = \frac{1}{R}$$

In other words the lower the resistance of any heat-exchanger system to the passage of heat, the greater will be the value of U, the overall heat transfer co-efficient.

In a clean heat exchanger the overall heat transfer co-efficient U is a combination of:

(a) The individual heat-transfer co-efficient of the process medium (h_1).

(b) The thermal conductivity of the tube wall (k).

(c) The individual heat-transfer co-efficient of the cooling medium (h_2).

This is conventionally expressed by the equation:

$$\frac{1}{U} = \frac{1}{h_1} + \frac{L}{k} + \frac{1}{h_2}$$

where L = thickness of the tube wall.

However, fouling deposits in heat-exchangers create an additional resistance to heat transfer, and this 'fouling factor' $\left(\frac{L_f}{k_f}\right)$ has to be inserted in the equation defining the overall heat transfer co-efficient. Thus for a heat-exchanger tube, fouled on one side of the tube, the heat-transfer co-efficient expression is modified to:

$$\frac{1}{U} = \frac{1}{h_1} + \frac{L}{k} + \frac{L_f}{k_f} + \frac{1}{h_2}$$

It can been seen from the modified equation that the lower the thermal conductivity (k_f) of the fouling deposit, and/or the greater the thickness of the fouling deposit, then the greater will be the value of $\frac{1}{U}$, that is, the greater will be resistance to heat transfer.

In fact, fouling deposits exert an affect on the overall heat transfer co-efficient out of all proportion to their thickness, due to the huge disparity between the thermal conductivity of a typical foulant and that of the tube metal. Table 1 compares the thermal conductivities of a number of conventional fabricating materials with those of typical fouling materials.

Table 2 illustrates how even very thin scale deposits cause a marked reduction in overall heat transfer co-efficient (U). The very large extent by which the heat-transfer surface area (A) would have to be increased to maintain the quantity of heat flow (Q) obtainable with a clean tube is highlighted in the last column of Table 2.

It is of course impractical to increase the heat-transfer surface area of a heat-exchanger, so the inevitable result of fouling is always a pronounced decrease in the total heat flow from process to cooling water.

It is standard practice for heat-exchanger manufacturers to incorporate a 'fouling factor', based on 'experience', when specifying equipment for particular cooling duties. In other words a deliberate degree of oversizing is practised, to compensate for the anticipated reduction in the overall heat transfer co-efficient due to fouling of the heat-exchanger surfaces.

When these 'fouling factors' are generous, as used to be the case, then the heat-exchanger can indeed tolerate a modest degree of fouling without seriously affecting product output. However, heat-exchanger manufacturers are not immune from the same economic pressures which affect the rest of us, and consequently much modern equipment is designed with very low fouling tolerances.

This means that the cooling tower operator can no longer afford to tolerate the slightest degree of fouling. Absolutely clean heat-transfer surfaces need to become the norm, and the tower operator must ensure that he is using the most technologically advanced approach to water treatment, which is designed specifically for the job. Too many modern plants are attempting to maintain efficiency with traditional treatments which are no longer capable of meeting today's more stringent requirements. A glance at Table 2 shows that any deposition which is even slightly in excess of that anticipated by the 'fouling factor' will result in a dramatic reduction in the rate of removal of heat from the process-side.

Under such circumstances, the cooling system will be unable to carry out its basic function of controlling the energy level at a critical point in the manufacturing process. The nett result will inevitably be a loss of production and a consequent wastage of the primary energy used to fuel the manufacturing process.

(c) The Effects on Pumping Costs

Fouling in the cooling system reduces the effective diameter of pipes and tubing, which results in an increase in system head pressure according to the equation for turbulent flow:

$$\triangle F + \frac{4 f G^2 L}{2 g \rho^2 D}$$

Where $\triangle F$ represents the pressure loss in a pipe expressed as ft. of liquid.

f = the friction factor

G = the mass flow velocity lb/(hr)(ft^2)

L = the length of the pipework (ft.)

g = acceleration of gravity ft/hr^2

ρ = the density of the liquid in the pipe

D = the internal diameter of the pipe (ft.)

This equation demonstrates how decreasing pipe diameter increases the pressure drop through the system. Calculations based on this equation show that a smooth coating of 0.1 inches of deposit would produce a three-fold increase in system head pressure in a typical industrial cooling system.

In order to maintain the design water velocity through a fouled system the circulating pump would be required to develop a higher head pressure, which means that its work output and hence power consumption, would increase proportionately.

Although a few of the more sophisticated packaged cooling systems have a variable speed pumps and motors capable of responding in this way, for most industrial cooling systems what usually happens in practice when pipework fouling occurs is that the pump motor's work output remains unchanged, and the increased head pressure is reflected instead by a fall-off in water throughput by the pump. This means that the water velocity through the system reduces, which has a significant bearing on the transfer of heat at the heat exchangers.

Reynolds Number

The expression used to define the degree of turbulence of a fluid in a pipe is its 'Reynolds Number' (Re). Increasing values of Reynolds Number reflect an increased degree of turbulence.

Since heat is transferred within a fluid mainly by convection, which increases with increased turbulence, this means that the individual heat transfer co-efficient of the cooling water is proportional to its Reynolds Number.

A reduction in water-velocity will reduce its Reynolds Number according to the following equation:

$$Re = \frac{\rho D V}{\mu}$$

Where:

ρ = Density of fluid (lbs. per ft^3)

D = Internal pipe dia. (ft.)

V = Velocity of fluid (ft. per sec.) in the pipe.

μ = Viscosity of fluid (lbs per ft. sec) in the pipe.

It follows then that a reduced water velocity will lower its individual heat-transfer co-efficient, and hence the overall heat-transfer co-efficient of the heat exchanger will also be reduced.

A further effect of a reduced water velocity is that its ability to maintain solid particulate matter in suspension in the cooling water will be impaired. The risk of sedimentation fouling is thereby increased, thus further compounding the problems discussed, and setting up a classic vicious circle.

Causes of Fouling

We have considered some of the effects of fouling. Table 3 summarises the main causes and preventative measures available to the water-treatment specialist to eliminate fouling in evaporative recirculating cooling water systems.

It is not the author's intention to explore the aspect of fouling prevention in detail in this paper. Most reputable water treatment companies should be able to appraise system conditions and offer programmes of water treatment for the control of scale, corrosion, silt and organic growths.

(2) WATER WASTAGE

Having considered Energy Wastage we now need to consider the second of our two areas, namely Water Wastage.

Table 3 indicates that bleed-off is an acceptable method of reducing the risk of crystallisation and sedimentation fouling. The effect of bleed-off is to de-concentrate the system, and it is conventional to regulate bleed-off by reference to the system water concentration relative to the make-up. This relationship, i.e. solids level in the circulation water divided by solids level in the make-up water, is termed the system "Concentration Factor".

Figure 2 shows the relationship between water usage and concentration factor. It will be seen that the water usage rises rapidly at the lower concentration factors but diminishes markedly at the higher values. With the increased cost of water, particularly in the last few years (see Figure 1), it is obviously important to minimise losses due to bleed-off.

The main cause of water wastage in evaporative recirculating cooling systems is undoubtedly due to over-enthusiastic application of bleed-off.

The answer to unnecessary water wastage is therefore to reduce the system bleed-off rate, but this has the effect of increasing the dissolved solids in the cooling water and water becomes progressively less stable as dissolved solids increase. In addition, the risk of sedimentation fouling from suspended solids is increased at the higher concentration factor.

However, modern non-acidic sequestrant treatments will effectively inhibit the formation of calcium carbonate scales at quite high dissolved solids levels, whilst polymeric antifoulants, sometimes coupled with side-stream filtration, will prevent sedimentation fouling.

CASE HISTORY

An evaporative recirculating cooling system sited in North West England has a recirculation rate of 100,000 gallons per hour and a temperature differential at the cooling tower of 20°F. Operation is continuous; 350 days per annum. Evaporative loss is estimated at 1,600 gallons per hour, some heat being lost by convection as well as evaporation.

System head pressure is 73 psi.

A water stability appraisal was carried out by reference to the circulating water calcium bicarbonate and solids content, the system pH level and the maximum water temperature in the system. The combined effect of these factors determine the likely scaling potential of the cooling water. These calculations were based on the classical work carried out by Langelier, and the corrosion/scaling tendency is expressed by means of the 'Langelier Saturation Index' of the cooling water, with negative values indicating a strong corrosive tendency and positive values indicating a strong scaling tendency.

Table 4 gives a general guide to the likely behaviour of cooling water according to the calculation value of Langelier Index for the particular system.

The operator had been employing a traditional organic/polyphosphate treatment since start-up and under this regime was able to operate up to a maximum water concentration factor of 2.3 with reasonable cleanliness.

The operator revised his water-treatment programme by changing to a more stable modern polymeric antifoulant/organo-phosphorus formulation.

Using the modified water-treatment approach, it was found possible to operate at 4.5 cycles of concentration, whilst still maintaining completely clean water-side conditions.

This was achieved by lowering the system bleed-rate from 1,231 gallons per hour to 457 gallons per hour, with a corresponding reduction in make-up water requirements, as illustrated in Table 5.

Power costs on this system, due to the operation of pumps and fans, were estimated as follows:

Pump : 60 Horsepower (for 73 psi head pressure)

Fan : 10 Horsepower

Total : 70 Horsepower = (70 x 0.746) KW

= 52.2 KW

Operation is 8,400 hours p.a. hence:

(8400 x 52.2) units of electricity are used p.a.

= 438,648 units of electricity p.a.

At a cost of 1.5p per unit, the annual electricity bill for operating this cooling system is £6,580.

CONCLUSIONS

Evaporative cooling water systems are essential equipment for the intelligent management and conservation of energy and water in the industrial sphere. An appreciation of the factors that impair their effectiveness in carrying out this function, coupled with a willingness to make a modest investment in an up-to-date programme of water-treatment, will be quickly repaid in reduced system operational costs and often also in enhanced process throughput.

It costs nothing to take advantage of the recent developments in water treatment technology which can ensure clean heat-transfer surfaces with a variety of water-types and plant conditions. Massive energy and water wastage is the almost inevitable result of not doing so.

WATER AVERAGE COST PER 1000 GALLONS

FIGURA 1

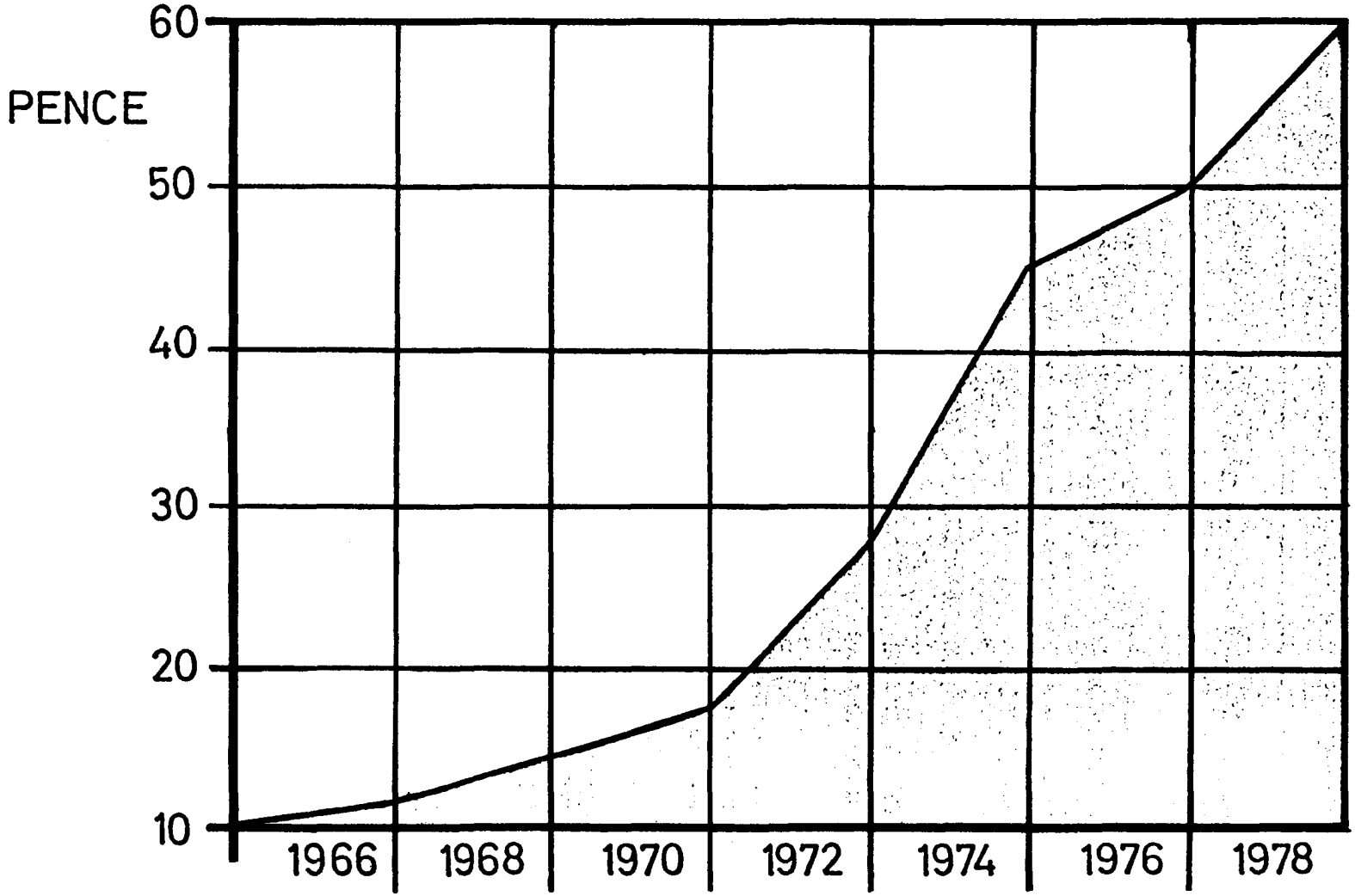

FIGURA 2

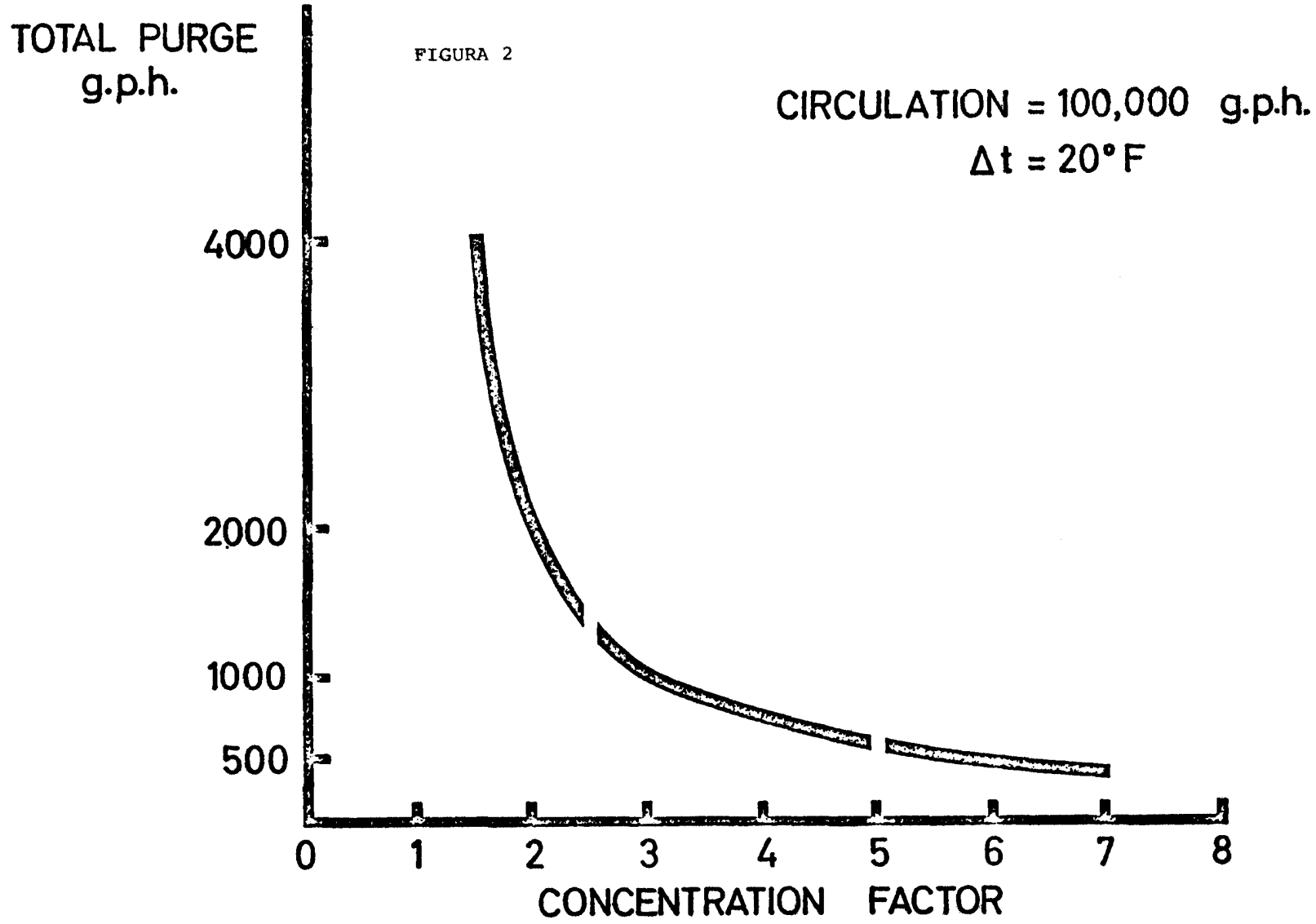
TOTAL PURGE
g.p.h.
CIRCULATION = 100,000 g.p.h.
Δt = 20° F
4000
2000
1000
500
0
1
2
3
4
5
6
7
8
CONCENTRATION FACTOR

TABLE 1

MATERIAL	THERMAL CONDUCTIVITY (Btu - ft./(ft^2).(hr.)($^\circ$F)
Copper	225
Admiralty Brass	64
Mild Steel	25 - 30
Porous Calcium Carbonate	0.2
Calcium Sulphate	0.34 - 1.34
Calcium Silicate	0.1 - 0.25

TABLE 2

HEAT TRANSFER SURFACE REQUIRED TO OFFSET FOULING

THICKNESS OF SCALE : APPROX. (in.)	FOULING THERMAL RESISTANCE † Btu/(hr)(sq.ft)(deg $^\circ$F)	OVERALL HEAT TRANSFER COEFFICIENT # Btu/(hr) (sq. ft.) (deg F)	INCREASE OF REQUIRED HEAT TRANSFER AREA* (Approx. %)
.000	Clean tubes	850	0
.006	0.0005	595	45
.012	0.001	460	85
.024	0.002	315	170
.036	0.003	240	250

† Assume a mean value for the thermal conductivity of the scale of 1.0 (Btu - ft./(ft.^{2}).(hr.)($^\circ$F)

The overall heat transfer coefficient U selected for this illustration is typical for a water-cooled refrigerant condenser. However, because it is possible to have different overall heat transfer coefficients depending on the system, the effect on the overall heat transfer by the scale will vary.

* Sq.ft. of inside surface of tube in heat exchanger.

TABLE 3

TYPE OF FOULING	DUE TO	PREVENTATIVE TECHNIQUES AVAILABLE
Crystallisation (Scale)	Presence of hardness salts in the make-up water.	. Limiting Water Concentration (i.e. Bleed-off) . Acid dosing . Use of threshold treatments . Pre-softening of make-up water
Corrosion Products	Presence of conductor, electrolyte & oxygen (i.e. effect of the cooling water on metal surfaces).	. Corrosion Inhibitors
Sedimentation (Silt/Clay)	Air-Scrubbing at The Cooling Tower or Turbid makeup water.	. Limiting Water Concentration (Bleed Off) . Antifoulants . Filtration (either pre-filtration if makeup water is turbid or otherwise by side-stream filtration). . Pre-clarification of make-up
Organic Growths (Algae; Bacterial spores)	Ingress of bacterial spores and nutrients for slime and algae growth.	. Chlorine . Non oxidising biocides
Process Contamination	Ingress of process materials. Ingress of Lubricating oils.	. Bleed off . Antifoulants . Filtration . Oil Separation

Please see page 27.12 for Table 4

TABLE 5

WATER ANALYSIS VALUES	MAKE-UP	COOLING WATER	
		INITIAL C/F = 2.3	ADJUSTED TO C/F = 4.5
Total Hardness (as ppm $CaCO_3$)	120	276	540
Calcium Hardness (as ppm $CaCO_3$)	90	207	405
Magnesium Hardness (as ppm $CaCO_3$)	30	70	135
Total Alkalinity (M) (as ppm $CaCO_3$)	80	184	360
Chloride (as Cl)	30	69	135
Sulphate (as SO^{2-}_4)	24	55	108
Total Dissolved Solids (TDS)	150	345	675
Measured/Anticipated pH	7.3	7.8	8.3
Calculated Langelier Index Value	-0.1	+1.1	+2.0
Threshold Ability Effectiveness — Natural Organic/ Polyphosphate		Effective	Not Effective
Polymer/ Phosphonate		"	Effective
WATER USAGE			
Hourly Make-Up Rate		2,831	2,057
Hourly Bleed-Off Rate.		1,231	457
WATER COSTS			
£0.50 per 1,000g for make-up		£ 34	£ 24.68
£0.20 per 1,000g disposal charges		£ 5.90	£ 2.19
CHEMICAL DAILY USAGE COSTS			
Organic/Polyphosphate costs approx. 7.5 pence per 1,000 gallons of water treated		£ 2.21	-
Polymer/Phosphonate costs approx. 40 pence per 1,000 gallons of water treated.		-	£ 4.39
Total daily water/water treatment costs		£ 42.12	£ 31.26

TABLE 4

LANGELIER SATURATION INDEX PREDICTION GUIDE

LANGELIER INDEX	LIKELY BEHAVIOUR OF COOLING WATER
+ 2.0	Severely Scale Forming
+ 0.5	Scale Forming/Slightly Corrosive
0.0	Nominally balanced
- 0.5	Non-Scale Forming/Corrosive
- 2.0	Severely Corrosive

TABLE 6

SUMMARY

At a system water Concentration Factor of:	2.3	4.5
Annual Power Costs:	£ 6,580	£ 6,580
Annual Water Costs:	£13,965	£ 9,405
Annual Water Treatment Costs:	£ 774	£ 1,537
Total Power/Water/Water Treatment Expenditure:	£21,319	£17,522
Hence annual operational SAVINGS Accruing from Rise in System Concentrations is:	£3,797	

An Optimal Strategy for Cleaning a Set of Four Condensers Subject to Rapid Fouling by Salt-water, Showing the Influence of Fouling Models on the Cleaning Cycle, and the Influence of Operating Conditions on the Parameters of the Model

D.A. Lihou
Z. Kabir

The University of Aston in Birmingham, Gosta Green, Birmingham, England

SUMMARY

Air for a process is supplied by two compressors, driven by two steam turbines. Each turbine has two identical condensers, working in parallel. These condensers are cooled by estuary water and require frequent tube-side cleaning. In order to avoid large losses in profits, the air supplied should not decrease during cleaning operations. While a condenser is isolated for cleaning, its turbine must deliver at least 43% of the total air. The other condenser of the pair must not be fouled more than a "limited amount". The optimal cleaning strategy is to clean one condenser from each pair, in succession. The time for cleaning arrives when the other two condensers have achieved the "limiting fouling resistance". The overall cycle time is twice the time taken to arrive at limiting fouling conditions.

The following equation, proposed by Weibull for correlating statistical data, enables a wide variety of trends between fouling resistance R and time t, to be correlated.

$$R/R_{\infty} = 1 - \exp\left(-(t/n)^{\beta}\right)$$

Correlations for the parameters, R_{∞}, β and n are proposed in the paper The principal operating conditions which affect the parameters, are cooling water velocity and temperature and the addition of a biocide at appropriate periods.

INTRODUCTION

The experimental data on which this paper is based, was collected during a six week summer project. The company operate a process which requires about $52m^3/s$ of air; this is provided by two turbo-blowers driven by steam turbines at 3480 revolutions per minute. The steam from each turbine is condensed by two identical condensers in parallel.

The condensers are cooled by estuary water, and require tube-side cleaning every one or two months.

As the condensers become more fouled, the inlet pressure of steam to the turbine is increased, in order to maintain turbine speed to deliver the requisite air. However, the turbine blades and thrust bearings would be damaged if the steam pressure exceed 650 kN/m^2. The more common constraint, which dictates the need to clean the condesers, is when the condensate temperature reaches 328K. Above about 325K, the pressure drop across the last stage of the turbine is insufficient to maintain the boundary layer on the blades and the stage effectively stalls. This causes the turbine to slow down; its speed is typically 90% when the condenser hotwell temperature is 328K.

The previous operating strategy was to wait until the hotwell temperatures reached 325K and then to isolate and clean each of the four condensers on consecutive days. Because all four condensers were fouled and the hotwell temperature was at the maximum value of 100% turbine speed, the steam supply had to be reduced during the four day cleaning operations. The resultant reduction in air flowrate was estimated to be causing £12000 loss of profit from the plant. The cleaning costs were about £100 per condenser.

Clearly, there was considerable financial incentive to develop a cleaning strategy which did not involve reducing the air flowrate to the plant. Previously, attempts had been made to prolong the

operating cycle of the condensers by injecting slugs of hydrogen chloride gas into the cooling water, when the hotwell temperature was approaching its limiting value of 325K. The objective of this doping was to kill the algae adhering to the tube surfaces and thereby dislodge the deposits. The effect of doping was erratic and it had been discontinued, because the nature of the deposits seemed to be more silt and less slime. However, the length of an operating cycle during winter was about 50% longer than in summer, suggesting that marine growth was instrumental in the fouling mechanism. Samples were taken of the water at strategic positions from the jetty intake to the condenser outlets, both at low and at high tide. The solid matter was analysed for organic and inorganic content by destroying the organic matter in a muffle furnace. These results were inconclusive and are not reported here; for example, the solid content seemed to increase from 18p.p.m. to 34p.p.m. over the condensers.

This could have been due to sediment being dislodged from stagnant areas in the outlet header, when the drain was opened to collect the samples. The organic content of all the samples ranged from 8 to 10p.p.m.; but this excludes the shell weight of the marine organisms; the shells being inorganic.

OPTIMAL CLEANING STRATEGY

The cleaning strategy proposed, enabled three condensers to handle the steam, equivalent to a total air flowrate of $52m^3/s$. At maximum speed, either blower can deliver $29.5m^3/s$; so that the blower with only one condenser in service, must deliver $22.5m^3/s$. This blower can be operated at 90% speed with the condenser hotwell temperature at 328K. This condenser must condense 4.7 kg/s of steam. The two condensers serving the blower which is delivering $29.5m^3/s$ of air, will be condensing 7.4 kg/s of steam at 325K.

Numbering the condensers 1,2,3,4 and assuming that 1 and 2 are connected in parallel to blower A, with condensers 3 and 4 serving blower B. For the situation when condenser 4 is isolated for cleaning, 3 will be condensing 4.7 kg/s and B will be delivering $22.5m^3/s$. Condensers 1 and 2 will be condensing 7.4 kg/s, which is less than twice 4.7 kg/s; so condenser 3 has a greater heat load than the average of 1 and 2. Becuase 3 is limiting, the cycle time between cleaning will be maximised if the overall heat transfer coefficient for 3 was proportionally larger than the average for 1 and 2.

The total cleaning costs will be minimised if the cycle time for each condenser is maximised and the number of times the cleaning crew is required on site is also minimised. The time taken to clean a condenser is the same, whether they are cleaned consecutively or in a staggered sequence

The strategy which maximises the operating cycle but minimises the number of calls on the cleaning crew, is to clean one exchanger from each pair consecutively, Thus if 2 and 4 are due for cleaning, 1 and 3 are at the half-cycle stage. At the half-cycle stage, exchangers 1 and 3 must be able to condense 4.7 kg/s of steam with the hotwell temperature not exceeding 328K. Condensers 1 and 3 are said to have attained the limiting fouling resistance. The overall cycle time will be twice as long as it takes to attain limiting fouling.

The maximum fouling which is permitted can be calculated by considering a pair of condensers, one at limiting fouling and the other at maximum fouling, able to condense 7.4 kg/s of steam with a hotwell temperature of 325K.

The way in which fouling resistance increases with time since the condenser was cleaned, may not result in condensers 2 and 4 attaining maximum fouling at the same time as 1 and 3 have attained limiting fouling.

Nevertheless, cleaning of 2 and 4 must be carried out when limiting fouling of land 3 has occurred. Thus there will be an optimal fouling model, which allows all four condensers to attain the appropriate critical values of fouling, simultaneously. Various fouling models are examined in a later section.

LIMITING AND MAXIMUM FOULING RESISTANCES

Each condenser contains 576 titanium tubes arranged in two passes. The tubes are 5m long, 25mm outer diameter by 2mm wall thickness; giving a total internal surface area of 190m^2.

Limiting Fouling Resistance in Condenser 3

The calculations were based on cooling water entering at 289K and leaving at 300K, with the condensate at 328K.

Steam condensation rate	= 4.725 kg/s
Heat load	= 11.276 MW
Cooling water flow rate, W	= 244.84 kg/s
Tube-side heat transfer coefficient	= 8684 W/m^2K
Shell-side heat transfer coefficient	= 6749 W/m^2K
Tube wall heat transfer coefficient	= 48468 W/m^2K
Overall clean coefficient, inside area	= 3869 W/m^2K

The minimum overall heat transfer coefficient based on the inside area of the tubes, was found by equating the rate of heat gain by the cooling water to the rate of heat transfer. This results in the following equation from which U_3 was found.

$$\ln \frac{T_w - T_1}{T_w - T_{23}} = \frac{U_3 A}{WC} \qquad (1)$$

A = total internal area = 190m^2

C = specific heat of water = 4186.8J/kgK

T_1 = inlet temperature of water = 289K

T_{23} = outlet temperature of water from condenser = 300K

T_w = hotwell temperature = 328K

From these values, U_3 was calculated as 1788 W/m^2K

Limiting fouling resistance = $R_3 = \frac{3869 - 1788}{3869 \times 1788} =$ 3 x 10^{-4} m^2K/W

Maximum Fouling Resistance of Condenser 2

Condensers 1 and 2 must condense 7.396 kg/s of steam at 325K. The overall heat transfer coefficient U_1 will be the same as U_3; that is 1788 W/m^2K. It is assumed that the cooling water flowrate through each condenser is also W; that is 244.84kg/s.

Condensers 1 and 2 will condense a proportion of the steam, according to the ratio of their overall coefficient to the sum of the coefficients (U_1+U_2). Let T_{21} and T_{22} be the temperatures of cooling water leaving condensers 1 and 2, respectively. The total latent heat removed Q_T by both condensers equals 7.396 x 2390 kW. A heat balance on the cooling water yields the sum of the outlet temperatures:

$$T_{21} + T_{22} = 2T_1 + \frac{Q_T}{WC} \qquad (2)$$

$$T_{21} + T_{22} = 2 \times 289 + \frac{17676}{244.84 \times 4.1868}$$

$$= 595K$$

Applying equation 1 with T_w = 325K and $U_1 = U_3$ = 1788 W/m^2K gives the following relationship for T_{21}:

$$\ln \frac{325 - 289}{325 - T_{21}} = \frac{1788 \times 190}{244.84 \times 4186.8}$$

$$T_{21} = 325 - \frac{34}{1.393} = 301K$$

From equation 2, T_{22} = 595 - 301 = 294K.

U_2 can be calculated from equation 1 as follows:

$$\ln \frac{325 - 298}{325 - 294} = \frac{U_2 \times 190}{244.84 \times 4186.8}$$

whence U_2 = 807 W/m^2K

Maximum fouling resistance of condenser 2:

$$R_2 = \frac{3869 - 807}{3869 \times 807} = 9.8 \times 10^{-4}\ m^2K/W$$

FOULING MODELS

Fig. 1 shows values of fouling resistance, determined from the data collected during the six week project. A Weibull model, curve A, has been fitted through the data except for days 28 to 30. Conversely, curve B has been fitted through the data for days 28 to 35, but ignores the earlier data.

The study was carried out while the policy was to clean all four condensers consecutively. The condensers were assumed to be identically fouled, because measurements were not available to determine the performance of individual condensers. The values of R which are plotted on Fig. 1, were calculated from the reported average overall coefficients and a clean overall coefficent of 3869 W/m^2K. The actual tube-side film coefficient would be directly related to the 0.8 power of water flowrate, and the shell-side coefficient would be inversely proportional to the cube root of steam condensation rate. Physical properties of cooling water and condensate are temperature

dependent also.

Clearly, more information about the operating conditions of each condenser would have been preferable. Nevertheless, some useful observations can be made about the curves drawn on Fig. 1:

(1) If curve A represents the growth of fouling, the limiting resistance would be attained in 21 days. With the staggered cleaning strategy, one condenser from each pair would be cleaned every 21 days and the overall cycle time for each condenser would be 42 days.

(2) Curve B illustrates a situation where the half-cycle time has been increased to 30 days, by increasing β from 0.98 to 2.46. The value of the scale parameter η remains unaltered at 38 days and the ultimate fouling resistance is still 7×10^{-4} m^2K/W. It will be seen that for the curve B, the initial rate of fouling is much less than for curve A. This may be achieved by adding a biocide to the cooling water before it enters those condensers which have been cleaned recently, in order to delay the growth of marine organisms on the tubes. These organisms could provide the necessary roughness for silt to adhere.

(3) Curve D represents an optimal fouling model, because the condensers would attain the maximum permitted fouling resistance just before they were cleaned at 60 days. Also, the ultimate fouling resistance has been allowed to rise to 15.5×10^{-4} m^2K/W. Note that the scale factor η has been put equal to the overall cycle time for curve D. This means that the maximum fouling resistance is 63.2% of the ultimate fouling resistance.

(4) Curve C illustrates the exponential model of fouling, where β is 1. The scale parameter is equal to the overall cycle time, as with curve D. But the fouling resistance just before cleaning is only 4.8×10^{-4} m^2K/W.

(5) Curves B, C and D all have the same lengths of half-cycle (30 days). But just before cleaning, the fouling resistance is higher for curve D than for curve B, which in turn, is higher than for curve C.

On Fig. 2, curve E is the best fit by the least squares method, of a Weibull model, through all the data from the six week study. For this curve, the scale parameter η was found to be equal to the half-cycle time, at which limiting fouling is achieved. The ultimate fouling resistance was found to be 4.65×10^{-4} m^2K/W and β is 1.19.

Curves F and G illustrate verly clearly that altering β will have no effect on the half-cycle time, when this is equal to η. However, the larger is the value of β the higher will R be at cleaning; thus the values of R/R_{∞} at 42 days, for the various curves is: curve F 86.5%, curve E 89.8%, curve G 98.2%.

FACTORS AFFECTING WEIBULL MODEL PARAMETERS

The fouling resistance correlated by the Weibull model can be calculated from the following equation.

$$R = R_{\infty} (1 - \exp - (t/\eta)^{\beta}) \qquad (3)$$

R_{∞} is the ultimate resistance which would be obtained after a very long time. If the shape parameter β is 1, equation 3 becomes the negative exponential relationship which has been suggested previously[1]. When the shape parameter β exceeds unity, the initial rate of fouling is zero. This can be shown by differentiating equation 3 and then eliminating the exponential term by means of equation 3.

$$\frac{dR}{dt} = (R_{\infty} - R) \left\{\frac{\beta}{\eta}\right\} \left\{\frac{t}{\eta}\right\}^{\beta-1} \qquad (4)$$

when β is 1, the initial rate of fouling is R_{∞}/η because $R(0)=0$. When $\beta<1$, the rate of fouling is inversely proportional to time, to the power $1-\beta$. Hence, the initial rate of fouling will be infinite.

The onset of fouling can be concieved as the silt particles filling the cavities between the surface perturbations in the tube wall. These surface irregularities would be supplemented by colonies of marine organisms (algae) adhering to the wall The rate of growth of the colonies should depend on their concentration in the water, with a negative exponential term containing an inhibition factor and the water temperature. This term is analagous to the Arrhenius factor in reaction

kinetics.

The following equation can be postulated for β, which contains all these factors in dimensionless form.

$$\beta = \frac{d_s}{\epsilon_w} \{1 - \frac{\epsilon_w}{\epsilon_a} p_a \exp(-\frac{I}{T})\} \quad (5)$$

ϵ_w and ϵ_a are the roughness of the wall and algae, respectively; d_s is the diameter of the silt particles; p_a is the concentration of algae expressed as parts per million by weight. I is an inhibition factor, analagous to the activation energy in reaction kinetics, and T is the absolute temperature of the wall. It is conceivable that I would be increased by chemical treatment of the cooling water with a biocide and by a deficiency of nutrients and oxygen, which the algae require to sustain growth. Note that I has the demensions of temperature. Bott and Pinheiro[2] give a good review of slime formation mechanisms. Their experiments[3] indicated that wall temperatures about 310K led to maximum growth rate.

It has been postulated[1] that the rate of fouling is the result of the difference between the rate of deposition of silt and its rate of erosion from the deposit. The review by Taborek et al[4,5] shows that most models are based on deposition and erosion. At $R = R_{\infty}$ these processes are in dynamic equilibrium.

The deposit should start with a large value of coherence, which may diminish as the layer gets deeper[5]; but may attain a higher, constant value independent of depth, if colonies of algae are intermingled with the silt deposit. The value of coherence at dynamic equilibrium can be considered as an effective kinematic viscosity μ_d,

$$R_{\infty} = \mu_d / 2 f V \rho_m K \quad (8)$$

Considering that the rate of increase of R due to deposition is proportional to R_{∞} while the rate of erosion is proportional to R, the deposition rate may be deduced from equation 4.

$$\{\frac{\partial \delta}{\partial t_D}\} = \frac{R_{\infty}^{\beta}}{\eta} \{\frac{t}{\eta}\}^{-1} \quad (9)$$

Note that when β is 1, the deposition is independent of time and equal to the initial rate of increase of R. When β is not equal to 1, equation 9 shows that the rate of growth of the fouling deposit depends upon β. From equation 5 it is seen that β depends upon the inhibiting factor I. In this way, the influence of factors such as pH, nutrients and oxygen, upon the growth of algae colonies is incorporated in the overall deposition rate. These effects are discussed by Bott and Pinheiro[2] for the case of algae growth in the absence of silt deposition.

Note than from the form of equation 5 and the inclusion of β in equation 9, that the model proposed here has similarities with the "transfer adhesion model" used by Watkinson and Epstein[6] to correlate their experimental results for sand deposition from water.

If silt is transported to the surface of the deposit by eddy diffusion only, the mass transfer coefficient is related to the Fanning friction factor as follows:

$$\frac{k}{V} = 0.023\, Re^{-0.2} = \frac{f}{2} \quad (10)$$

Beal[7] postulated an eddy diffusion model for dust deposition from gas streams. But all previous authors dealing with liquid streams have used a molecular diffusion model. In order to allow for the time dependence of the deposition rate, required by equation 9, the mass transfer rate is scaled by $(.368\,\delta/(\delta_{\infty} - \delta))^{\beta-1}$. Furthermore, since V is measured m/s and t in days a numerical factor of 8.64×10^4 s/day is included also. It was found that values of η which were similar to those used in Fig. 1 could be correlated by scaling the deposition rate by $(\delta_{\infty}/D)^{1.5}$; where D is the inner diameter of the tubes. Whith all these factors included, the mass flux rate of silt may be predicted by

$$\rho_s \{\frac{\partial \delta}{\partial t_D}\} = 8.64 \times 10^4\, k\, C_s \{\frac{\delta_{\infty}}{D}\}^{1.5} \{\frac{0.368\delta}{\delta_{\infty} - \delta}\}^{\beta-1} \quad (11)$$

In equation 11, C_s is the mass of silt per unit volume of water. Also the function of δ in equation 11, allows the deposition rate to be independent of δ for $\beta=1$; but for $\beta>1$ it is zero initially and infinite when $\delta=\delta_{\infty}$. Also, for $\beta<1$, the initial rate is infinite. The factor

0.368 has been included because when $t=\eta$ in equation 9, $\delta=.632\delta_{\infty}$ in equation 11, for all values of β.

It is assumed that the rates predicted by equations 9 and 11 become equal to $t=\eta$. Thus, substituting $\delta=KR$ in equation 11 and equating the rate of increase of R due to the deposition at $t=\eta$, with k coming from equation 10, gives the following relationship for η.

$$\eta = \frac{\beta D}{4.32 \times 10^4 fV} \left\{\frac{\rho_s}{C_s}\right\} \left\{\frac{D}{KR_{\infty}}\right\}^{.5} \qquad (12)$$

Prediction of Weibull Parameters for Fig. 1

The following analysis is based upon reasonable estimates of unknown operating parameters, plus typical values of measured variables. For the prediction of β, the values assigned to the variables in equation 5, are listed in Table 1. Similarly, in Table 2, the appropriate values of velocity were selected, so that the values of η used in Fig. 1 could be predicted by equation 12. These values of V were then used in equation 8 to find μ_d, as listed in Table 3. In Table 3, the values of the cohesion of the deposit are listed, which would predict the values of R_{∞} used in Fig. 1.

Comparing the values of μ_d, it can be seen that to change from curve A to curve B, the cohesion has to increase from 5.3 to 13.1 centipoise (g/ms); whereas R_{∞} is identical for both curves. In order to obtain curve B, a high inhibition factor I and/or low water temperature T are required, coupled with a water velocity of 5.2m/s; these conditions would not be conducive to high cohesion, so curve B seems unattainable.

Curve D on Fig. 1 was postulated because it represents a situation where the condensers to be cleaned attain the maximum permissible fouling, at the same time as the other two condensers attain the limiting fouling resistance. Curve D is rather more feasible than curve B, insofar as the velocity is comparable with curve A. Curve D could arise if dosing of the cooling water with biocoide was carried out for a limited period, immediately after cleaning. After the treatment ceased, the colonies of algae would tend to bind in the silt, giving rise to the higher value of μ_d, between curves A and D. Thus curve D would be expected at periods of high algae concentration.

Table 1 shows that curve A can be transformed into curve C by a small change in I. The principal difference between curves A and C is that η is increased from 38 to 60 days, by using a lower water velocity of 1.3m/s. The cohesion is also reduced to 3.6 centipoise; perhaps by continual addition of biocide.

The advantage of curve C over curve A, is that the half-cycle time has been increased from 21 days to 30 days.

Note that the ultimate thickness of the deposit is equal to KR_{∞} which for curves A, B and C is equal to about 210 microns. This is in good agreement with reported data[3].

CONCLUSIONS

The optimal cleaning strategy is to clean one condenser from each pair in succession. The time for cleaning arrives when the other two condensers have achieved the "limiting fouling resistance". The overall cycle time is twice the time taken to arrive at limiting fouling conditions.

The Weibull equation enables a wide variety of trends between fouling resistance and time, to be correlated. The principal operating parameters, which affect the constants of the Weibull equation, are cooling water velocity and temperature and the addition of a biocide at appropriate periods.

LITERATURE

1. Kern D.Q. and Seaton R.E. Chem.Eng.Prog. 1959, 55 No.6, 71
2. Bott T.R. and Pinheiro M.M. 16th Nat.Conf. Heat Trans. 1976, St. Louis, U.S.A.
3. Bott T.R. and Pinheiro M.M. Can.J.Chem.Engng. 1977, 55, 473
4. Taborek J., Aoiki T., Ritter R.B., Palen J.W. and Kundsen J.G. Chem.Eng.Prog. 1972, 68, No. 2, 59
5. Ibid.Chem.Eng.Prog. 1972, 68 No. 7, 69
6. Watkinson A.P. and Epstein N. 4th Int.Conf. Heat Trans., 1970, Vol. 1, Paris
7. Beal S.K. Nuclear Sci.Eng. 1970, 40, 1.

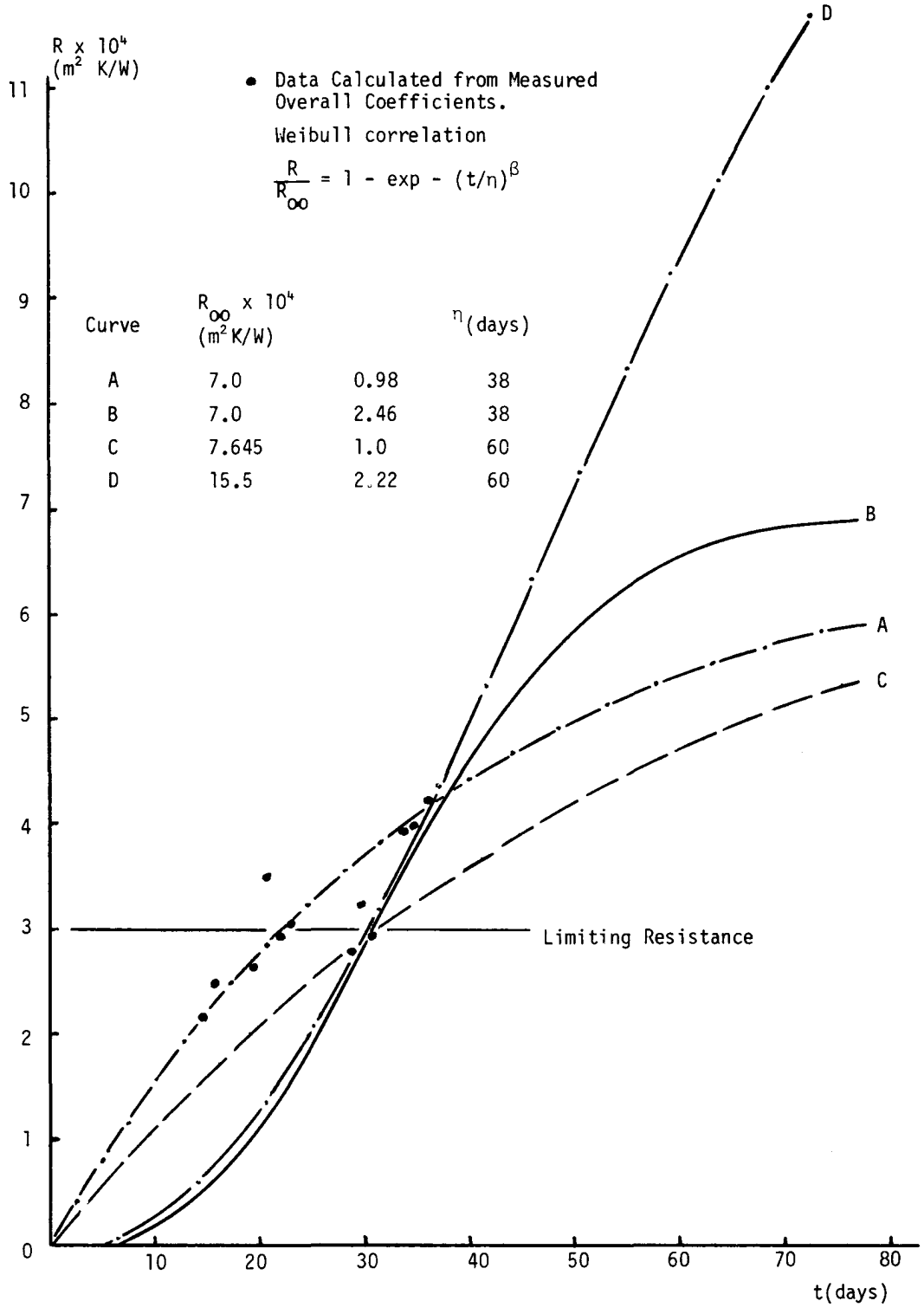

Figure 1 - Illustration of Fouling Models

Table 1. Prediction of β for Fig. 1

Estimated Variables		Typical Measured Values			
d_s = 0.5mm		p_a = 10 parts per million			
ε_w = .02mm		T = 294 K			
ε_a = .002mm					
Prediction from equation 5					
β		0.98	1.0	2.22	2.46
I		1500K	1504K	2000K	2570K
Curve on Fig. 1		A	C	D	B

Table 2. Prediction of η for Fig. 1

Estimated Variables		Typical Measured Values			
K = .3W/mK		f = .006			
ρ_s = 2000kg/m^3		C_s = .02kg/m^3			
		D = 21mm			
Prediction from equation 12					
V(m/s)		2.1	5.2	1.3	2.0
β		0.98	2.46	1.0	2.22
R_{oo} x 10^4(m^{2}K/W)		7	7	7.645	15.5
η(days)		38	38	60	60
Curve on Fig. 1		A	B	C	D

Table 3. Prediction of R_{oo} for Fig. 1

Estimated Variables		Typical Measured Values			
K = .3W/mK		f = .006			
ρ_m = 1000kg/m^3					
Prediction from equation 8					
R_{oo} x 10^4(m^{2}K/W)		7	7	7.645	15.5
V(m/s)		2.1	5.2	1.3	2.0
μ_d x 10^3(Ns/m^2)		5.3	13.1	3.6	11.2
Curve on Fig. 1		A	B	C	D

• Data from Measured Overall Coefficients
• R_{oo} = 4.65 x 10^{-4} (m^2 K/W)

Curve	E	F	G
β	1.19	1.0	2.0

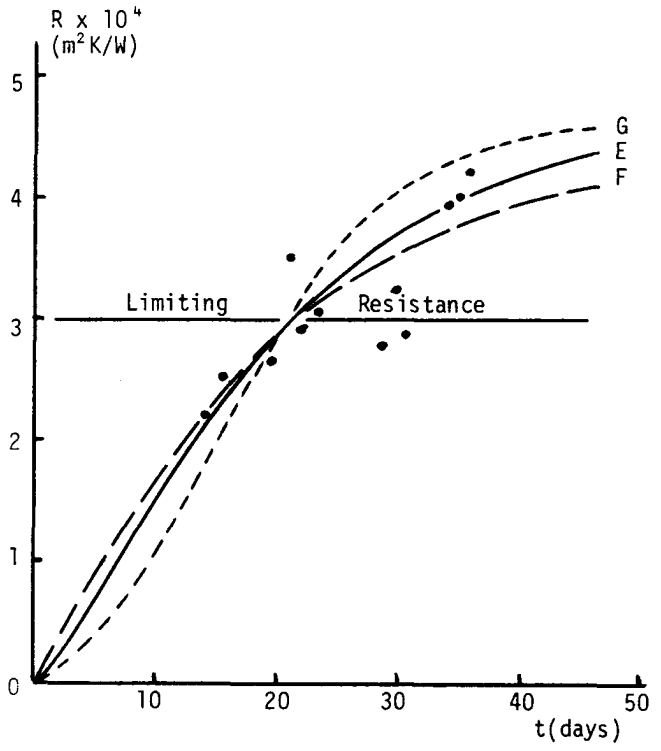

Figure 2 - Fouling Models with The Scale Parameter Equal to the Half-Cycle Time

SYMBOLS USED

A	Surface area inside the tubes in one condenser	(m^2)
C	Specific heat of water	(J/kgK)
C_s	Mass of silt per unit volume of cooling water	(kg/m^3)
D	Inner diameter of tubes	(m)
d_s	Diameter of silt particles	(m)
f	Fanning friction factor	
I	Inhibition factor	(K)
K	Thermal conductivity of silt deposit	(W/mK)
k	Mass transfer coefficient of silt to the deposit layer	(m/s)
p_a	Parts per million (w/w) of algae in cooling water	
Q_1	Heat transfer rate in condenser 1	(W)
Q_2	Heat transfer rate in condenser 2	(W)
Q_T	Sum of Q_1 and Q_2	(W)
R	Fouling resistance inside the tubes	(m^2K/W)
R_∞	Ultimate fouling resistance	(m^2K/W)
Re	Reynolds number	
T_1	Cooling water inlet temperature	(K)
T_{21}	Temperature of cooling water leaving condenser 1	(K)
T_{22}	Temperature of cooling water leaving condenser 2	(K)
T_{23}	Temperature of cooling water leaving condenser 3	(K)
T	Mean temperature of cooling water in a condenser	(K)
T_w	Hotwell temperature at which steam condenses	(K)
t	Time elapsed since last cleaning operation	(days)
U	Overall heat transfer coefficient based on the inside area of tubes (Subscripts are condenser number)	(W/m^2K)
V	Superficial velocity of water in the tubes	(m/s)
W	Mass flowrate of cooling water to each condenser	(kg/s)

Greek Letters

β	Shape parameters	
δ	Thickness of silt deposit	(m)
δ_∞	Ultimate thickness of silt deposit	(m)
∂	Partial derivative (subscript D: for deposition)	
ε_w	Roughness of wall	(m)
ε_a	Roughness of algae growing on wall	(m)
μ_d	Cohesion of silt deposit	(Ns/m^2)
η	Scale parameter	(days)
ρ_m	Density of silt and water mixture flowing in the tubes	(kg/m^3)
ρ_s	Bulk density of the silt deposit	(kg/m^3)
τ	Shear stress	(N/m^2)

MODELLING OF LIQUID-LIQUID EXTRACTION COLUMNS - THE DISPERSED PHASE PROBLEM

W.J. Korchinsky and J.J.C. Cruz-Pinto

Department of Chemical Engineering,
University of Manchester Institute of Science and Technology,
Manchester, England.

ABSTRACT

Theoretical models of the liquid-liquid extraction process in countercurrent flow columns have been developed to take into account the influence of drop size distribution and of size-dependent residence time distributions and interphase mass transfer rates. The rigid drop and Handlos and Baron turbulent circulation/oscillating drop model equations have been solved exactly, taking into account variations in mass transfer rates with position and variation in boundary conditions due to changing continuous phase concentrations. Significant differences from the approximate solutions previously published were obtained.

Experimental data verifying the influence of drop size distribution (independent of mean drop size) on extraction rates have been obtained. These data have been compared with the 'exact' predictions of the rigid drop and Handlos-Baron drop models. The importance of controlling drop size distributions cannot be over-estimated.

INTRODUCTION

The complex nature of the behaviour of the dispersed phase in an extraction column makes difficult the modelling of the hydrodynamic and mass transfer processes. Factors which should be considered in any model include at least the following

I Drop size distribution, which will depend on
- a) method of introduction of the dispersed phase,
- b) degree of coalescence and breakup in the column,
- c) level of solute concentration,
- d) influence of surfactants,
- e) physical properties.

II Drop residence time distribution, which will depend on
- a) drop size distribution,
- b) degree of agitation,
- c) degree of axial mixing,
- d) level of surfactants, influence on drop mobility,
- e) physical properties.

III Distribution of mass transfer rates, which will vary with
- a) drop size,
- b) position - during formation
  - during rise or fall due to changing boundary conditions and driving force, changing physical properties, degree of coalescence and/or breakup
  - during settling and coalescence at the outlet end,
- c) level of surfactants, resulting interfacial resistance.

IV Multicomponent mass transfer due to
- a) miscibility of solvent and raffinate,
- b) multiple solutes.

Until recently, none of these factors was considered in the modelling of countercurrent flow extraction columns. First models were formulated by analogy to gas - liquid contacting in absorption columns. Plug flow of the two phases in countercurrent flow was assumed, the required number of transfer units was determined and the only experimental data required were the heights of transfer unit. Differential and stage models were then modified to attempt a more realistic description of two phase flow in extraction columns. Backmixing of both phases, with the resulting reduction in mass transfer driving force, was assumed. The unsuccessful attempts at measurement and correlation of the model parameters has not given much confidence to engineers in designing extraction columns using these models.

The objective of our work is to construct a realistic model which will take into consideration as many of the above factors as possible, and to obtain the appropriate data to test the model.

MODEL DEVELOPMENT

In developing the model, the following assumptions have been retained:

1) A single component, in low concentration, transfers between immiscible carrier phases;
2) Phase flows remain constant over the height of the column;
3) Physical properties are constant;
4) No unusual influence of 'surfactants';
5) No interfacial resistance to mass transfer.

Models may be developed from either the basic differential, or stagewise, contacting models. Both have been employed by the authors (1,2). However, in this work, the model developments based on the differential contacting model will be detailed.

One further assumption is made throughout this work. The continuous phase is assumed to flow in plug flow, with axial mixing within the phase represented by eddy diffusion, and the extent of axial mixing is given by the size of the diffusion, or dispersion, coefficient E_C.

The dispersed phase is assumed to consist of drops of varying sizes passing through the continuous phase at varying velocities. Drops of a given size are assumed to have a given velocity or residence time in the column, but the influence of variability of residence time within drops of a given size has been estimated (3). The theory is first developed for the case where there is no coalescence or breakup. The associated problems which arise when coalescence and breakup are considered then will be discussed.

-Hydrodynamics

Chartres (3) started with the usual definition of slip velocity

$$V_s = \frac{V_D}{\phi} + \frac{V_C}{1 - \phi} = V_k(1 - \phi) \qquad (1)$$

and assumed that the individual drop slip velocities, could be similarly defined as follows:

$$V_{s,i} = V_{d,i} + \frac{V_C}{1 - \phi} = V_{k,i}(1 - \phi) \qquad (2)$$

and summing over all the drops in the dispersion, the following is obtained:

$$\sum_i f_i V_{d,i} \equiv \frac{V_D}{\phi} = \Sigma f_i V_{k,i}(1 - \phi) - \frac{V_c}{1 - \phi} \quad (3)$$

Chartres then assumed that individual drop characteristic velocities, $V_{k,i}$, were proportional to the single drop terminal settling or rise velocities, $V_{t,i}$. Misek (4), in work on Rotating Disc Columns, used

$$V_{s,i} = V_{t,i}(1 - \phi) \exp(a_i \phi) \quad (4)$$

whereas Olney (5) suggested a simpler relation

$$V_{s,i} = C_R V_{t,i}(1 - \phi) \quad (5)$$

where C_R is a constriction factor to account for internals within the column.

Pinto (6) has modified the above relations slightly, considering the relative flows of the two phases at the most constricted cross-sectional area ($C_R S$) and defining the drop velocities there by

$$V_{d,i}^* + \frac{V_c}{C_R(1 - \phi)} = V_{s,i} \quad (6)$$

where $V_{d,i}^* = V_{d,i} \cdot \frac{S_a}{SC_R}$

When summed up over all drops Equation 6 leads to

$$\Sigma f_i V_{d,i}^* = \sum_i f_i V_{s,i} - \frac{V_c}{C_R(1 - \phi)} \quad (7)$$

and substituting for the mean rise velocity $V_{d,i}$, the following is obtained:

$$\Sigma f_i V_{d,i} \equiv \frac{S}{S_a} \frac{V_D}{\phi} = \frac{S}{S_a}\left[C_R \Sigma f_i, V_{s,i} - \frac{V_c}{(1 - \phi)}\right] \quad (8)$$

To obtain expressions for the slip velocities the approach of Chartres was again used, but in addition the work of Barnea and Mizrahi (7,8) was applied. They corrected particle slip velocities for

a) density variation with dispersed phase holdup

b) viscosity effect due to presence of dispersion,

and

c) wall effects.

Ideally, drop size dependent residence times ($\theta_i = Z/V_{d,i}$) should be measured. Instead, however, measured holdup, ϕ, and drop size distributions, f_i, are used with calculated single drop terminal velocities, $V_{t,i}$, to calculate a 'constriction factor', C_R, from Equation 8. Equation 6 is then used to calculate $V_{d,i}^*$. These values will depend on the method used for calculating the slip velocities so each method, i.e. Misek, Olney, Barnea et al, was used, and the effect on predicted residence time and extraction efficiency determined.

-Mass Transfer

The model equations applying to dispersions with varying drop size distributions are those developed and used by Chartres, with only minor modification to correct for the presence of internals, which reduce the effective column working volume. The equations are repeated below (6).

$$\frac{dx}{dz} = \frac{Q_c}{SE_c}(X - x) \quad (9)$$

$$\frac{dX}{dz} = \frac{6\phi S_a \rho_D}{Q_c \rho_c} \sum_i \frac{K_{OD,i} f_i (y^* - y_i)}{d_i} \quad (10)$$

$$\frac{dy_i}{dz} = \frac{6K_{OD,i}(y^* - y_i)}{V_{d,i} d_i} \quad (11)$$

The publications of Rod (9) and Olney (5) were used to develop these model equations.

To use these equations, values of the overall dispersed phase mass transfer coefficient, $K_{OD,i}$, are required. As drop size dependent coefficients have not been measured under column condi-

tions, the procedure used has been to predict the coefficients from single drop theoretical models, and then to compare predicted theoretical extraction efficiencies with experimental values. Rigid drop (10), viscous circulating drop (11), turbulent circulating drop (12), and oscillating drop (13,14) models have been developed, and the resulting equations solved for single drop situations. When applied to swarms of drops in an extraction column some of the basic assumptions made are of doubtful validity, particularly the assumption of constant continuous phase concentration!

To obtain more accurate predictions of drop models for column conditions, the model equations have to be solved for the appropriate conditions. This has been done for two models - the rigid drop, and the Handlos-Baron turbulent circulating drop (also generally applied to the oscillating drop).

Molecular diffusion within a rigid drop rising with constant velocity through a continuous phase may be represented by the following equation:

$$\frac{\partial^2 y}{\partial r'^2} + \frac{2}{r'}\frac{\partial y}{\partial r'} - \frac{V_d}{4}\frac{d^2}{D_{AD}}\frac{\partial y}{\partial z} = 0$$

Handlos and Baron proposed a 'turbulent circulating' model, which has since been widely applied to oscillating drops, for mass transfer within drops. The following equation was derived:

$$\frac{\partial y}{\partial z} = \frac{V_s}{128 d\, V_d (1 + \mu_D/\mu_c)(1 - \xi')} \cdot \frac{\partial}{\partial \xi'}\left[(1 - 5\xi' + 10\xi'^2 - 6\xi'^3)\frac{dy}{\partial \xi'}\right]$$

These model equations were first solved assuming the following:

1) uniform continuous phase concentrations
2) infinite continuous phase mass transfer coefficients, k_c
3) long contact times

Dispersed phase mass transfer coefficients were calculated, in each case, averaged over the infinite time of contact, and then combined with a finite continuous phase mass transfer coefficient, assuming the two film resistance model for mass transfer between phases, to calculate an overall mass transfer coefficient K_{OD}. The equations have since been solved for finite contact times (15) and finite continuous phase mass transfer coefficients (16,17,18). In the latter case average values of the overall coefficient which are directly dependent on k_c are used in the column model equations. However, the errors involved in the averaging process, and in neglecting the change in continuous phase concentrations, have not been previously determined.

The authors have solved the rigid drop, and Handlos-Baron drop, model equations and, using experimental data from a number of runs on a Rotating Disc Contactor, have determined the errors in predicted mass transfer rates due to each of the above assumptions. Values of $K_{OD,i}$, for rigid and oscillating drops, were calculated for different combinations of assumptions and the effect on the extraction efficiencies calculated using the column model equations. To determine the influence of changing continuous phase concentration, however, the drop model equations had to be solved simultaneously with the column model

equations, by numerical methods. In this case values of $K_{OD,i}$ are not calculated, but are eliminated from Equations 10,11 by combining them. Details of the mathematical, and numerical, methods may be obtained from the Ph.D. thesis of Pinto (19).

-Coalescence and Breakup

It is recognized that extraction columns will generally be operated under conditions where breakup at least will occur due to the agitation method employed in the column. Coalescence, too, may occur, especially if high dispersed phase holdups are present. Previous work (20,21) has resulted in the derivation of drop population balances which take into account drop coalescence and breakup, thus predicting changing drop size distributions with time or position. Parameter values have been measured (21,22) for the single stage mixer for which the theory was developed, but the data are still too limited to adequately establish the mechanism of these processes.

The drop population balances have been incorporated into the column hydrodynamic model equations. Experimental conditions which result in drop breakup, but not significant coalescence, with resulting reduction in mean drop size have been used in an attempt to predict drop breakage parameters. No attempt has been made to include any direct influence on mass transfer rates of the breakup and coalescence processes.

EXPERIMENTAL

The first objective of the experimental programme was to establish conditions in a pilot plant Rotating Disc Contactor which might closely approximate single drops in an infinite continuous phase, i.e. by preventing if possible any interdrop interactions. That is, the theory was to be checked against experimental for the case where the column was operated at low rates, and low dispersed phase holdup, and with the dispersed phase introduced into the column at a drop size near the steady state size for the particular operating conditions. The distributor was designed, and the agitation rate controlled so that the drops formed at the distributor retained their identity through the column. Agitation rates were low to avoid excessive backmixing of the dispersed phase.

The Rotating Disc Column was operated with two sets of internals, the dimensions of which are given in Fig. 1. Measurements of

a) drop size distributions (photographically),
b) dispersed phase holdup,
c) both phase inlet and outlet concentrations, and in some cases
d) continuous phase concentrations at several points within the column,

were made for a range of operating conditions with the toluene-acetone-water system.

RESULTS

Experimental - Drop Size

Initial attempts by Chartres to obtain an unchanging drop size over the column height were unsuccessful. With the introduction into the column of relatively large (0.6 - 0.7 cm. dia.) drops, the break-up rate was not high enough to produce a steady state drop size through increased agitation alone. However, this problem was overcome by changes in distributor

design, and the drop size variation was reduced to the minor level indicated for 2 Runs (No.2 and 5) in Fig. 2. Very little change with height indicates a minimum of drop break-up. Some redistribution of drop sizes does occur, as indicated for Run 5 in the plotted drop size distributions in Fig. 3 but the effect on mean drop size is minimal.

Different distributors were used in order to effect changes in drop size distributions, while keeping the mean drop size unchanged, so that the influence of drop size distribution on extraction efficiency could be demonstrated directly.

Runs 3 and 4, 2 and 5, and finally 6 and 7 are three pairs of runs where operating conditions are identical except for the dispersed phase distributor used. As the results in Table 1 indicate, the mean drop size within each pair of runs did not change significantly. Dispersed phase holdup decreased when large drops were introduced to widen the drop size distribution, with the predicted detrimental effect on extraction efficiency (see below).

Experimental - Mass Transfer

Extraction efficiencies in dispersed phase units (E_{OD}) were calculated from the inlet and outlet concentrations and are tabulated in Table 1. Equilibrium data for the system were obtained over the range of temperatures employed, and the extraction efficiencies are therefore corrected for temperature. As the comparison of efficiencies leads to difficulties because of changing extraction factors and of the increasing importance of a given increment of efficiency as the efficiency approaches one, the plug flow number of transfer units, N_{ODP}, was calculated in each case and used to compare column performance under different conditions.

The influence of drop size distribution is clearly demonstrated by the changes in E_{OD}, and N_{ODP}, obtained when different distributors are used - see Table 1. Increases in N_{ODP} of up to 50% resulted from more uniform drop size distribution obtained in Runs 2, 4 and 7, when compared with those in Runs 5, 3 and 6 respectively.

Over the limited range of conditions employed, efficiencies changed little with flow rates and disc speed, though they increased with both due to increasing dispersed phase holdup.

Theoretical - Hydrodynamics

In order to predict dispersed phase holdup for a given drop size distribution, flows, etc., a value of C_R in Equation 8 is required. Values of C_R were determined for a large number of runs, and compared with values calculated from the internal dimensions to see whether the constriction factor could be related to the latter. Some of the results are tabulated in Table 2. These data indicated that the values of C_R are always higher than what would be predicted from column dimensions (see Fig. 1), which suggests that the actual drop velocities through the column may have been slightly under-estimated. However, the relation for $V_{s,i}$ which was used made little difference to the results except that the more complex models of Misek and Barnea-Mizrahi predicted higher C_R values than Olney's simple approach.

Within engineering accuracy, the constriction

factor is approximately constant for each column geometry. However, some variability of the values obtained requires further analysis. If we compare the values of C_R for the three pairs of runs (2,5), (3,4) and (6,7), it is apparent that the broadening of the size distribution, by forming some of the drops from larger distributor holes, caused an increase in that factor, even though the average drop diameters were similar. It is not clear, however, at this stage, whether the difference could be due to a specific drop size effect, or rather to the holdup itself which is consistently higher for the narrower size distributions.

This problem may still be in need of study, but this more fundamental type of approach should definitely be preferred to the usual correlations for RDC dispersed phase holdup (e.g., Kung and Beckmann (23) or Murakami et al. (24), which totally ignore the real structure of the dispersed phase, particularly its size distribution, which often changes dramatically with column height. The advantages of the treatment discussed here are clearly illustrated if we compare, for a few cases, our measured holdups with the predictions by the two correlations mentioned above (see Table 3).

No matter how recent some of these correlations may be (24), the fact that the method of introducing the dispersed phase into the column is never reported, neither its size distribution nor how it changes with height, make this type of correlation entirely useless for design purposes.

Theoretical - Mass Transfer

First, experimental drop size distributions and other data from two runs were used in order to determine the accuracy of prediction of the rigid drop, and the Handlos-Baron drop, model equations when these were solved for different boundary conditions, etc.. The results of this study showed that the simple equations used to predict mass transfer rates are not always very accurate, with differences between the simplest and the most complex, exact numerical, solution as high as 30% possible. This is due mainly to the assumptions of constant continuous phase concentration with column height and very large contact times, and to the neglect of the continuous phase transfer resistance when evaluating the dispersed phase partial transfer coefficient. The differences in predicted results are further illustrated in Table 4, where predictions for the most approximate (Case I*) and the exact numerical solution are tabulated with the corresponding experimental data. The result of simplifying assumptions made in the solution of either model equations cannot be ignored if one wishes to draw conclusions regarding the drop behaviour in an extraction column.

Comparing experimental and model-predicted values for E_{OD} and N_{ODP}, one finds that nearly all experimental values fall below the predicted ones for the Handlos-Baron model, the exceptions being slightly higher than predicted by this model. Although the major variable, that of drop size distribution, has been measured and accounted for, some assumptions still were required in applying the models, and these could well explain any differences between experimental and theor-

etical values. For instance, a previously published correlation for E_c (25,26) was utilized, though the state of the dispersed phase will undoubtedly affect continuous phase axial mixing, and the applicability of the E_c correlation, when dispersed phase properties are not comparable, is questionable. Experimental continuous phase concentration profiles could be utilized to provide values of the axial dispersion coefficient, and hence to provide more accurate predictions of extraction efficiencies. This is one of the objectives of continuing work.

In connection with this, one should question how the inaccuracy of the predicted continuous phase axial mixing affected the results. To answer this, we resolved the column model equations for Runs 2, 3, 4 and 5, assuming plug flow (no axial mixing) in the continuous phase, and the results are shown in Table 5. The striking conclusion is that, for rigid drops, the effect of the usual simplifying assumptions regarding the drop boundary conditions is far more important (over a factor of 3) than, as in the early design methods, the assumption of no axial mixing! And for oscillating drops the effect, even though smaller, cannot be neglected.

Composition profiles for Runs 2 and 5 are shown in Figures 4 and 5. They provide another means of comparing the different calculation methods with each other, and how closely they predict the actual (experimental) composition profile. It is clear that for the two cases illustrated the extent of axial mixing has been overestimated, which only stresses the conclusion of the paragraph above.

Theoretical - Coalescence and Breakup

Drop sizes and size distributions were obtained at three column levels, for conditions where drop breakup was extensive, but in the absence of any significant coalescence (see Run 12 in Table 1). The Sauter mean diameters are plotted in Figure 2. A model and the corresponding algorithm were developed (19), and utilized in an attempt to predict the experimental changes in drop size, and size distribution, with column height. The model-predicted d_{32}'s are also plotted in Figure 2, and the fit may be considered very good. The local size distributions are also output by the calculation routine, together with the values of three parameters characterizing the breakage distribution function, the fraction of drops that actually break, and the breakage time. The local predicted size distributions were, however, broader than the experimental.

CONCLUSIONS

1. A realistic model of the countercurrent flow liquid-liquid extraction process has been developed and tested under carefully controlled experimental conditions.
2. Drop size distributions, and the factors affecting them, must be accounted for in any theoretical model, and must be carefully considered in the design of extraction column internals, particularly of the inlet distributor.
3. Single drop model equations must be solved for more realistic boundary conditions if

they are to be used to predict extraction efficiencies for swarms of drops in an extraction column.

ACKNOWLEDGEMENTS

The financial assistance of a NATO Fellowship obtained by Mr. Pinto through the Junta Nacional de Investigacao Cientifica e Tecnologica, Lisboa, Portugal, is gratefully acknowledged.

NOTATION

a	coalescence coefficient (Equation 4)
C_R	constriction factor
C_R', C_R''	geometrical factors (Fig.1)
d	drop diameter
D	disc diameter
d_{32}	Sauter-mean drop diameter $\Sigma nd^3/\Sigma nd^2$
D_c	column diameter
D_s	opening diameter
D_{sh}	shaft diameter
E_C	axial dispersion coefficient, continuous phase
E_{OD}	extraction efficiency, dispersed phase basis
f	volume fraction of dispersed phase in particular drop size interval
h_c	compartment height
k_C,k_D	partial mass transfer coefficients, continuous and dispersed phases
K_{OD}	overall mass transfer coefficient, dispersed phase basis
N_{ODP}	plug flow number of transfer units, dispersed, phase basis
Q_C	volumetric flow, continuous phase
r	radial coordinate
r'	reduced dimensionless, radial coordinate (2r/d)
S	column internal cross sectional area
S_a	column average cross-sectional area for flow
V_C	Superficial velocity, continuous phase
V_d	drop vertical velocity based on mean available column cross-sectional area
V_d^*	drop vertical velocity based on minimum column cross-sectional area
V_k	drop characteristic velocity
V_s	drop slip velocity
V_t	drop terminal settling (rise velocity)
x	weight fraction solute, continuous phase
X	weight fraction solute, continuous phase, plug flow basis
y	dispersed phase solute weight fraction
y*(x)	weight fraction solute in dispersed phase, equilibrium with x
z	column vertical position
Z	total column height

Greek symbols

μ_C,μ_D	viscosity, continuous and dispersed phases
ρ_C,ρ_D	densities, continuous and dispersed phases
ξ	reduced radial coordinate, oscillating drop (4r/d)
ξ'	$1 - \xi$
ϕ	fraction dispersed phase holdup
θ	drop residence time in column

Subscripts

C,D referring to continuous, dispersed phases

i referring to drops in a particular size interval

REFERENCES

(1) Chartres, R.H. and Korchinsky, W.J., Trans. Inst. Chem. Engrs. 1975 53 247.

(2) Korchinsky, W.J. and Azimzadeh-Khatayloo, S., Chem. Eng. Sci. 1976 31 871.

(3) Chartres, R.H., Ph.D. Thesis, The Victoria University of Manchester, 1975.

(4) Misek, T., Coll. Czech. Chem. Commun. 1964 29 1755.

(5) Olney, R.B., A.I.Ch.E.Jl. 1964 10 (6) 827.

(6) Cruz-Pinto, J.J.C., Transfer Report, University of Manchester Institute of Science and Technology, 1976.

(7) Barnea, E. and Mizrahi, J., Chem. Eng. Jl. 1973 5 171.

(8) Barnea, E. and Mizrahi, J.,Can. J. Chem. Eng. 1975 53 461.

(9) Rod, V., Br. Chem. Eng. 1966 11 483.

(10) Newman, A.B., Trans. A.I.Ch.E. 1931 27 310.

(11) Kronig, R. and Brink, J.C., Appl. Sci. Res. 1950 A-2 142.

(12) Handlos, A.E. and Baron, T., A.I.Ch.E.Jl. 1957 3 127.

(13) Rose, P.M. and Kintner, R.C., A.I.Ch.E.Jl. 1966 12 530.

(14) Angelo, J.B., Lightfoot, E.N. and Howard, D.W., A.I.Ch.E.Jl. 1966 12 751.

(15) Olander, D.R., A.I.Ch.E.Jl. 1966 12 1018.

(16) Elzinga, E.R. and Banchero, J.T., Chem.Eng. Prog. Symp. Series 1959 55 (29) 149.

(17) Wellek, R.M. and Skelland, A.H.P., A.I.Ch.E.Jl. 1965 11 557.

(18) Patel, J.M. and Wellek, R.M., A.I.Ch.E.Jl. 1967 13 384.

(19) Cruz-Pinto, J.J.C., Ph.D. Thesis (Univ. Manchester) - in preparation.

(20) Valentas, K.J. and Amundson, N.R., Ind. Eng. Chem. Fund. 1966 5 538.

(21) Coulaloglou, C.A. and Tavlarides, L.L., Chem. Eng. Sci. 1977 32 1289.

(22) Park, J.Y. and Blair, L.M. Chem. Eng. Sci. 1975 30 1057.

(23) Kung, E.Y. and Beckmann, R.B., A.I.Ch.E.Jl. 1961 7 319.

(24) Murakami, A., Misonou, A. and Inoue, K., Int. Chem. Eng. 1978 18 (1) 16.

(25) Misek, T., "Longitudinal Mixing Phenomena in Rotating Disc Contactors" meeting in Prague, 9th April, 1970.

(26) Misek, T., Coll. Czech. Chem. Comm. 1975 40 1686.

(27) Calderbank, P.M. and Moo-Young, M.B., Chem. Eng. Sci. 1961 16 39.

TABLE 1

Operating Variables for Liquid-Liquid Extraction Runs

Run No.	Geometry	Distributor*	Column Temp. (°C)	Volumetric Flowrates (cm^3/sec) Cont. Phase	Disp. Phase	Dispersed Phase Holdup (%)	Disc Speed (r.p.m.)	Average Drop Diameter - d_{32} (cm)	Efficiency - N_{ODP} (Dispersed Phase Basis)
1	A	I	19.0	10.0	20.0	4.9	225	0.123	0.718	3.67
2		IV	17.8	29.5	51.0	9.2	240	0.178	0.734	2.87
3		III	20.5	20.0	34.5	4.4	240	0.181	0.643	1.94
4		IV	8.7	20.0	34.5	5.7	240	0.190	0.788	3.02
5		III	16.5	29.5	51.0	7.0	240	0.174	0.690	2.24
6		V	22.5	28.5	45.3	7.7	307	0.159	0.695	2.35
7		IV	22.1	28.5	45.3	9.3	307	0.165	0.763	3.32
8		IV	23.6	20.0	30.8	5.7	307	0.161	0.764	3.30
9	B	IV	26.5	20.0	34.5	3.9	293	0.175	0.615	1.91
10		IV	22.9	29.5	51.0	5.5	293	0.172	0.651	2.12
11		IV	24.3	39.0	61.8	7.0	293	0.175	0.670	2.15
12	A	II	-	25.8	51.5	6.4	300	See Fig. 2	No mass transfer with solute present	

*Distributors: I - 220 irregular holes of 0.1 cm. diam.
II - 220 holes of 0.159 cm. diam.
III - 12 holes of 0.159 cm. diam. + 40 holes of 0.099 cm. diam.
IV - 85 holes of 0.099 cm. diam.
V - 40 holes of 0.099 cm. diam. + 9 holes of 0.159 cm. diam. + 3 holes of 0.24 cm. diam.

TABLE 2

TABLE 2

Calculated Value of the Column Constriction Factor, C_K (Based on Experimental Drop Size Distributions)

Run No.	C_K - Based on Average Column Holdup: Hydrodynamic Model: Olney	Misek	Barnea-Mizrahi	C_K - Based on Predicted* Local Holdups: Hydrodynamic Model: Olney	Misek	Barnea-Mizrahi
1	0.274	0.289	0.314	0.274		
2	0.276	0.323	0.328	0.287		
3	0.337	0.365	0.382	0.334		
4	0.263	0.291	0.303	0.284		
5	0.351	0.395	0.407	0.358		
6	0.301	0.341	0.352	0.335		
7	0.260	0.301	0.310	0.269		
8	0.273	0.298	0.315	0.288		
9	0.412	0.440	0.469	0.408	0.436	0.465
10	0.447	0.490	0.514	0.458	0.502	0.532
11	0.427	0.481	0.498	0.432	0.486	0.505
12	0.292	0.331	0.309	0.287	0.329	

*Local holdups were predicted by applying Equation 9 to each of the compartments for which size distributions were measured and interpolating between them.

TABLE 3

Experimental vs Predicted Column Holdup by Previous Correlations

Run No.	Dispersed Phase Holdup, %: Experimental	Kung and Beckmann (23)	Murakamietal (24)
1	4.9	1.4	1.5
2	9.2	3.5	4.0
11	7.0	4.1	4.0
12	6.4	5.6	4.4

TABLE 4

TABLE 4

Comparison of Experimental with Theoretically Predicted* Data

Run No.		Experimental	Theoretical: Rigid: Approx.	Rigid: Exact	Handlos-Baron: Approx.	Handlos-Baron: Exact
1	E_{OD}	0.718	0.622	0.647	0.666	0.685
	N_{ODP}	3.67	2.032	2.327	2.599	2.925
2	E_{OD}	0.734	0.579	0.655	0.734	0.774
	N_{ODP}	2.87	1.403	1.952	2.863	3.605
3	E_{OD}	0.643	0.468	0.552	0.652	0.696
	N_{ODP}	1.94	0.910	1.296	2.023	2.520
4	E_{OD}	0.788	0.569	0.659	0.764	0.808
	N_{ODP}	3.02	1.217	1.716	2.692	3.335
5	E_{OD}	0.690	0.525	0.613	0.714	0.759
	N_{ODP}	2.24	1.107	1.586	2.505	3.164
6	E_{OD}	0.695	0.556	0.633	0.714	0.754
	N_{ODP}	2.35	1.273	1.766	2.582	3.189
7	E_{OD}	0.763	0.616	0.683	0.745	0.781
	N_{ODP}	3.32	1.629	2.198	3.006	3.688
8	E_{OD}	0.764	0.586	0.653	0.720	0.755
	N_{ODP}	3.30	1.426	1.904	2.611	3.143
9	E_{OD}	0.615	0.448	0.515	0.609	0.643
	N_{ODP}	1.91	0.882	1.190	1.851	2.208
10	E_{OD}	0.651	0.467	0.542	0.646	0.684
	N_{ODP}	2.12	0.927	1.277	2.067	2.512
11	E_{OD}	0.670	0.481	0.559	0.673	0.715
	N_{ODP}	2.15	0.949	1.314	2.186	2.698

*Calderbank-Moo Young (27) k_c used, influences of drop size distribution, small settling zone, included.

TABLE 5

Comparing the Effects of Different Boundary Conditions and of Axial Mixing

Run No.	Predicted Efficiencies (N_{ODP})							
	Rigid				Handlos-Baron			
	Approx.		Exact		Approx		Exact	
	$E_c \neq 0$	$E_c = 0$	$E_c \neq 0$	$E_c = 0$	$E_c \neq 0$	$E_c = 0$	$E_c \neq 0$	$E_c = 0$
2	1.403	1.644	1.952	2.459	2.863	4.088	3.605	5.796
3	0.910	1.050	1.296	1.598	2.023	2.864	2.520	3.991
4	1.217	1.420	1.716	2.158	2.692	3.993	3.335	5.636
5	1.107	1.249	1.586	1.890	2.505	3.397	3.164	4.757

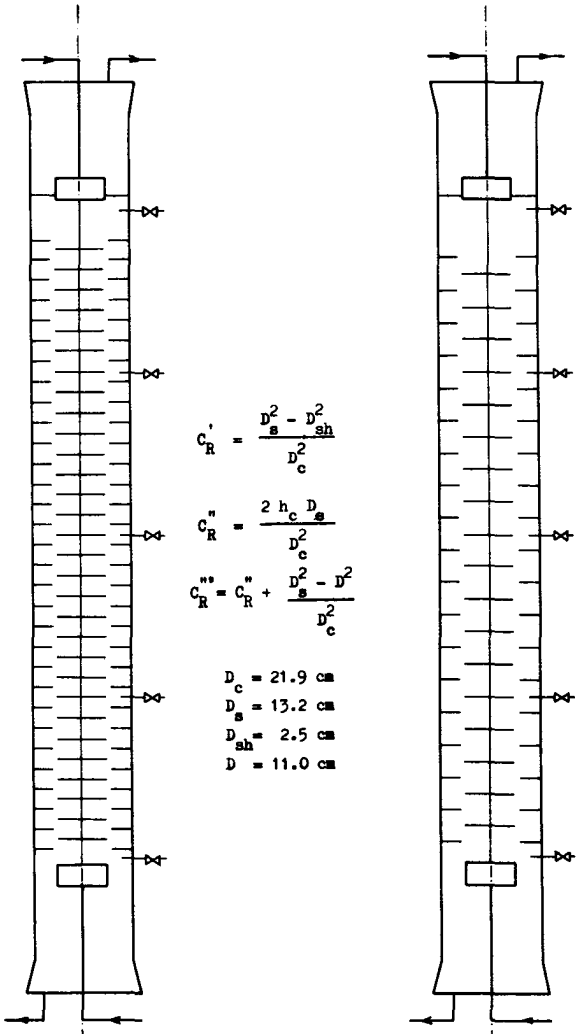

$$C_R' = \frac{D_s^2 - D_{sh}^2}{D_c^2}$$

$$C_R'' = \frac{2 h_c D_s}{D_c^2}$$

$$C_R''' = C_R'' + \frac{D_s^2 - D^2}{D_c^2}$$

D_c = 21.9 cm
D_s = 13.2 cm
D_{sh} = 2.5 cm
D = 11.0 cm

Geometry A
h_c = 4.5 cm
C_R' = 0.35
C_R'' = 0.25
C_R''' = 0.36

Geometry B
h_c = 7.2 cm
C_R' = 0.35
C_R'' = 0.40
C_R''' = 0.51

Figure 1: Rotating Disc Contactor (RDC) Geometrics Used

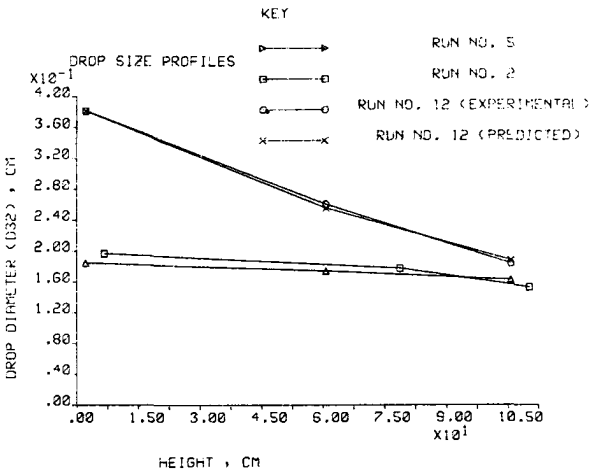

Figure 2: Drop Size Profiles

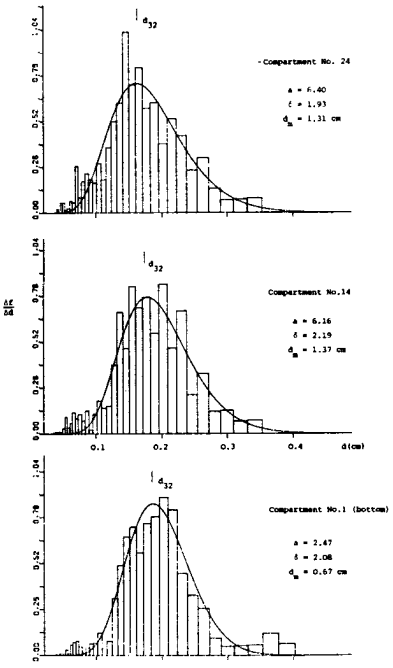

Figure 3: Measured Drop Size Distributions and Best-Fit Mugele-Evans* functions (Run No.5)

$$*\frac{df}{dd} = \frac{\delta}{\sqrt{\pi}} \cdot \frac{d_m}{d(d_m - d)} \cdot \exp\left[- \left(\ln \frac{ad}{d_m - d}\right)^2 \delta^2 \right]$$

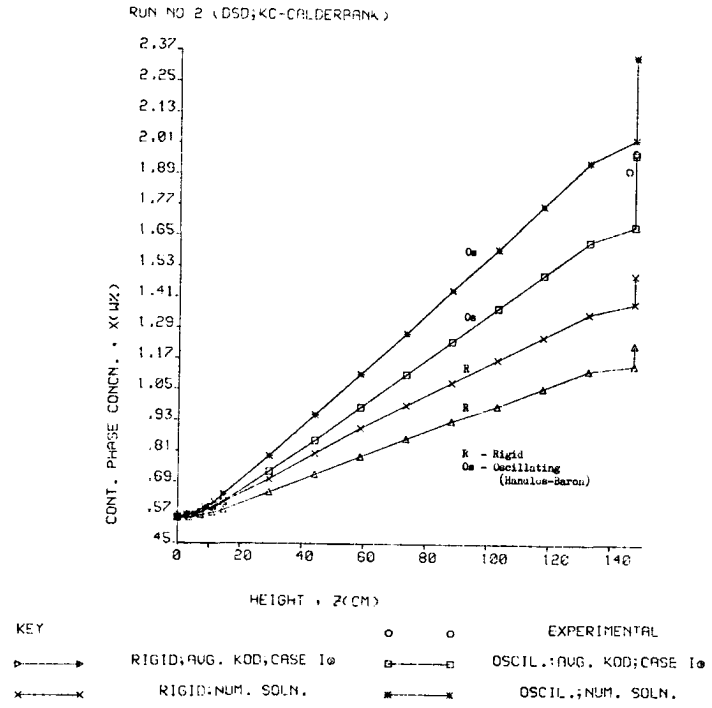

Figure 4: Model Concentration Profiles, Continuous Phase, Run 2

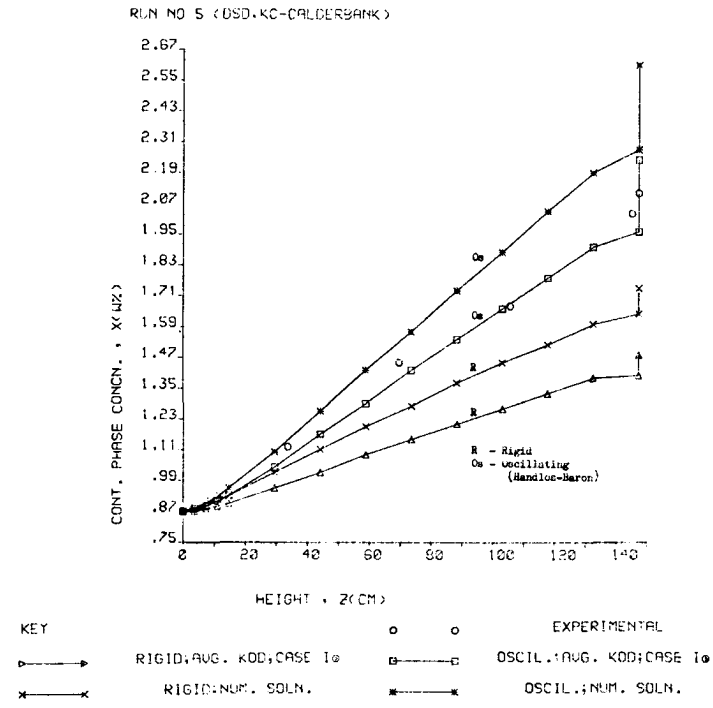

Figure 5: Model and Experimental Concentration Profile, Continuous Phase, Run 5

ABSORPTION ACCOMPANIED BY LARGE HEAT EFFECTS FOR THE SYSTEM CHLORINE-CARBON TETRACHLORIDE

Dr. W. Peier
Professor A.B. Ponter †
Dr. N.Q. Hien

Swiss Federal Institute of Technology, Lausanne, Switzerland.
Now † University of Aston in Birmingham, Gosta Green, Birmingham.

ABSTRACT

Absorption rates of chlorine into films of carbon tetrachloride have been measured using a short wetted wall column. When comparing the results with those obtained using a laminar jet column where the contact times between the gas and liquid are much lower, the influence of this parameter on mass transfer enhancement, has been ascertained. Temperatures at the wall and in the liquid film have been determined using microthermocouples, which have allowed a model to be developed to predict absorption rates for systems where heat is generated. Reasonable agreement between predicted and experimental values is obtained except at low flowrates and causes for this are postulated.

INTRODUCTION

At the present time there is no reliable method to predict the rates of gas absorption into a liquid film when the process is accompanied by large heat releases. Chiang and Toor (1) developed a model which took into account volume change due to the heat effects in the liquid phase and were able to predict rates of absorption for ammonia into water with reasonable success but failed when considering the chlorine-carbon tetrachloride system. Clegg and Mann (2) measured the absorption rates of chlorine in a jet of carbon tetrachloride and the experimentally determined rates were found to be approximately three times higher than that predicted by the Penetration Theory under isothermal conditions. These workers concluded that the observed increase was caused by turbulence in the liquid phase since Ruckenstein and Berbente (3) had previously suggested a similar mechanism for mass transfer enhancement in liquid-liquid systems.

In the work now presented a model is developed to describe the process where a gas is absorbed in a liquid film flowing down a vertical surface and where heat is generated. The validity of the model is assessed by comparing the predicted absorption rates with those measured using the chlorine-carbon tetrachloride system with a short wetted-wall column.

MODEL

The physical model shown in Figure 1 comprises a

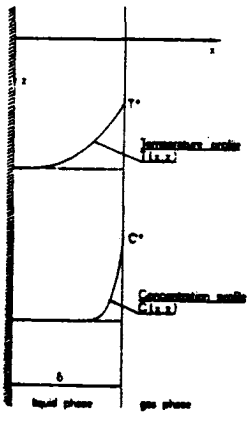

Fig. 1 FALLING FILM MODEL

liquid film flowing down a vertical wall in contact with a one-component gas. The liquid is assumed to be non-volatile.

To simplify the mathematical treatment the following assumptions are made:

1. The concentration c^* at the liquid-gas interface is the equilibrium value corresponding to the interfacial temperature T^*.
2. The interfacial temperature T^* is considered constant along the film.
3. The heat of solution is released instantaneously at the gas-liquid interface.
4. Dufour and Soret effects are negligible.
5. The gradients of density, specific heat and transport coefficients with the exception of the viscosity across the film are negligible.
6. The heat of solution is propagated into the liquid phase only, the heat conduction into the gas phase being insignificant.

For the considered geometry Schlichting (4) and Eckert and Drake (5) have shown, taking into account the above assumptions, that the rate equations reduce to

$$v_x \frac{\partial v_z}{\partial x} + v_z \frac{\partial v_z}{\partial z} = \frac{\partial U}{\partial x} \frac{\partial v_z}{\partial x} + \nu \frac{\partial^2 v_z}{\partial x^2} + g \qquad (1)$$

$$\frac{\partial v_x}{\partial x} + \frac{\partial v_z}{\partial z} = 0 \qquad (2)$$

$$v_x \frac{\partial c}{\partial x} + v_z \frac{\partial c}{\partial z} = D \frac{\partial^2 c}{\partial x^2} \qquad (3)$$

$$v_x \frac{\partial T}{\partial x} + v_z \frac{\partial T}{\partial z} = \alpha \frac{\partial^2 T}{\partial x^2} \qquad (4)$$

In equation (1) the kinematic viscosity has been introduced.

The above system of differential equations has to be completed by appropriate boundary conditions. In particular the mass flux $\underline{j}$ and the heat flux $\underline{q}$ at the interface are related by the equation

$$\Delta H_s j_x = q_x, \qquad (5)$$

where H_s is the heat of solution.

Firstly, the velocity field is determined by solving equations (1) and (2). The transformation

$$\hat{v}_x = v_x - \frac{\partial v}{\partial x} \qquad (6)$$

yields the more familiar equation of motion.

(CONTINUED NEXT PAGE)

EXPERIMENTAL

Absorption rates for the chlorine/carbon tetrachloride system were measured using a 3.86 cm diameter wetted-wall column whose length could be adjusted up to a maximum of 11 cm (Figure 2).

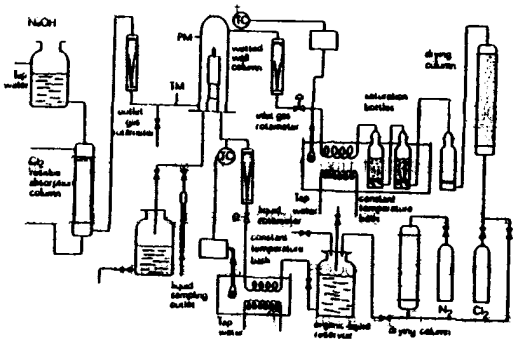

Fig 2 EXPERIMENTAL ARRANGEMENT.

The liquid inlet temperature was maintained at 293°K and the temperatures at the wall and in the liquid film were determined using calibrated micro-thermocouples. The densities and viscosities of the chlorine/carbon tetrachloride mixtures were measured at different temperatures and chlorine concentrations and have been reported elsewhere by Hien et al. (8). Absorption rates

were measured using liquid flow rates ranging from 1.275×10^{-3} kg/s to 1.448×10^{-2} kg/s and five different column lengths of 2.5×10^{-2} m to 1.1×10^{-1} m.

$$\hat{v}_x \frac{\partial v_z}{\partial x} + v_z \frac{\partial v_z}{\partial z} = g + \nu \frac{\partial^2 v_z}{\partial x^2}, \qquad (7)$$

where $\hat{v}_x$ is the relative velocity in the x-direction after subtraction of the velocity caused by the temperature gradient. The transformed equation of continuity then reads

$$\frac{\partial \hat{v}_x}{\partial x} + \frac{\partial v_z}{\partial z} + \frac{\partial^2 \nu}{\partial x^2} = 0. \qquad (8)$$

A solution of these two coupled differential equations where equation (7) is non-linear is complex. As the absorption rate is determined by the hydrodynamics taking place near the interface, it is sufficient to find a solution which is valid for this domain.

Assuming that

$$\frac{\partial^2 \nu}{\partial x^2} \simeq 0 \qquad (9)$$

near the interface the equations (7) and (8) reduce to the well-known boundary layer equations whose solutions can be found by a power series expansion when the boundary conditions

$$\hat{v}_x = v_z = 0 \quad \text{at } x = 0 \qquad (10)$$

$$v_z \to U(z) \quad \text{for } x \to \infty \qquad (11)$$

are valid (see Schlichting (4), Falkner (6), Hartree (7).

With the variable

$$\zeta = x \sqrt{\frac{(m+1)\,U}{2z\nu}} \qquad (12)$$

the components of the velocity field are

$$v_z = U \frac{df}{d\zeta} \qquad (13)$$

and

$$\hat{v}_x = -\sqrt{\nu \frac{(m+1)\,U}{2z}} \cdot \{f + \frac{m-1}{m+1} \zeta \frac{df}{d\zeta}\}, \qquad (14)$$

where f is a solution of the differential equation

$$\frac{d^3 f}{d\zeta^3} + f \frac{d^2 f}{d\zeta^2} + \frac{2m}{m+1}\left(1 - \left(\frac{df}{d\zeta}\right)^2\right) = 0 \qquad (15)$$

and

$$U = az^m, \qquad (16)$$

a being an arbitrary constant.

f can be approximated by a power series in ζ.

In this case

$$U = \sqrt{v_o^2 + 2gz}, \qquad (17)$$

where v_o is the initial velocity at the interface.

From equation (17) it is evident that for $z \ll \frac{v_o^2}{2g}$, $m = 0$; for $z \gg \frac{v_o^2}{2g}$, $m \simeq \frac{1}{2}$. In the case of $m=0$ the boundary layer becomes thicker, i.e. $\hat{v}_x$ is directed away from the wall. For $m=\frac{1}{2}$ the boundary layer becomes thinner and $\hat{v}_x$ has the opposite direction. As the mean absorption rate is calculated by integrating the local rate over the wall length it is assumed that $\hat{v}_x$ can be approximated by some mean value

$$\hat{v}_x = 0. \qquad (18)$$

From the continuity law it then follows that

$$\frac{\partial v_z}{\partial z} = 0, \qquad (19)$$

and

$$v_z = \frac{g}{2\nu}(2\delta x - x^2), \qquad (20)$$

where δ is the film width.

Insertion of equation (18) into equation (6) yields

$$v_x = \frac{\partial \nu}{\partial x}, \qquad (21)$$

which is a constant because of equation (9). There exists a constant flux of liquid from the gas-liquid interface towards the wall caused by the large temperature gradients near the interface. Since no liquid can penetrate the wall, mass conservation is only respected if there

exists a counterflow of liquid with the same velocity $|v_x|$ towards the interface. In this way energy and mass are transferred by convection from the interface into the film.

The diffusion equation (3)

$$v_x \frac{\partial c}{\partial x} + v_z \frac{\partial c}{\partial z} = D \frac{\partial^2 c}{\partial x^2}$$

can be solved subject to the following initial and boundary conditions

$$c = 0 \quad \text{at } z = 0, \quad x = 0 \tag{22}$$

$$c = c^* \quad \text{at } x = \delta, \quad z > 0 \tag{23}$$

$$\frac{\partial c}{\partial x} = 0 \quad \text{at } x = 0, \quad z > 0. \tag{24}$$

Assuming that v_x is a more slowly varying function of z than the concentration c, then the Laplace transform L of equation (7) reads

$$v_x \frac{\partial \bar{c}}{\partial x} + v_z s\bar{c} = D \frac{\partial^2 \bar{c}}{\partial x^2}, \tag{25}$$

where

$$\bar{c} = L(c) \equiv \int_0^\infty dz\, e^{-zs}\, c. \tag{26}$$

The solution of equation (25) subject to the boundary conditions (22) to (24) is

$$\bar{c} = \frac{c^*}{s} \frac{\left(e^{q_1 x} - \frac{q_1}{q_2} e^{q_2 x}\right)}{\left(e^{q_1 \delta} - \frac{q_1}{q_2} e^{q_2 \delta}\right)} \tag{27}$$

with

$$q_{1,2} = + \frac{v_x}{2D} \pm \sqrt{\frac{v_x^2 + 4 v_z D s}{4D^2}} \tag{28}$$

The concentration profile is then determined by the inverse Laplace transform

$$c = L^{-1}(\bar{c}). \tag{29}$$

The mass flux at the gas-liquid interface at z into the film is defined by

$$j_x = D \left.\frac{\partial c}{\partial x}\right|_{x=\delta} - v_x (c^* - c_o), \tag{30}$$

where c_o is the concentration near the wall. The first term on the right-hand side of equation (30) describes the mass transfer caused by diffusion. The second term takes account of convection; liquid with the concentration c^* leaves the interface into the film whereas liquid from the interior arrives with the concentration c_o.

Since

$$D \frac{\partial c}{\partial x} = D \frac{\partial}{\partial x} (L^{-1}(\bar{c})) = L^{-1}\left(D \frac{\partial \bar{c}}{\partial x}\right) \tag{31}$$

holds, $\frac{\partial \bar{c}}{\partial x}$ has to be calculated yielding

$$D \left.\frac{\partial \bar{c}}{\partial x}\right|_{x=\delta} = c^* v_z \frac{1}{\sqrt{\frac{v_x^2 + 4 v_z D s}{4D^2}} \operatorname{cot} \sqrt{\frac{v_x^2 + 4 v_z D s}{4D^2}} - \frac{v_x}{2D}} \tag{32}$$

Only small values of z ($z < 0{,}1$) or equivalently large values of s are of interest. $D \left.\frac{\partial \bar{c}}{\partial x}\right|_{x=\delta}$ can therefore be expanded as a power series in $\frac{1}{s}$, giving

$$D \left.\frac{\partial \bar{c}}{\partial x}\right|_{x=\delta} = c^* \sqrt{\frac{v_z D}{s}} + O\left(s^{-\frac{3}{2}}\right), \tag{33}$$

where O indicates the order.

The inverse Laplace transform yields as a first approximation

$$D \left.\frac{\partial c}{\partial x}\right|_{x=\delta} = c^* \sqrt{\frac{v_z D}{\pi z}}. \tag{34}$$

The first approximation neglects the effects of convection on the diffusional part of the mass flux.

Insertion of equations (21) and (34) into equation (30) yields

$$j_x = c^* \sqrt{\frac{v_z D}{\pi z}} - \frac{\partial v}{\partial x} \Delta c, \tag{35}$$

where

$$\Delta c = c^* - c_o. \tag{36}$$

As c_o is very small in all cases considered it can be approximated by the solution of the penetration model

$$c_o = c^* \operatorname{erfc} \frac{\delta}{2\sqrt{\frac{D z}{v_z}}}, \tag{37}$$

Therefore

$$\Delta c = c^* \operatorname{erf} \frac{\delta}{2\sqrt{\frac{D z}{v_z}}} \qquad (38)$$

The heat flux q_x at the interface into the film is

$$q_x = \rho C_p \left(\alpha \frac{\partial T}{\partial x}\Big|_{x=\delta} - \frac{\partial \nu}{\partial x} \Delta T\right), \qquad (39)$$

where ΔT is the difference between the constant interfacial temperature T^* and the liquid temperature near the wall, i.e.

$$\Delta T = T^* - T_o. \qquad (40)$$

The first term on the right-hand side of equation (39) describes heat conduction, the other describing heat convection. Again it is assumed that T_o can be approximated by the solution of penetration theory yielding

$$\Delta T = \Delta T^* \operatorname{erf} \frac{\delta}{2\sqrt{\frac{\alpha z}{v_z}}}, \qquad (41)$$

where

$$\Delta T^* = T^* - T_i. \qquad (42)$$

and T_i indicates the initial temperature of the liquid.

The temperature gradient can be determined by equation (5) which relates heat and mass flux at the interface, together with the fact that $\frac{\partial \nu}{\partial x}\Big|_{x=\delta}$ can be approximated by

$$\frac{\partial \nu}{\partial x}\Big|_{x=\delta} = \frac{\partial \nu}{\partial T} \frac{\partial T}{\partial x}\Big|_{x=\delta} \qquad (43)$$

since temperature is the only variable changing significantly. $\frac{\partial \nu}{\partial T}$ can be considered constant over the temperature range of interest.

Thus

$$\frac{\partial T}{\partial x}\Big|_{x=\delta} = \frac{c^* \Delta H_s}{\alpha \rho C_p - \rho C_p \Delta T \frac{\partial \nu}{\partial T} + \Delta H_s \Delta c \frac{\partial \nu}{\partial T}} \sqrt{\frac{D v_z}{\pi z}} \qquad (44)$$

and insertion of equation (43) into the expression for the local absorption rate yields

$$j_x = c^* \sqrt{\frac{v_z D}{\pi z}} \left(\frac{\frac{\alpha}{\left|\frac{\partial \nu}{\partial T}\right|} + \Delta T}{\frac{\alpha}{\left|\frac{\partial \nu}{\partial T}\right|} + \Delta T - \frac{\Delta H_s \Delta c}{\rho C_p}} \right) \qquad (45)$$

where

$$\left|\frac{\partial \nu}{\partial T}\right| = - \frac{\partial \nu}{\partial T}. \qquad (46)$$

The mean absorption rate is defined by

$$\bar{j}_x = \frac{1}{L} \int_o^L dz \, j_x, \qquad (47).$$

where L is the observed wall length.

If concentration and temperature near the wall are approximated by some mean values $\bar{c}_o$ and $\bar{T}_o$ respectively then after the insertion of equation (45) into equation (47) the integration is straightforward to yield

$$\bar{j}_x = 2c^* \frac{\frac{\alpha}{\left|\frac{\partial \nu}{\partial T}\right|} + \overline{\Delta T}}{\frac{\alpha}{\left|\frac{\partial \nu}{\partial T}\right|} + \overline{\Delta T} - \frac{\Delta H_s \overline{\Delta c}}{\rho C_p}} \sqrt{\frac{D}{\pi \theta}}, \qquad (48)$$

or equivalently

$$\bar{j}_x = 2c^* \left(1 + \frac{\frac{\Delta H_s \overline{\Delta c}}{\rho C_p}}{\frac{\alpha}{\left|\frac{\partial \nu}{\partial T}\right|} + \overline{\Delta T} - \frac{\Delta H_s \overline{\Delta c}}{\rho C_p}}\right) \sqrt{\frac{D}{\pi \theta}}. \qquad (49)$$

In equations (48) and (49) the contact time θ defined by

$$\theta = \frac{L}{v_z} \qquad (50)$$

and the mean values $\overline{\Delta T}$ and $\overline{\Delta c}$ defined by

$$\overline{\Delta T} = T^* - \bar{T}_o \qquad (51)$$

$$\overline{\Delta c} = c^* - \bar{c}_o \qquad (52)$$

have been introduced.

The particular form of the expression for the mean absorption rate allows one to introduce an effective diffusivity D_{eff} defined by

$$D_{eff} = D\left[1 + \left(\frac{\frac{\Delta H_s \overline{\Delta c}}{\rho C_p}}{\frac{\alpha}{\left|\frac{\partial \nu}{\partial T}\right|} + \overline{\Delta T} - \frac{\Delta H_s \overline{\Delta c}}{\rho C_p}}\right)\right]^2, \quad (53)$$

which in addition to the molecular diffusion constant D depends on the thermal diffusivity , the heat of solutions H_s and the gradient of the kinematic viscosity with respect to the temperature $\left|\frac{\partial \nu}{\partial T}\right|$.

COMPARISON OF THEORY AND EXPERIMENT

The experimentally determined wall temperatures T_o indicate that the interfacial temperature of the chlorine/carbon tetrachloride system is constant at about 15°K above the initial liquid temperature T_i of 293°K and that the difference between interfacial and wall temperature T is well approximated by equation (41) with $T^* = 15$, i.e. $\Delta T = 15 \operatorname{erf} \frac{\delta}{2\sqrt{\alpha\theta}}$. For the lowest measured flow rate corresponding to a film width δ of 1.1×10^{-4} m and the longest contact time of 1 sec, ΔT falls to about 3°K. For the highest measured flow rate ($\delta = 2.5 \times 10^{-4}$ m) and the shortest contact time of 0.05 sec, ΔT is nearly zero. The difference between interfacial and wall concentration Δc is calculated from equation (38), i.e. $\Delta c = c^* \operatorname{erf} \frac{\delta}{2\sqrt{\theta D}}$. Except for the lowest flow rate $c \cong c^*$ holds.

For low flow rates and long contact times the model does not describe the experiment well. For the restricted domain of validity of the model it is consistent to approximate Δc by

$$\Delta c = c^*. \quad (54)$$

If the mean value $\overline{\Delta T}$ is approximated by

$$\overline{\Delta T} = \frac{15}{2}\left(1 + \operatorname{erf} \frac{\delta}{2\sqrt{\alpha\theta}}\right) \quad (55)$$

($\Delta T = 15$ for $\theta = 0$), the mean absorption rate as a function of the film width and the contact time can be determined.

All physical properties at 308°K are listed in Table 1.

TABLE I - Physical Properties of Chlorine/Carbon Tetrachloride at 308°K.

C_p ($m^2/sec^2\ ^oK$)	8.71×10^2
ρ (kg/m^3)	1.564×10^3
α (m^2/sec)	7.79×10^{-8}
c^* (mol/m^3)	1.400×10^3
ΔH_s (J/mol)	1.85×10^4
D (m^2/sec)	3.34×10^{-9}
η (kg/sec m)	8.4×10^{-4}
$\frac{\partial \nu}{\partial T}$ ($m^2/sec\ ^oK$)	6.4×10^{-9}

Insertion of equations (54) and (55) as well as the numerical values of Table I into equation (49) yields

$$\overline{j_x} = 0.091\left(1 + \frac{19.0}{0.66 + 7.5 \operatorname{erf} \frac{1790\delta}{\sqrt{\theta}}}\right)\frac{1}{\sqrt{\theta}}. \quad (56)$$

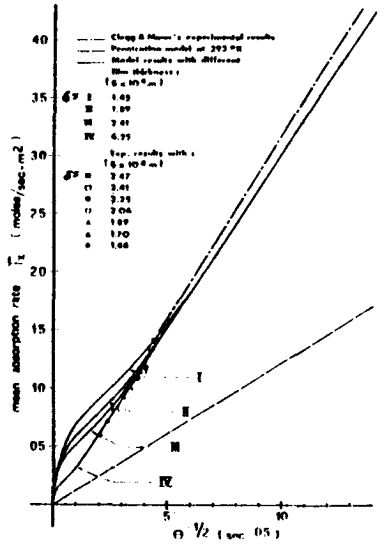

Fig 3 COMPARISON OF MODELS AND EXPERIMENTAL RESULTS.

In Figure 3 the mean absorption rate calculated by equation (56) is represented as a function of $\theta^{-\frac{1}{2}}$ for four different film widths. The experimental results obtained in this investigation with a falling film and the results obtained by Clegg and Mann (2) with a laminar jet are plotted for comparison and the values predicted by penetration theory at 293°K are added for completion.

The model gives a satisfactory description of the experiment when

$$\frac{\delta}{\theta} > \frac{1}{1790} \qquad (57)$$

holds, the mean absorption rate becoming proportional to $\theta^{-\frac{1}{2}}$ which is in accord with the rate determined from experiments. The laminar jet can be treated in a similar manner as the falling film, since the widths and the contact times of the jet are always such that equation (57) is satisfied. Thus the model curve fits very well the experimental values found by Clegg and Mann (2). For very low flow rates and a long contact time equation (57) is not satisfied however since the absorption rates calculated with the model are then too high. Reasons why the model description fails in this case is that several approximations made in the derivation of the mean absorption rate are then not justified namely

1. The influence of convection on the diffusional part of the mass flux cannot be neglected, and
2. The relative velocity component $\hat{v}_x$ cannot be approximated by a mean value $\hat{v}_x = 0$.

In addition, for very thin films the interfacial tension has probably to be included explicitely into the description of the system.

CONCLUSIONS

The model developed to describe gas absorption with large heat effects clearly shows that the enhancement in the absorption rate is due to convection taking place in the liquid phase caused by large viscosity gradients near the interface. The results obtained with the model are in accord with those determined by experiment except in the case of very low flow rates and long contact times where the criterion (57) does not hold.

NOMENCLATURE

c	concentration of dissolved gas in the film
c_o	concentration of dissolved gas near the wall
c^*	concentration of dissolved gas at the interface
Δc	difference of concentrations defined by (36)
$\overline{\Delta c}$	mean value of c
C_p	specific heat
D	molecular diffusion coefficient
D_{eff}	effective diffusivity
f	function defined by equation (15)
g	gravity acceleration
ΔH_s	heat of solution
$\underline{j}$	mass flux of dissolved gas at the interface
$\overline{j}_x$	mean absorption rate
L	observed wall length
$\underline{q}$	heat flux at the interface
T_i	initial liquid temperature
T_o	temperature at the wall
T	temperature in the liquid

T^*	temperature at the interface
ΔT	temperature difference defined by equation (40)
ΔT^*	temperature difference defined by equation (42)
$\overline{\Delta T}$	mean value of T
U	velocity of the potential flow
$\underline{v}$	velocity field
$\hat{v}$	relative velocity
v_i	initial velocity in z direction
x,z	spatial coordinates

GREEK SYMBOLS

α	thermal diffusivity
δ	film width
ν	kinematic viscosity of liquid
η	viscosity of liquid
ρ	density of liquid
ξ	variable defined by equation (12)
θ	contact time

ACKNOWLEDGEMENT

To Suisse Fond Nationale for financial support (N.Q.H.).

REFERENCES

1. Chiang S.H. and Toor H.L., AIChE J. 1964 10 398.
2. Clegg G.T. and Mann R., Chem. Eng. J. 1972 4 243.
3. Ruckenstein E. and Berbente C., Chem.Eng.Sci. 1970 25 475.
4. Schlichting H., Boundary Layer Theory. McGraw-Hill, New York 1968.
5. Eckert E.R.G. and Drake R.M., Heat and Mass Transfer. McGraw-Hill, New York 1959.
6. Falkner V.M. and Skan S.W., Phil.Mag.S. 1931 12 865.
7. Hartree D.R., Proc. Cambr. Phil. Soc. 1937 33 223.
8. Hien N.Q., Ponter A.B. and Peier W., J.Chem. Eng.Data. 54, 23 (1978).

I THE CHOICE OF A SUITABLE EFFICIENCY MODEL

A.G. Medina[1], M. Ashton[2], G. McDermott[2]

1. Centro de Engenharia Química da Universidade do Porto, Portugal
2. University of Birmingham, Birmingham, England

ABSTRACT

The design of industrial distillation columns is normally based on estimated values of plate efficiencies. Although several plate efficiency models have been proposed in the literature Murphree's model is still widely used. However it has already been shown that the model proposed by Hausen overcomes limitations of Murphree's model and is in agreement with physical reality.

In the present paper the differences between both models are reviewed and the merits of Hausen's model are emphasized. It is shown that Hausen plate efficiencies can be easily calculated and also used in plate to plate calculations.

An analysis of point efficiency definitions is also presented and a previous Hausen point efficiency model is discussed.

Three phase distillation processes are considered and Hausen plate efficiencies for a typical situation are defined.

INTRODUCTION

The design of industrial distillation columns involves the calculation of the number of theoretical stages and the estimation of plate efficiencies.

A different number of algorithms has been proposed in the literature for the calculation of the number of theoretical stages[12,13,16]. Computer programs for the simulation and optimization of distillation columns are now freely available[2].

The problem of the simulation of plate efficiencies is a more delicate one as experimental values are not always known ; although correlations for the prediction of binary plate efficiencies have been published, little is known as far as multicomponent systems are concerned. Reports published as a result of the work sponsored by the American Institute of Chemical Engineers[1,3] recommended the use of a constant plate efficiency for the different components based on an estimated value for the key components: however this is unsatisfactory as efficiencies may be different for the different components[6,8,10].

Although several plate efficiency models have been proposed in the literature, Murphree's model is still widely used. However it has already been shown[7] that the model proposed by Hausen[4] overcomes limitations of Murphree's model and is in agreement with physical reality.

In the present paper the differences between both models are reviewed and the merits of the former are emphasized. A critical discussion of point efficiency definitions based on both models is presented. Reference is also made to the use of Hausen efficiencies in plate calculations and in three phase distillation processes.

MURPHREE AND HAUSEN EFFICIENCY MODELS

Plate efficiencies

Murphree vapour phase plate efficiency

for component i and plate n can be written as:

$$E_{MV_{n,i}} = \frac{y_{n,i} - y_{n+1,i}}{(y^*_{n,i})_M - y_{n+1,i}} \qquad (1)$$

where

$y_{n,i}$ and $y_{n+1,i}$ - mole fraction of component i in the vapour leaving and entering plate n respectively.

$(y^*_{n,i})_M$ - mole fraction of component i in the vapour in equilibrium with the liquid that leaves plate n.

Murphree liquid phase plate efficiency can be defined in a similar way and it is well known that the numerical values of the two efficiencies, for the same plate, are usually different.

Hausen efficiency for component i and plate n can be defined as:

$$E_{H_{n,i}} = \frac{y_{n,i} - y_{n+1,i}}{(y^*_{n,i})_H - y_{n+1,i}} \qquad (2)$$

where

$(y^*_{n,i})_H$ - mole fraction of component i in the vapour which results from a flash calculation with a feed equal to the sum of the streams entering the plate.

It can be easily shown that there is no difference between the numerical values of vapour and liquid Hausen plate efficiencies.

The distinction between the two models has been established for binary systems by Ho and Prince[5]; These authors defined the operating lines for the real plate and for the ideal plates, as considered by Hausen and Murphree, showing that the operating line for Hausen's ideal stage was parallel to the other two and that these coincided.

The different compositions and lines can be seen in Figs. 1 and 2 where the point $((x_n^*)_H , (y_n^*)_H)$ is defined by the intersection of the line that contains C' and D with the equilibrium line. It is clear that for the situation considered in Fig.1 $1 > E_H > E_{MV}$ and for that considered in Fig.2, $1 < E_H < E_{MV}$.

The algebraic relationship between Murphree's and Hausen's definitions can be written as:

$$E_{MV,i} = \frac{E_{H,i}}{\lambda_i + 1 - \lambda_i E_{H,i}} \qquad (3)$$

where

λ_i - ratio between the slopes of the equilibrium and operating lines; the equilibrium line refers to the locus of equilibrium points calculated from theoretical tray to theoretical tray.

A graphical representation of equation (3) is shown in Fig. 3.

Point efficiencies

Efficiency models can be used to describe the separation occuring in specific points of distillation plates.

Adopting Murphree's model , vapour phase Murphree point efficiency relates the vapour composition change occuring in a real plate along a vertical streamline with the separation to be obtained if the leaving vapour could reach equilibrium with the liquid existing in the vertical streamline. This liquid is assumed to have a uniform composition. Refering to Fig. 4 it can be written that:

$$E_{OV_{m,i}} = \frac{y_{m,i} - y_{m+1,i}}{(y^*_{m,i})_M - y_{m+1,i}} \qquad (4)$$

where

$y_{m,i}$ - mole fraction of component i in

the vapour leaving plate n at "point" m.

$y_{m+1,i}$ - mole fraction of component i in the vapour entering the plate at "point" m.

$(y^*_{m,i})_M$ - mole fraction of component i in the vapour in equilibrium with the liquid existing in the vertical streamline.

In a similar way Murphree liquid phase point efficiency can be defined (Fig.4) as:

$$E_{OL_{m,i}} = \frac{x_{m-1,i} - x_{m,i}}{x_{m-1,i} - (x^*_{m,i})_M} \qquad (5)$$

where

$x^*_{m,i}$ - mole fraction of component i in the liquid in equilibrium with the vapour leaving the liquid streamline for which the mole fraction of component i in the entering and leaving liquid streams are $x_{m-1,i}$ and $x_{m,i}$ respectively.

This definition is based on the assumption that the vapour leaving an horizontal streamline has an uniform composition and this will rarely occur[14].

Previously Ho and Prince[5] presented an Hausen point efficiency definition and wrote that the relationship between Hausen and Murphree point efficiencies was the same as the one existing between plate efficiencies; Hausen point efficiency definition was written as:

$$E_{OH_{m,i}} = \frac{y_{m,i} - y_{m+1,i}}{(y^*_{m,i})_H - y_{m+1,i}} \qquad (6)$$

Although the equilibrium composition is not defined by Ho and Prince it can be seen that $(y^*_{m,i})_H$ is considered as the mole fraction of component i in the vapour resulting from a flash calculation with a feed formed by the mixture of a liquid stream with composition $x'_{m,i}$ and flowrate L (total liquid flowrate entering the plate) with a vapour stream of composition $y_{m+1,i}$ and flowrate V (total vapour flowrate entering the plate).

This definition seems to be unsatisfactory as it is based on total flowrates and not local flowrates. It can be shown that if local flowrates are considered Hausen and Murphree vapour phase definitions do not differ. This is also true as far as liquid definitions are concerned.

Considering the vapour phase and Fig.5 it becomes clear that the total liquid stream is contacted by a small vapour stream wich will tend to zero when dz also tends to zero. Denoting by L' and V' the local streams it can be written that

$$L'x'_{m,i} + V'y_{m+1,i} = L'x^*_{m,i} + V'y^*_{m,i} \qquad (7)$$

For the limit situation dz=0, V'=0, $x'_{m,i} = x_{m,i} = x^*_{m,i}$ and

$$y^*_{m,i} = (y^*_{m,i})_M \qquad (8)$$

A more detailed discussion on point efficiency definitions will be published elsewhere[9].

HAUSEN EFFICIENCIES AND PLATE CALCULATIONS

In spite of its advantages Hausen's model is very rarely used and experimental distillation results are normally expressed in terms of Murphree efficiencies. However the calculation of Hausen efficiencies from experimental data can be easily achieved as $(y^*_{n,i})_H$ can be evaluated from the following equations:

$$Lx_{n-1,i} + Vy_{n+1,i} = L(x^*_{n,i})_H + V(y^*_{n,i})_H$$

$$(y^*_{n,i})_H = K_{n,i}\,(x^*_{n,i})_H \qquad (9)$$

$$\sum_{i=1}^{c} (y^*_{n,i})_H = 1 \; ; \quad \sum_{i=1}^{c} (x^*_{n,i})_H = 1$$

For binary systems composition-composition diagrams are often used and in that case $(y^*_{n,i})_H$ is easily calculated (Fig.2 and 3).

The knowledge of numerical values of Hausen plate efficiencies allows the graphical calculation of the number of real stages for a specified distillation separation. Such calculation involves, for each plate, a trial and error procedure since a value of $y_{n,i}$ has to be assumed before $(y^*_{n,i})_H$ can be calculated. The knowledge of $y_{n,i}$, $(y^*_{n,i})_H$ and $y_{n+1,i}$ allows the evaluation of Hausen efficiency and the calculated value can then be checked against the specified value.

Refering to Fig. 6 it can be seen that if the equilibrium line is linear between points M and N the trial and error method can be avoided. In fact it can be written that:

$$E_H = \frac{BC}{AC} = \frac{B'C'}{A'C'} = \frac{B''C''}{A'C''} \qquad (10)$$

and so the consideration, on any line of slope - L/V (L/V slope of the operating line), of two segments BC and AC with a ratio equal to Hausen efficiency allows the location of point B' and the definition of the real plate.

HAUSEN EFFICIENCES AND THREE PHASE DISTILLATION PROCESSES

Either by accident or design some of the plates of a distillation column may enter the two liquid phase region for systems exhibiting partial miscibility over a part of the composition range.

There is a growing interest by industry on such processes and it becomes clear that research is needed in areas such as phase equilibrium, column calculations and equipment design. It is also apparent that a new approach is needed as far as plate efficiencies are concerned.

In an ideal three phase distillation plate the vapour stream leaving the plate will be in equilibrium with both liquid phases . It can be written that:

$$y^*_{n,i} = K^{I}_{n,i}\, x^{*\,I}_{n,i}$$

$$y^*_{n,i} = K^{II}_{n,i}\, x^{*\,II}_{n,i} \qquad (11)$$

$K^{I}_{n,}$, $K^{II}_{n,}$ - vapour liquid equilibrium ratios.

Also the two liquid phases are in equilibrium and so:

$$x^{*\,I}_{n,i} = K^{III}_{n,i}\, x^{*\,II}_{n,i} \qquad (12)$$

$K^{III}_{n,i}$ - liquid-liquid equilibrium ratio.
It is obvious that one of the above equations is not independent and that:

$$K^{III}_{n,i} = \frac{K^{II}_{n,i}}{K^{I}_{n,i}} \qquad (13)$$

The Hausen efficiency concept seems to be

adequate for the description of three phase distillation processes. For each real plate an ideal plate with the same entering streams can be considered and the separation occuring in the real plate can be compared with the one achieved in the ideal plate; in this the leaving streams are assumed to be in equilibrium.

Although a different number of situations is possible and need to be considered a typical case is highlighted in Fig. 7. For such situation Hausen plate efficiencies can be defined as follows

$$E_{HV_{n,i}} = \frac{y_{n,i} - y_{n+1,i}}{(y^*_{n,i})_H - y_{n+1,i}} \qquad (14)$$

$$E_{HL_{n,i}}^{I} = \frac{x_{n-1,i}^{I} - x_{n,i}^{I}}{x_{n-1,i}^{I} - (x^{*\,I}_{n,i})_H} \qquad (15)$$

$$E_{HL_{n,i}}^{II} = \frac{x_{n-1,i}^{II} - x_{n,i}^{II}}{x_{n-1,i}^{II} - (x^{*II}_{n,i})_H} \qquad (16)$$

CONCLUSIONS

1. The differences between the efficiency models proposed by Hausen and Murphree were reviewed; it was shown that Hausen plate efficiencies can be easily calculated and also used in plate to plate calculations: in certain situations graphical calculations are possible without trial and error.

2. An analysis of point efficiency definitions was presented and a previous Hausen point efficiency model was discussed. It was shown that, adopting local flowrates, there is no difference between Murphree's and Hausen's models.

3. Three phase distillation processes were considered and Hausen plate efficiencies for a typical situation were defined.

NOMENCLATURE

c - number of components
E_H - Hausen plate efficiency
E_{HL} - Hausen liquid phase plate efficiency
E_{HV} - Hausen vapour phase plate efficiency
E_{OH} - Hausen point efficiency as defined by Ho and Prince
E_{ML} - Murphree liquid phase plate efficiency
E_{MV} - Murphree vapour phase plate efficiency
E_{OL} - Murphree liquid phase point efficiency
E_{OV} - Murphree vapour phase point efficiency
K - equilibrium ratio
L - liquid flowrate
V - vapour flowrate
x - liquid mole fraction
y - vapour mole fraction

Subscripts

H - Hausen
i - component
M - Murphree
n - plate number

Superscripts

I - liquid phase I
II - liquid phase II
* - equilibrium

REFERENCES

[1] American Institute of Chemical Engineers, "Bubble Tray Manual", New York, 1958

[2] Fredenslund A., Gmehling J., Rasmussen P., "Vapour-liquid equilibria using UNIFAC", Elsevier, Amsterdam, 1977

[3] Gerster J.A. et al., "Tray efficiencies

in distillation columns - Final report of the University of Delaware", Am. Inst. Chem. Engrs., New York, 1958

[4] Hausen H., Chem. Ing. Tech., 25,595,1953

[5] Ho G.E., Prince R.G.H., Trans. Inst.Chem. Engrs., 48,101,1970

[6] Krishna R. et al., Trans. Inst. Chem. Engrs., 55,178,1977

[7] Medina A.G., "Multicomponent distillation efficiency studies", Ph.D. Thesis, University of Birmingham, Birmingham, England, 1976

[8] Medina A.G., McDermott C., Ashton N., accepted for publication in Chemical Engineering Science

[9] Medina A.G., Jerônimo M.S., to be published

[10] Miskin L.G., Ozalp U., Ellis S.R.M.,Brit. Chem. Eng. and Proc. Tech.,17,153,1972

[11] Murphree E.V., Ind. Eng. Chem.,17,747, 1925

[12] Naphtali L.M., Sandholm D.P., AIChE J., 17,748,1971

[13] Sargent R.W.H., Murtagh B.A., Trans.Inst. Chem. Engrs., 47,85,1969

[14] Standard G., The Chem. Engr., 716,Nov. 1974

[15] Stroud S.E., "Studies in two and three phase steady state distillation simulation", Ph. D. Thesis, University of Birmingham, Birmingham, England, 1976

[16] Wang J.C., Henke G.E., Hydrocarbon Processing, 45(8),155,1966

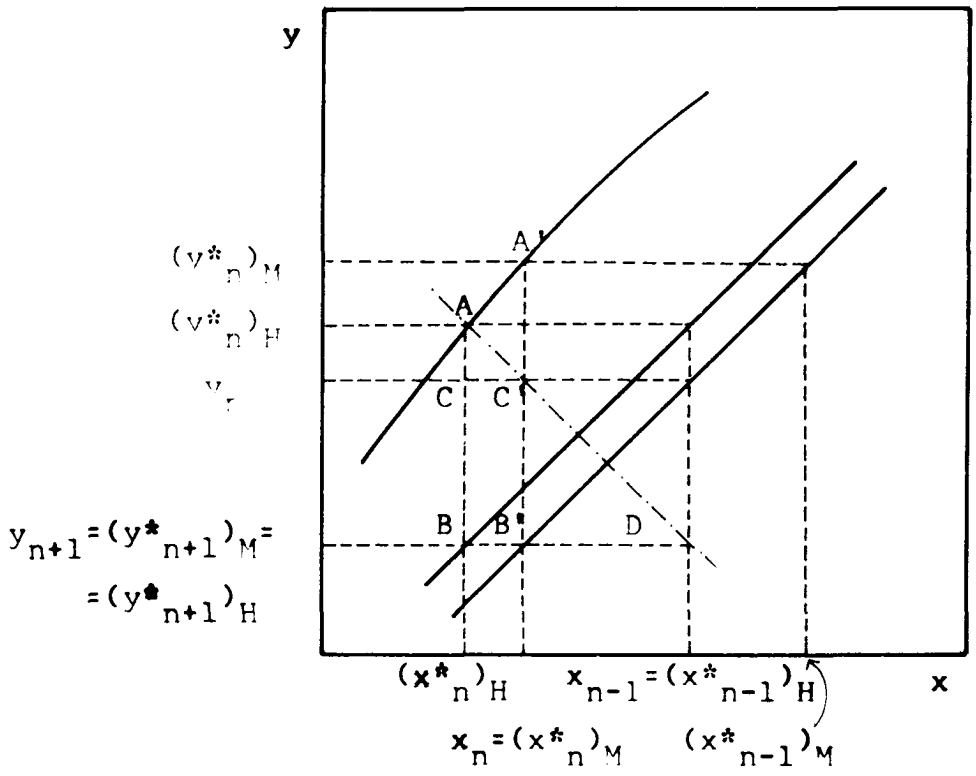

Fig 1 : Murphree and Hausen plates (efficiencies smaller than unity)

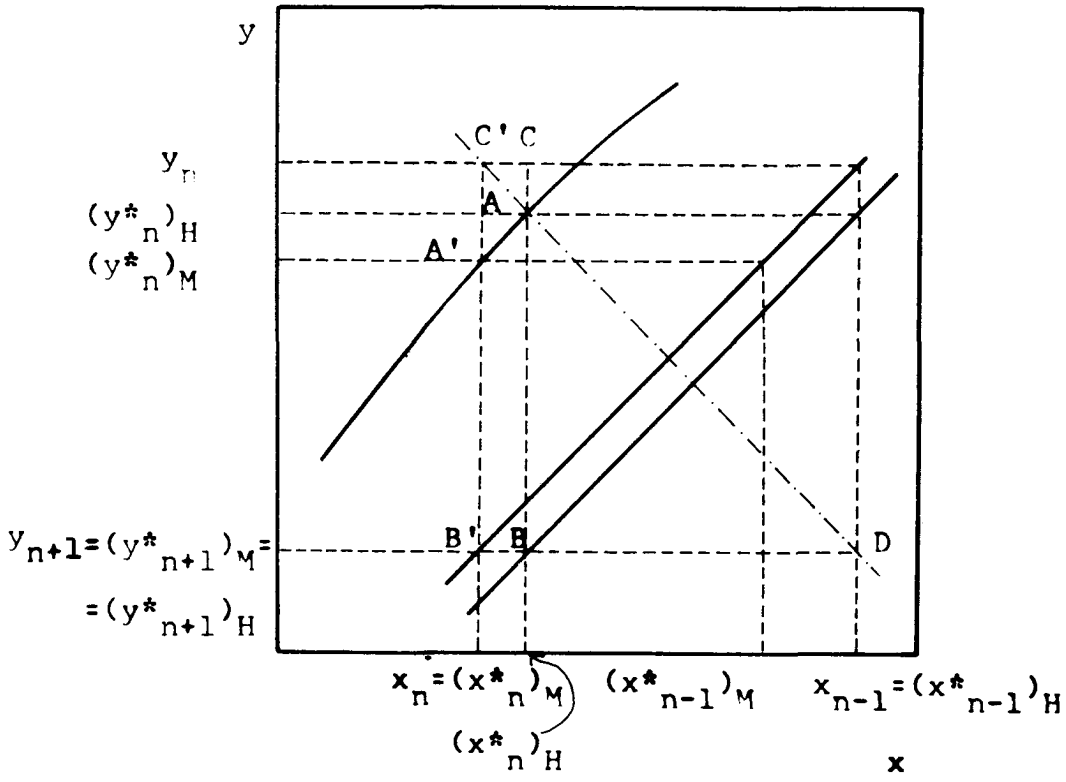

Fig 2 : Murphree and Hausen plates (efficiencies greater than unity).

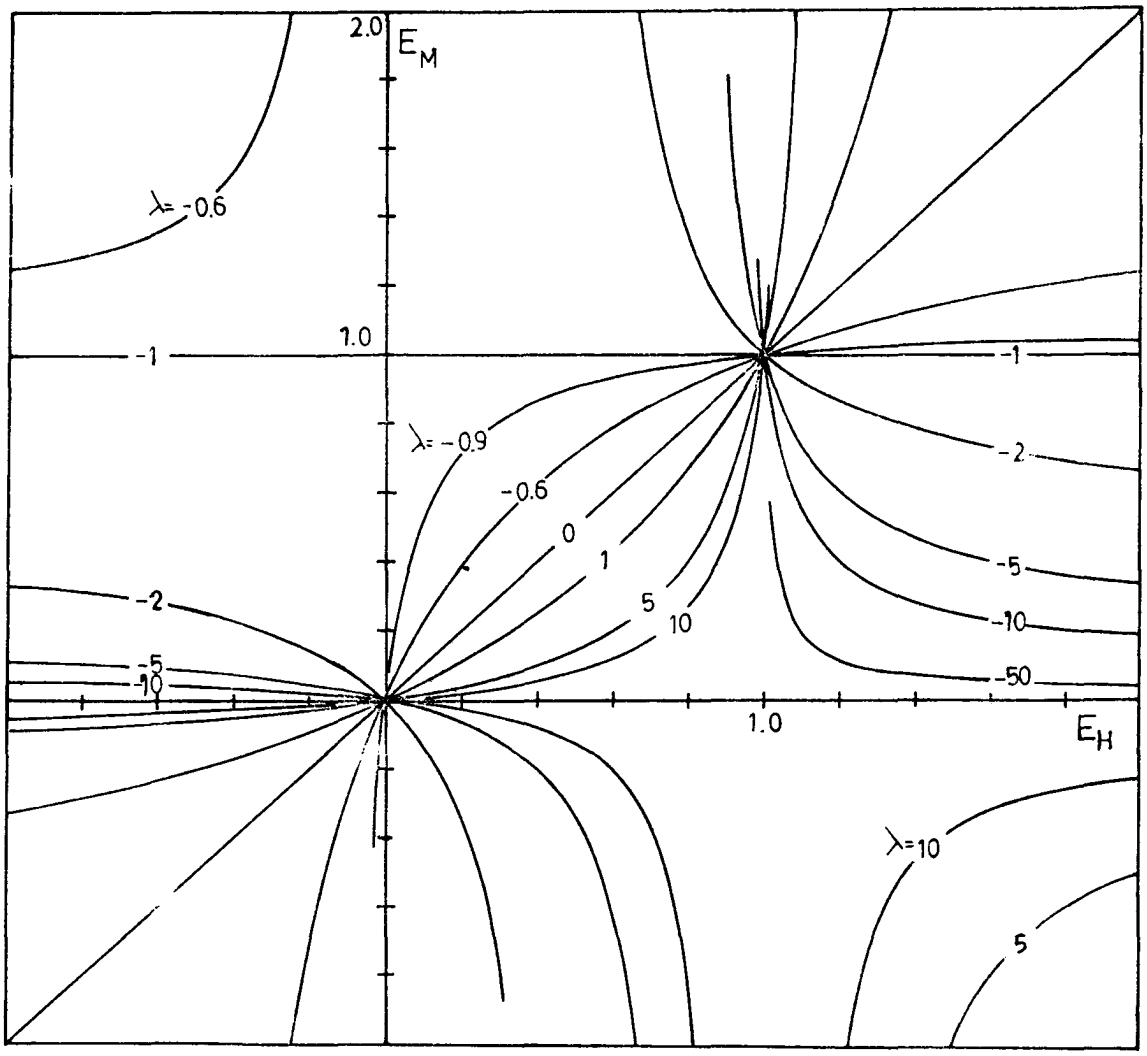

Fig 3 : Relationship between Hausen and Murphree efficiencies – binary and multicomponent systems.

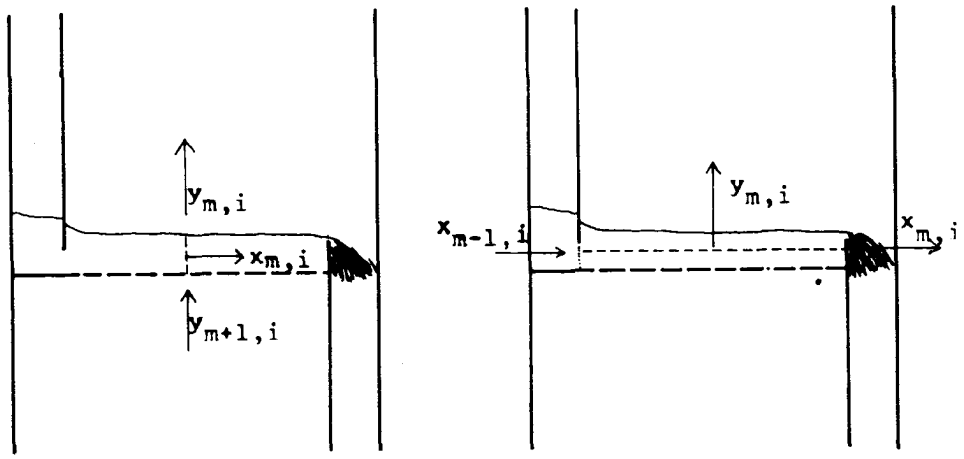

Fig 4 : Murphree point efficiencies.

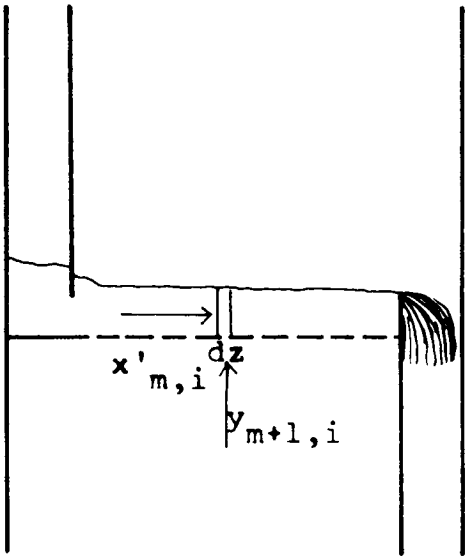

Fig 5 : Hausen point efficiencies

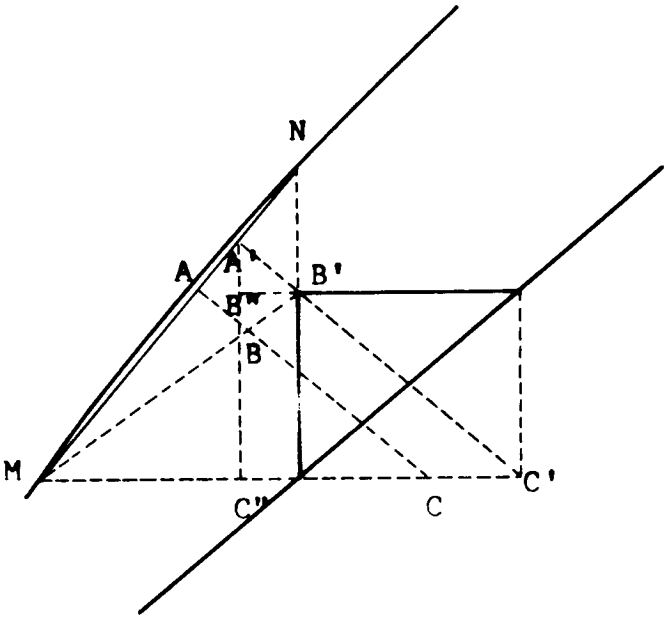

Fig 6 : Hausen efficiencies and plate calculations

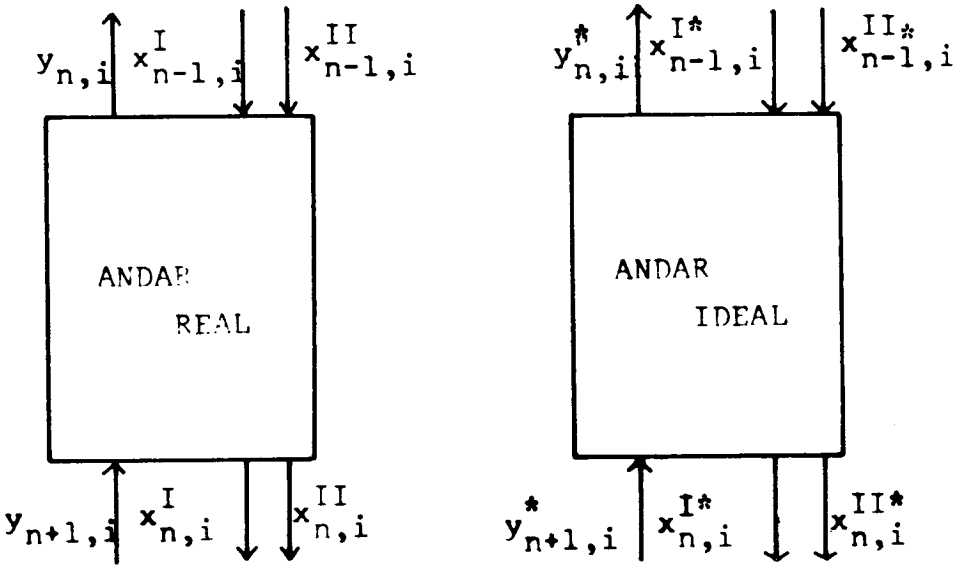

Fig 7 : Three phase distillation

THE VALIDITY OF THE HOFFMAN AND EMERY EQUATION IN THERMAL DIFFUSION

M.F.L.S. MORGADO
J.de D.R.S. PINHEIRO
J.J.B. ROMERO

Centro de Quimica Pura e Aplicada da Universidade do Minho,Braga,Portugal

ABSTRACT

The most widely used equation in thermal diffusion is discussed in what concerns its range of validity. It is shown that when the separation curves are non-symmetrical with respect to the initial composition the error involved in the Hoffman and Emery equation when using a value of $t=0.3\ t_r$ for the lower limit of the time, may be significantly larger than those predicted by their original authors.
Experimental cases described in the literature are discussed on the light of previous analysis.

INTRODUCTION

Thermal diffusion techniques have been increasingly used not only to separate difficult mixtures but also as a means of testing kinetic theories of the liquid state[1]. In many instances, though, discrepancies have been observed between the experimental results and the established phenomenological theories of the columns, leading sometimes to the introduction of "correction factors" into the phenomenological equations involved. Of these, one of the most widely used is the so-called Hoffman and Emery equation which relates the degree of separation between the two ends of the column to the physical variables affecting the process, including the time. Hoffman and Emery[2] claim that the usual simplified form of their equation may be used with an error less than 1% for separation times greater than $0.3\ t_r$, where t_r is a relaxation time that measures the rate of approach of equilibrium, or, roughly, the time required for the degree of separation to attain 70% of its steady-state value. This lower limit of the time - $0.3\ t_r$ - has, however, been questioned by Pinheiro[3] who showed that the criteria to estimate this lower limit should also take into account the value of the parameter λ - the "separation potential" of the system. Otherwise, the error introduced in the simplified form of the Hoffman and Emery equation for $t=0.3\ t_r$ could be much larger than 1%. Pinheiro discussed only symmetrical separations of equimolar mixtures. Yet, the vast majority of separations are non-symmetrical and non-equimolar, i.e., the value of $c_T - c_o$ is different from $c_o - c_B$ and $c_o \neq 0.5$ (the subscripts mean, respectively: - T = top, B = bottom 0= feed compositions)which would apparently reinforce Pinheiro's comments. The present paper is, then, an attempt to shed further light into the subject by considering firstly different kinds of theoretical cases and discussing, finally, experimental situations reported in the literature.

THE HOFFMAN AND EMERY EQUATION

Derivation

In a batch thermogravitational column, the concentration profile along the column length as a function of the time is given by the following equation[4]

$$\mu \frac{\partial c}{\partial t} = - H (1 - 2c) \frac{\partial c}{\partial z} + K \frac{\partial^2 c}{\partial z^2} \qquad (1)$$

with

$$\mu = \rho_M (2\omega) B \qquad (2)$$

$$H = \frac{\alpha \beta \rho_M g B (\Delta T)^2 (2\omega)^3}{6 ! < T > \mu} \quad (3)$$

$$K = K_c + K_d \quad (4)$$

$$K_c = \frac{\beta^2 \rho_M g^2 B (\Delta T)^2 (2\omega)^7}{9 ! D \mu^2} \quad (5)$$

$$K_d = (2\omega) \rho_M D B \quad (6)$$

(see Nomenclature for physical meaning of the variables)

Equation (1) was linearized by Majundar[5] who firstly introdured the dimensionless variables

$$Z = \frac{H z}{K} \quad (7)$$

$$\Theta = \frac{H^2 t}{\mu K} \quad (8)$$

so that equation (1) becomes

$$\frac{\partial c}{\partial \theta} = - (1 - 2c) \frac{\partial c}{\partial Z} + \frac{\partial^2 c}{\partial Z^2} \quad (9)$$

and afterwards used the transformation

$$c (Z, \theta) = \frac{1}{2} + \frac{1}{\psi} \frac{\partial \psi}{\partial Z} \quad (10)$$

where

$$\psi = \psi (Z, \theta) \quad (11)$$

to obtain the following equation linearized in ψ :

$$\frac{\partial \psi}{\partial \theta} = \frac{\partial^2 \psi}{\partial Z^2} \quad (12)$$

Majundar integrated equation (10) using the Laplace Transform to get:

$$\psi (Z,\theta) = \frac{e^{\theta/4} \quad (e^{c_o \lambda} - 1) e^{Z/2} + (e^{\lambda} - e^{c_o \lambda}) e^{- Z/2}}{e^{\lambda} - 1} +$$

$$+ \sum_{n=1}^{\infty} \frac{2 n \pi}{\lambda} \frac{(\frac{1}{4} - b_o^2) \quad 1 - (-1)^n e^{-b_o \lambda}}{(\frac{1}{4} + \frac{n\pi^2}{\lambda^2}) (b_o^2 + \frac{n^2 \pi^2}{\lambda^2})}$$

$$(\exp - \frac{n^2 \pi^2}{\lambda^2} \theta) . \sin \frac{n\pi}{\lambda} \quad ...(13)$$

where λ is the adimensional length of the column **(for Z = L) and**

$$b_o = \frac{1}{2} - c_o \quad (14)$$

Now, to determine the degree of separation Δ , i.e., the difference between the concentration at the top (c_T) and bottom (c_B) of the column, one evaluates $\partial \psi / \partial Z$ from equation (13) substitutes this value into equation (10) and obtains c_B for $Z=0$ and c_T for $Z=\lambda$.

In doing so, the degree of separation is obtained in terms of a sum of two terms, one of which involves a infinite series, as :-

$$\Delta = c_T - c_B = (e^{c_o \lambda} - 1)(e^{\lambda} - e^{c_o \lambda}) +$$

$$+ (-1)^n e^{b_o \lambda} - 1 . \frac{2\pi^2}{\lambda^3} (\frac{1}{4} - b_o^2).$$

$$\sum_{n=1}^{\infty} \frac{1 - (-1)^n e^{-b_o} \quad n^2}{(\frac{1}{4} + \frac{n^2 \pi^2}{\lambda^2}) (b_o^2 + \frac{n^2 \pi^2}{\lambda^2})} .$$

$$\exp \left(- \frac{\frac{1}{4} + \frac{n^2 \pi^2}{\lambda^2}}{\frac{1}{4} + \frac{\pi^2}{\lambda^2}} \frac{t}{t_r} \right) \quad (15)$$

where

$$t_r = \frac{\mu K}{H^2 (\frac{1}{4} + \frac{\pi^2}{\lambda^2})} \quad (16)$$

is the relaxation time.

Hoffman and Emery claim that for times greater than 0.3 t_r all the terms of the infinite series in equation (15) can be neglected with an error less than 1%. This rapid convergence enables the simplification of equation (15) to

$$\Delta = \Delta_\infty \left(1 - k_3 \; e^{-t/t_r} \right) \qquad (17)$$

where Δ_∞ is the steady-state degree of separation:

$$\Delta_\infty = \frac{(e^{c_o\lambda} - 1)\,(e^{\lambda} - e^{c_o\lambda})}{e^{c_o\lambda}\,(e^{\lambda} - 1)} \qquad (18)$$

and k_3 is a coefficient given by

$$k_3 = \frac{2\,c_o\,(1-c_o)\,\pi^2(1 + c^{-b_o\lambda})\,(e^{\lambda}-1)(e^{c_o\lambda} + e^{\lambda/2})}{\lambda^3\,(b_o^2 + \frac{\pi^2}{\lambda^2})\,(\frac{1}{4} + \frac{\pi^2}{\lambda^2})(e^{c_o\lambda} - 1)(e^{\lambda} - e^{c_o\lambda})}$$

$$\simeq \frac{8}{\pi^2} \qquad (19)$$

Equation (17) is the so-called Hoffman and Emery equation.

Validity

In obtaining equation (17), Hoffman and Emery introduced the limitation of $t > 0.3\ t_r$ so that, and with an error less than 1% as claimed, a simplified form for the degree of separation could be attained Hoffman and Emery have based their criterium on the analysis of the two most important factors concerning the convergence of the infinite series in equation (15) :- n and t/t_r. The other parameters involved, b_o and λ were neglected in the analysis.

In what concerns b_o, it may be easily seen that, in fact, its value is of no importance for the series convergence. Yet, for λ the same is not true since it affects remarkably the relative magnitude of the terms of the series.

To define new criteria for the lower limit of validity of the Hoffman and Emery equation it is necessary to analyse further the infinite series involved in equation (15). In doing so it may be noticed that

- Regardless of the value of c_o, the even terms are positive and the odd terms are negative. Thus, the series may be thought as composed of two sub-series, one being positive (n even) and the other negative (n odd).
- Both sub-series are rapidly convergent with n
- The absolute values of the negative sub-series are much larger than those involved in the positive sub-series and therefore the convergence of the series may be studied with relation solely to the odd terms

In neglecting all the terms beyond the first, an error is implicitly introduced, which may be defined as

$$\varepsilon\ (\%) = \frac{\sum_{n=2}^{\infty} f\ (n)}{\sum_{n=1}^{\infty} f\ (n)} \times 100 \qquad (20)$$

where f (n) goes for the argument of the infinite series.

Representing the i^{th}-term of the series as $f_i(n)$ and noting that for n-even and n >3 the terms become negligible as compared to the first term., equation (20) becomes

$$\varepsilon\ (\%) = \frac{f_3\ (n)}{f_1(n) + f_3(n)} \times 100 \qquad (21)$$

But, since $f_1(n) >> f_3\ (n)$ one may simply write

$$\varepsilon\ (\%) = \frac{f_3\ (n)}{f_1\ (n)} \times 100 \qquad (22)$$

ε is therefore a measure of the error involved in neglecting all the terms of the series beyond the first. From equation (15) it is seen that its value will depend strongly on t/t_r and λ.

Now, the influence of λ may be analysed in two different ways, either

a) Making ε = 1% and evaluating t/t_r vs. λ

or

b) Making $t/t_r = 0.3$ and evaluating ε vs. λ

In this work an attempt is made to tackle both approaches since both are of interest:- Case b) to give an idea of the errors possibly committed in the past and case a) to provide some guide-lines for the future.

SYMMETRICAL SEPARATIONS

Symmetrical separations ocurr when the separation attained in the upper half of the thermogravitational column equals the separation in the lower half, i.e.,

$$c_T - c_o = c_o - c_B = \frac{\Delta}{2} \qquad (23)$$

Symmetrical separations have been reported for several hydrocarbon mixtures[6] for which the dependence of Δ on the composition is a parabola.

For symmetrical separations the value of λ associated with a certain degree of separation may be obtained theoretically either through equation (18) or more accurately using its definition[4]

$$\lambda = \ln \frac{c_T\,(1-c_B)}{c_B\,(1-c_T)_\infty} \qquad (24)$$

where the subscript ∞ indicates a steady-state condition, i.e., $\Delta_\infty = C_T - C_{B_\infty}$

The results obtained using equation (24) are shown in Fig 1 for several values of the initial composition c_o.

(Note that the curves obtained for c_o are exactly the same as obtained for $1-c_o$)

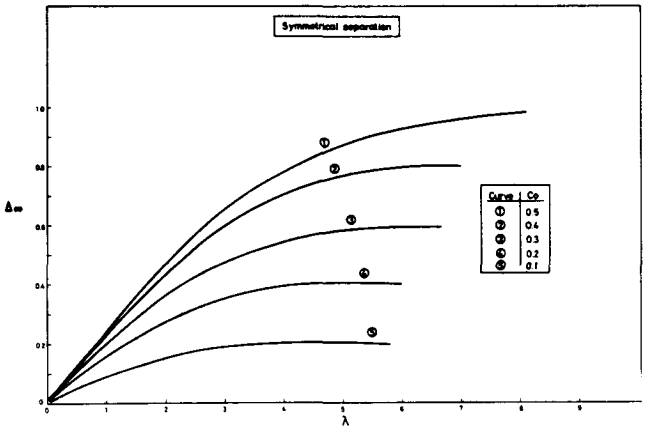

FIGURE 1 - The relationship between Δ_∞ and λ for various values of feed composition in symmetrical separations.

It is seen that regardless of the values of c_o or Δ_∞ involved the values of λ may vary from zero to infinite, although in pratice they remain relatively small.

In fact, equation (24) clearly shows that λ only reaches high values if one of the extreme compositions (c_T or c_B) approaches either zero or unity.

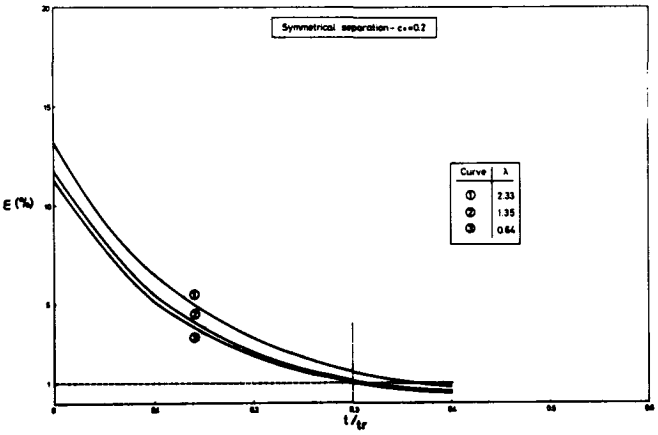

FIGURE 2 - ε vs. t/tr for different values of λ for $c_o = 0.2$ and symmetrical separation

Thus if, for instance, $c_B \sim 0$, then $c_T \sim 2\,c_o$ and equation (24) becomes

$$\lambda = \ln \frac{2\,c_o/(1-2\,c_o)}{c_B} \qquad (25)$$

clearly showing that when c_B approaches zero, λ approaches infinite.

One may also conclude that when $c_o = 0.5$ equation (24) simplifies to

$$\lambda = 2 \ln \frac{c_T}{c_B} \qquad (26)$$

It is now possible for different values of the initial composition c_o, to evaluate

a) ε vs. λ for $t/t_r = 0.3$

and

b) t/t_r vs. λ for $\varepsilon = 1\%$

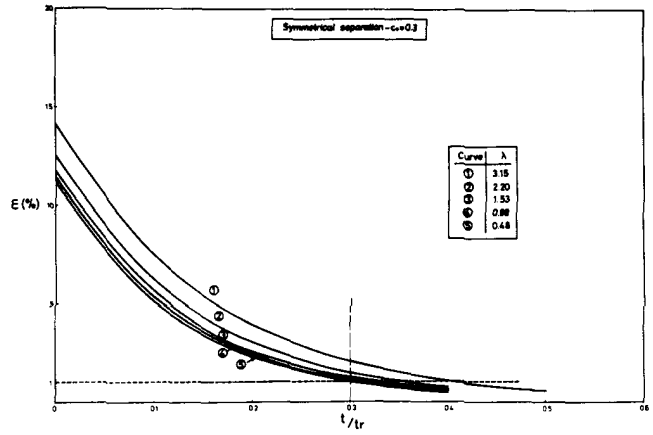

FIGURE 3 - ε vs. t/tr for different values of λ for c_o = 0.3 and symmetrical separation

The results obtained are presented graphically in Figs.2 to 4 where it may be seen that in the vast majority of cases (for which λ is not large, i. e. λ < 5 say),the error ε although larger than 1%, is comparatively small and most probably smaller than the usual experimental error.

One may then conclude, that the Hoffman and Emery equation represents fairly accurately the symmetrical separations.

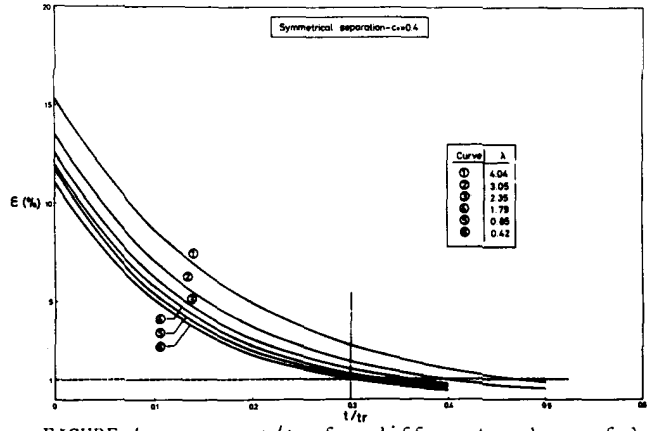

FIGURE 4 - ε vs. t/t_r for different values of λ for c_o = 0.4 and symmetrical separation

NON - SYMMETRICAL SEPARATIONS

Non-symmetrical separations, i.e., when

$$c_T - c_o \neq c_o - c_B$$

are, by far, the most common case in practice, though in many instances the "degree of assymetry" (7) is small.

Theoretical discussion

For non-symmetrical separations it is virtually impossible to use equation (24) to evaluate the value of λ associated with a given value of Δ_∞ mainly because there are several pairs of values (c_T, c_B) that may satisfy the contition $\Delta_\infty = c_T - c_B$.

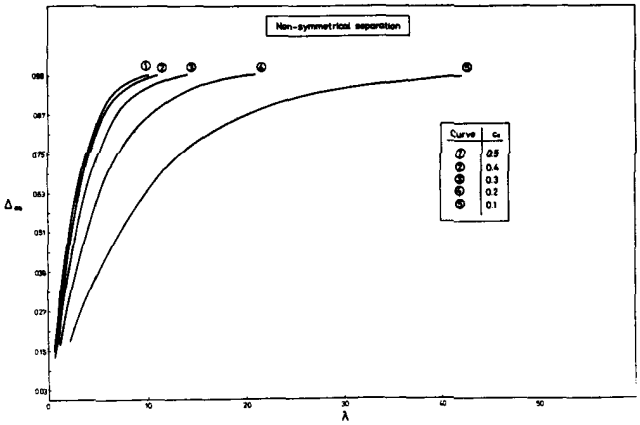

FIGURE 5 - The relationship between Δ_∞ and λ for various values of feed composition in non-symmetrical separations

To overcome this difficulty one may use equation (18) to determine the dependence of λ on Δ_∞ for various values of c_o. The consequent results are shown in Fig. 5, where it may be noticed that (contrary to what happened with the symmetrical situation) the values of λ may reach relatively high values, even though the end compositious may be far from zero or unity.

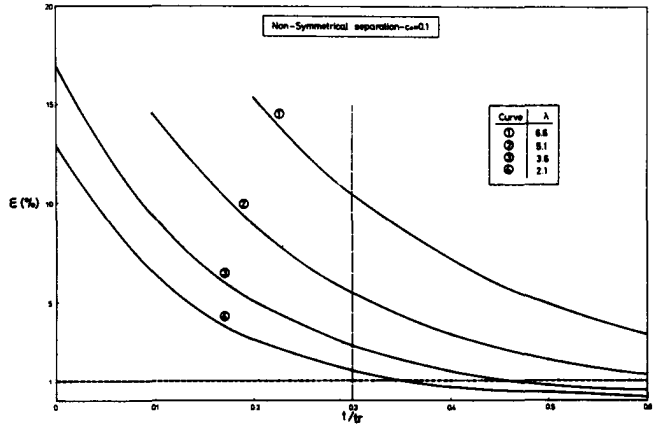

FIGURE 6 - ε vs. t/t_r for different values of λ for c_o = 0.1 and non-symmetrical separation

Not surprisingly the curves of ε vs. t/t_r for different values of λ and c_o (Figs. 6 to 10) show a quite distinct behavior. In fact, for t/t_r = 0.3 the corresponding values of ε are larger than 1% even for moderate values of λ (or, which is the same, ε = 1% only for t/t_r greater than 0.3).

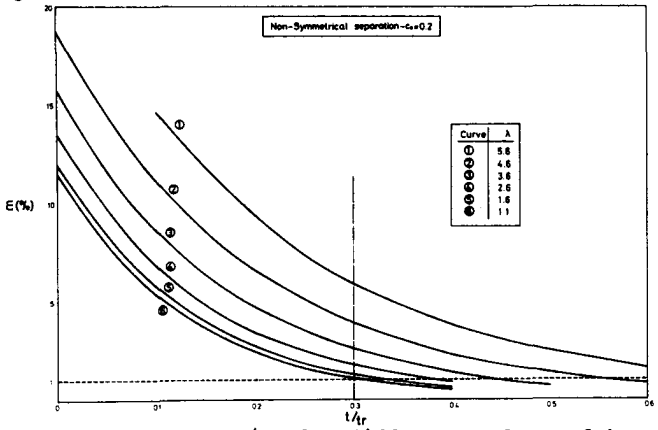

FIGURE 7 - ε vs. t/t_r for different values of λ for c_o = 0.2 and non-symmetrical separation

Experimental cases

It is interesting to analyse the range of values of λ and c_o that have been involved in experimental separations reported in the literature in order to estimate (with the help of Figs. 5 to 10) the implicit values of ε involved in such cases.

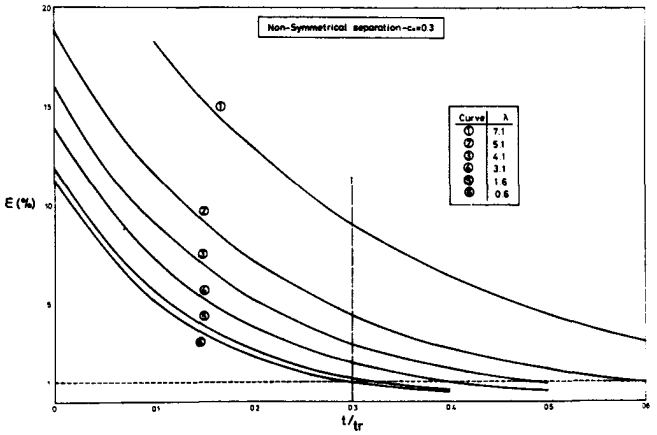

FIGURE 8 - ε vs. t/t_r for different values of λ for c_o = 0.3 and non-symmetrical separation

A summary of this analysis is presented in Table 1 where one may clearly note that the values of ε for t/t_r = 0.3 is, in some instances, of the order of 10% or more. This may explain some of the discrepancies that have been reported when attempting to the experimental results to the Hoffman and Emery equation.

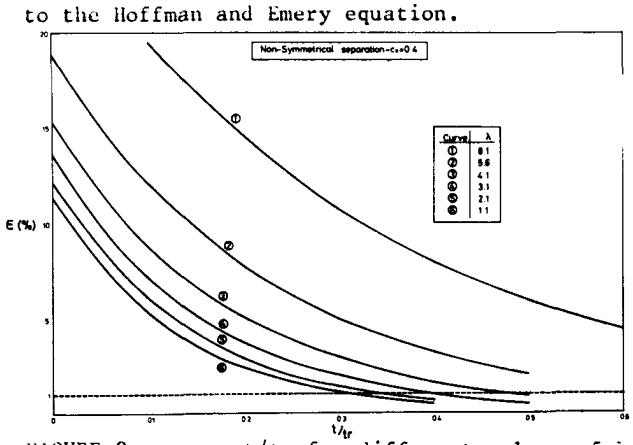

FIGURE 9 - ε vs. t/t_r for different values of λ for c_o = 0.4 and non-symmetrical separation

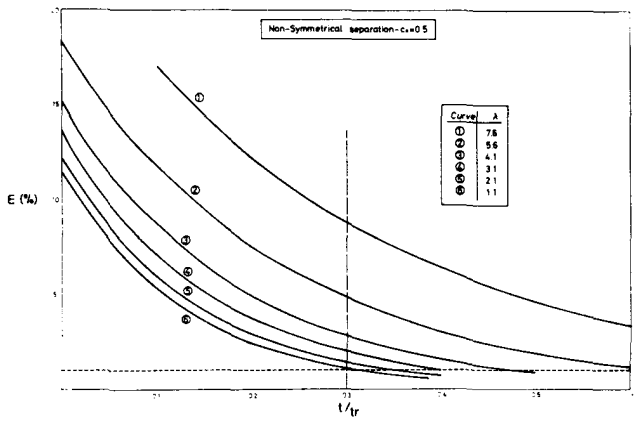

FIGURE 10 - ε vs. t/t_r for different values of λ for c_o = 0.5 and non-symmetrical separation

CONCLUSIONS

The use of the Hoffman and Emery equation to correlate the experimental separation vs. time curve involves an error of the order of 1% for t/t_r = 0.3 when the separation is symmetrical. For non-symmetrical separations, the error involved for t/t_r = 0.3 is generally quater than 1%, its value increasing with the value of λ and with the "degree of assymetry" of the curve relating the evolution of c_T and c_B with the time. It is therefore strongly recomended that for values of λ greater than about 4-5 an inspection of the lower limit of time is carried out before using the Hoffman and Emery equation to correlate the experimental data.

NOTATION

b_o = $1/2 - c_o$

B column dimension in the horizontal non-thermogravitational direction

c molar fraction of the reference component

c_o feed composition

c_T top composition

c_B botton composition

D ordinary diffusion coefficient

g accelaration of gravity

H thermogravitational transport coefficient

k_3 coefficient defined by eq. (19)

K transport coefficient associated with the parasitic remixing

K_c transport coefficient associated with the convective remixing

K_d transport coefficient associated with the ordinary back-diffusion

L column length

t time

t_r relaxation time

T absolute temperature

ΔT temperature difference between the column walls

<T> average absolute temperature

Greek Letters

α thermal diffusion factor

β temperature coefficient of density

Δ degree of separation = $C_T - C_B$

Δ_∞ equilibrium degree of separation

ε truncation error defined by eq. (20)

λ dimensionless length = $504 \times D\xi L/\beta g \Delta T (2\omega)^4$

μ number of moles per unit of column length

ζ viscosity

ω one-half of the distance between the hot and cold walls

ρ_M molar concentration of the solution

T A B L E I

Mixture	Reference	c_o	λ	$\varepsilon \leq 1\%$ t/t_r	$t/t_r = 0.3$ ε %
n-dodecane/ carbon tetrachloride	(8)	0.4846	7.65	0.98	9.02
n-heptane/cetane	(9)	0.6659	2.31	0.36	1.52
n-octane/decane	(9)	0.5459	1.37	0.32	1.17
iso-octane/n-octane	(9)	0.4961	0.73	0.31	1.05
n-heptane/triptane	(9)	0.4977	5.14	0.59	4.10
n-hexane/carbon tetrachloride	(8)	0.6599	13.74	2.95	39.14
n-heptane/carbon tetrachloride	(8)	0.6346	12.28	2.31	28.30
n-octane/carbon tetrachloride	(8)	0.6133	8.25	1.13	11.34
cumene/cetene	(10)	0.324	0.63	0.31	1.04
cumene/cetene	(10)	0.324	0.89	0.31	1.08
cumene/cetene	(10)	0.324	1.09	0.31	1.11
cumene/cetene	(10)	0.324	1.17	0.32	1.13
cumene/cetene	(10)	0.324	1.20	0.32	1.14
cumene/cetene	(10)	0.317	0.77	0.31	1.06
cumene/cetene	(10)	0.317	1.11	0.31	1.12
cumene/cetene	(10)	0.317	1.85	0.34	1.33
cumene/cetene	(10)	0.317	2.32	0.36	1.53
cumene/cetene	(10)	0.317	2.41	0.37	1.58
cumene/cetene	(10)	0.317	3.14	0.41	2.04
cumene/cetene	(10)	0.317	3.30	0.42	2.17
benzene/n-heptane	(8)	0.484	5.71	0.67	5.01
toluene/n-hexane	(8)	0.5268	4.60	0.53	3.38
o-xylene/n-hexane	(8)	0.5816	5.33	0.62	4.45
benzene/carbon tetrachloride	(8)	0.6638	9.36	1.43	16.44
benzene/carbon tetrachloride	(9)	0.5211	6.09	0.72	5.67
benzyl alcohol/ethylenodiol	(9)	0.7035	1.20	0.32	1.14
cumene/methyl-naphtalene	(9)	0.5028	1.46	0.32	1.19
Folvene/chlorobenzene	(9)	0.4974	1.11	0.31	1.11
β-methylnaphtalene/α-methyl-naplitalene	(9)	0.4936	0.52	0.30	1.03
cetane/benzene	(9)	0.7670	1.48	0.33	1.22
cetane/toluene	(9)	0.7332	0.61	0.31	1.04

T A B L E I (Cont.)

Mixture	Ref^{-ce}	c_o	λ	$\varepsilon \leq 1\%$ t/t_r	$t/t_r = 0.3$ ε %
cetane/m-xylene	(9)	0.7043	0.73	0.31	1.06
n-heptane/benzene	(9)	0.6228	6.42	0.78	6.64
n-heptane/methylcyclohexane	(9)	0.5349	5.16	0.59	4.14
cyclohexane/carbon tetrachloride	(9)	0.6471	7.96	1.08	10.95
cyclohexane/n-hexane	(8)	0.4759	7.95	1.04	9.78

REFERENCES

(1) STORY, M. and TURNER, J. Trans. Far. Soc., 65, 1523, 349, (1969)

(2) HOFFMAN, D. and EMERY Jr, A.H., A.I.Ch.E. Journal 9, 653 (1963).

(3) PINHEIRO, J.de D.R.S., M.Sc. Thesis, Birmingham University (UK), 1974

(4) ROMERO, J.J.B., Rev. Fis.Quim. Eng. ULM, vol.II, 1, Ser.A, 1 (1970)

(5) MAJUMDAR, S.D., Phys. Rev. 81, 844, (1955)

(6) BOTT, T.R. and WHYSALL, M. J.Chem.Engn.Japan 7, 167 (1974)

(7) PINHEIRO, J.de D.R.S., Ph.D.Thesis, Birmingham University (UK), 1976

(8) NIKOLAEV, B., NIKOLAEV, N. and TUBIN, A. theor. J. Chem. Engn 4, 144, (1977)

(9) JONES, A.L. and MILBERGER, E., Ind. Eng. Chem. 45, 2689, (1953)

(10) HOFFMAN, D., Ph.D. Thesis, Purdue University (USA), 1959

LIQUID THERMAL DIFFUSION IN A BATCH ROTARY COLUMN

T.R. BOTT,[1]
J.de D.R.S. PINHEIRO,[2]

1. Chemical Engineering Department, The University of Birmingham, Birmingham, U.K.
2. Centro de Química Pura e Aplicada da Universidade do Minho, Braga, Portugal

ABSTRACT

Experimental observations of separation by thermal diffusion in rotary columns have been published, but no adequate theory to explain the column perfomance has been given. By consideration of the hydrodymanics within the annular space an approximate theory has been developed wich shows that for a geometrically perfect column the relevant parameters affecting separation can be simply related to the corresponding static column. The relaxation--time and separation are virtually independent of the speed of rotation and separation values are more favourable for the rotary column. The application of the theory to non-perfect pratical colums requires the consideration of the " equivalent annulus width " concept similar to the static case. Experimental tests conducted at different speeds of rotation in two geometrically different columns whose inner cylinder rotates and the outer is static, showed that the rotation at moderate speeds increased the equilibrium separation by about 7%, reducing, simultaneously the relaxation time by an average of 3%. These results are in good agreement with the theoretical predictions.

INTRODUCTION

Since Clusius and Dickell[(1)] introduced the thermogravitational thermal diffusion column, several modifications on the basic design have been proposed aiming at a better perfomance of the apparatus, i.e. larger degrees of separation or smaller separation times.

More recently, the interest of some investigators has been focused on the so-called."rotary column"- a concentric cylinder apparatus in which one or both cylinders may rotate about the common axis. Yet, in spite of some experimental and theoretical studies that have been reported in the literature[(2-5)] it has not been possible to appreciate adequately the separation potential of the rotary column or even to draw clear conclusions about the influence of the process variables on the overall efficiency. The reasons are to be found on the lack of agreement between the experimental results so far reported and the apparent inadequacy of the theoretical models that have been suggested.

In the present work an attempt is made to obtain some information which may help to clarify the situation. The two essential aspects under consideration are : -

1. Development of a phenomenological model similar to (and based on) the conventional thermogravitational theory by Furry, Jones and Onsager[(6)] (FJO)
2. Experimental investigation of the influence of the speed of rotation in the laminar regime below the critical Taylor Number.

The first objective requires, in the first place, a strategy to tackle the problem since the unique characteristics of the 3-dimensional transport in the rotary column virtually excludes the possibility of a simple analytical integration

of the resulting non-linear partial differential equation of continuity for mass transport.

It would appear that the suggestion of Romero[2] to reduce the problem to 2-dimensions through the introduction of some simplifying assumptions, so that a derivation-pattern analogous to that of the thermogravitational column could be followed is, in fact, a realistic compromise which, once accomplished, would enable the translation of conventional methods of design and optimization to the 3-dimensional rotary apparatus. The procedure requires, though, a somewhat detailed analysis of the existing physical situation, namely the hydrodynamics involved.

2. THE HYDRODYNAMICS

2.1 The velocity profiles and flow-path.

In a rotary thermal diffusion column the convective fluxes are of two types : -

1. Vertical natural convection originated by the thermal gradient across the width of the annulus.
2. Tangential forced convection caused by the rotation of one or both of the cylinders.

The profiles of the velocity components corresponding to the above convective fluxes may be obtained from the Navier-Stokes equations which, for the laminar flow of an incompressible Newtonian fluid at the steady-state are, in the coordinate system shown in fig 1 :

$$\frac{\delta}{\delta z}(\rho v) = 0 \qquad \ldots\ldots(1)$$

$$\frac{\delta P}{\delta x} = 0 \qquad \ldots\ldots(2)$$

$$\eta \frac{\delta^2 v_y}{\delta x^2} = 0 \qquad \ldots\ldots(3)$$

$$\eta \frac{\delta^2 v_z}{\delta x^2} = \frac{\delta P}{\delta z} + \rho g \qquad \ldots\ldots(4)$$

Assuming the wall velocites to be V_h and V_c, the boundary conditions are

$$v_y = V_h, \quad v_z = 0 \quad \text{at } x = -+\omega \qquad \ldots\ldots(5)$$

$$v_y = V_c, \quad v_z = 0 \quad \text{at } x = -\omega \qquad \ldots\ldots(6)$$

$$\int_{-\omega}^{+\omega} v_z \, dx = 0 \qquad \ldots\ldots(7)$$

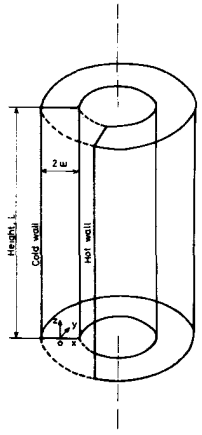

Fig. 1 - Concentric cylinder thermal diffusion column.

Equations (3) and (4) can be integrated separately and using the above boundary conditions the following well known solutions are obtained(*)

$$v_y = \frac{V_h - V_c}{2\omega} x + \frac{V_h + V_c}{2} \qquad \ldots\ldots(8)$$

$$v_z = \frac{\beta g (\Delta T)}{12 \eta \omega} * (\omega^2 - x^2) \qquad \ldots\ldots(9)$$

in which ω is the half distance between the walls, β is the temperature coefficient of density, η is the viscosity coefficient, g is the gravitational acceleration and (ΔT) is the temperature difference between the hot and cold walls.

The combination of these two components yields a resultant velocity, $v_R(x)$, which has a magnitude of

---

* FOOTNOTE

It is considered that $\frac{\delta T}{\delta x} = \frac{\Delta T}{2\omega}$ in accordance with the conclusions of TACHIBANA et al.[7]

$$v_R(x) = \sqrt{v_y^2 + v_z^2} \qquad \ldots\ldots(10)$$

and makes an angle $\psi(x)$ with the horizontal xy--plane defined by

$$\tan \psi(x) = \frac{v_z}{v_y} \qquad \ldots\ldots(11)$$

$$\sin \psi(x) = \frac{v_z}{\sqrt{v_y^2 + v_z^2}} \qquad \ldots\ldots(12)$$

Equations (8) to (12) are, in fact, the mathematical representation of a physical situation of which the following aspects must be emphasised:

1. The rotation deflects the particles streamlines from the vertical forcing them to follow a helical-path, the inclination of which, like the local velocity, is a function of the x-distance.

2. The vertical component, $v_z(x)$, is independent of the rotation and therefore the residence-time t_p - taken as the time required for a particle to travel from the top to bottom of the column or vice-versa- is not altered.

3. The column length being, indeed, the length of the particicle streamlines is not constant but rather a function of the x-distance. Hence, noting that t_p is constant and representing the length of the rotary streamlines by L* it is possible to write for a column of a vertical height of L:

$$\frac{L}{|v_z|} = t_p = \frac{L^*}{|v_R|} \qquad \ldots\ldots(13)$$

or, using equations (10) and (12) :

$$L^* = \frac{L}{|\sin \psi|} \qquad \ldots\ldots(14)$$

4. By substituting for the variables involved in equations (11), (8) and (9), specific values it may be readily seen that even for low speeds of rotation (of the order of, 5 RPM) the angle ψ is close to zero (*). As a consequence, the magnitude of the local velocity, v_R, and the local shear rate $\delta V_R/\delta x$ are practically identical to the corresponding local magnitudes of the tangential component:

$$|v_R| = |v_y| \sqrt{(\tan \psi)^2 + 1} = |v_y| \qquad \ldots\ldots(15)$$

$$\frac{\delta v_R}{\delta x} = \sin \frac{\delta v_z}{\delta x} + \cos \psi \frac{\delta v_y}{\delta x} \simeq \frac{\delta v_y}{\delta x} \qquad \ldots(16)$$

2.2 Types of rotary columns

A characteristic of the free-convection profile given by equation (9) is that, whatever the values of the variables involved may be, v_z is always an-odd-function of x, i.e.

$$v_z(+x) = -v_z(-x) \qquad \ldots\ldots(17)$$

which is equivalent to saying that the free convection streams for $x > 0$ and < 0 move countercurrently.

The same, however, is not true for the tangential component $v_y(x)$ which depends on the actual values of V_h and V_c . These may be combined in several different ways to which correspond different types of rotary flow patterns (simply designated by letters): -

Type A : Both walls rotate in the same direction with equal velocities

i.e, $V_h = V_c$

Type B : Both walls rotate in the same direction but with different velocities,

$V_h = V_c$, $V_h/V_c > 0$

---

*FOOTNOTE

For a column with one wall rotating with a speed N(r.p.m.) and assuming the followings CGS values for the variables : $\beta \sim 10^{-3}$, $g \sim 10^3$, $r \simeq 3$, $2\omega = 0.06$, $T = 20$ and making $\varepsilon = x/\omega$ the numerical value of tan ψ is approximately given by

$$|\tan \psi| \simeq \left| \frac{\varepsilon(1-\varepsilon)}{N} \right|$$

Type B_o: A subtype of the previous case in which one wall is static, $V_c = 0$ or $V_h = 0$

Type C : The walls rotate in opposite directions with the same absolute velocity , $V_h = - V_c$

Type C : The walls rotate in opposite directions with the same absolute velocity, $V_h = -V_c$

Type D : The walls rotate in opposite directions but with different velocities , $V_h = - V_c$, $V_h / V_c < 0$

Form equation (8) it may be easily seen that only type C corresponds to a profile that is an odd-function of x, i.e., only the tangential profile of type C is of true countercurrent nature relative to x=0. All the other cases, thus, have a combination of a tangential co-current profile with a vertical countercurrent profile. The net result, however, must be considered as a countercurrent--type process since it is clear that each atream contacts "fresh" fluid as it moves inside the annulus (see Fig.2).

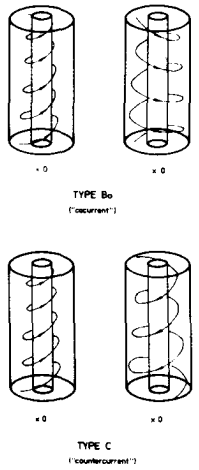

Fig.2 - Flow-paths in rotary columns

The fact that the overall flow inside a rotary column may be considered of the countercurrent type is of primary importance from the viewpoint of using the existing 2-dimensional derivation pattern which is based on that type of flow symmetry.

3. EARLIER WORK

3.1 Experimental reports

So far, it would seem that only columns of type B_o have been used experimentally. The first report was by Sullivan and co-workers[5] who , however, appeared to have worked at speeds above the critical Taylor Number and therefore out of the scope of the present work. A more detailed study at speeds below the critical Taylor Number was reported by Romero[2,8] who claimed that the rotation decreased the separation-time without increasing, though, the separation attainable. Romero also observed that the equilibrium separation decreased as the speed of rotation increased. A somewhat different conclusion was reached by Bott[3,9] who, using a column identical to Romero's but with a larger annulus width, noted that in the transient period of the separation (broadly, in the regious where the Ruppel--Coull[10] equation applies) the rotation increased the separation, the largest degree of separation being obtained for the higher speed of rotation studied.

Meanwhile, theoretical studies by Yeh and co-workers[4] suggested that a large increase in the degree of separation should occur where one of the cylinders rotates. (This work is discussed in the next section).

3.2 Theoretical studies

The first attempt to derive a phenomenological theory for the rotary column was by Romero[2]. This author rationalised the problem through an "elementary theory" in which the problem dimensions were reduced by neglecting the natural convection as compared to the forced convection and substituting the rotary column by a parallel plate one with the walls set in opposite motion. In the nomenclature of the present work, the substituition is equivalent to use type C instead of type B_o, keeping the rate of shear across the annulus unchanged.

Neglecting v_z in comparison with v_y is acceptable if the effect of v_z on the shape of the particles streamlines is taken into account. This Romero does in a clear discussion of the physical situation involved but somewhat surprisingly , the author uses for the column length the vertical height . As a consequence the theory predicts

degrees of separation far lower than those obtained experimentally.

Using the substitution of a type B_0 column by a type C one is acceptable from the viewpoint of Romero - the development of a " first approach " to the rotary column - although they are not strictly equivalent.

A more recent study has been presented by Yeh and Cheng[3] who developed a phenomenological model for continuous rotary columns[*] whose basic characteristics were :-

1. The introduction of the Brinkman Number , N_{Br}, - defined as $N_{Br} = \frac{\eta V^2}{k(\Delta T)}$ (where k is the thermal conductivity of the mixture) - to account for the distortions in the temperature profile (and consequently on the velocity profile) caused by the viscous heat generation.
2. The use of the "wired column" approach to derive the rotary column equation. (The "wired column" is a concentric tube column in which a wire of diameter equal to the annulus width is helically wrapped along the inner cylinder forcing therefore the particles to follow a helical-path inside the annulus).

As far as the Brinkman is concerned, its introduction appears to be unrealistic since it may be easily demonstrated, by substituting the variables involved by common (usual) numerical values, that N_{Br} is negligible for the vast majority of conditions encountered in practice.

As to the second aspect - the analogy between rotary and wired columns - it is indeed restricted to the shape and length of the particles streamlines. Wide differences do exist in values of the local velocity, residence-time or local shear rate, as may be seen by comparing the rotary equations (15) and (16) with the corresponding "wired equations" (where "w" stands for "wired")

$$(v_R)_w = v_z \sin \psi_w \qquad \ldots\ldots(17)$$

$$\left(\frac{\delta v_R}{\delta x}\right)_w = \sin \psi_w \frac{\delta v_z}{\delta x} \simeq 0 \qquad \ldots\ldots(18)$$

Moreover, the application of the Yeh and Cheng approach to the batch operation predicts that the value of the equilibrium degree of separation is cncreased by a factor equal to $(1/\sin \psi)$ which is quite large even for moderate speeds of rotation and, indeed, not vindicated by the experimental results so far available.

Before finalising this section it is interesting to note that the approach of Yeh and Cheng is, ultimately, an attempt to reduce the problem dimensions though by quite a different technique from Romero's and apparently unaware of the latter

4. THE TRANSPORT EQUATION

4.1 Simplifying approximations

To obtain the rotary transport equation through a pattern similar to the FJO derivation for the static column, it is necessary to introduce some approximations so that only two spacial coordinates are required to describe the transport involved and, simultaneously, to substitute the actual velocity profile by an approximate function with an odd-symmetry with respect to the x-distance.

The first approximation is to consider that the rotary column length, L*, defined by equation (14) has a constant value which implies that the angle ψ must also be considered as a constant:

$$\psi = \psi_a = \text{constant}$$

Physically, the aproximation introduced means that the particles streamlines have a constant inclination (independent from x) and, as a consequence, the resulting velocity profile exists in a xy-plane that makes an angle ψ_a with the horizontal xy-plane. It may also be concluded that this xy-plane together with equations (15) and (8) fully described the velocity profile that results from the approximation introduced.

---

* FOOTNOTE

The distinction betwenn batch and continuous phenomenological theories is immaterial from the viewpoint of establishing a body of rotary concepts or parameters since the continuous theories are, in fact, extensions of the corresponding batch ones.

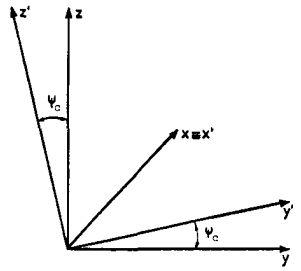

Fig.3 - Coordinate system x'y'z'

The actual value of ψ_a may be simply determined from the condition that the flowrates in the y and z directions are related by

$$\bar{v}_R \sin \psi_a \simeq \bar{v}_y \cdot \sin \psi_a = \bar{v}_z \qquad \ldots\ldots(20)$$

noting, now, that ψ_a is small and therefore sin $\psi_a \simeq \tan \psi_a$, the rotary length is

$$L^* = \frac{L}{|\sin \psi_a|} = \frac{L}{|\tan \psi_a|} = L.\frac{\bar{v}}{\bar{v}_y} \qquad \ldots\ldots(21)$$

It is worth emphasising that, at the present stage, the natural convection term, v_z, is neglected in evaluating the local velocity or shear stress i.e. similar to Romero's approach, but it is taken into account by defining a value $\psi_a \neq 0$.

The second basic approximation is related to the symmetry of the flow relative to the plane x=0 . First, it is considered that due to the countercurrent character of the "upwards" and "downwards" streams corresponding to the two column halves for $x > 0$ and $x < 0$ (briefly referred as x^+ and x^-). They are independent entities which only share a common boundary at $x = 0$. Secondly and in accordance with the approximation (19), the flow-rates in each half must be identical. Finally, it is also considered that within each half the sign of the shear stress is unimportant but rather its absolute value.

Under the above conditions it is possible to separate the rotary column into two halves having the velocity profiles shown schematically in fig 4 and 5 for columns of type A and B_o .
(see Fig 4)

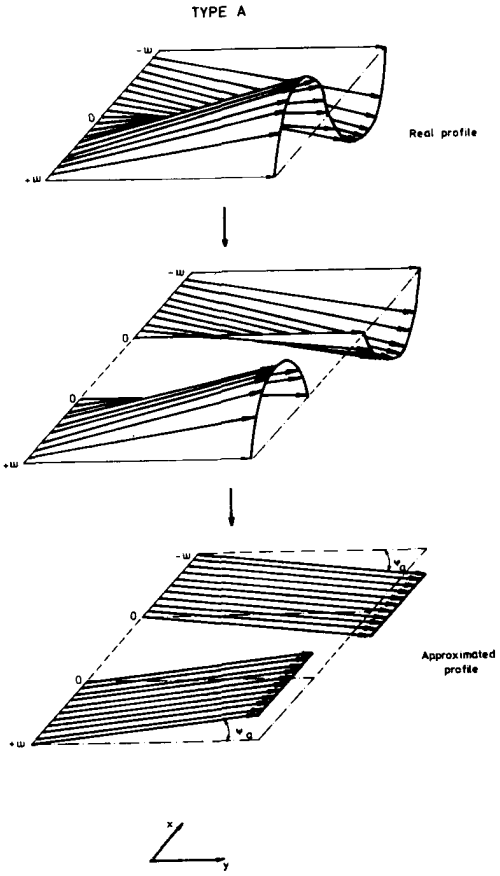

Fig.4 - Velocity profile in a rotary column of type A

Their mathematical representation is

$$v_y,(x^+) = \frac{V_h - V_c}{2\upsilon} x + \frac{V_h + 3V_c}{4} = R\omega(\varepsilon+A) \ldots(22)$$

$$v_y,(x^-) = \frac{V_h - V_c}{2\upsilon} x - \frac{V_h + 3V_c}{4} = R\omega(\varepsilon-A) \ldots.(23)$$

where $R = \frac{V_h - V_c}{2\omega}$

is the rate of shear across the annulus,

$$A = \frac{1}{2}\left(\frac{V_h + V_c}{R\omega} - 1\right) \qquad \ldots\ldots(25)$$

and

$$\varepsilon = \frac{x}{\upsilon} \qquad \ldots\ldots(26)$$

It is clear from equations (22) and (23) that the overall approximate profile is an odd--function of x.

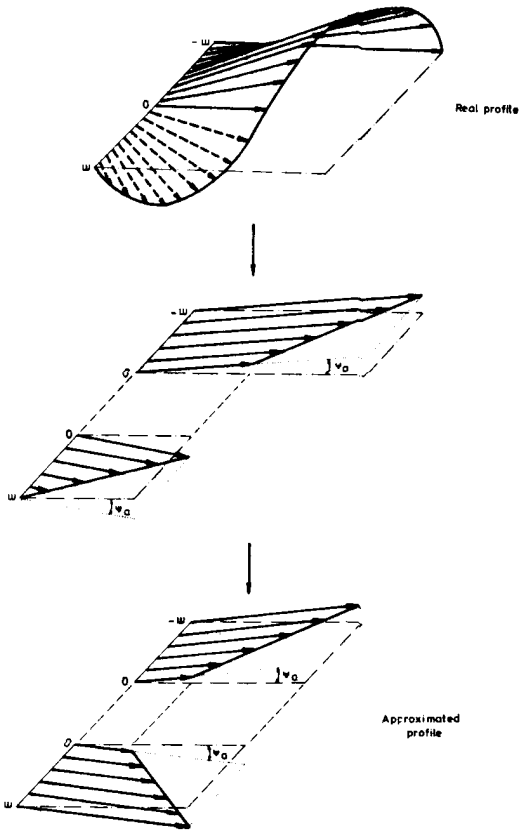

Fig.5 - Velocity profile in a rotary column of type B_o

4.2 The transport equation

In the xy'z' system of coordinates obtained from the xy system by rotating it around the x--axis by and angle ψ_a - see fig 3 - the velocity profile resulting from the approximations introduced has only one component : $v_{y'}(x)$. The mass fluxes existing in each half of the column have then the (usual) form

$$J_x = - \rho D \frac{\delta c}{\delta x} + \frac{\alpha \rho \; D(\Delta T)}{T_{av}(2\omega)} \; c \; (1-c) \qquad .....(27)$$

$$J_{y'} = \rho D \frac{\delta c}{\delta y'} + v_{y'} \; c\rho \qquad .....(28)$$

$$J_z = - \rho D \frac{\delta c}{\delta z'} \qquad .....(29)$$

in which c is the molar fraction of the specified component and T_{av} is the average absolute temperature inside the column, with the boundary conditions

$$J_x = 0 \quad \text{at} \quad x = \pm \omega \qquad .....(30)$$

$$c = c_o \quad \text{at} \quad t = o \qquad .....(31)$$

The equation of continuity is thus written as

$$\frac{\delta(c\rho)}{\delta t} = - \frac{\delta J_x}{\delta x} + \frac{\delta}{\delta y'} \; \rho D \frac{\delta c}{\delta y'} - v_{y'} \frac{\delta(c\rho)}{\delta y'} + \frac{\delta}{\delta z'} \; \rho D \frac{\delta c}{\delta z'} \qquad .....(32)$$

In this form, equation (32) does not allow the FJO-approach to be followed due to the existence of the z' term which makes the equation 3-dimensional (in spacial terms). The problem may however be overcome by noting that, for small values of the angle ψ it is possible to assume that $(\delta c/\delta z) \simeq (\delta c/\delta z')$. Since the process may be "followed" either through the y' - direction or the vertical z - direction due to the helical shape of the streamlines, it is possible to write the approximate relationship

$$\frac{\delta c}{\delta z'} \simeq \frac{\delta c}{\delta z} \simeq \frac{L^*}{L} \; \frac{\delta c}{\delta y'} \qquad .....(33)$$

Using identical arguments for $(\delta \rho / \delta z')$ and noting that $(L^*/L) >> 1$, the equation of continuity becomes under these conditions

$$\frac{\delta(c\rho)}{\delta t} = - \frac{\delta J_x}{\delta x} + \frac{\delta}{\delta y'} \left[\rho D \left(\frac{L^*}{L} \right)^2 \frac{\delta c}{\delta y'} \right] - v_{y'} \frac{\delta(c\rho)}{\delta y'} \qquad .....(34)$$

This equation is a function of only two spacial dimensions (x and y') and is formally similar to the continuity equation obtained by FJO for the static column and with the same boundary conditions which means that hereafter it is possible to follow the classical derivation pattern.

Without entering into details which have been fully described in the literature[6,11,12] it suffices to say that the conventional derivation

arrives at an equation - the transport equation - - to describe the transport of the reference component along the column of the type

$$\tau = H\, c\,(1-c) - k\,\frac{\delta c}{\delta y} \qquad \ldots\ldots(35)$$

where τ is the mass flow-rate of the specified component and H and K, designated by "transport coefficients" have the following expressions

$$H = \frac{B\,\rho\,\alpha\,(\Delta T)}{T_{av}\,(2\omega)} \int_{-\omega}^{+\omega} G(x)\,dx \qquad \ldots\ldots(36)$$

$$K = K_c + K_d \qquad \ldots\ldots(37)$$

$$K_c = \frac{B\rho}{D} \int_{-\omega}^{+\omega} G(x)^2\,dx \qquad \ldots\ldots(38)$$

$$K_d = B\,\rho\,D(2\omega) \qquad \ldots\ldots(39)$$

where B is the column width in the y-direction and G(x) is an auxiliary function introduced in the derivation and such that

$$\frac{\delta\,(c\rho)}{\delta y'} \cdot G(x) = J_x \qquad \ldots\ldots(40)$$

and

$$\frac{\delta}{dx}\,G(x) + v_{y'} = 0 \qquad \ldots\ldots(41)$$

Also according to condition (30) and equation (40)

$$G(+\omega) = G(-\omega) = 0 \qquad \ldots\ldots(42)$$

In the present case the derivation is carried out independently for the two halves ($x \geq o$ and $x \leq o$) subjected to the condition:

$$J_x(x^+) = J_x(x^-) \text{ at } x=o \qquad \ldots\ldots(43)$$

or, in accordance with equation (40)

$$G(x^+) = G(x^-) \text{ at } x=o \qquad \ldots\ldots(44)$$

The overall transport of the specified component is thus the sum of the contributions of each half:

$$\tau = \int_0^{+\omega} J_{y'}(x^+)\,dx + \int_{-\omega}^{o} J_{y'}(x^-)\,dx =$$

$$= H^*\,c(1-c) - K^*\,\frac{\delta c}{\delta y'} \qquad \ldots\ldots(45)$$

The principal differences from the static theory of FJO concern the auxiliary function G(x) which, for the profiles described by equations (22) and (23) and in accordance with conditions (41) (42) and (44), has the form:

$$G(x^+) = \frac{-R\omega^2}{2}\left[\,\varepsilon^2 + 2A\varepsilon - (2A+1)\,\right] \ldots(46)$$

$$G(x^-) = \frac{-R\omega^2}{2}\left[\,\varepsilon^2 - 2A\varepsilon - (2A+1)\,\right] \ldots(47)$$

After performing the integrations indicated in equations (36) and (38) the following expressions are obtained for the transport coefficients of a rotary parameters: (the absence of asterisk identifies the static ones):

$$H^* = \frac{B^*\rho\,(\Delta T)}{T_{av}\,(2\omega)}\,\frac{R\omega^3}{3}\,(2+3A) \qquad \ldots\ldots(48)$$

$$K_c^* = \frac{B^*\rho}{D}\,\frac{R^2\omega^5}{30}\,(8 + 25A + 20A^2) \qquad \ldots(49)$$

$$K_d^* = B^*\,\rho\,(2\omega)\left(\frac{L^*}{L}\right)^2 D \qquad \ldots\ldots(50)$$

The physical meaning of the terms involved in the rotary transport equation is analogous to the static one:- The term $H^*c\,(1-c)$ representing the contribution of the thermal diffusion effect to the transport of the specified component and the terms $K_c^*\,\frac{\delta c}{\delta y}$, and $K_d^*\,\frac{\delta c}{\delta y'}$, accounting, respectively, for the remixing effects of the convective currents and ordinary molecular diffusion.

As a " corolarium ", any conceptual relation between these or other phenomenological parameters of equivalent physical significance will have the same form in both rotary and static columns. By analogy, then, with the static theory

it is possible to obtain steady and unsteadystate solutions for the transport equation using the methods described by Majumdar[13] and others[10,14]. The corresponding final equations are presented in the next section.

5. SEPARATION EQUATIONS

5.1 Theoretical equations

By analogy with the static theory the following rotary parameters may be defined :

- Dimensionless length $\lambda^* = \frac{H^* L^*}{K^*}$ .....(51)

-Equilibrium separation $\Delta^*_\infty = \frac{(e^{c_o\lambda^*}-1)\ (e^{\lambda^*}-e^{c_o\lambda^*})}{e^{c_o\lambda^*}\ (e^{\lambda^*}-1)}$ .....(52)

-Relaxation-time $t^*_r = \frac{\mu^* K^*}{H^{*2}} \quad \frac{1}{\frac{1}{4} + \left(\frac{\pi}{\lambda^*}\right)^2}$ .....(53)

-Moles/unit of length $\mu^* = B^* \rho\ (2\omega)$ .....(54)

-Dimensionless time $\theta^* = \frac{H^{*2}}{\mu^* K^*}\, t$ .....(55)

For large values of time such that $t > 0.3 t^*_r$ the solution of the transport equation by Hoffman and Emery[14] yields the following equation for the dependence of the degree of separation, Δ^*, on the values of Δ^*_∞ , t^*_r and t:

$$\Delta^* = \Delta^*_\infty \left(1 - \frac{8}{\pi^2}\ e^{-t/t^*_r} \right) \qquad .....(56)$$

For short experimental times such the $\theta^* < 0.05 \left| \lambda^* \right|^{1.82}$, the dependence of the degree of separation, Δ^* , on the variables involved may be obtained from the solution presented by Ruppel and Coull[10] for the static case. The equation is: (The subscript RC stands for "Ruppel and Coull"):

$$\Delta^*_{RC} = 4\, c_o(1-c_o) \sqrt{\frac{\theta^*}{\pi}} = s^* \sqrt{t} \qquad ...(57)$$

with

$$s^* = \delta\, \Delta^*_{RC} \,/\, \delta\sqrt{t} \qquad .....(58)$$

i.e.s^* is the critical slope of the curve relating Δ^*_{RC} and $\sqrt{t}$.

For columns of type B_o the value of the parameter A defined by equation (25) is 1/2 and the value of L^* defined by equation (21) may be obtained using equations (8) and (9):

$$L^* = 96\ \frac{\eta\, V\, L}{\beta g\ (\Delta T)(2\omega)^2} \qquad .....(59)$$

The phenomenological parameters involved in the separation equations (56) and (57) may now be determined from equations (48) (49) and (59):

$$\lambda^* = 527.1\ \frac{\alpha\ D\ \eta\ L}{\beta g\ T_{av}(2\omega)^4} = 1.046\ \lambda \qquad ...(60)$$

$$t_r = 1.25 \left[\frac{T_{av}\ (2\omega)}{\alpha\ (\Delta T)\sqrt{D}} \right]^2 \quad \frac{1}{0.25 + \pi^2/\lambda^2} =$$

$$= 0.875 \left[\frac{0.25 + \pi^2/\lambda^2}{0.25 + \pi^2/\lambda^{*2}} \right] \cdot t_r \qquad .....(61)$$

$$s^* = 2.019\ \frac{c_o\ (1-c_o)\ \alpha\ (\Delta T)\sqrt{D}}{T_{av}\ .\ (2\omega)} = 1.068\ s \qquad (62)$$

Equations (60) and (62) respectively show that s^* , λ^* (and, hence Δ^*_∞) are larger than the corresponding static parameters. In contrast the rotary relaxation-time t^*_r is smaller than the static one as shown by equation (61). On the whole, therefore, it may be conclued that the theory predicts the perfomance of rotary columns of type B_o is better than the perfomance of a static column under the same experimental conditions although the improvement is moderate. If the procedure described for columns of type B_o ($A = \frac{1}{2}$) was carried out for the other types mentioned , the results would be similar in regard to the relaxation-time and the short-time separation,but would show significant differences in the ratio

λ^*/λ. A semi-quantitative comparison is shown in Table 1 where it may be appreciated that the lar - gest equilibrium separation attainable is for the type A column (both walls rotating in the same direction with equal velocities).

TABLE 1

Comparison between the theoretical performances of rotary and static columns

Type of column	$\frac{\lambda^*}{\lambda}$	$\frac{\Delta_{\infty}^*}{\Delta_{\infty}}$	$\frac{t_r^*}{t_r}$	$\frac{s^*}{s}$	$\frac{\Delta_{RC}^*}{\Delta_{RC}^*}$	Rotary performance relative to the static
A	1.143	>1	<1	1.034	>1	Better
B(A=1)	1.078	>1	1<	1.059	>1	Better
B_o	1.046	>1	1<	1.068	>1	Better
C	0.952	1<	1<	1.090	>1	Comparable

Another interesting aspect worth mentioning and somewhat surprising is the fact the phenomenological parameters are independent of the speed of rotation apart from the limitations imposed by the critical Taylor Number ("upper limit") and by the assumption that the angle ψ_a is small (" lower limit ").

In connection with the " lower limit " it is also of importance to note that the error involved in the simplifying approximations introduced decreases as the speed of rotation increases. Hence, the " lower limit " is defined by imposing a maximum value for the error. This means, on the other hand, that the separation equations derived are the asymptotic solutions which apply at speeds below $N = \infty$ with a certain degree of error which, in turn, is negligible at apeeds above the " lower limit ".

5.2 Equivalent annulus width of a rotary column

The assumption of a constant annulus width implicit in the FJO-approach is seldom acceptable when considering real columns due to the high $L/(2\omega)$ rations which because of constuctional difficulties, implies the existance of small eccentricities along the column height. This problem has been discussed by several authors [14,16] and ultimately has led to the introtuction by Bott and Romero[16] of the "equivalent annulus width" concept - the annulus width of a geometrically perfect column which yields the same separation as the actual imperfect one under the same experimental conditions. This concept was further developed by Romero and Pinheiro[17] who proposed a method for the evaluation of the " equivalent annulus width " which is discussed below.

The introduction of the concept for the static column was essentially based on hydrodynamical considerations which, however, may not be strictly applied to the rotary case mainly because the spacial location of the "funnels" originated by the eccentricities are continuously displaced by the rotation, It may, though, be admitted that a certain degree of instability is transmitted to the flow by the eccentricities and therefore one must accept that the overall perfomance of the column is affected. Whether or not an " equivalent annulus width " for the rotary column may be defined by analogy with the static column is a question whose answer requires the application of the Romero and Pinheiro[17] method to the experimental data abtained.

The method derived for the static column allows the independent evaluation of the equivalent annulus width and thermal diffusion factor and is simply based on the fact that the static parameters λ and s may be written as

$$s = \frac{\alpha}{2\omega} \cdot m \qquad \ldots\ldots(63)$$

$$\lambda = \frac{\alpha}{(2\omega)^4} \cdot n \qquad \ldots\ldots(64)$$

where

$$m = 1.89 \frac{c_o(1-c_o)\ (\Delta T)\sqrt{D}}{T_{av}} \qquad \ldots\ldots(65)$$

and

$$n = 504 \frac{D\ \eta\ L}{\beta g\ T_{av}} \qquad \ldots\ldots(66)$$

The coefficients m and n may be evaluated separately with accuracy independent from α and (2ω), and the values of s and λ may be determined experimentally. Under these conditions,

equations (63) and (64) form a system of 2 equations with 2 unknowns whose solution is

$$2\omega = \left(\frac{n\,s}{m\,\lambda}\right)^{-\frac{1}{3}} \qquad \ldots\ldots(67)$$

$$\alpha = 2\omega \cdot \frac{s}{m} = \frac{s}{m} \cdot \left(\frac{ns}{m\lambda}\right)^{-\frac{1}{3}} \qquad \ldots\ldots(68)$$

In the rotary case the basic differences are in the numerical factors of equations (65) and (66) which become, in accordance with equations (60) and (62):

$$m^* = 2.019\,\frac{c_o\,(1-c_o)\,(\Delta T)\sqrt{D}}{T_{av}} \qquad \ldots\ldots(69)$$

$$n^* = 527.1\,\frac{D\,\eta\,L}{\beta g\,T_{av}} \qquad \ldots\ldots(70)$$

and

$$(2\omega^*) = \left(\frac{n^*\,s^*}{m^*\,\lambda^*}\right)^{-\frac{1}{3}} \qquad \ldots\ldots(71)$$

$$\alpha = \frac{s^*}{m^*}\left(\frac{n^*\,s^*}{m^*\,\lambda^*}\right)^{-\frac{1}{3}} \qquad \ldots\ldots(72)$$

It is seen that to examine the adequacy of the " rotary equivalent annulus width " is also to examine the separation equations in which its evaluation is based. This adequacy may however be tested in two complementary ways :

- By comparing the value(s) of α obtained from equations (32) with others cited in the literature.

- By comparing the experimental separation curve with the two theoretical curves obtained using:

a) The equivalent annulus width given by equation (71)

b) The mechanically measured annulus width, $(r_2 - r_1)$.

6. EXPERIMENTAL WORK

6.1 Experimental apparatus and conditions

The experimental apparatus used in this work has already been described elsewhere [3,9] so that only the principle characteristics are described. It is comprised of two concentric cylinders made of brass, the height being 102 cm, the mechanically measured[3,9] annulus width 0.0571 cm and the annular volume 80cm^3. The inner cylinder may rotate at speeds up to 300 RPM while the outer cylinder is static. The heating and cooling of the walls is made through a thermostatic water circuit which flows inside the inner cylinder (hot wall) and through a water-jacket surrounding the outer cylinder (cold wall). The wall temperatures are measured through a group of 8 thermocouples placed in each wall at four different heights. The column is also provided with eleven sampling ports equally spaced along the height.

The test mixture used was n-heptane-benzene with an initial composition of $c_o = 0.560$ (molar fraction of benzene), each component being of high purity[18]. The analysis of the mixture composition was by refraetometry with an accuracy greater than 0.001 of the molar fraction.

The temperature difference between the walls was 18.5 ± 0.25°C and the average temperature 293 ± 2°K. The vertical variation of the temperature was in no case larger than 0.5°C.

The rate of sampling was 1 sample/run in accordance with the recommendations of Vichare and Powers[19], i.e. after a sample is withdrawn the column is emptied, washed with fresh mixture, emptied again and finally filled up with fresh mixture for a new run.

In the runs referred to as 1B the column was operated at full height (102 cm) and in the runs 2B with a height of 90 cm by leaving the upper section empty. This was intended as a means of assessing the influence of a suspected imperfect zone located near the top of the column (between L = 91 cm and L = 102 cm) on column efficiency.

Before assembling the column (which has self-aligning devices) the inner and outer cylinder diameters were carefully measured[8,9] at 9 different points equally spaced along the height.

The mechanically measured (or theoretical) annulus width is obtained by subtracting the cylinder radii at corresponding heights. The average values for the annulus width are listed in Table 2 for runs 1B and 2B and it is seen that it may be considered that two geommetrically different columns were used as shown in Table 2. The Table also shows the speeds of rotation at which the columns were operated.

TABLE 2

Column dimensions and operational velocities

	Height, L (cm)	$(r_2-r_1)_{av}$ (cm)	Speed of rotation, N (rpm)
COLUMN 1 (runs 1B)	102	0.0571	0, 1, 3, 6, 12, 28, 48, 88,
COLUMN 2 (runs 2B)	91	0.0565	0,1,3,10,20,44

6.2 Results and discussion

For each column and speed of rotation, the degree of separation, Δ , was determined for , at least, 13 different experimental times ranging from very short times of about 0.25 hrs up to times near equilibrium of the order of 30 hrs. or more. This set of (t_i, Δ_i) pairs constituted the input of computer programmes specially devised, whose output inclued the best valus - as determined by least squares methods - of the parameters λ^*, Δ_∞^* , t_r^* and s^* (or λ, Δ_∞, t_r and s). The values of Δ_∞^* and t_r^* are determined so that the (theoretical) curve of Δ^* vs. t obtained by substituting those values of Δ_∞^* and t_r^* into equation (57), yields the minimum deviation between the experimental points (Δ_i^* , t_i) and the corresponding points in the theoretical curve (Δ^* , t). In this work , it was found that in no case was the deviation (*) greater than 5% which means that (with an error less than 5%) the experimental results are well described by the two values of Δ_∞^* (or λ^*) and t_r^* given by the computer and presented in Tables 3 and 4 .

TABLE 3 Experimental and calculated parameters - column 1

N (RPM)	Δ_∞^*	λ^*	t_r^* (hr)	$s^*.10^2$ ($min^{-\frac{1}{2}}$)	$2\omega .10^2$ (cm)	α	$\frac{\lambda^*}{\lambda}$
0	0.462	2.03	3.82	2.35	6.14	1.36	-
1	0.464	2.04	3.78	2.40	6.13	1.31	1.004
3	0.477	2.11	3.43	2.44	6.10	1.32	1.032
6	0.490	2.18	3.29	2.47	6.06	1.33	1.061
12	0.495	2.20	3.58	2.29	5.90	1.29	1.071
28	0.500	2.23	3.87	2.46	6.00	1.31	1.080
48	0.471	2.08	3.54	2.43	6.12	1.32	1.019
88	0.410	1.77	2.14	2.43	6.23	1.34	0.888

$m.10^3 = 1.056$ $m^*.10^3 = 1.128$ $n.10^5 = 2.11$ $n^*.10^5 = 2.21$

The values of λ^* and s^*, together with the values of m^*, n^*, m and n determined, respectively, from equations (69), (70), (65) and (66) using the appropriate values of the variables involved (c_o=0.560, ΔT=18.5°C, T_{av}=293.5°K, $\beta.10^3$=0.88 $g.cm^{-3}.{}^oC^{-1}$, $\eta.10^2$=0.461 $g.cm^{-1}.s^{-1}$, $D.10^4$=0.216 $cm^2.s^{-1}$, ρ=0.767 $g.cm^{-3}$, g=980 $cm.s^{-2}$) allow the evaluation of the "equivalent annulus width" and thermal diffusion factor using the method of Romero and Pinheiro described earlier. The results thus obtained are summarized in Tables 3 and 4 and suggest the following observations:-

1. Although in theory for a given speed of rotation column 1 equilibrium separation should be nearly 6% higher than that of column 2, it is seen that, in practice, it is of the order of 10% lower than the equilibrium separation obtained in column 2. This discrepancy must be attributed to the geometric irregularities existing near the top of column 1 which promote extra-remixing effects that affect the whole apparatus efficiency. Not surprisingly, therefore, the ratio between the equivalent annulus width, and mechanically measured gap, $2\omega/ (r_2 - r_1)$, (which may be considered as a measure of the degree of imperfection of the column)-

* FOOTNOTE

The percentage deviation between the experimental ponts (Δ_I^* , t)and the theoretical value of separation, Δ^*, for the same value of the time, t_i is given by $\frac{\sqrt{(\Delta^* - \Delta_i^*)^2}}{\Delta_i^*}$

is considerably higher for column 1 for the same value of N as may be seen from the tables.

2. The values of the thermal diffusion factor, α, determined from the data of either column 1 or 2 show a very good agreement between themselves and with other values reported in the literature and determined in thermogravitational columns[17].

TABLE 4 - Experimental and calculated parameters - column 2

N (rpm)	Δ^*_∞	λ^*	t^*_r (hr)	$s^*.10^2$ ($min^{-\frac{1}{2}}$)	$2\omega.10^2$ (cm)	α	$\frac{\lambda^*}{\lambda}$
0	0.516	2.32	4.22	2.48	5.76	1.35	-
1	0.516	2.32	4.11	2.56	5.79	1.31	1.000
3	0.523	2.36	4.19	2.61	5.79	1.34	1.017
10	0.564	2.60	4.29	2.63	5.62	1.31	1.121
20	0.558	2.56	4.25	2.65	5.66	1.33	1.103
44	0.541	2.46	4.27	2.63	5.73	1.34	1.060

$m.10^3 = 1.056$ $\quad m^*.10^3 = 1.128$ $\quad n.10^5 = 1.89$ $\quad n^*.10^5 = 1.98$

3. The equivalent annulus width, in both columns, appears to decrease first as the s speed increases, to reach a minimum and then to increase with increasing speeds of rotation. This suggests that the role of the geometric irregularities in a rotary column tend to become more important for higher speeds due probably to some local fluid instability arising at large values of the rotation.

Conversely, $\lambda^* \propto (2\omega)^{-4}$ reaches a relative maximum and then decreases monotonically as the speed of rotation increases as shown in Fig 6 through the experimental curves for column 1 (curve E_1) and column 2 (curve E_2).

By comparing the experimental λ^* vs. N curves (E_1 and E_2) with the theoretical curves predicted by the theory for perfect columns 1 and 2, (curves T_1 and T_2 , respectively, in fig 6) it is seen that for column 2 the twoo curves (E_2 and T_2) are not far apart in contrast to what happens to column 1 (E_1 and T_1). Furthermore the shape of the experimental curves suggest that may considered as distorted theoretical curves.

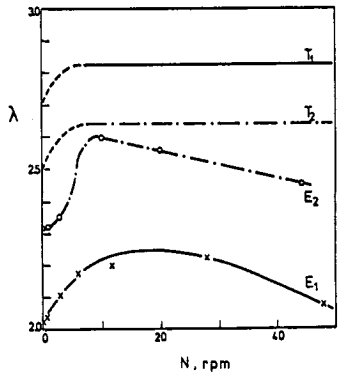

Fig. 6 - Comparison between experimental and theoretical values of parameter λ^*

T_1 - Theoretical curve for a perfect column 1

E_1 - Experimental curve for column 1

T_2 - Theoretical curve for a perfect column2

E_2 - Experimental curve for column 2

4. The existance of geometric imperfections with the need to consider "equivalent annulus widths" clearly alters the theoretical ratio of $\lambda^*/\lambda \simeq 1.05$ as shown by the last column in Tables 3 and 4. It is interesting to note, though, that, not only is that ratio larger than unity in all cases except for N=88 RPM in column 1, but also that the average value of that ratio ($\lambda^*/\lambda = 1.04$ for column 1 and $\lambda^*/\lambda = 1.06$ for column 2) are quite close to the theoretical value of 1.05.

5. The comparatively low separation obtained in column 1 for N = 88 RPM assumes a larger significance if it is noted that the "upper limit" of velocity, N^L, defined through the critical Taylor Number[20,21] is not far apart from the speed of 88 RPM:

$$N^L = \frac{(N_{Ta})_c}{\pi^2/900} \left[\frac{(r_2+r_1)\,\eta^2}{4\, r_1^2\, (2\omega)^3 \rho^2} \right]^{\frac{1}{2}} = 95 \text{ RPM} \qquad .....(73)$$

It is logical, therefore, that some degree of instability with a possible change of

flow regime may have occurred in the (imperfect) column 1 at that high speed.

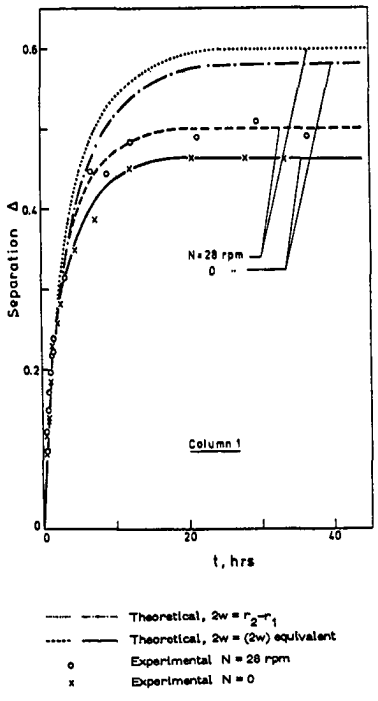

Fig. 7 - Typical comparisons between the theoretical curves (for $2\omega = r_2 - r_1$ and $2\omega = (2\omega_{equiv.})$ and the experimental points in column 1

The above comments generally suggest that the experimental results obtained show a trend that is in agreement with the theory derived earlier. The most meaningful test is , though, the comparison between the separation vs. time curve predicted by equation (56) and the experimental points. Typical examples of these comparisons are shown in figs. 7 and 8 in which two theoretical curves for each speed are represented: one using the " equivalent annulus width " and the other calculated for $2\omega = (r_2 - r_1)$. The comparisons for other speeds show similar trends which may be summarised as :-

1. The use of the "equivalent annulus width" in equation (56) produces a curve that has a much better agreement with the experimental points than the curve obtained from equation (56) using $2\omega = r_2 - r_1$. This is particularly true for column 1 and for the static operation of column 2.

2. In column 2 the two theoretical curves for N=0 are distinctly apart whereas for N=10 RPM the curves are close together sugesting that at this speed of rotation the irregularities are not so important as they become for N=0 or for higher speeds of rotation.

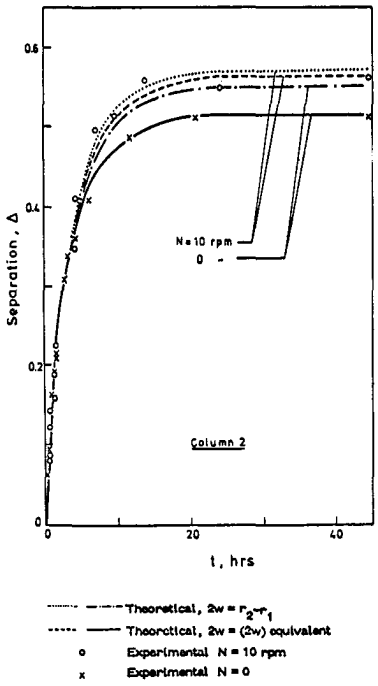

Fig. 8 - Typical comparisons between the theoretical curves (for $2\omega = r_2 - r_1$ and $2\omega = (2\omega_{equiv.})$ and the experimental points in column 2.

7. CONCLUSIONS

It is thought that the main conclusinos to be drawn from the present work may be summarised as follows:

1. The approximate phenomenological theory of the rotary thermal diffusion column derived using some simplifying approximations to reduce the problem dimensions and with an approach similar to that of FJO appears to describe satisfactorily the behaviour of a geometrically perfect column.

2. For real rotary columns (geometrically imperfect) it is necessary to consider, by analogy with the static column, an "equivalent annulus width" whose value may be determined by a method similar to the static case. When this rotary " equivalent annulus width " is used a good agreement is observed between theory and experiment (even for non-perfect columns).

3. The column efficiency improved when rotated at speeds up to about 50 RPM. The average increase in the equilibrium separation relative to the static operation was 6% and 7% for the two columns used. These figures agree fairly with the theoretical prediction of a 5% improvement.

AKNOWLEDGEMENT

The authors acknowledge, with sincere thanks, the provision of laboratory facilities by Professor J.T. Davies and the University of Birmingham in support of the research reported.

One of the authors (J.D.R.S. Pinheiro) wishes to express his gratitude to the Calouste Gulbenkian Foundation, Lisbon, Portugal for the provision of a scholarship which made this work possible.

NOTATION

A	parameter defined by eqn(25)
B, B^*	column width in the y and z directions, respectively
C	molar fraction of the reference component (benzene)
C_o	initial composition
D	ordinary diffusion coefficient
g	gravitational acceleration
G, G^+, G^-	auxiliary functions defined respectively by eqns (40), (46) and (47)
H, H^*	transport coefficients defined, respectively, by eqns(36) and (48)
J_k	mass flux of the reference component
K_c, K_c^*, K_d, K_d^*	thermal conductivity transport coefficients given by, respectively, eqns (38),(49),(39), and (50)
L	column height
L^*	lenght of the rotary column, defined by eqn (21)
m, m^*	coefficients defined by, respectively, eqns (64) and (68)
n, n^*	coefficients defined by, respectively, eqns (65) and (69)
N	speed of rotation of the inner cylinder in r.p.m.
N_{Br}	Brinkman Number, $N_{Br}=\eta V^2/k(\Delta T)$
N_{Ta}	Taylor Number, $N_{Ta}=4\pi^2 r_1^2 \rho^2 (2\omega)^3 N^2/900(r_1+r_2)\eta^2$
$(N_{Ta})c$	critical Taylor Number , $(N_{Ta})_c \simeq (3 \pm 0.3).10^3$
p	local pressure
r_1, r_2	cylinder radii
R	shear rate across the annulus, defined by eqn.(24)

s, s^*	initial slope of the separation vs. square root of the time curve given by eqn (61)
t	time
t_p	residence-time, defined by eqn (13)
t_r, t_r^*	relaxation-times defined in equation (60)
T	absolute temperature
v_i	velocity component (in the i-direction)
V_R	resultant velocity defined by eqn (10)
V_h, V_c	tangential velocities of the hot and cold walls
x, x'	horizontal coordinate normal to the walls surfaces
y	horizontal coordinate parallel to the walls surfaces
y'	coordinate direction defined in fig 3
z	vertical coordinate
z'	coordinate direction defined in fig 3

Greek symbols

α	thermal diffusion factor
β	temperature coefficient of density $= -(\partial\delta/\partial T)_p$
Δ, Δ^*	difference in composition between the top and bottom of the column
ΔT	temperature difference between the walls
ε	dimensionless horizontal distance defined by eqn (26)
η	viscosity of the mixture
θ	dimensionless time, defined by equation (55).
λ, λ^*	dimensionless length, defined , by eqns (51) and (59)
μ^*	no. of moles per unit length of the column
π	3.141592...
ρ	mass density of the mixture
τ	total transport of specified component in the direction of convection, eqn (35)
ψ	deflection angle of the particles strealines from the horizontal plane
ψ_a	deflection angle defined by eqn. (20)
ω	one-half the distance between hot and cold walls

Subscripts

av	average
RC	"Ruppel and Coull"
x,x',y,y'	coordinate direction
w	wired column
∞	steady-state

Superscripts

*	rotary column
-	average (velocity)

REFERENCES

1. CLUSIUS,K.and DICKELL,G. Naturwissenschaften 1938,26,546
2. ROMERO, J.J.B Dechema-Monogr. 1971,65,337
3. BOTT, T.R. Chemeca 70,p.35, Butterworths, Australia 1970
4. YEH, H.M. and CHENG, S.M. Chem. Eng. Sci., 1973, 28,1803
5. SULLIVAN,L.J.,RUPPEL, T.C. and WILLINGHAM, C.B. Ind. Eng.Chem. 1955,47,208
6. FURRY, W.H.,JONES, R.C.and ONSAGER, L.Phys. Rev.1939, 55, 1083

7. TACHIBANA, F.,FUKUI, S. and MITSUMURA , H. Bull J.Soc. Mech.Engrs 1960,3,119

8. ROMERO, J.J.B. Ph.D. Thesis, Univ of Birmingham 1967

9. BOTT, T.R. Ph.D. Thesis, Univ of Birmingham, 1968

10. RUPPEL, T.C. and COULL, J. Ind. & Eng. Chem., Fundamentals 1964, 3 ,368

11. ROMERO, J.J.B Rev. Fis. Quim. Eng. ULM,1970, 2 A,1

12. POWERS, J.E. "Thermal Diffusion" in "New Chemical Engineering Separation Techniques", ed. Schoen Interscience Pub., 1962

13. MAJUMDAR, S.D. Phys. Rev., 1951,81,844

14. HOFFMAN, D. and EMERY, A.H. A.I.CH.E. Journal, 1963,9,653

15. KORCHINSKY, W.and EMERY, A.H. A.E.CH.E. Journal, 1967, 13, 224

16. BOTT, T.R. and ROMERO, J.J.B Trans. Instn. Chem Engrs 1969, 47,T166

17. ROMERO, J.J.B. and PINHEIRO, J.D.R.S. Chem.Eng. Sci., 1975, 30, 1459

18. PINHEIRO, J.D.R.S., PINHEIRO, H.M.P.S., ROMERO J.J.B. Rev. Fis. Quim. Eng : ULM,1973,5 A, 1

19. VICHARE, G.and POWERS, J.E. A.I.CH.E. Journal, 1961, 7 , 650

20. CHANDRASEKHAR, S.Mathematics, 1954, 1, 5

21. PINHEIRO, J.D.R.S. M.Sc. Thesis, Univ. of Birmingham, 1974

GASIFICATION OF CARBON DEPOSITED ON STEAM REFORMING CATALYSTS - MASS TRANSFER LIMITATIONS

C.A. Bernardo [1]
D.L. Trimm [2]

1. Universidade do Minho, Largo do Paço, Braga, PORTUGAL
2. University of Trondheim, 7034-Trondheim-NTH, NORWAY

ABSTRACT

Mass transfer limitations were detected in the gasification by carbon dioxide and steam of carbon deposited on steam reforming catalysts. By using the kinetic data obtained and the calculated effectiveness factor for the gasification, it can be shown that the limitations occur in the pores of the coke deposit. As the mass transfer effects are mainly determined by the structure of the deposits, the possibility of an effective "clean-up" of the catalyst by the gases present in the steam reforming reaction is necessarily limited. Therefore, to prevent the deactivation of the catalyst, attention should be focussed on inhibiting carbon lay-down.

INTRODUCTION

The deactivation by carbon deposition of catalysts used in many industrial processes poses problems of regeneration and optimum operation control. The regeneration of fouled catalysts is mainly achieved by burning-off the carbon with air, steam or mixtures of both. Sometimes complete regeneration is not possible and the catalyst has to be replaced. Thus, it is important to define the operating conditions that promote the formation of desired products while supressing the formation of carbon. For instance, in the steam reforming of hydrocarbons, this could be achieved by enhancing the removal of the coke deposited on the catalyst by some of the gases present in the system. With these ideas in mind, the study of the gasification by steam, hydrogen and carbon dioxide of carbon deposited on foils and supported nickel catalysts was undertaken (2).

The catalytic gasification of carbons was found to be important above ca. 475°C, and thus to be unaffected by the uncatalysed gasification (3). As the reaction kinetics depend on the availability of the metal and on the structure of the carbon (4,5), it was necessary to have an idea about these factors. Some information in given in the next section and more can be found elsewhere (1, 2). It is important, however, to emphasise here that a very high reactivity for the gasification was observed, much greater than that of other carbon deposits with similar metal content (1,5). Consequently, mass transfer limitations could be affecting the gasification data obtained. These limitations are the object of the present communication.

EXPERIMENTAL

The experimental arrangement consisted of a microbalance (C.I. Electronics, MK 2B) and associated flow reactor, furnace and temperature controller ($\pm$ 0.5°C). It is represented diagrammatically in Figure 1. Reactants and products were analysed by gas chromatography using a column filled with porapak-R (2m,70°C), and a thermal conductivity detector. Water

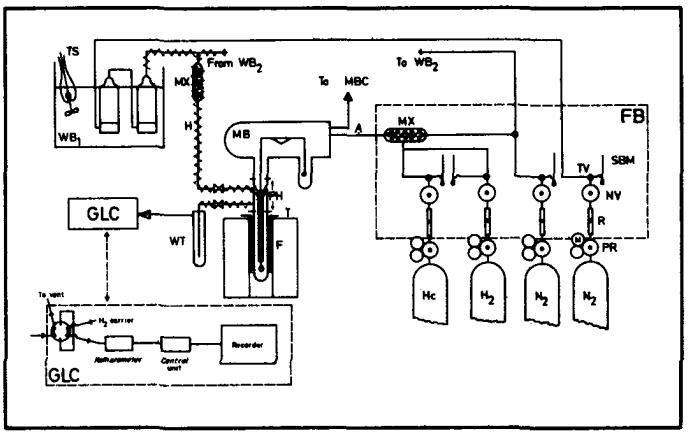

Fig. 1 The Flow system

Key. MB-microbalance; WB-water bath; F-furnace; HW-heating wire; WT-water trap; T-thermocouple; M-manometers; NV-needle valves; R-rotameters; PR-two stage pressure regulator; SBM-soap bubble meter; H-heated lines; PH-preheater; GLC-analysis system; MX-mixer; MBC-microbalance cabinet, matching box and recorder

vapour was produced in a bubbler system, where a carrier nitrogen stream was saturated at known temperatures (1). Where it was necessary to study the dependence of the rate on the pressure of a gasifying agent, the total pressure was maintained at one atmosphere by the addition of oxygen free nitrogen or argon.

Nickel foils were obtained from Goodfellow Metals, and were of 99.7% purity, 0.125 mm thickness and had a geometric area of about 20 $cm^2\ g^{-1}$. Supported catalysts were prepared by impregnation. A low surface area alumina was crushed to BS 40-60 mesh and soaked in 0.3 M $Ni(NO_3)_2.6H_2O$. The excess solution was removed by slow evaporation. The nitrate was decomposed to nickel oxide (450°C,2h) and reduced to metal (500°C, 3h). The final catalysts contained 18 wt % Ni and had a total and metal surface area of 8.5 and 1.1 $m^2\ g^{-1}$, respectively.

Since gasification was shown to be dependent on the characteristics of the deposits, a common carbon deposition procedure was followed. A mixture of n-hexane (13.5 molar %), hydrogen (25%) and nitrogen (61,5%) was passed over the catalyst maintained at 600°C, the uptake of carbon being continued until the desired amount had accumulated. The reactor was then flushed with nitrogen at the gasification temperature for half an hour, before starting the carbon removal. Weight changes were registered continuously.

In certain cases, prior to the gasification, the carbon deposits were analysed by Electron Micro Probe (EPMA) and wet chemical methods and examined under optical and stereoscan electron microscopes (Olympus N-TR and Cambridge MK IIA, respectively). In the case of foils, the average nickel concentration in the carbon was 1,5% (w/w) while, for the supported catalysts, nearly all the available nickel was distributed in the carbon, the concentration depending on the relative amounts of the catalyst and the deposit. Changes in the structure of the deposits during the gasification were also monitored by determining the surface area of the carbon at various percentages of burn-off. The determination was made by the BET nitrogen adsorption procedure using a gravimetric method (7). The total pore volume was obained by applying the Gurvitsch Rule (7).

RESULTS

The gasification of carbon deposits by carbon dioxide was studied over the temperature range 475-850°C for nickel foils and supported catalysts. In most cases, the reaction was characterised by a short induction period, followed by a period of constant rate that lasted from ca. 15 to ca. 75% of burn-off. No significant amount of nickel oxide was formed during the gasification and the only detectable product was carbon monoxide (2).

Measurements of the steady rates of gasification are summarised in Figure 2 for both foils and supported nickel catalysts.

The rates were normalised by dividing by the weight of carbon. Either initial weights or critical weights were used, to take into account

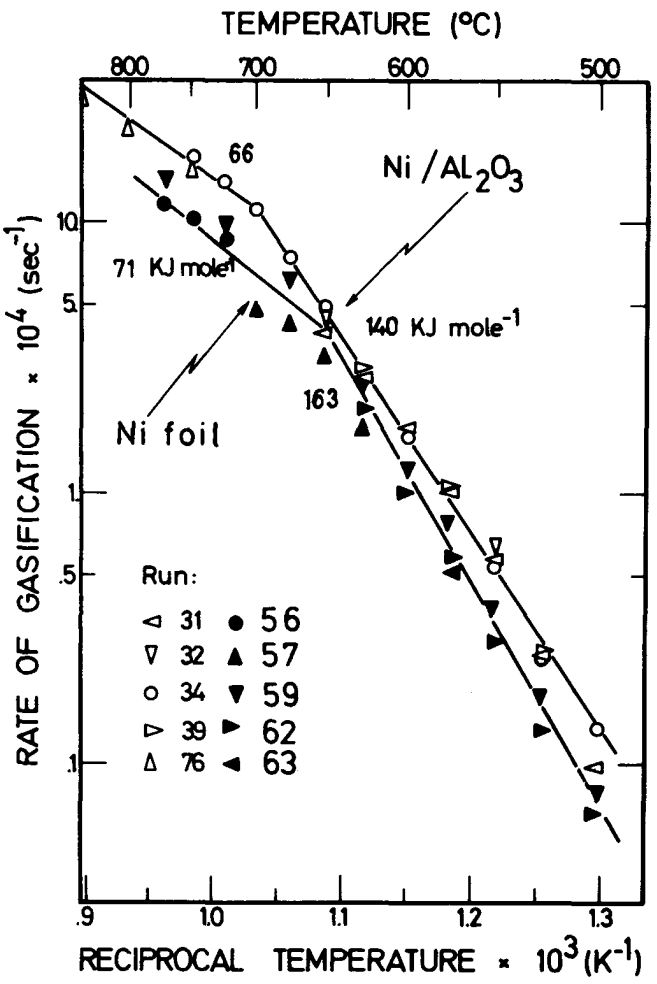

Fig. 2 Arrehenius-type plot of the gasification rates at a constant CO_2 flow rate (3.3 cm^3 (STP) sec^{-1}) and atmospheric pressure.

the accessibility of the metal inside the coke deposits (1,2). Arrehenius-type plots are seen to exhibit two distinct regions, with a change over at about the same rate and temperature. At the higher temperatures, the dependence of rate on carbon dioxide concentration was approximately linear (order ca.1). At lower temperatures, the order was complex, increasing from near zero at 550°C to near unity at 625°C .

The general features of the experiments of hydrogen gasification were the same as those observed with carbon dioxide. At temperatures above 700°C, however, the gasification rate decreased when the temperature increased. This has been explained in terms of the approach of the system to the conditions corresponding to the equilibrium of the gasification reaction (1,6).

The gasification of carbon deposits with steam was studied at temperatures varying between 500 and 825°C and steam partial pressures varying between 7 and 30 KN m^{-2}. Hydrogen and carbon dioxide were the major products of the reaction, with smaller amounts of carbon monoxide being detected. The general features of the experiments were similar to those of the previous cases. The Arrhenius-type plot of the gasification rates bears many resemblances to Figure 1 below 725°C (1,2). At higher temperatures, the activation energy drops to zero. In this zone, the order of the reaction with respect to steam was unity and the gasification rates were dependent on the total flow rate from $5x10^{-5}$ to $2.5x10^{-4}$ moles sec^{-1}. As a result of instabilities in the microbalance head the flow rate could not be further increased.

For comparison, the rates of gasification of carbon by carbon dioxide, steam and hydrogen are presented in Figure 3. The figure refers to nickel/alumina catalysts only. The rates were normalised to refer to the same weight of carbon and to one atmosphere of the gasifying agent.

DISCUSSION

The results summarised in figure 2 show a change in activation energy as the temperature increases. The change is not due to an approach to equilibrium, since the carbon monoxide concentration in the gas phase only reached 15% of that expected for equilibrium of the reaction of carbon dioxide with pure graphite (8). The change is also not due to modifications in the structure of the carbon, since the rate of gasification at 650°C was not affected by heating to 850°C for two hours. On the other hand, when the temperature raises above 675°C, the value of the apparent

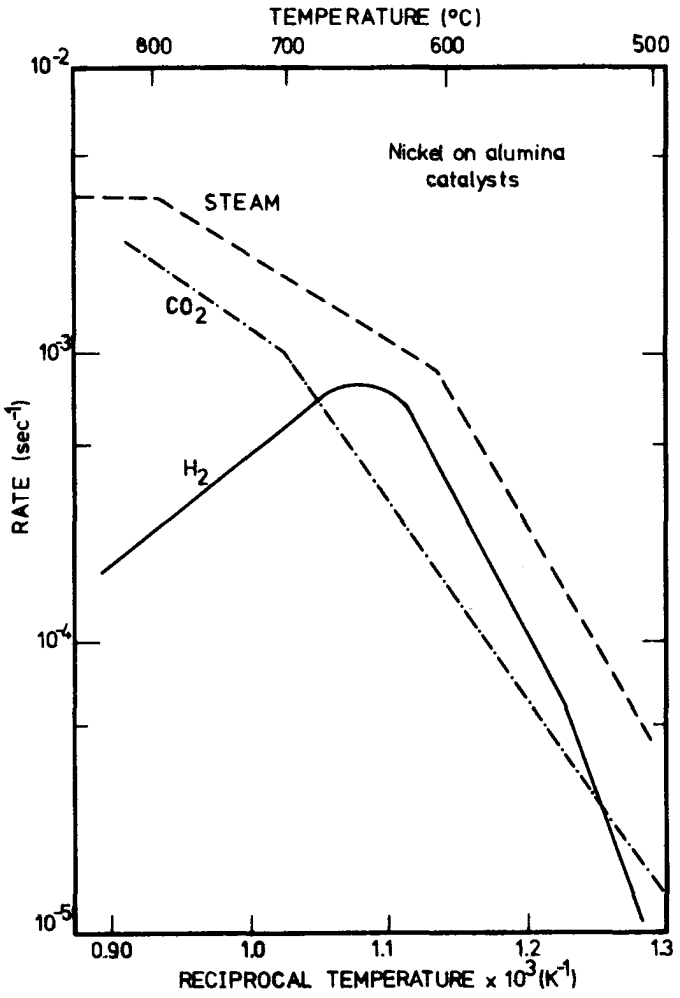

Fig. 3 Arrhenius-type plot of the rates of carbon gasification (Atmospheric pressure; inlet flow=3.3 cm^3 (STP) sec^{-1}). Rate expressed as g carbon gasified per g initial carbon deposited per second.

activation energy is nearly halved and the orders of reaction move towards unity. This seems to indicate the presence of limitations by diffusion in the pores of the carbon (7). In order to test for this hypothesis, the treatment of Roberts and Satterfield (7) was applied.

This treatment is based in the determination of an effectiveness factor, η, as a function of the thiele modulus, ψ, for different values of KP_{CO_2}. ψ and K are defined as:

$$\psi = (L_c^2 \, RT/D_e \, P_{CO_2}) \, R_{CO_2} \qquad (1)$$

and

$$K P_{CO_2} = \frac{k_1/k_2 - 1.6 \, k_1'/k_2'}{1 + 1.6 \, k_1'/k_2} P_{CO_2} \qquad (2)$$

where:

P_{CO_2} - partial pressure of CO_2 outside the carbon

L_c - characteristic dimension of the carbon particle in cm (L_c=R/3 in the case of spheres)

D_e - effective diffusivity of CO_2 into the pores in cm^2 sec^{-1}

R_{CO_2} - rate of the reaction in moles cm^{-3} sec^{-1}

k_1, k_1' and k_2 - direct and reverse specific rates for the oxygen exchange between the gas phase and the carbon surface and the specific rate for the carbon gasification step, respectively.

Assuming that the rate equation in the chemical reaction controlled zone is of the type:

$$\text{Rate} = \frac{kP_{CO_2}}{(1 + b_{CO_2} P_{CO_2} + \varepsilon_i b_i P_i)} \qquad (3)$$

The value of η can be obtained directly as a function of ψ, for spherical geometry (7, page 192).

In the case of supported catalysts the deposits were formed by roughly spherical carbon particles whose diameter was estimated (by microscope observation), to be 0.1 cm in average. The effective diffusivity, D_e, was estimated with data from reference (7), for CO_2 diffusing through a carbon with an average porosity during burn-off of 0.36 (0.26 in the present case). For 725°C and one atmosphere, if the diffusion occurs in the transition region between bulk and Knudsen diffusion:

$$D_e = 0.013 \left(\frac{T}{294}\right)^{0.98} = 4.3 \times 10^{-2} \; cm^2 \; sec^{-1}$$

In figure 2, Run 34, for example, the rate at 725 °C is 1.4×10^{-3} mg sec mg^{-1}. The apparent density, d_a, of the carbon particles at an average burn-off of 50%, can be calculated from the value of the total pore volume, 0.186 $cm^3 g^{-1}$, and the density of the pore walls (1.95 in Table 1, reference 9):

$$d_a = \frac{1}{d_p} + V_p = 1.43 \text{ g cm}^{-3}$$

The value of the rate is then 1.7×10^{-4} moles sec^{-1} cm^{-3}. Thus, from eqn.1, $\psi \simeq 0.090$. K can be calculated from table III in reference (10). At 725°C, K =-0.99. Then from reference (8), $\eta \simeq 0.4$. The intrinsic rate would be $R^i_{CO_2} = R_{CO_2}/\eta \simeq 4.25 \times 10^{-4}$ moles $sec^{-1} cm^{-3}$. Although a calculation of this type can only be taken as an approximation, it is evident that diffusion limitations are affecting the rates observed at 725°C. The fact that similar kinetics are observed above 675°C for both foils and supported nickel catalysts confirms the assumption underlying the calculation: that the diffusion limitations should occur in the pores of the carbon. In these conditions, carbon monoxide, the main product of the gasification, accumulates within the porous structure of the carbon. Even if the gas phase is composed mainly by carbon dioxide, the reaction inside the pores is akin to the gasification by carbon dioxide--carbon monoxide mixtures.

No diffusion limitations were detected in the case of the gasification with hydrogen. As the reaction rate decreased with temperature above 700°C, due to the approach to equilibrium conditions, this was probably to be expected.

In the case of the gasification with steam (see figure 3), the changes in apparent activation energy are believed to be caused by the onset of pore diffusion limitations at ca. 600°C (second zone) and film diffusion limitations at ca. 750°C (third zone).

First, the apparent activation energy decreased from 164 to near zero KJ $mole^{-1}$ and the orders of the reaction increased from 0.6 to 1 when the temperature increased from the first to the third zones. Second, at 750°C , The gasification rates were dependent on the inlet flow rate. Finally, the rates became closer to those of carbon dioxide gasification as the temperature increased.

As the limitations occur in the pores of the coke deposits it is impossible to increase significantly the rates of gasification by any of the gases studied. In the steam reforming of hydrocarbons, carbon can be formed either by the direct decomposition of the hydrocarbon or by carbon-forming gas-phase reactions. In commercial operations, coke originating from these reactions is usually prevented by using excess steam. However, as the present results show, the possibility of a complete "clean-up" of the catalysts is necessarily limited. Rostrup-Nielsen (11), noted that the ability of the catalyst for steam adsorption was important in depressing carbon formation. Thus, a correct formulation of the catalyst, by using selected additives, seems to be the only way of preventing deactivation.

ACKNOWLEDGMENT

The work upon which this communication was based was carried out at the Chemical Engineering Department, Imperial College of Science and Technology. C.A. Bernardo wishes to thank the Universidade do Minho for leave of absence and the Invotan Commission for a scholarship.

REFERENCES

1. Bernardo, C.A., PhD thesis, University of London (1977).
2. Bernardo, C.A. and Trimm, D.L., in preparation.
3. Figueiredo, J.L. and Trimm, D.L., J.Catalysis 40, 154, (1975).
4. Tomita, A.and Tamai Y., Carbon 12, 143 (1974).
5. Marsh, H. and Adair, R.R., Carbon 13, 327, (1975).
6. Nishyiama, Y. and Tamai Y., Carbon 14, 13, (1976)
7. Satterfield, C.N., Mass Transfer in Heteroge-

neous Catalysis, MIT Press, Massachussets (1970).
8. Catalyst Handbook, Wolfe Scientific Books (1970).
9. Marsh,H. and Rand, B., Carbon 9, 47 (1971).
10. Rao, Y.K., Jalan, B.P., Metall. Trans. 3, 2465 (1972).
11. Rostrup-Nielsen, J.R., J.Catalysis 33, 184 (1974).

POLYMER ENGINEERING AND PROCESSES THEORY

M . FRIAS

Quartermaster Laboratories, Lisbon
and Polytechnic Institute, Covilhã

ABSTRACT

The characteristic properties of polymeric materials are associated to engineering problems not accounted in general by the so called unit operations. The association of deformation and flow with physicochemical structure is the scope of polymer engineering, of which stereospecific catalysis and viscoelasticity are typical topics.

When in 1948 Nitschman and Schrade postulated that polymeric systems should exhibit Trouton viscosity to be spinnable, analysis of flow in spinning, as well as in extrusion and injection, where high shear prevails, called for nonlinear viscosity models, that were obtained either by curve fitting or submolecular approach like Bueche's one. It appeared that these models miss important physical effects, in general due to unsufficient thermodynamical and mechanical foundation, taking for granted that qualitative description was correct in linear approach and so giving a too simplified picture of the physics involved in volume shearing. In view to further progress, a review of continuum mechanics and thermodynamics involved in high polymer viscosity and shearing seems worthwhile.

1. POLYMER PROCESSING MOLECULAR APPROACH

Polymer processing is the conversion of polymeric materials or resins into products, including injection, extrusion, calendering, dispersion of pigments and surface activation. Deformation and flow cannot here be generally accounted by hydrodynamics, unless molecular flow and relaxation effects be kept frozen by the involved time scale and by sufficiently low angular and other momenta. On the other hand, characterization of rheological properties should permit the control of molecular weight distribution and the degree of long chain branching of a polymer or a polymeric system, in order to provide an optimum processing condition or a particular desired set of physical behaviour in the final product, as well as optimum design of processing equipment. Some of the molecular approach relationships are those of:

- BUECHE and HARDING, between molecular weight and viscosity of concentrated polymer solutions at various shear rates;
- ROUSE, between relaxation time of a spring and bead molecular element and viscosity of dilute polymer solutions;
- ROUSE, between complex viscosity for oscillatory shear flow and shear rate;
- ZIMM, alternative to Rouse's relations;
- WILLIAMS, between the normal stress difference for steady shearing flow and molecular weight, concentration and temperature;
- BUECHE, submolecular theory, combining friction losses due to solvent motion with friction losses due to molecular rotation under shear;
- LODGE, relating both viscosity and normal stress difference to concentration and temperature, for concentrated polymer solutions;

- GRAESSLEY, between viscosity in steady shearing flow and shear rate as well as relaxation time, predicting also fluid elasticity at low shear rates;
- MIDDLEMAN, between viscosity of polydisperse materials and molecular weight distribution function;
- FERRY, between elastic modulus of a monodisperse polymer and fluid density, molecular weight and temperature;
- FERRY, between elastic modulus of o polydisperse polymer and fluid density, average molecular weight and temperature;
- BUECHE, between the viscosity of a branched polymer and the viscosity of the linear polymer;
- ZIMM and KILB, also between the viscosity of a branched polymer and the viscosity of a linear polymer;
- PETRAGLIA and COEN, between molecular weight and relaxation times spectrum;
- WILLIAMS, LANDEL and FERRY, between viscosity and temperature;
- BUECHE, between polymer viscosity and viscosity of respective solutions;
- BUECHE, between glass transition temperatures of a copolymer and glass transition temperatures of constituent polymers.

These molecular approaches must be used with care, specially as far as quantitative predictions are required. Nevertheless, in certain situations e.g. for polymers of molecular weight of several million, rheological measurements can be the only practical way of determining molecular weight and molecular weight distribution.

It is out of question that a better knowledge of the relationships between the molecular parameters and the rheological and mechanical and thermodynamical parameters in general will be of great help in the design of new polymers or in modifying the existing ones, permitting also the desired material as well as mechanical modifications whenever a processability problem arises.

2. HIGH VISCOSITY FUNDAMENTALS

NITSCHMAN and SCHRADE postulated in 1948 that liquid systems can only be spinnable if their viscosity is anomalous and much greater than Newtonian viscosity. NITSCHMAN and SCHRADE (1) called it Trouton viscosity,reviving old suggestions by TROUTON(2) on the "coefficient" of viscous traction. Since then, analysis of elongation flow of polymers attracted researchers interested in both polymer engineering and non-Newtonian flow.As molecular approaches are unsufficient and in many cases misleading in this domain, it is worthwhile to try to put high viscosity fundamentals on a sound basis and so review its mechanical as well as thermodynamical background.

When introducing rheological linear relations like $\tau=\eta\gamma$, relating the shearing stresses to the rate of shear we are taking an oversimplified picture of the process, hiding for instance rotating momenta and cross effects between degrees of freedom. It is a historical fact that Hooke's law,

$$\sigma = Ee \qquad (2.1)$$

relating the longitudinal stress σ to longitudinal strain e was an experimental law but that Newtonian relation

$$\tau = \eta\gamma \qquad (2.2)$$

was a hypothesis, as Newton himself called it, as reminded by TRUESDELL,

(3). As TRUESDELL well emphasizes, the classical equations of elasticity,

$$T = \lambda E_s U + 2\mu E \qquad (2.3)$$

and of fluid dynamics,

$$T = -pU + \lambda D_s U + 2\mu D \qquad (2.4)$$

have been discovered by theory alone. Let us remind that E and E_s are, respectively, the infinitesimal strain matrix and its trace or scalar and that D and D_s are, respectively, the rate of deformation tensor and its trace, U being the unit tensor and unit matrix.

Both NAVIER and POISSON have used hypothesis to simplify a system of mass points and both CAUCHY and STOKES used molecular hints. Some of their working hypothesis are today known to be incorrect but they arrived to fortunate results. Decades of curve fitting and empirical nonlinear models followed.

A direct lecture of Newtonian flow is that shearing strain can be maintained by shearing stress only i.e., in a shearing experiment, both the stress and strain tensors are proportional to the tensor

$$\begin{vmatrix} 0 & 1 & 0 \\ 1 & 0 & 0 \\ 0 & 0 & 0 \end{vmatrix} \qquad (2.5)$$

When, as many authors have done, we admit a nonlinear viscous law like, e.g.

$$\tau = \eta_1 \gamma + \eta_2 \gamma^2 + \eta_3 \gamma^3 \qquad (2.6)$$

we are wrongly admitting that shearing stresses alone are sufficient to maintain shearing strains or rates of shearing.

It is of common experience that if a rod of steel is pulled or twisted, the linear relations (2.1) and (2.2) are valid only for very small strains. POYNTING experiments by 1912 revealed that a steel wire when twisted increases in volume in proportion to the square of the angle of twist. REYNOLDS discovered this effect independently and called it "dilatancy" i.e. a change in bulk associated to a change in shape. He admitted that bodies are composed of small particles and constructed a "Sub-Mechanics of the Universe", today considered, like many other molecular approaches, a molecular speculation kept in the archives of the bypasses of physics.

POYNTING repeated the steel rod experiment with a rubber cord and observed a change of its length in proportion also to the square of the angle of twist i.e. he observed two qualitatively new phenomena, not predicted by linear theory or its refinements like (2.6).

Much later, on the forties, RIVLIN repeated Poynting's experiments and was able to predict on 1947 the surface stresses necessary to be applied to the ends of a rubber rod in order to obser ve a pure torsional displacement. Also on the forties, WEISSENBERG observed the climbing up of the free surface of a fluid sheared between two concentric circular cylinders. Classical theories predicted instead a flat surface. We do not consider here the small meniscus due to capillarity, as this is a detail, bounded to a special important special treatment. We refer by the way the work of GONÇALVES (4) , on capil larity and viscometric capillars. It is particularly interesting to note that REINER predicted Weissenberg ef-

fect by theory but referred to it as not observed.

POYNTING, RIVLIN and WEISSENBERG experiments have here been revived because they are the milestones of the actual large deformation and non-Newtonian flow science, so important for polymer science and engineering. Of particular importance was the introduction by RIVLIN of the Helmholtz free energy from thermodynamics into continuum mechanics. As a matter of fact, it is an essential feature of the modern processes theory that processes are irreversible in essence and so that thermodynamics in specific sense i.e. in contradistinction to thermostatics must play a fundamental role in the analysis of processes. A unified treatment of mechanics and thermodynamics is today still to be completed specially under the statistical physical viewpoint (5).

A relatively simple analysis is possible for isotropic media, as is the case of melt polymers in processing. In this case, as the strain or deformation rate strain matrix must in any case satisfy its own Cayley-Hamilton equation and as due to the isotropy of the material, the stress matrix may be supposed to be a power series in the strain or rate of deformation matrix, third and higher powers may be eliminated so that T , the stress matrix can be expressed in the strain or rate of deformation matrix D by the exact and general relation

$$T = aU + bD + cD^2 \qquad (2.7)$$

where a, b, c are power series in the principal invariants of D matrix i.e. intrinsic functions of the deformation or rate of deformation matrix or tensor.

Shearing characterizing experiments must of course use simple deformation patterns e.g. a deformation tensor like (2.5) or a multiple of it i.e.

$$r \times \begin{vmatrix} 0 & 1 & 0 \\ 1 & 0 & 0 \\ 0 & 0 & 0 \end{vmatrix} \qquad (2.8)$$

Calculating the respective strain matrix invariants, (2.7) yields

$$T = (A + Br^2) \times \begin{vmatrix} 1 & 0 & 0 \\ 0 & 1 & 0 \\ 0 & 0 & 1 \end{vmatrix} + \qquad (2.9)$$

$$+ r(C + Dr^2) \times \begin{vmatrix} 0 & 1 & 0 \\ 1 & 0 & 0 \\ 0 & 0 & 0 \end{vmatrix} +$$

$$+ \quad r^2F \quad \times \begin{vmatrix} 1 & 0 & 0 \\ 0 & 1 & 0 \\ 0 & 0 & 0 \end{vmatrix}$$

The classical result, that shearing strain can be maintained by shearing stress only,only follows if B, D and F be zero or physically negligible. For the general case we see very well that a hydrostatic pressure of magnitude $-Br^2$ and normal tension of magnitude Fr^2 must be supplied against the deformation tensor. If not, the medium or material will contract or expand according to the sign of B except if it is incompressible. If normal stresses be missing, then the material or medium will elongate or shorten, according to the sign of F. These two effects are characteristic of nonlinear rheology either for solids or liquids and are observed in polymers, namely in injection, extrusion and spinning processes.

From (2.9), we see also that bulk dilatancy and elongation are governed by independent material qualities, as the respective coefficients occur one

at time, in one term each. Nevertheless, this important theoretical and practical fact does not appear clearly in general in the literature and so it must be well emphasized.

3. POLYMER MELT SPINNING PROCESS

Injection and extrusion and particularly melt spinning are processes under high shear, involving so nonlinear transport phenomena and eventually a change in physical state.

We have so far analysed that to an elementary simple strain input corresponds a complex stress output, degenerating into a simple output only under limiting conditions for quadratic terms, before defined, those limiting conditions not existing for spinning and also for related high shear polymer flows. This means in practice that instead of

$$\tau = \eta\gamma \qquad (2.2)$$

with a well defined viscosity η, we have to consider that

$$\tau = f(\gamma) \qquad (3.1)$$

Of course, $f(\gamma)$ must have the dimensions of $\eta\gamma$ i.e. a time parameter must be involved. This is typical of viscoelastic flow, like polymer melt flow, where the time parameter may be associated to a material parameter or material constant. Subjecting the melt flow to the same viscometric apparatus as in low viscometry, namely to capillary high-pressure viscometers, that time constant is assimilated to a viscosity, in case that stresses do not result so high that viscometric measures are hampered of course. In the case of spinning, the polymer melt exhibits both elastic and viscous aspects i.e. it is a typical viscoelastic medium. In spinning technology it is usual to define a spinning viscosity as the rate of the tension under which the filament emerges from the spinnerette and the relative decrease in cross section per unit time, so resulting a parameter with different dimensions of those of rheological viscosity, an important comment to be taken in mind in spinning process analysis.

In contrast to low-shear viscometry, the status of research in high-shear viscometry is far from satisfactory. EYRING (6) modified his rate of process theory of jumping molecules into one of "flow groups" of polymer segments, each group having an intrinsic relaxation time. Nevertheless, probably due to unsufficient definition of grouping of polymer segments, quantitative results are poor.

4. CONCLUSION

Polymer processing, namely high-shear operations involve transport phenomena of complex analysis from the physical viewpoint, hidden by mathematical empirical models but foreseen by the variety of molecular approaches. Terms are often improperly used and so care must be taken in collecting information from the literature. Progress in transport phenomena in this domain seems to depend on a deeper association of viscoelastic flow with polymeric parameters distinct from those employed in low-shear, newtonian case. Temperature aspects have not here been considered not only by paper length

reasons but because temperature is just one of several parameters to add to viscous parameters on a compreensive thermodynamical framework, whose contours are under work, (7),(8),(9).

ACKNOWLEDGEMENT

We thank Universidade do Minho for the kind invitation and particularly prof. J. ROMERO for the honour of old friendship. We also thankfully remind critical advices of RIVLIN and of GYARMATI on the structure of process fundamentals.

REFERENCES

(1) NITSCHMAN,H.,SCHRADE,J. J. Helv. Chem.Acta 31 297 1948 ;

(2) TROUTON, T. Proc.Roy.Soc. A77 326 1906 ;

(3) TRUESDELL, C. J.Math.Pur.Appl. 113-158 1951 ;

(4) GONÇALVES, F. Thesis Cl.Un.Lis. 1977 ;

(5) FRIAS, M. Portugaliae Physica 10 under publ. ;

(6) EYRING, H. J.Appl.Phys. 26 793 1955 ;

(7) FRIAS, M. Colloque de Rhéologie 1978 under publ. ;

(8) VERHÁS, J. Per.Polytech.,Ch.Eng. 21 311-322 1977 ;

(9) EDELEN, D. Adv.Chem.Phys. XXXIII 399-442 1976 .

PROCESSABILIDADE DE ÓLEOS ESSENCIAIS EM CCC

Aquiles C. Gomes[1]
M. Fátima Farelo[1]

1. Centro de Processos Químicos das U.L. I.S.T, Lisboa

RESUMO

Investiga-se a processabilidade de óleos essenciais por Cristalização Contínua em Coluna, estudando a separação do 1-8 cineol do óleo de Eucaliptus Globulus e o L-mentol da dL-mentona (principais constituintes do óleo de Menta Arvensis Brasil), em equipamento piloto CCC tipo Schildknecht.
Certos dados físico-químicos destes sistemas, não existentes na literatura e necessários para este trabalho, são determinados: apresentam-se aqui os principais diagramas de equilíbrio sólido-líquido e caracterizam-se os cristais quanto ao hábito cristalino. As determinações de hábito por foto-microscopia a baixas temperaturas permitem a sua comparação e observar as modificações introduzidas pelo processo de arrefecimento.
Conclui-se relacionando o hábito cristalino com a processabilidade de óleos essenciais na coluna Schildknecht.
Tais conclusões são generalizáveis para o processamento de outros sistemas orgânicos nos vários tipos de equipamento de CCC.

INTRODUÇÃO

A Cristalização Contínua em Coluna-CCC é um processo de separação de grande interesse potencial para a industria química, que tem deparado com dificuldades apreciáveis na passagem das escalas laboratorial e piloto para as semi-industrial e industrial. Estas dificuldades têm originado numerosos insucessos, quer em técnicas específicas para a sua concretização, quer em vias teóricas para a sua análise e projecto, que se traduzem na incapacidade de transposição das técnicas ou das formulações para contexto diferente daquele em que foram concebidas, (seja no aumento da escala, ou na aplicação a novos sistemas).
Esta situação induziu-nos a procurar uma diferente abordagem para a operação abandonando muitas das formulações existentes para a CCC (1) decidimos recorrer aos conhecimentos acumulados para a cristalização, isto é, separação por cristalização a partir de soluções. Esta, apesar das limitações da sua análise teórica (2), sentidas nas dificuldades de projecto e previsão de resultados de operação para novos equipamentos e sistemas, beneficia duma longa experiência industrial, com uma contribuição decisiva para a realização de numerosos processos.
Aplicámos estes conhecimentos e as novas análises propostas aos óleos essenciais. Trata-se de produtos naturais obtidos de plantas ou arbustos, por extracção ou destilação. O óleo "bruto", assim obtido é, em vários casos, submetido a purificação, às vezes por Cristalização (tradicional).
A CCC tem grande interesse nesta aplicação, por poder permitir um processamento sem degradação térmica do produto (de molécula complexa, e ponto de ebulição elevado o que dificulta a destilação, mesmo sob vácuo), contínuo e com adequado controle de qualidade (o que a cristalização tradicional não garante facilmente).
Dos óleos essenciais a processar eventualmente em Portugal, por CCC, tem especial interesse o óleo de eucalipto de que somos um dos maiores produtores mundiais, e óleo de menta Arvensis não obtido em quantidades apreciáveis, mas de interesse potencial significativo.
Do óleo de menta Arvensis separa-se o L-mentol seu constituinte principal e exclusivamente (em nosso conhecimento) obtido por cristalização tradicional. Esta separação é muito complexa e permite apenas a redução do teor de L-mentol de 70% no óleo "bruto" a cerca de 50% no óleo "desmentolado". (3) Do óleo de eucalipto separa-se o 1,8 - cineol, vendido comercialmente sob a designação de eucaliptol, e que é o seu principal componente. Actualmente separação é feita predominantemente por cristalização tradicional.
Para esta investigação consideraram-se os sistemas mais importantes que constituem aqueles óleos. Assim, e para o óleo de menta, estudou-se o binário do L-mentol com a dL-mentona, 2ª constituinte do óleo de menta e que dele representa cerca de 18%. (4).
Para o óleo de eucalipto caracterizaram-se experimentalmente os binários 1-8 cineol/α-pineno, 1,8-cineol/d-limoneno, α-pineno/d-limoneno e também o ternário 1-8 cineol/α-pineno/d-limoneno (5)
Nos ensaios piloto deste óleo utilizou-ze o próprio óleo, dado que 99% da sua composição corresponde aquele ternário.
Os resultados aqui apresentados são parte de uma investigação de muito maior dimensão, realizada sobre o mesmo tema e que abordou, com resultados experimentais e análises teóricas, vários factores que influenciam a CCC e a processabilidade dos óleos essenciais. Neste trabalho retem-se para análise dois aspectos básicos:o equilíbrio sólido-líquido e o hábito cristalino que são dos mais importantes daqueles factores.

EQUILÍBRIO SÓLIDO-LÍQUIDO (ESL)

Os dados de esl são indispensáveis para o estudo da aplicação de CCC a qualquer sistema; não se tendo encontrado na literatura dados experimentais, foi necessário fazer a sua determinação que se revelou aliás, difícil dadas as temperaturas baixas a que foi necessário trabalhar e os problemas de cristalização vítrea surgidos para os sistemas com L-mentol.

Técnicas experimentais

As curvas de aquecimento permitem a determinação do liquidus pela simultânea leitura de temperaturas e observação visual da massa cristalina em fusão; o fim da fusão corresponde ao desaparecimento da turvação causada por finas partículas sólidas dispersas no líquido.
Parte-se de amostras sólidas obtidas por arrefecimento brusco, que distribui homogeneamente as impurezas. A amostra de 6 cm^3, contida na célula de vidro transparente de dupla parede, é aquecida num banho termostalizado com controlo fino de temperatura, a ritmo muito lento (0,1°C/min), com agitação rápida. A temperatura é medida por termopar Ni-Cr/Ni-Al referido a gelo fundente, num registador Phillips PM8100.
Esta técnica só foi usada acima de 0°C, dada a dificuldade de, a temperaturas negativas, manter o aquecimento lento e realizar observação visual.
Nas curvas de arrefecimento o liquidus, início da solidificação, é determinado por um "pico" no diagrama temperatura-tempo. O solidus é dificilmente detectado.
O equipamento é semelhante ao da técnica anterior; o meio arrefecedor é um banho termostatizado entre 0 e 100°C; para temperaturas negativas utilizaram-se misturas de neve carbónica/acetona, azoto líquido/álcool ou apenas azoto líquido.
Esta técnica tem boa reprodutibilidade, mas dá um desvio constante de alguns graus, em relação ao liquidus real, correspondente à curva de supersolubilidade de Miers.
Para sistemas com solidificação vítrea a sua aplicação é difícil; ou não há transição e não há "pico", ou a transição é muito lenta e origina um pico largo.
As determinações por curvas de arrefecimento e aquecimento supõem o equilíbrio termidinâmico entre as fases sólida e líquida: a pequena velocidade de transferência de massa no sólido, impede esse equilíbrio para cristais mistos (6). Em particular, no traçado das curvas de aquecimento, em que apenas a camada superficial está em equilíbrio com o líquido, também o pré-tratamento das amostras sólidas influencia a forma das curvas. A técnica de arrefecimento, por partir de amostras líquidas não tem estas limitações, mas a cristalização é muito mais lenta que a fusão e as temperaturas de equilíbrio sofrem grandes desvios.
A microscopia permite a determinação do solidus e do liquidus pela observação de lâminas com o sistema estudado.
Por arrefecimento lento da platina observa-se o início da solidificação com o aparecimento de pequenissimos cristais que actuam como núcleos de cristalização. Numa amostra congelada rapidamente determina-se o solidus observando-se o início da fusão na intersecção de planos de cristalização com orientações diversas.
Utilizou-se um microscópio Leitz, com platina arrefecida por circulação de álcool; a fonte fria é uma unidade de refrigeração Hectofrig Flow Cooler CA3, com regulação de temperatura. O aquecimento da platina é feito por resistência eléctrica, sendo a potência calorífica regulada num transformador de voltagem. A temperatura da lâmina lê-se em termómetros cuja escala se observa no microscópio.
Os resultados são concordantes com os obtidos nas curvas de aquecimento. Não foi possível trabalhar a temperaturas negativas: a congelação do vapor de água sobre a lâmina falseia os resultados.

Produtos utilizados

Os produtos utilizados nas determinações experimentais de esl têm as seguintes origens e especificações: 1-8 cineol: eucaliptol comercial "Codex", com um teor mínimo de 99%; a principal impureza é o α-pineno; α-pineno: produto comercial com teor mínimo de 99% (m/m), avaliado por cromatografia em fase gasosa; d-limoneno: produto BDH, de qualidade média, 96% (m/m).
L-mentol: produto Fluka, a cromatografia em fase gasosa revelou um teor de 99.4 (m/m).
DL-mentona Produto Fluka, de baixa qualidade; a análise cromatografia revelou em teor de 5,9% (m/m) de uma impureza não identificada.

Esl para o L-mentol/dL-mentona

O solidus e o liquidus determinados indicam solubilidade sólida total entre os dois compostos (pontos de congelação afastados de 140°C, Fig.1).

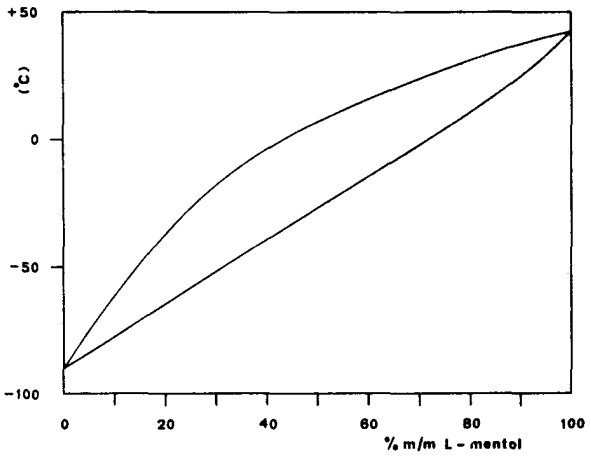

Fig.1 - Esl para o L-mentol/dL-mentona

A linha solidus foi apenas parcialmente determinada devido à dificuldade de utilizar o microscópio a temperaturas negativas. O aquecimento e a microscopia, aplicados para misturas contendo de 100 à 40% de L-mentol, permitiram obter valores concordantes das temperaturas liquidus; por arrefecimento obtêm-se, nesta gama de concentrações, um desvio de 8-8,5ºC (linha de supersolubilidade com que se corrigiu o liquidus para teores inferiores.

Esl para sistemas com 1,8-cineol

Para os binários1,8-cineol/α -pineno e 1,8 cineol/ /d-limoneno a forma dos liquidus e solidus indicam tratar-se de sistemas com solubilidade sólida nula ou muito baixa (Fig 2, Fig 3).

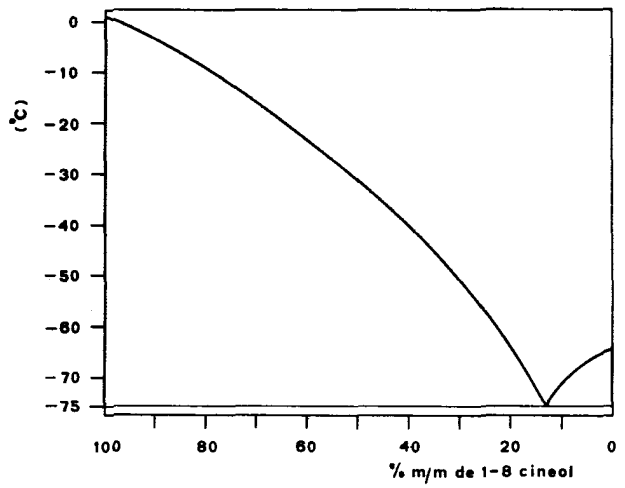

Fig.2 - Esl para o 1,8-cineol/α-pineno

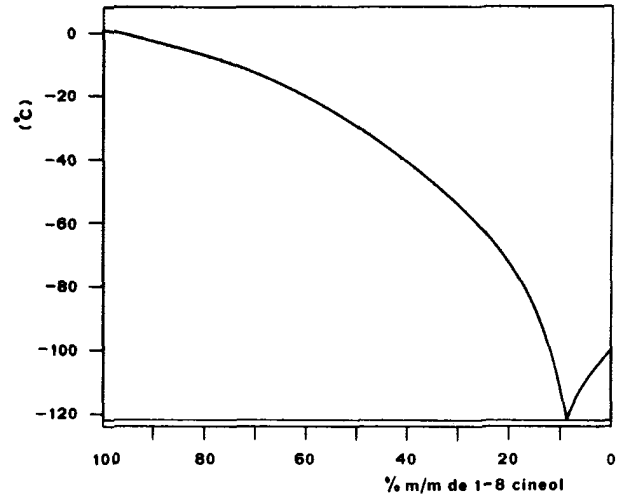

Fig.3 - Esl para o 1,8-cineol/d-limoneno

Para o binário α- pineno/d-limoneno os resultados são apresentados na Fig. 4. Trata-se de um sistema com solubilidade sólida total, que origina um composto com um ponto de fusão mínimo (duas moléculas de d-limoneno associadas a uma molécula de α -pineno). No entanto, a dificuldade de observação visual da congelação do líquido devido à elevada viscosidade, à temperatura muito baixa a que tem início (o composto tem um ponto de fusão de aproximadamente 170º C), conjuntamente com as dificuldades de interpretação das curvas de aquecimento e arrefecimento quando varia acentuadamente o gradiente de temperaturas durante a medida, diminuem fortemente a reprodutibilidade dos valores obtidos.
Para o ternário 1,8-cineol/ α-pineno/d-limeno os resultados (Fig . 5) são obtidos sobretudo no campo do 1-8 cineol (zona de concentrações do ternário em que a solidificação se inicia com a formação de cristais de 1-8 cineol);

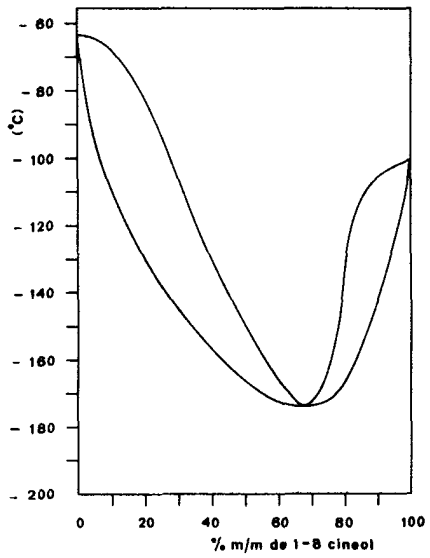

Fig.4 - Esl para o α-pineno /d-limoneno

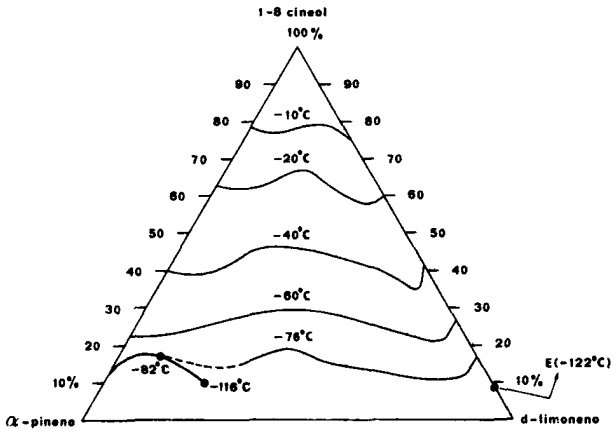

Fig.5 - Esl para o 1,8-cineol/α-pineno/ d-limoneno

HABITOS CRISTALINOS

Fig.6 - Cristais de L-mentol/ dL-mentona

Os hábitos cristalinos dependem do modo de crescimento dos cristais; aqui ,foram estudadas duas situações distintas: a formação de cristais a partir de uma massa de solução ou fundido, por arrefecimento rápido com agitação ;os cristais têm pequenas dimensões; corresponde à situação real em CCC onde há tempos de residência de alguns minutos. A formação de cristais, a partir de uma camada fina de líquido, contido entre lâmina e lamela; embora não corresponda a uma situação em CCC e nem sempre possa dar indicações sobre o hábito cristalino porque por vezes o destrói, este tipo de cristalização permite conhecer a possível tendência para a formação de agregados dendríticos.

Equipamento

No estudo dos hábitos cristalinos recorremos à fotografia em microscópio a várias temperaturas, utilizando equipamento de dois tipos: microscópio Reichert, do Departamento de Metalurgia do IST, permitindo fotografia à temperatura ambiente; microscópio Olympus X-Tr, com platina substituida por uma câmara de circulação de líquido termostatizado, permitindo a formação de cristais a qualquer temperatura. A máquina fotográfica deste equipamento é uma Olympus PM-10-35A com fotómetro automático; a unidade frigorífica é uma Hectofrig Flow Cooler CA 3, com circulação de álcool termostatizado. O conjunto formado pela objectiva, lâmina e platina foi isolado em atmosfera de azoto arrefecido (resultante da vaporização de azoto líquido), impedindo a formação de cristais de gelo, a baixas temperaturas.

Fotomicroscopias

A fotomicroscopia dos cristais formados por arrefecimento rápido do sistema L-mentol/dL-mentona revela hábito acicular , fibro-radiado, de dimensões microscópicas. Estas agulhas enovelam com extrema facilidade formando aglomerados cristalinos que, sem o auxílio de microscópio, são facilmente tomadas por "cristais" de aspecto f'oculento. Notam-se ainda dendrites negativas (aglomerados cristalinos em que a interface sólido-líquido tem curvatura negativa com centro no líquido). Por arrefecimento em camada fina, produzem-se curiosíssimas formações dendríticas, tipicamente arborescentes (Figs. 6,7).

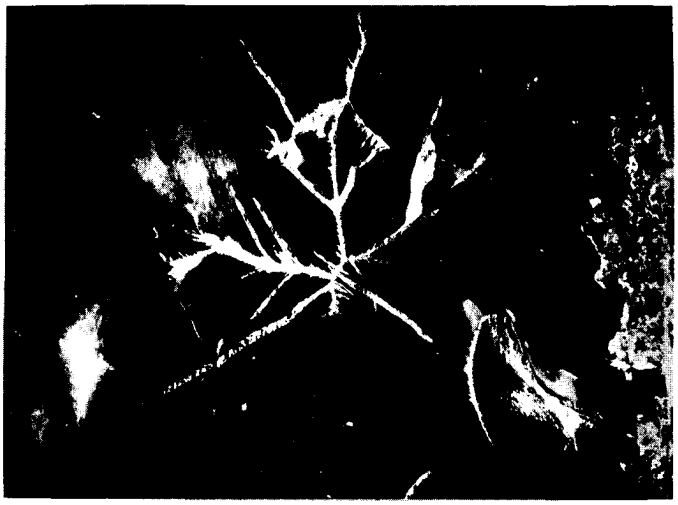

Fig.7 - Cristais de L-mentol/ dL-mentona em camada fina

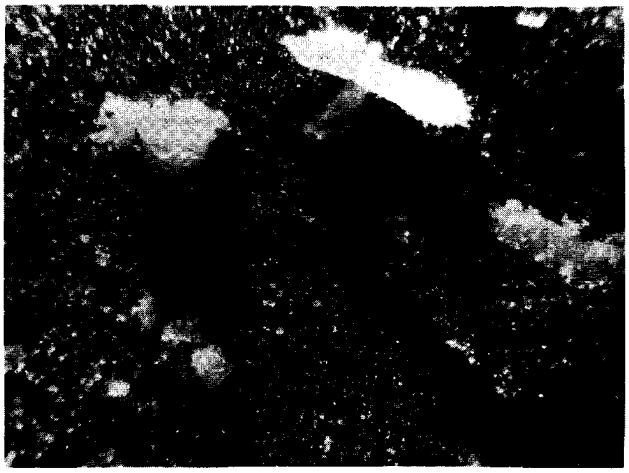

Fig.8 - Cristais microgranulares de 1,8-cineol

Por arrefecimento rápido do 1,8 cineol obtêm-se cristais de hábitos micrograrnular solto (Fig.8). Por arrefecimento em camada fina, não se observam dendrites.

EXPERIMENTAÇÃO PILOTO

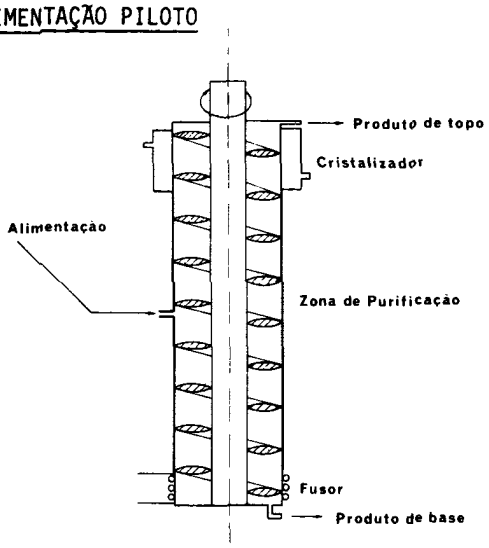

Fig. 9 - Coluna piloto Schildknecht

Os ensaios foram conduzidos numa unidade piloto Schildknecht realizada pela Newton-Chambers, adquirida e modificada pelo "GEPS" (Grupo de Estudos de Processos de Separação).
Descrevem-se as duas versões da coluna: a inicial, Newton-Chambers, e a resultante das alterações introduzidas pelo GEPS.

Equipamento piloto-versão básica

A coluna piloto é essencialmente o espaço compreendido entre dois tubos concêntricos de 800 mm de altura, onde se move um hélice. O tubo interno, ou veio, é de aço inox (diâmetro 37 mm); o tubo externo de vidro é de grande precisão para garantir com rigor um diâmetro interno de 2" (Fig. 9).
Na coroa circular definida pelos dois tubos, move-se o hélice em aço inox (secção quadrada de 6,5 mm de lado, declive de 14º, folga às paredes de 1/100 de polegada). Um sistema de motor eléctrico, correia e variador de velocidade (0-200 rpm), comunica movimento ao hélice.
A mistura a processar é alimentada por bomba de duas cabeças e passo regulável, usualmente a meio da coluna. O nível da alimentação separa a zona de enriquecimento (purificação da corrente de cristais), da zona de esgotamento (acima da alimentação onde se esgota o líquido no produto).
O fusor, na base da coluna, é realizado pela aplicação sobre o tubo de vidro de uma resistência eléctrica (duas dezenas de espiras, 61Ω a 25ºC). Um regulador de tensão controla a potência calorífica. O produto de mais alto P.F. é daqui retirado, sob a forma líquida.
No topo da coluna o cristalizador é realizado pela circulação de um líquido frigorífico entre a coluna e uma parede de vidro, exterior, concêntrica (Ø = 85 mm) ; o álcool é arrefecido numa unidade de frio Hectofrig Flow Cooler CA 3, com regulação de temperatura. No extremo superior do cristalizador um overflow descarrega o produto de mais baixo P.F., com um caudal determinado pela diferença entre a alimentação e o caudal imposto na base.

Equipamento piloto-versão GEPS

A aplicação de potências frigoríficas elevadas pode originar aglomerados cristalinos densos que, bloqueando o movimento do hélice, exercem tensões muito elevadas na parede de vidro da coluna, cuja fragilidade é aumentada pelas perfurações para alimentação e medidas de temperatura.
Para evitar a sua rotura frequente substituiu-se o tubo de vidro por um tubo de aço inox maquinado interiormente com grande precisão; manteve-se uma zona para observação visual no fusor, em vidro resistente a altas temperaturas (110 mm de altura), onde se aplica a resistência eléctrica.
A zona de enriquecimento (360 mm de altura) dispõe de perfurações laterais para amostragem do líquido e medida da temperatura por termopar; a leitura destas é feita num leitor Comark (-50; + 160ºC; menor divisão 0,1ºC; zero calibrado com gelo fundente). O isolamento da coluna, usado em ensaios com a versão inicial (meias canas cilíndricas com espuma rígida de poliuretano) tornou-se insuficiente dado que o aço inox tem uma condutibilidade térmica cerca de 70 vezes superior à do vidro. Recorreu-se então a isolamento duplo: espessa camada de fibra de amianto e camisa de vidro de dupla parede.

Operação da coluna

Enchimento da coluna: ligar a bomba de alimentação, até o overflow descarregar o líquido. Ler a temperatura de alimentação por termopar.
Accionar o motor eléctrico do hélice e ajustar a velocidade de rotor para o valor pretendido.
Ligar a unidade frigorífica e a bomba de circulação do álcool.
Programar o arrefecimento do alcool (rápido, de 30ºC/h, ou lento, de 10ºC/h, conforme a composição da alimentação).
Alimentar periodicamente à coluna mais líquido para compensar a redução de volume provocada pela cristalização.
Registar a intervalos regulares as temperaturas indicadas pelos termopares nos diferentes níveis na zona de enriquecimento, (curvas temperatura-tempo de operação). Medir a temperatura ambiente.
Ligar o aquecimento quando os cristais chegarem ao fusor, regulando o variador de tensão para o funcionamento óptimo da coluna (últimos cristais fundindo ao nível da última espira).
Estabilizar a coluna a refluxo infinito, controlando sempre o nível dos cristais na base; na estabilização as temperaturas são constantes.
Para operar a refluxo finito, regular o passo da bomba de alimentação para o caudal pretendido;

TABELA 1 - Ensaios com L-mentol/dL-mentona

	L-mentol na alimentação (% m/m)	N (rpm)	Arrefecimento		Aquecimento		Tempo de operação (h)
			Periodo (h)	T_ℓ (°c)	Período (h)	P (cal/min)	
M 3	63,6	63	0 -1,33 1,33-8,4	-10 -20	0 -1,5 1,5 -2,67 2,67-5,5 5,5 -8,4	0 23,0 34,0 70,0	8,4
M 5	72,5	63	0 -1,5 1,5 -3,5 3,5 -5,25 5,25-7,5 7,5 -8,75	+2 +1 -5 -13 -18	0 -2 2 -3,83 3,83-8,75	0 51 47	8,75
M 6	72,5	60/44 (1)	0 -4,5 4,5 -8,75	-3 -24	0 -2,67 2,67-4,44 4,44-5,83 5,83-8,75	0 28 97 143	8,75
M 7	72,5	44	0 -4,2 4,2 -8,33	-7 -24	0 -2 2 -3 3 -5 5 -6,5 6,5 -8,33	0 425 90 105 145	8,33

TABELA 2 - Ensaios de separação do 1,8-cineol

	1-8 cineol na alimentação	N rpm	Arrefecimento		Aquecimento		Tempo de operação (hr)		Caudais (cm^3/h)		
			Período (h)	T_ℓ (°C)	Período (h)	P Cal/min	Refluxo infinito	Refluxo finito	A	B	B/T
C18	87	98	0 - 4,0	- 30	0 - 0,5 0,5 - 4,0	0 85	4	-	-	-	-
C21	80	62	0 - 1,0	- 30	0 - 0,5 0,5 - 1	0 25	1	-	-	-	-
C23	86	74	0 - 10,7	- 21	0 - 1,0 1,0 - 10,7	0 68	10,7	-	-	-	-
C24	89	86	0 - 1,7	- 20	0 - 1,0 1,2 - 1,7	0 60	1,7	-	-	-	-
C17	88	20	0 - 1,5	- 32	0 - 0,3 0,3 - 1,5	0 6	0,5	1	80	35	0,78
C20	87	62	0 - 1,5	- 30	0 - 0,3 0,3 - 1,5	0 24	0,5	1	500	350	2,34
C22	86	62	0 - 6,5 6,5 - 9,0	- 29 - 2,7	0 - 3,5 3,5 - 4,0 4,0 - 9,0	0 53 24	4	5	920	430	0,87

regular grosseiramente a válvula de descarga de base; reduzir o aquecimento do fusor; ligar a bomba doseadora da alimentação e ajustar por aproximações o caudal de base para a razão de caudais base/topo pretendido; controlar o aquecimento. Exceptuando ocasionais perturbações externas, o sistema é estável por períodos longos.

Ensaios com L-mentol/dL-mentona

Conduziram-se ensaios sobre o binário L-mentol/dL-mentona., com a versão GEPS da coluna.
Não se referem aqui, nem os ensaios prévios para exploração do comportamento do sistema em coluna e afinação da operação desta essencialmente não programados e de resultados não explorados, nem os ensaios em que se estuda a influência de parâmetros não relevantes neste estudo: isolamento, temperatura ambiente, ... Os ensaios foram conduzidos a refluxo infinito, todos com tempos de estabilização longos, de várias horas.
O arrefecimento depende da evolução da temperatura do fluido frigorífico no tempo. A potência calorífica de aquecimento foi variada descontinuamente. O teor em L-mentol nas alimentações foi de 63,6% e 72,5% m/m. Para esta última ensaiaram-se diferentes velocidades do rotor, de 44 a 63 rpm. A temperatura da alimentação foi em todos os ensaios, a ambiente.
As estratégias de arrefecimento variaram consoante o teor de L-mentol na alimentação: para o teor mais baixo usou-se arrefecimento rápido; para o teor mais elevado, em que a probabilidade de colagem da coluna era previsivelmente maior, o arrefecimento foi lento e progressivo, (Tab. 1).

Ensaios de separação de 1-8 cineol

Os oito ensaios com o óleo de eucalipto para separação de 1,8-cineol foram conduzidos com a versão básica da coluna; num deles (ensaioC19) houve descontrole do aquecimento do fusor, originando sobreaquecimento de toda a parte inferior da coluna e não foram recolhidas amostras.
Dos sete ensaios válidos, quatro foram conduzidos a refluxo infinito e três a refluxo finito; a alimentação variou quanto ao teor em 1,8 - cineol na gama 80-90% m/m (Tab. 2).
O arrefecimento foi em todos os casos extremamente rápido, dado que este sistema não origina colagem da coluna. A potência calorífica, aplicada após a chegada de cristais à base, manteve-se praticamente constante ao longo da operação, com ligeira redução na passagem a refluxo finito.
Os tempos de estabilização foram muito mais reduzidos que para o binário; a duração de alguns ensaios não ultrapassou 1-1,5 horas. Nos ensaios a refluxo finito ensaiaram-se dois níveis para a razão base-topo (ligeiramente inferior a 1 e superior a 3).

RESULTADOS E CONDUÇÃO DA COLUNA

Os ensaios realizados com o equipamento piloto descrito permitiram obter informação muito detalhada sobre o comportamento dos sistemas e condução da coluna. Os resultados suportam as conclusões sobre a processabilidade apresentadas à frente (tais resultados foram ainda submetidos a análise aprofundada, não apresentada aqui, sobre a separação obtida e sua evolução no tempo).

Ensaios com L-mentol /dL -mentona

As amostras recolhidas na base e topo da coluna após estabilização, foram analisadas por cromatografia em fase gasosa. As composições médias são indicadas na Tab. 3 que contêm ainda a temperatura T_ℓ do líquido no cristalizador, e a potência calorífica na estabilização; a diferença $T_\ell - Tf$, (Tf é a temperatura na fonte fria) foi de 25 a 30ºC. O teor de L-mentol nas amostras de base variou acentuadamente, de 73,6% no ensaio M3 até 95% no ensaio M6, evoluindo paralelamente ao aumento da potência calorífica aplicada no fusor.
Das leituras periódicas da temperatura em vários níveis da zona de enriquecimento, são apresentados na Tab. 4 extractos para apenas 3 secções: o nível mais ao topo S2, o nível intermédio S5, o nível mais próximo do fusor S8 (tempo desde o início da operação).
A representação gráfica da evolução da temperatura ao longo do tempo para o ensaio M3, nas secções S2, S3, S4, S5 e S8 é feita na Fig. 10;

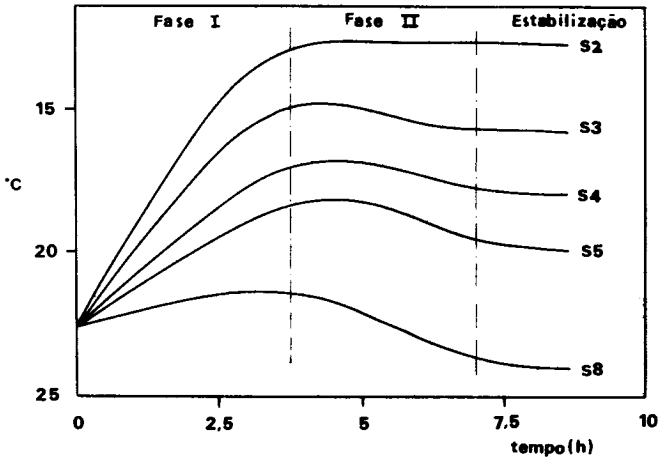

Fig.10 - Evolução das temperaturas no ensaio M3

a escala das temperaturas cresce para baixo para que a curva S2 apareça no topo e a S8, na parte inferior do gráfico. No arranque da coluna distinguimos duas fases: a primeira, inicia-se com a circulação do fluído frigorífco no cristalizador e conclui-se com a aplicação de potência de aquecimento no fusor. O arrefecimento não é uniforme em toda a coluna, sendo mais rápido e acentuado no topo (cristalizador e S2); com a descida dos cristais a temperatura sofre aí um decréscimo ligeiro. A acumulação de cristais no fusor obriga à aplicação de potência calorífica e define no tempo o fim da primeira fase (e o início da segunda). Da estratégia de arre-

TABELA 4 - Evolução das temperaturas nos ensaios com o L-mentol/dL-mentona

Tempo de operação	ENSAIO M3				ENSAIO M5				ENSAIO M6				ENSAIO M7			
	Níveis na zona de enriquecimento			Cristais no fusor	Níveis na zona de enriquecimento			Cristais no fusor	Níveis na zona de enriquecimento			Cristais no fusor	Níveis na zona de enriquecimento			Cristais no fusor
(h)	2	5	8		2	5	8		2	5	8		2	5	8	
0	22,5	22,5	22,5	-	25,8	25,8	25,8	-	28,0	28,0	28,0	-	25,0	25,0	25,0	-
0,5	21,5	21,8	22,1	-	24,8	25,5	25,8	-	26,5	27,0	27,8	-	23,6	24,4	24,8	-
1,0	19,5	21,2	22,0	-	23,9	25,3	25,8	-	24,6	25,0	27,8	-	23,0	24,1	24,6	-
1,5	17,5	20,6	22,0	-	22,8	24,8	25,9	-	23,7	25,6	26,8	-	22,8	23,3	24,4	-
2,0	16,0	20,0	21,9	-	21,6	24,4	26,1	S	22,6	25,0	26,2	-	21,2	23,6	24,4	S
3,0	13,5	18,9	21,6	-	20,6	24,1	26,7	S	20,8	23,8	25,5	-	18,7	23,3	25,5	S
4,0	12,4	18,1	21,6	S	20,2	24,3	27,4	S	19,0	23,2	25,6	-	17,4	23,3	27,1	S
5,0	12,7	18,4	21,9	S	19,8	24,3	27,5	S	17,2	22,7	26,0	S	16,6	23,0	27,8	S
6,0	12,6	18,8	22,8	S	19,2	24,2	27,6	S	16,3	23,5	27,5	S	16,3	23,2	28,9	S
7,5	12,6	19,5	24,0	S	19,1	24,7	28,5	S	14,7	22,9	30,7	S	15,2	23,5	31,8	S
8,0	12,6	19,6	24,1	S	19,1	25,0	28,9	S	14,7	22,9	31,8	S	15,2	24,0	33,8	S
8,5	12,6	19,7	24,1	-	19,1	25,3	29,2	S	14,1	23,5	33,1	S	15,2	24,2	35,6	-

TABELA 3 - Resultados nos ensaios com o binário

	TOPO			BASE	
	Teor de L-mentol (%m/m)	T_2 (ºC)	$T_c - T_f$ (ºC)	Teor de L-mentol (%m/m)	P (cal/min.)
M3	49,2	+ 5	25	73,6	70
M5	52,8	+ 8	26	81,2	47
M6	49,5	+ 5	29	95,0	143
M7	50,7	+ 6	30	92,3	145

TABELA 5 - Resultados nos ensaios com 1,8-cineol

	TOPO		BASE	
	Teor de 1,8-cineol (%m/m)	T_c (ºC)	Teor de 1,8-cineol (%m/m)	P (cal/min.)
C 18	63	- 18	99,9	85
C 21	63	- 18	98,7	25
C 23	80	- 9	99,3	68
C 24	82	- 8	99,5	60
C 17	61	- 20	96,8	6
C 20	63	- 18	98,7	24
C 22	63	- 15	98,7	24

fecimento depende a diferença então verificada, entre as temperaturas nos níveis de enriquecimento S8 e S2, indicador a ter em atenção no arranque da coluna.
Na segunda fase, o aquecimento na base funde os cristais e origina um refluxo líquido ascendente que eleva as temperaturas; esta inflexão é acentuada nos níveis S7 e S8 (tanto maior quanto mais elevado fôr o caudal de cristais), e muito atenuado em S2. Quando as temperaturas se apresentam constantes, a coluna está estabilizada e o arranque concluído, eventualmente prosseguido com operação a refluxo finito.
Estas duas fases, distinguíveis no diagrama temperatura-tempo (Fig. 10) são mais claras na Fig. 11 com os perfis de temperatura na coluna, em vários tempos de operação, para o ensaio M6 (em ordenadas os níveis da zona de enriquecimento e em abcissas temperaturas decrescentes para a direita). No início há crescente inclinação dos perfis: às 4 h de operação há já um abaixamento de 9ºC em 52 e apenas de 2,5ºC na base; no período 4-4,25 h a acumulação de cristais no fusor, obriga à aplicação de potência calorífica.

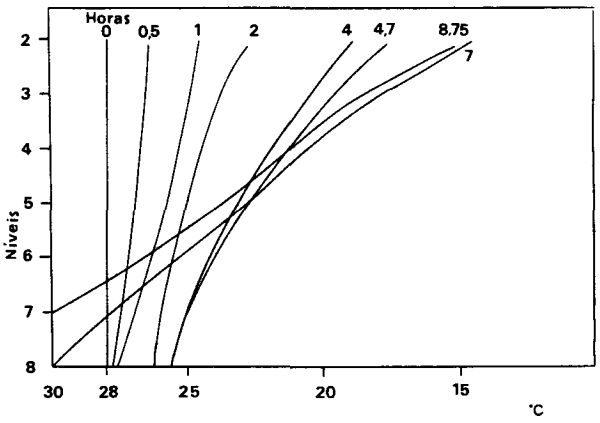

Fig.11 - Perfis de temperatura para o ensaio M6

Os perfis de temperatura da segunda fase cruzam os da primeira; a crescente potência de aquecimento aplicada no fusor, faz subir as temperaturas em S6, S7 e S8 (em especial para esta última ,subida de 8ºC). Por outro lado, em S5 e acima,a temperatura mantém-se relativamente constante; neste ensaio a temperatura em S2 desce mesmo 2ºC.
No ensaio M3, a 63 rpm, os primeiros cristais aparecem no fusor às 4 h de operação; no fim da 1ª fase (às 4,5 h) ΔT 8,2 foi de 9ºC. Na 2ª fase conseguiu-se apenas um aquecimento pequeno do fusor; verificou-se no final do ensaio sensível redução na quantidade de cristais presentes no fusor, atribuível ao facto de a temperatura do álcool ter sido mantida em -20ºC ao longo de todo o ensaio (noutros ensaios foi gradualmente diminuída até - 25ºC).
No ensaio M5, também a 63 rpm, os primeiros cristais surgiram no fusor rapidamente sem que tivesse havido arrefecimento pronunciado do cristalizador, (arrefecimento muito lento e com temperatura limite do álcool de apenas - 22ºC.) No final da 1ª fase (2,5 h) ΔT8-2 foi de apenas 5,3ºC. O caudal de cristais que atingiram o fusor foi pequeno, sendo a potência calorífica máxima de 47 cal/min. ΔT8 durante a 2ª fase foi assim de apenas 3,1ºC.
No ensaio M6 iniciado a uma velocidade de 60 rpm com uma estratégia de arrefecimento média (-24ºC às 4,2 horas) os cristais atingiram o fusor às 4,75 horas, sendo ΔT8-2 de 8,0ºC. Este fluxo de cristais permitiu a aplicação de uma potência calorífica pequena (26 cal/min); reduziu-se então a velocidade do rotor para 44 rpm, obtendo-se significativo acréscimo do número de cristais e tornando possível o aumento gradual da potência até 143 cal/min. Assim, no final da 2ª fase, depois de 9 horas de operação, ΔT8 atingiu os 8ºC.
No ensaio M7 utilizando a estratégia de arrefecimento e a alimentação do ensaio anterior, obteve-se uma velocidade de descida dos cristais sensivelmente maior, concluindo-se a 1ª fase da operação às 2,25 horas, sendo então ΔT8-2 relativamente pequeno, de 3,8ºC. Na 2ª fase do ensaio, devido a um abundante caudal de cristais, obteve-se um ΔT8 de 11ºC; a potência calorífica máxima aplicada foi de 145 cal/min.

Ensaios com óleo de eucalipto

As fracções enriquecidas de teor elevado em 1-8 cineol foram caracterizadas pela temperatura de congelação, de que facilmente se deduz aquele teor; algumas determinações (Tab. 5) foram confirmadas por cromatografia em fase gasosa ou pelo método de O-cresol (5).
As fracções esgotadas foram igualmente caracterizadas pelo O-cresol, pelo desvio polarimétrico e pela cromatografia em fase gasosa. A tentativa de caracterização por espectro I.V. revelou-se de difícil interpretação. Todos os métodos revelam a presença de α-pineno em teor elevado e de d-limoneno em teores médios (além de teores baixos de outros componentes); os teores indicados pela cromatografia acompanham o teor total de impurezas e o desvio Polarimétrico das fracções.
Os ensaios de separação a refluxo infinito permitiriam a obtenção de produtos de base de qualidade elevada, sobretudo para velocidades do rotor de 60 - 80 rpm; para os ensaios a refluxo finito, verificou-se que para alcançar a qualidade pretendida, a razão base-topo deve depender da alimentação; o caudal não influencia a riqueza até ao limite ensaiado (1,6 Kg/h, no ensaio C22).
A evolução do teor em cineol na base da coluna foi acompanhada em vários ensaios. Apresenta-se na Fig. 12 a evolução verificada para o ensaio C23 conduzido a refluxo infinito. Anota-se a rápida evolução de tal teor no período inicial de arranque de 1 hora, seguido de subida progressiva mas lenta ao longo das 10 h seguintes.
Do teor em 1-8 cineol nas fracções esgotadas depende o rendimento do processamento; tal teor depende da temperatura atingida no topo da coluna T_ℓ que em condições normais de funcionamento é igual à temperatura de congelação das fracções

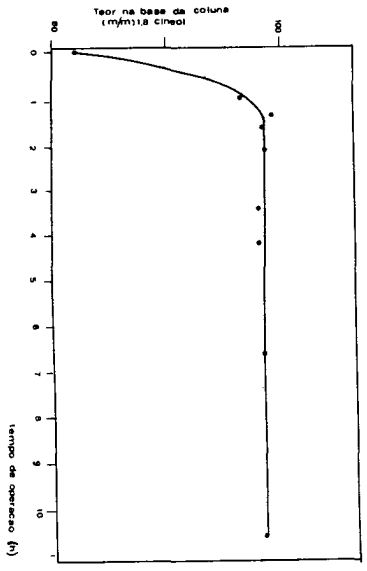

Fig. 12 - Evolução do teor de 1,8-cineol

esgotadas e depende de Tf, temperatura do fluído frigorífico. Dadas as limitações de equipamento disponível não foi possível ensaiar sistematicamente temperaturas muito diferenciadas no cristalizador.

Tamanho dos cristais e seu transporte

A utilização da CCC tem sido limitada pela dificuldade de assegurar o funcionamento regular e eficaz de colunas industriais e piloto.Para abordar os aspectos práticos da operação, em especial os que se relacionam com o transporte de cristais, analisam-se o tempo de descida dos cristais(duração da fase I definida atrás), a colagem da coluna e o fluxo máximo de cristais que atinge o fusor na fase II, correlacionando-os com o tamanho dos cristais.
Este é fortemente influenciado pela velocidade do rótor,aumentando quando esta diminui, o que a observação visual nos ensaios piloto comprova.
Esta influência deriva da dependência entre os tempos de residência e aquela velocidade - no cristalizador, o tempo médio de residência dos cristais é função de N, velocidade do rótor em rpm:(atendendo ao comprimento do cristalizador de 29,5 cm e ao passo do hélice de 2,5 cm)

$$t_r = \frac{29,5}{2,5} \cdot \frac{1}{N} = \frac{11,6}{N} \quad \text{(min.)}$$

Para N=100 rpm, o tempo de residência é de 7 seg. e os cristais são pequenos e portanto mais solúveis; para N=12 rpm o tempo sobe a cerca de 1 min., o que origina cristais maiores.
Nos ensaios piloto com L-mentol/dL-mentona apareceu clara relação entre a velocidade do rótor e o tempo de descida dos cristais (a diminuição de N reduz o tempo de descida), o que pode explicar -se por: as baixas velocidades de rotação, ao originarem cristais de grandes dimensões, favorecem o seu transporte para a base, apesar da diminuição da velocidade imprimida aos cristais pelo rótor.
Nos ensaios com o óleo de eucalipto os tempos foram tão baixos que não foi possível detectar uma influência deste género.
A colagem verificada na operação de equipamentos de cristalização é factor muito perturbador pela interrupção de funcionamento que impõe, pela atenção que exige do operador e pelo risco de avaria mecânica que introduz. Embora impossível de eliminar, pelo menos em equipamento piloto,há que procurar condições de operação que a minimizem.
Nos ensaios com o binário verificou-se colagem para velocidades do rótor elevadas; com valores médios não houve colagem.Nos ensaios com óleo de eucalipto não se verificou colagem da coluna.
A colagem explica-se pelo tamanho e hábito dos cristais formados:Para baixas velocidades do rótor os cristais têm bom tamanho e elevada transportabilidade, o que conjuntamente com a diminuição da capacidade do rótor, pode criar bloqueamentos.Para altas velocidades a pequena dimensão dos cristais, menores que a folga entre a parede e o rótor,pode explicar as colagens.
O fluxo máximo de cristais que atinge o fusor, na fase II do arranque das colunas de CCC, é outro factor importante na separação obtida.Este fluxo, que não pode ser medido, é avaliado visualmente e quantificado pela potência calorífica aplicada no fusor.
Nos ensaios realizados com o L-mentol/dL-mentona estabeleceu-se uma relação inversa entre o fluxo de cristais e a velocidade do rótor;em particular, no ensaio M6, depois de o fluxo de cristais ter estabilizado a 60 rpm, conseguiu-se a sua quase duplicação (avaliada pelo aument da potência calorífica), ao reduzir-se a velocidade do rótor para 44 rpm. Portanto, no processamento de sistemas com L-mentol,as elevadas velocidades do rótor não permitem fluxos abundantes,que se obtêm para velocidades reduzidas.
Pelo contrário,no processamento do óleo de eucalipto,o caudal máximo de cristais que atinge a base, em refluxo infinito, varia no mesmo sentido de N : o maior caudal foi obtido no ensaio C18, a 98 rpm; o menor, foi obtido no ensaio C21 , a 62 rpm. Esta diferença de comportamento dos dois sistemas ensaiados relaciona-se com a natureza dos cristais formados (tamanho, hábito,...).

Condução da coluna

Os ensaios realizados sugerem modos operatórios para melhorar a condução dacoluna e a separação obtida.Assim, como o teor da fracção descarregada do topo da coluna, depende da temperatura no cristalizador, quanto mais baixa for esta, mais esgotado é o produto de topo no constituinte de mais elevado P.F.. Esta temperatura no cristalizador é função da potência frigorífica aplicada ,pelo que poderia ser relacionada com a temperatura do álcool de arrefecimento; no entanto, factores difíceis de quantificar (como a colagem da coluna e a entrada de entalpia nela e nas tubagens) não permitem determinar com exactidão essa relação.
Para cada sistema, verificam-se diferenças aproximadamente constantes entre as temperaturas do cristalizador (considerada como temperatura liquidus)

e a temperatura na fonte fria. Assim,a temperatura do álcool de arrefecimento que deverá ser a mais baixa possível no fim da estabilização, será gradualmente diminuida, de modo a manter um fluxo de cristais constante, durante a estabilização. Esta requer fluxos de cristais regulares e tão elevados quanto possível; um tempo de estabilização curto exige, além da adiabaticidade da coluna, a rápida formação e descida dos cristais, só possível com um arrefecimento inicial intenso mas sem colagem do hélice.
De acordo com o diagrama de esl e para refluxo infinito, quando a temperatura no cristalizador se torna constante, o fluxo de cristais desaparece no cristalizador e posteriormente em toda a coluna , originando,no limite, uma coluna sem cristais mas cheia de um líquido onde existiria um qradiente axial de concentrações. Assim, deve procurar-se que o arrefecimento máximo no cristalizador, seja apenas atingido na estabilização da coluna - uma conclusão não óbvia, que não foi respeitada nos ensaios realizados.
A temperatura ambiente influencia a operação da coluna, porque dela dependem as trocas de entalpia com o exterior e a entalpia inicial do líquido que enche a coluna: quanto mais elevadas forem, mais difíceis serão a formação e descida dos cristais para o fusor. Este parâmetro é difícil de controlar em equipamento semi-piloto; sendo a temperatura de processamento próxima da ambiente, este efeito perde importância.

HÁBITO CRISTALINO E PROCESSABILIDADE

Os ensaios piloto realizados confirmam que certas misturas orgânicas não são facilmente processáveis por algumas técnicas que aliás têm sido aplicadas a um número restrito de sistemas; ensaios com outras misturas não deram resultados esperados ou apresentaram dificuldades "mecânicas" de processamento.

Processabilidade

Para analisar este problema , propõe-se e explora-se o conceito de processabilidade que depende muito significativamente do hábito cristalino, factor de que investigámos a influência no processamento por CCC.
Entedemos a processabilidade como o conjunto de características físico-químicas de um sistema de que depende a facilidade e a possibilidade do seu processamento por CCC, condicionando a escolha do equipamento de cristalização e a separação que nele pode ser obtida. É um conceito que integrando influências estudadas na literatura e conclusões induzidas pela experimentação piloto realizada neste trabalho, permite a sistematização de experiências, a normalização da recolha de informação e a previsão do comportamento de sistemas.
De acordo com esta formulação, a processabilidade de uma mistura orgânica depende simultaneamente da taxa de retenção e da transportabilidade, isto é, da possibilidade de promover o seu transporte dentro de uma coluna de cristalização.
A taxa de retenção influencia o grau de separação que é obtido num andar de equilíbrio; determina pois o número de andares requeridos para uma separação pretendida ou reciprocamente, a separação que pode ser obtida com um determinado equipamento. Por outro lado, a transportabilidade permite avaliar a capacidade de um certo equipamento para operar um sistema, determinando a escolha da técnica para a sua realização.
Assim a processabilidade de um sistema condiciona a escolha e o dimensionamento do equipamento de CCC capaz de fazer a separação pretendida permitindo sempre avaliar a capacidade do equipamento pré-definido para a sua execução .
A taxa de retenção e a transportabilidade dependem de características da solução (viscosidade,densidade, etc.) e dos cristais (hábito, tamanho, etc.). Analisaremos a influência das características mais significativas na transportabilidade, dado que a análise aprofundada da taxa de retenção, como condicionante da separação e como factor de processabilidade,ultrapassa o âmbito deste trabalho.
A transportabilidade de um sistema num determinado equipamento resulta de duas contribuições:
. do transporte de cristais na coluna, em contra-corrente com o líquido.
. de funções complementares indispensáveis à operação CCC (formação de cristais, promoção do contacto sólido-líquido, filtração para separação do líquido esgotado a fusão).
Para determinar a influência destas contribuições na transportabilidade e para deduzir a sua dependência de características básicas da solução e dos cristais, importa analisar o transporte da fase sólida nas colunas de CCC, tendo em atenção as diferentes técnicas e a sua realização.

Transportabilidade

Pode-se identificar três tipos de forças que promovem o transporte de cristais em colunas de CCC: gravidade, impacto forçado dos cristais e arrastamento pelo líquido.No primeiro caso, o transporte é provocado pela diferença entre as forças de gravidade e de impulsão, dado que os cristais estão imersos na solução.O impacto forçado dos cristais resulta da deslocação do leito cristalino,imposta por forças mecânicas através de hélice, parafuso ou êmbolo. O terceiro tipo de forças é a tensão de arrastamento que surge quando o transporte de sólidos é feito pelo líquido durante o movimento deste.
Para a técnica Schildknecht os cristais são fundamentalmente transportados por impacto forçado pelo hélice.
A transportabilidade resulta de contribuições do transporte de cristais e de funções complementares das colunas de CCC. O transporte não é definido por um indice único: é em relação a cada tipo de forças que se determina a influência no transporte de cristais das características do sistema, tanto as físicas (en particular a densidade relativa dos cristais e a viscosidade da solução) como as cristalinas.
Se uma mistura orgânica tem cristais e solução de densidades muito próximas, o balanço gravidade impulsão tem pequena influência no transporte dos cristais e a transportabilidade por gravidade é muito pequena, eventualmente nula.

Por outro lado o aumento de viscosidade no estado líquido reduz a transportabilidade por impacto forçado pois a pressão necessária para deslocar o leito cristalino, em contra-corrente com o líquido, aumenta com a viscosidade da solução. De facto, a deslocação do leito cristalino faz-se aplicando nos sólidos uma força que consiga vencer a perda de carga através do leito, do líquido que se desloca em contra-corrente. Aumentando a perda de carga, aumenta aquela pressão que vai assim comprimir ainda mais o leito, dificultando o fluxo de líquido. Como os sistemas são processados em zonas de temperatura em que usualmente a sua viscosidade é máxima , (próximo do ponto de congelação) , são assim facilmente atingidas , para misturas muito viscosas, elevadas forças de impacto o que põe problemas mecânicos (de transmissão de força, resistência de materiais, etc.) e de compactação excessiva dos cristais, levando o leito a colar.
A transportabilidade por gravidade surge também reduzida quando a solução tem uma viscosidade elevada. Se a driving force do movimento laminar dos cristais é apenas a diferença de densidades entre a fase sólida e a solução, a velocidade terminal das partículas, além de depender muito acentuadamente do diâmetro equivalente, varia inversamente com a viscosidade da solução.
O transporte de cristais por arrastamento não é afectado negativamente por características do sistema: a velocidade da partícula resulta da adição algébrica da velocidade do líquido e da velocidade de queda da partícula. Como esta é pequena em relação à primeira, o seu valor não afecta de maneira sensível a velocidade global dos cristais. No entanto, este transporte pode conduzir a transportabilidade reduzida pela eventual exigência de promoção de contacto sólido-líquido.
São ainda relevantes para a transportabilidade dos cristais o tamanho e o hábito cristalino, este último a justificar atenção especial, à frente.
As pequenas dimensões dos cristais (que no limite podem ser microscópicos) não favorecem qualquer tipo de transportabilidade. No transporte por gravidade e em regime laminar, a velocidade terminal é directamente proporcional ao quadrado do diâmetro equivalente da partícula: assim a velocidade de partículas muito pequenas é reduzidissima.
No transporte por impacto a dependência do tamanho dos cristais surge através da força necessária para deslocar o leito cristalino, que sendo proporcional à perda de carga no leito, depende do tamanho : ao diminuir este (avaliado pelo diâmetro médio equivalente) aumenta a força de deslocamento. Esta variação (equação de Karman-Kozeny) relaciona-a por um lado com o diâmetro da partícula e por outro com a porosidade do leito, portanto mais uma vez com aquele diâmetro.

Hábito cristalino

O hábito cristalino é factor determinante da transportabilidade por afectar a densidade da fase sólida, o diâmetro equivalente dos cristais e a porosidade dos leitos cristalinos.
O hábito cristalino é a forma externa do cristal determinada pelas velocidades de crescimento das suas faces; usualmente umas têm um crescimento mais rápido do que outras. Por exemplo, um arrefecimento brusco favorece o hábito cristalino acicular(crescimento acentuado numa direcção) que permite a rápida dissipação da entalpia de cristalização; origina-se assim um cristal alongado, frequentemente com crescimento dendrítico.
A influência do hábito na densidade da fase sólida evidencia-se para cristais com hábitos aciculares ou tabulares que, dada a sua tendência para formar aglomerados, retêm no seu interior solução-mãe , pelo que a densidade da fase sólida se afasta da do cristal, aproximando-se da da solução, o que reduz a transportabilidade por gravidade.
O hábito influencia também o diâmetro equivalente dos cristais: duas partículas com a mesma massa, para efeito de transporte em fluidos, têm diâmetros equivalentes muito diferentes se uma delas for muito alongada (acicular) e a outra tabular. Através desta influência são assim afectadas as transportabilidades por gravidade: as partículas mais alongadas, de menor diâmetro equivalente para a mesma massa média, são menos transportáveis.
O hábito influencia ainda a porosidade dos leitos cristalinos:partículas de hábito mais alongado para a mesma massa média originam leitos que têm maior perda de carga específica, dado o seu diâmetro equivalente mais pequeno.Assim é afectada a transportabilidade por impacto, que é diminuida para partículas alongadas.
O hábito cristalino é condicionado pelo arrefecimento e meio de crescimento ; pode por isso ser alterado pela adição de modificadores (solventes, compostos iónicos, etc.)e por mudança de condições de cristalização (agitação, temperatura, etc.). Assim se pode eventualmente favorecer a formação de cristais de hábitos mais adequados.
O hábito é ainda factor importante no comportamento dos cristais face às funções complementares indispensáveis à operação das colunas de CCC. Destas, a fusão não impõe limitações em nenhum equipamento; há que analisar as três restantes. A promoção do contacto sólido-líquido (apenas usada na técnica TNO , em que pratos de rede suportam bolas metálicas mantidas em vibração) impõe limitações à transportabilidade de sistemas que formem cristais ou aglomerados cristalinos de grandes dimensões e difíceis de partir ou desagregar.
A filtração da solução esgotada, requerida por várias técnicas, limita a transportabilidade de sistemas que originem elevada perda de carga através do leito cristalino e rede metálica de suporte, o que obriga a maior pressão de funcionamento da coluna e dificulta a alimentação, sobretudo se esta for parcial ou totalmente cristalizada. Como a perda de carga depende dos mesmos factores que afectam o transporte por impacto (viscosidade da solução, diâmetro das partículas, hábito cristalino), cria-se assim uma limitação a técnicas com transporte por gravidade ou arrastamento e descarga por filtração.
A formação de cristais afecta diferentemente as colunas de que o cristalizador é parte integrante e aquelas em que é uma peça de equipamento autónoma. Os graus de liberdade destas permitem adequado ajuste sem dificuldades. Para as primeiras há que procurar condições de funcionamento (em particular, velocidades de transporte e raspagem) simultaneamente adequadas à formação e ao transporte de cristais. Assim, sistemas com cristalização vítrea levantam dificuldades em ambos os

casos , mas mais acentuadas no segundo, por mais facilmente "colar" o cristalizador.

NOMENCLATURA

A = caudal de alimentação da coluna, cm^3/h
B = caudal retirado na base da coluna, cm^3/h
N = velocidade do rótor , rpm
P = potência calorífica média, aplicada no fusor, cal/min
T_f = temperatura média do álcool na fonte fria,ºC
T' = temperatura do líquido no cristalizador,ºC
T = caudal descarregado do topo da coluna,cm^3/h
$\Delta T_{8,2}$ = diferença de temperatura nos extremos da zona de enriquecimento,no fim da fase I,ºC
ΔT_8 = acréscimo de temperatura na S8 , durante a fase II,ºC

AGRADECIMENTOS

Ao INIC, Instituto Nacional de Investigação Científica, pelo apoio dado ao Centro de Processos Químicos das Universidades de Lisboa, em cuja Linha 1 - Processos de Separação, foi realizado este trabalho. Ao Eng. Barbosa de Sousa, pelas modificações na coluna piloto usada nos ensaios com o binário L-mentol/dL-mentona.

BIBLIOGRAFIA

1.Zief,M.;W.Wilcox - "Fractional Solidification ", vol.I, ed. Marcel Dekker, New York (1967).
2. Mullin,J.W. - " Crystallisation", 2ª ed. , Butterworths .
3. Guenther, E. - " The Essential Oils", vol.III, Van Nostrand Company, Princeton (1950).
4. Farelo, F. - Trabalho em publicação.
5. Gomes. A. - "Processos de Separação para Óleos Essenciais com recurso à Cristalização Contínua em Coluna", Tese de doutoramento (1973).
6. Wiyk, H.; W.Smit - " Impurity determination by Thermal Analysis"(I,II), Anal. Chim. Acta, 23 (1960) 545-551; Anal. Chim. Acta ,24 (1961),41-45 .

PROCESSOS DE SEPARAÇÃO COM CCC
- Análise e Rendimentos de Separação -

Aquiles C. Gomes (1)
M. Fátima Farelo (1)

(1)Centro de Processos Químicos das Universidades de Lisboa

RESUMO

O recurso à Cristalização Contínua em Coluna (CCC) como técnica de separação em processos químicos, levanta o problema do rendimento desta operação;para a sua análise propõem-se três definições diferentes de rendimento.
Esta metodologia de análise é depois aplicada por um lado, a um processo bem conhecido (o processo Phillips Petroleum de separação dos xilenos) e por outro a processos novos, propostos ou em desenvolvimento. Em particular,analisa-se para um esquema de separação do 1,8-cineol a partir do óleo de eucalipto, os rendimentos da operação de CCC e do processo integrado.

FUNDAMENTOS

A Cristalização Contínua em Coluna é uma técnica de separação de grande interesse e elevado potencial de aplicação, por razões que se detalharão seguidamente; no entanto a sua integração em processos químicos levanta alguns problemas complexos, decorrentes em particular do rendimento da operação. Uma análise destes processos pressupõe assim cuidadosa utilização das várias definições possíveis de rendimentos (como as que se propõem à frente).

A Cristalização Contínua em Coluna

A CCC é uma operação de separação ou purificação realizada através da transição sólido-líquido numa coluna alimentada com a solução que se pretende separar,ou com o produto que se pretende purificar. Num dos extremos da coluna - habitualmente o superior, nalguns casos numa peça exterior - origina-se, por arrefecimento,a formação de cristais que são transportados por qualquer meio adequado — parafuso, hélice , êmbolo ou pressão pulsante — até ao outro extremo. Neste provoca-se a fusão total dos cristais, obtendo-se assim uma corrente líquida que passa a circular no interior da coluna em contra-corrente com os cristais. Fazendo uma alimentação contínua,retira-se,também continuamente, num dos extremos parte da corrente que está a sofrer cristalização e no outro parte da corrente que resulta da fusão dos cristais.
A CCC pode funcionar segundo dois mecanismos bem diferenciados que estão relacionados com os dois tipos extremos de esl (equilíbrio sólido-líquido):
.Solubilidade sólida total,com formação de cristais mistos, (fig.1): o processo baseia-se essencialmente na operação de"rectificação" ou purificação por contracorrente, por analogia com o que se passa na destilação.De cada"andar" sai um sólido (cristais) e um líquido com composições diferentes daquelas com que entraram, porque ao atingir o equilíbrio o líquido sofre um enriquecimento no componente de maior ponto de fusão. Portanto,quando há solubilidade sólida total o mecanismo básico

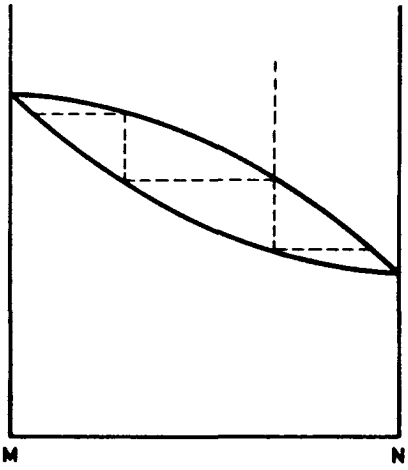

Fig. 1 - Diagrama de equilíbrio para sistemas com solubilidade sólida total

é o da recristalização, sem excluir a lavagem que, no entanto, é aqui um fenómeno secundário. Esta purificação só permitirá obter compostos puros se não existirem pontos de fusão congruente (equivalentes dos azeotropos na destilação), caso em que fica estabelecido o limite para a purificação máxima que se pode atingir.

. Solubilidade sólida nula, com formação de eutético, (fig. 2): a partir de uma solução contendo M e N que formam um eutético, e sendo o teor de M na solução superior à sua concentração no eutético, obtém-se por arrefecimento cristais de M (e apenas de M); os cristais de N só se formam ao ser atingido o eutético, mas em tais condições corre-se o risco de toda a solução cristalizar o que impediria o funcionamento da coluna.

Estes cristais de M, formados num extremo, contêm solução aderente, rica em N ; ao circularem em contracorrente com uma solução que é mais rica em M vai-se dando a "lavagem" dos cristais. A fase sólida, cristais e líquidos aderente e ocluido, que chega ao outro extremo da coluna, onde vai ser fundida, é por isso muito mais pura; o mecanismo da purificação é basicamente por lavagem dos cristais. O rendimento da operação é condicionado pelo teor em M no eutético, que não é possível ultrapassar na coluna; portanto,a corrente de " impurezas" que sai da coluna tem uma concentração em M superior à do eutético.

Processos com CCC

A integração da CCC em processos de separação levanta assim um problema importante: a partir de uma alimentação que constitua um eutético(o que é o caso mais corrente de aplicação), só é possível separar um dos componentes (seja M); a corrente esgotada é, no limite, o eutético que contém, portanto, um teor apreciável - eventualmente elevado - de M. A menos que seja muito baixo o valor deste composto ou que haja utilização directa para a corrente esgotada, há que a submeter a uma operação que a enriqueça em M, tornando possível o seu reprocessamento por CCC; esta segunda operação será provavelmente uma destilação, mas pode ser uma extracção ou qualquer outra operação de separação (fig.3). Para que o processo seja viável economicamente é necessária esta operação, mas a obtenção de M em determinado grau de pureza não depende dela, que apenas assegura a separação do segundo componente, N. Depende das aplicações de N o grau de pureza que lhe é exigido e portanto a separação imposta a tal operação; para o processo de purificação de M exige-se apenas que a corrente não reciclada obtida nesta operação contenha uma quantidade de M suficientemente baixa para permitir um determinado rendimento. Por exemplo, um teor de 95% em N (5% em M), facilmente atigido em muitos casos, assegura um rendimento elevado do processo,

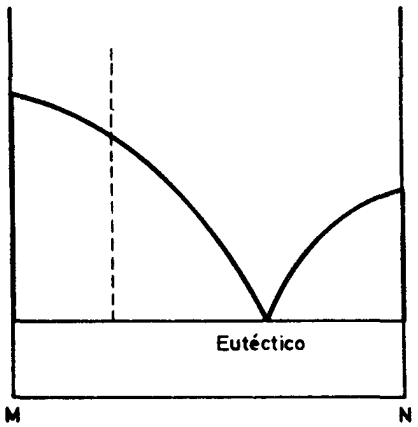

Fig.2 - Diagrama de equilíbrio para sistemas com solubilidade sólida nula

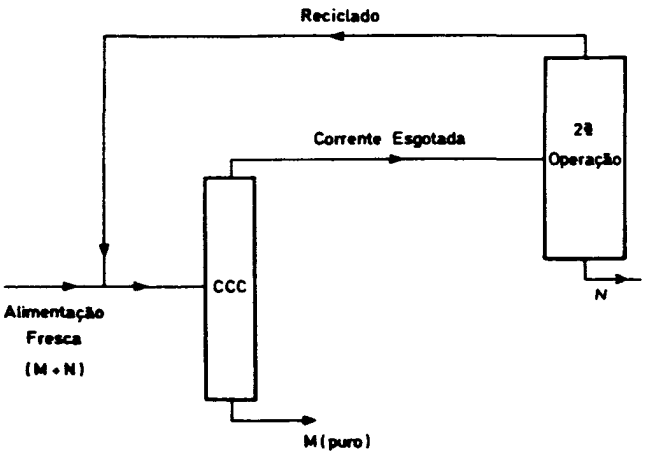

Fig.3 - Esquema geral de um processo de separação com CCC

já que a quantidade de M perdida será apenas de 5,3% da quantidade de N entrada na alimentação fresca ao processo (o rendimento depende, pois, do teor desta).

A segunda operação poderia ser dispensada se o teor do eutético em M for muito baixo e fazendo a operação da coluna de modo a obter uma corrente esgotada com teor próximo do eutético. Mas para que seja muito baixo aquele teor é necessário que o ponto de fusão de N seja muito inferior ao de M, e a temperatura no cristalizador, próxima da do eutético, seria muito afastada da temperatura do fusor (praticamente igual à temperatura de fusão de M). Ora a operação de colunas de cristalização com gradientes de temperatura elevados, de muitas dezenas de graus centígrados, levanta problemas delicados, frequentemente impeditivos de funcionamento regular, devidos a elevado fluxo longitudinal de energia calorífica.

Sendo a alimentação fresca pobre em M, é preferível, dadas as características da CCC, fazer a separação do composto M a partir de uma corrente relativamente rica, deixando à 2ª. operação o enriquecimento da alimentação (fig.4).

A 2ª. operação não seria necessária no processamento de sistemas formando soluções sólidas sem composto; como os sistemas complexos deste tipo, são raros, é reduzido o interesse prático da análise dos processos aplicáveis a tais casos, que não são aqui abordados.

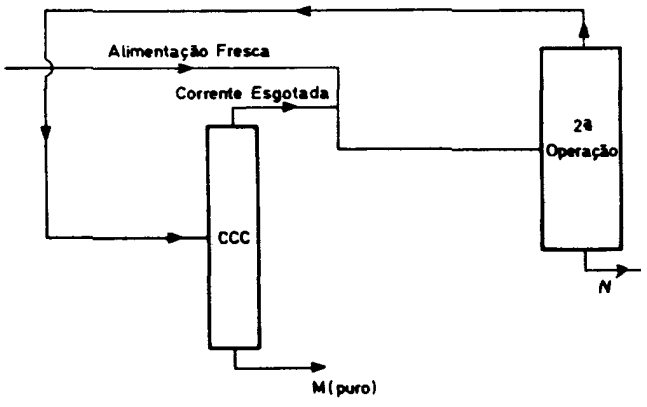

Fig. 4 - Esquema geral de um processo de separação com CCC (alimentação pobre em M)

Rendimento

Sendo o rendimento o problema básico da separação por CCC, é importante defini-lo de modo inequívoco. Para os rendimentos por passe é possível distinguir:

- rendimento aparente: em fracção é a relação entre os caudais mássicos do produto purificado (corrente de base) e a da alimentação à unidade

$$Z_a = \frac{q_b}{q_a} = 1 - \frac{q_t}{q_a}$$

ou, em percentagem,

$$Z_a(\%) = 100 \cdot \frac{q_b}{q_a} \quad ;$$

- rendimento industrial. relação entre os caudais mássicos do produto purificado e o do composto M alimentado à unidade

$$Z_i = 100 \cdot \frac{q_b}{x_a \cdot q_a}$$

$$Z_i(\%) = 10^4 \cdot \frac{q_b}{x_a \cdot q_a} \quad ;$$

- rendimento real: relação entre os caudais mássicos de M no produto purificado e na alimentação

$$Z_r = \frac{x_b \cdot q_b}{x_a \cdot q_a}$$

$$Z_r(\%) = 100 \cdot \frac{x_b \cdot q_b}{x_a \cdot q_a}$$

O conceito de rendimento aparente é muito limitado, embora seja comum a sua utilização no controle fabril de processos de separação; o rendimento industrial já tem em atenção a riqueza da alimentação e é perfeitamente aceitável na condução de unidades industriais, mas tem a limitação de poder ser superior a 100 %. O conceito mais adequado à análise e desenvolvimento de processos é o rendimento real, que difere pouco do rendimento industrial se o produto obtido for puro:

$$Z_r = Z_i \cdot \frac{x_b}{100}$$

Os mesmos rendimentos são usados para a análise global do processo, substituindo na definição a alimentação à unidade pela alimentação fresca do processo (habitualmente muito diferentes); distingue-se assim o rendimento final, do processo, e o rendimento por passe,da operação.

SEPARAÇÃO DOS XILENOS

A separação dos xilenos isómeros é um dos mais difíceis processos de separação realizado em grande escala. Assim este problema tem motivado inúmeras investigações, contribuindo para o desenvolvimento de novas operações e conduzindo à realização em escala industrial de processos inovados. Por isso serve também habitualmente de padrão na avaliação e análise de técnicas de separação.
A CCC foi uma das operações cujo desenvolvimento foi grandemente impulsionado por esta separação;em particular uma das suas técnicas, criada nos laboratórios da companhia norte-americana Phillips Petroleum, foi especificamente desenvolvida e encontrou realização industrial para esta finalidade.

Os xilenos

Os xilenos utilizados industrialmente são, na quase totalidade, de origem petrolífera e obtidos pela extracção por solventes sobre a saída de uma unidade de " reforming" catalítico; dispõe-se assim, de uma corrente que contém basicamente m-xileno (35 -40 %), o-xileno (19-26 %), p-xileno (16-20 %), e etilbenzeno (17-20 %), além de 2 a 4% de tolueno e outros aromáticos.
Dos xilenos produzidos anualmente (milhões de toneladas) menos de um terço é empregue tal qual, como solventes, aditivos de gasolina, etc.; servem sobretudo como intermediários na produção de outros compostos:
- o p-xileno é usado no fabrico de fibras poliester, que exige uma pureza de 99%;
- o o-xileno é usado no fabrico de anidrido ftálico, que exige uma pureza de 95% ;
- o etilbenzeno é convertido em estireno;
- o m-xileno, com menor procura, permite o fabrico do ácido isoftálico, que exige uma pureza de 98,5% ou a produção por isomerização de p-xileno.
Os pontos de ebulição e de fusão e as volatilidades relativas destes compostos são dados na Tabela 1 : obviamente é facil a separação por destilação do o-xileno de qualquer dos outros compostos, podendo -se obter o-xileno a 98% com colunas de 100 a 150 pratos. A separação do etilbenzeno por destilação levanta dificuldades consideráveis porque a volatilidade relativa etilbenzeno/p-xileno é muito baixa e para obter etilbenzeno a 99% são necessárias colunas de 300 a 400 pratos operadas a uma razão de refluxo de 25/1 a 50/1. A separação p-xileno/m-xileno por destilação é realizável mas economicamente inviável: a produção de p-xileno a 99% exigiria colunas de 800 pratos, operadas a razões de refluxo de 50/1 e 100/1.Aquela separação p-xileno/m-xileno exige o recurso

TABELA 1

Características dos xilenos

Composto	P. ebulição (ºC)		Volatilidade em relação a						Ponto de fusão (ºC)
			o-xileno		m-xileno		p-xileno		
	100 torr	760 torr	100 torr	760 torr	100 torr	760 torr	100 torr	760 torr	
o-xileno	100,2	144,4	-	-	-	-	-	-	- 25,2
m-xileno	76,8	139,1	1,94	1,14	-	-	-	-	- 47,9
p-xileno	75,9	138,3	1,99	1,16	1,027	1,020	-	-	+ 13,3
etilbenzeno	74,1	136,2	2,15	1,20	1,083	1,075	1,054	1,054	- 94,9

* Supostas perfeitas as soluções - os desvios são inferiores a 0,3% (1).

a técnicas de cristalização ou de absorção; as primeiras são possíveis porque, além da diferença notável de pontos de fusão, o p-xileno e o m-xileno formam um eutético com 14% de p-xileno à temperatura de -57ºC (2). A cristalização pode ser realizada por três vias distintas: a clássica (com separação do líquido esgotado por filtração ou centrifugação), a cristalização"ajudada" (extractiva, adutiva ou com clatratos) e a cristalização em coluna - esta última via desenvolvida pela Phillips-Petroleum, que para tal concebeu uma técnica específica de CCC.

A técnica Phillips-Petroleum

Esta técnica de CCC foi desenvolvida no período 1950- 1964, vindo a ser a primeira a atingir a escala industrial (há bastantes anos, em dimensões significativas e com resultados interessantes). A versão final resultou de muitas tentativas, iniciadas por colunas com transporte mecânico, até ao equipamento pulsante (3,4), característico desta técnica. O transporte de cristais por pulsação foi inicialmente conseguido pela exclusiva utilização do êmbolo que ao descer impele a alimentação, interrompida durante esse período, por ser também forçada por êmbolo com movimento alternativo, e força a descida do conteúdo da coluna; durante a subida retoma-se a alimentação. Como o êmbolo põe um problema difícil de comando mecânico dada a elevada pressão, de 15 a 60 kg/cm^2 (4), que nestas condições é necessário transmitir à massa de cristais, depois de terem sido realizadas algumas unidades industriais deste tipo, passou-se a aplicar uma pressão pulsante na tubagem de descarga do produto purificado para deslocar os cristais na coluna e a utilizar um parafuso para a alimentação da suspensão dos cristais à coluna. Foi assim possível construir unidades com diâmetros até 70 cm.

Na última versão desta coluna (fig.5) a alimentação é uma papa de cristais que um filtro separa da solução -mãe, já esgotada no composto de mais alto ponto de fusão. Os cristais movem-se por acção de uma pressão pulsante aplicada na base da coluna (frequência de 90 a 350 ciclos/min),(5) e formam um leito compacto por acção de um pistão com movimento alternativo. A potência calorífica aplicada na base funde os cristais mais próximos desta; parte do líquido assim obtido é o produto final e o

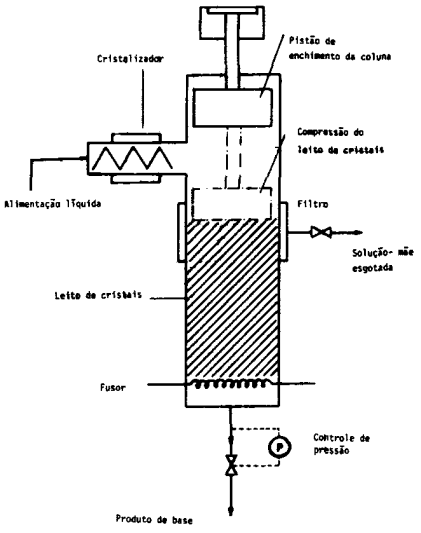

Fig. 5 - Equipamento Phillips Petroleum para CCC

restante constitui o refluxo. Este, forçado a ascender através do leito compacto por um gradiente de pressão, contribui para a purificação promovendo simultaneamente uma lavagem e uma recristalização (o líquido em contacto com um sólido a temperatura inferior congela parcialmente; a correspondente entalpia de transição provoca a fusão dos cristais de menor pureza e o deslocamento do líquido ocluído).

O processo Phillips Petroleum

A integração da técnica descrita no esquema de separação dos xilenos, faz-se com o processo Phillips Petroleum (fig.6); das quatro colunas de destilação fraccionada, três permitem a obtenção do o-xileno, m-xileno e etilbenzeno; o p-xileno é obtido na CCC.

Para a análise do processo e cálculo dos rendimentos estabeleceu-se o balanço de massas(Tab. 2).Assim a unidade de CCC é alimentada com a corrente 7, com um teor em p-xileno de 70%, e dela saiem o p-xileno a 98,5% e a corrente esgotada, com apenas 35,0% de p-xileno; o teor relativamente baixo em p-xileno nesta corrente é conseguido graças a uma temperatura no topo da coluna de cristalização de -25ºC, inferior em cerca de 40 ºC à temperatura no fusor. Os rendimentos por passe da operação são:

- rendimento aparente - Z_a = 53%
- rendimento industrial - Z_i = 76%
- rendimento real - Z_r = 75%

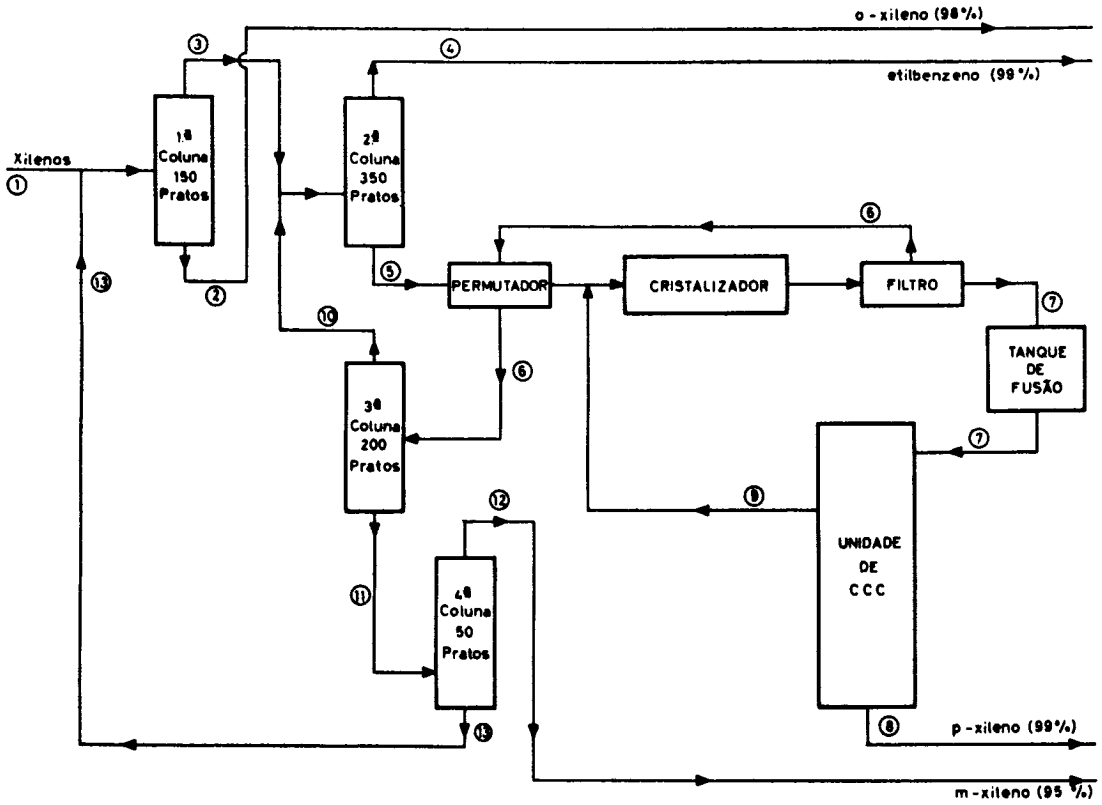

Fig.6 - Processo Phillips Petroleum para separação de xilenos

Uma operação prévia de cristalização clássica permite obter aquela alimentação de CCC a partir de uma corrente que contém 33% de p-xileno; com temperaturas de operação muito baixas, a fracção esgotada desta operação (corrente 6) tem apenas 13,5% de p-xileno, praticamente igual ao eutético. A fracção esgotada da coluna de CCC (corrente 9) é reciclada para esta operação; os rendimentos globais desta "secção de cristalização" do processo (cristalizador +unidade de CCC) são:

- rendimento aparente - Z_a = 23%
- rendimento industrial - Z_i = 70%
- rendimento real - Z_r = 69%

Ao considerar uma alimentação diferente, varia o rendimento aparente, sem que seja possível dar

TABELA 2

Balanço de massas no processo Phillips Petroleum (6)

Correntes	nº	1	5	6	7	8	9
	identificação	Alimentação do Processo	Alimentação da secção Cristalização	Reciclado da secção Cristalização	Alimentação da CCC	p-xileno	Reciclado da CCC
MASSA TOTAL		100	80,5	61,8	35,2	18,7	16,5
(kg)	etilbenzeno	25,0	1,6	1,6	0,3	-	0,3
	p-xileno	20,0	26,8	8,4	24,6	18,4	5,8
	m-xileno	35,0	50,2	49,9	9,9	0,3	9,6
	o-xileno	20,0	1,9	1,9	0,4	-	0,4
Composição (% m/m)	etilbenzeno	25,0	2,0	2,6	0,9	-	2,2
	p-xileno	20,0	33,2	13,5	70,0	98,5	35,0
	m-xileno	35,0	62,4	80,8	28,8	1,5	60,1
	o-xileno	20,0	2,4	3,1	1,1	-	2,7

significado a tal variação; são mais significativas as variações dos rendimentos industrial e real.
Os rendimentos por passe da primeira operação de cristalização (alimentação = corrente 5 + corrente 9) são :

- rendimento aparente - Z_a = 36%
- rendimento industrial - Z_i = 124%
- rendimento real - Z_r = 87%

o que evidencia o inconveniente do rendimento industrial que pode exceder 100%, se a corrente final for impura.
Portanto, apenas o rendimento real permite a análise de processos de cristalização; para o processo Phillips Petroleum o rendimento final em p-xileno é de

- rendimento real Z_r = 92%

conseguido graças a reciclagem para anteriores operações das sucessivas correntes esgotadas obtidas.

SEPARAÇÃO DO 1,8-CINEOL

Os conceitos para a análise de processos com CCC, definidos e aplicados atrás, foram desenvolvidos para análise da separação do 1,8-cineol a partir do óleo de eucalipto. Na sequência de ensaios em que esta separação foi investigada com equipamento piloto tipo Schildknecht (7,8), foi estabelecido um esquema prévio para a realização industrial deste processamento (7,9), que aqui se analisa detalhadamente recorrendo aqueles conceitos.

A técnica Schildknecht

Esta técnica de CCC, concebida em 1961 por Schildknecht (10), foi inicialmente usada como técnica laboratorial de purificação de compostos orgânicos.No entanto, despertou grande interesse e a partir de 1963 sucederam-se os estudos e publicações sobre a sua transposição à escala industrial, realizados em particular na Grã-Bretanha. Apesar destes esforços, esta técnica não ultrapassou a escala semi-industrial com colunas de 10 cm de diâmetro, pois surgem grandes dificuldades na operação de colunas de 20 a 25 cm .
Esta técnica tem transporte mecânico de cristais, conseguido por hélice que se move no espaço delimi-

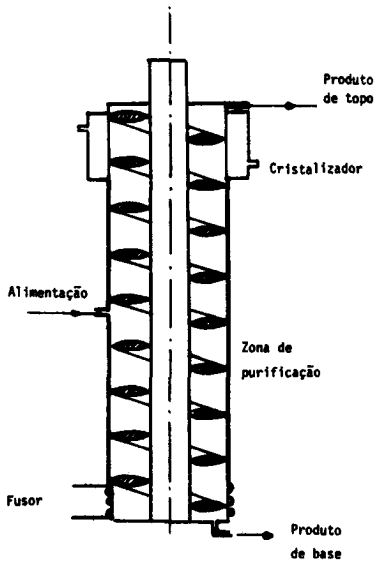

Fig.7 - Equipamento tipo Schildknecht

do por dois cilindros. No processamento de produtos com cristais mais densos que o líquido, há um cristalizador, colocado no topo da coluna (fig. 7),onde se formam cristais que a gravidade e o movimento de rotação do hélice fazem descer em contra-corrente com o líquido livre. Este é obtido,num fusor colocado na base da coluna, a partir dos cristais, sendo parte retirado como produto de base e constituindo o restante o refluxo que contribui para a purificação dos cristais que descem ao longo da coluna. O líquido livre que sobe até ao cristalizador congela parcialmente ao ser arrefecido; os cristais formados são arrastados para baixo pela hélice;do líquido que resta por cristalizar, empobrecido no composto a isolar, parte significativa deve ser descarregada, constituindo o produto de topo.
As dificuldades de scale-up deste equipamento resultam de:

- o transporte de cristais deve ser capaz de assegurar caudais o mais elevados possível, mas garantindo um contacto efectivo entre a massa cristalina e o líquido livre e impedindo a aglomeração daquela;

- a congelação no cristalizador deve impedir a aglomeração de cristais, o que ocluiria líquido fortemente impurificado e que poderia bloquear o transporte dos cristais;

- a transmissão de energia calorífica para o fusor deve assegurar a fusão total dos cristais, mas não

pode afectar o regime térmico da coluna - apenas os cristais que atingiram o fusor devem ser fundidos e o líquido deve ficar à sua temperatura de congelação.

Ensaios piloto

Foi com equipamento piloto Schildknecht de 1" e 2" de diâmetro que se realizaram os ensaios piloto de separação do 1,8-cineol do óleo de eucalipto, detalhadamente apresentados em (6,7). Anotam-se aqui as principais conclusões sobre os equilíbrios estudados, os ensaios realizados e sobre a própria operação de CCC, que suportam o processo proposto.
Sobre o esl do sistema estudado concluiu-se que:

- Os sistemas 1,8-cineol/α-pineno e 1,8-cineol/ d-limoneno formam eutéticos; o sistema α-pineno / limoneno tem solubilidade sólida total, com formação de composto;

- para o sistema 1,8-cineol/α-pineno/ d-limoneno há um campo eutético do cineol que cobre cerca de 80% do diagrama;

- não se apurou a influência neste sistema ternário do pinocarveol, que pode surgir em teores significativos na alimentação à coluna de CCC.

Dos ensaios piloto concluiu-se que:

- o 1,8-cineol a 99% pode ser separado do óleo de eucalipto rectificado por CCC, em colunas de 1 e 2" tanto a refluxo infinito como finito;

- o tempo de estabilização mínimo a refluxo infinito foi de 60 minutos; a velocidade óptima do rotor foi de 100 rpm para a coluna de 1" e de 70 rpm para a de 2" ;

- o controle da unidade de 2" foi mais fácil que o da unidade de 1";

-dentro dos limites de caudal ensaiado melhoraram-se as condições de operação e a pureza do produto ao elevar o caudal;não se apurou quaquer influência da razão base/topo sobre a pureza;

- a temperatura no cristalizador acompanhou a temperatura do fluido frigorífico (diferença de cerca de 12 ºC), excepto com alimentação muito rica;

- o ponto de congelação dá uma indicação válida do teor em cineol para a corrente enriquecida; para a corrente esgotada indicação idêntica é dada pelo desvio polarimétrico;

- a determinação do cineol por cromatografia em fase gasosa e pelo o-cresol,dão indicações úteis sobre os ensaios; a espectrofotometria IR e as propriedades físicas têm interesse reduzido.

Sobre a operação de CCC pode concluir-se que:

-a razão de refluxo não pode ser calculada apenas a partir do balanço energético da coluna; pode ser obtida pela medida dos caudais na base da coluna;

- a taxa de retenção de líquido aderente aos cristais pode ser avaliada através das temperaturas na base da coluna;

- a contribuição da recongelação para a purificação em colunas de CCC operando com eutéticos pode ser avaliada em condições determinadas de razão de refluxo e de razão base/topo.

Rendimento da operação

A análise seguinte da operação de CCC para a produção de eucaliptol toma em consideração o teor em 1,8-cineol da alimentação (X, expresso em % m/m) , a razão base/topo (R, para os caudais em massa) e a temperatura no cristalizador (T,em ºC); determina-se o rendimento real por passe (Z_r, em %).Não se consideram as variáveis de comando da operação (refluxo, estado e temperatura da alimentação, velocidade do rótor); não é explicitado o caudal da alimentação que serve de base aos cálculos realizados.
A temperatura no cristalizador T, imposta pela circulação do fluido frigorífico, determina o teor em 1,8-cineol da corrente esgotada Y, através do esl do sistema. Aqui adopta-se uma relação Y(T) que supõe na alimentação uma razão constante entre os teores de α-pineno e d-limoneno; esta relação traduz analiticamente a fig. 8 que resulta de um corte no diagrama ternário passando pelo vértice e pelo ponto 86 -10 -4 (7,8).
Numa primeira aproximação determina-se em computador, por um programa de cálculo simples, os valores máximos de R que, para determinados X e T, permitem processualmente obter um produto a 100% (na realização industrial é tecnicamente viável atin-

gir os 99,5% mas não é economicamente interessante ultrapassar os 99%, o que dá uma pequena margem de segurança ao cálculo). Os resultados são apresentados na fig.9 : só à esquerda de cada curva a combinação dos factores indicados dá a possibilidade de atingir a pureza pretendida. (Exemplo: a operação com R=4 a T= -30ºC só dá o produto especificado se na alimentação X⩾91%). Quanto mais baixo for X, menor será R e mais baixa a temperatura T; Ora, baixos valores de R implicam baixos rendimentos, baixos caudais de produto e dificuldades de operação da coluna; valores fortemente negativos de T são tecnicamente difíceis e economicamente inviáveis (a temperatura do fluido frigorífico no cristalizador terá de ser de 10 a 15 ºC inferior a T). Assim a operação só parece viável para X= 80% (com T ⩽ -30ºC e R⩽1,1), ou de preferência para X= 90 % (o que permitiria a operação para T⩽-10 ºC e R⩽1, ou para T⩽-30ºC e R⩽4).

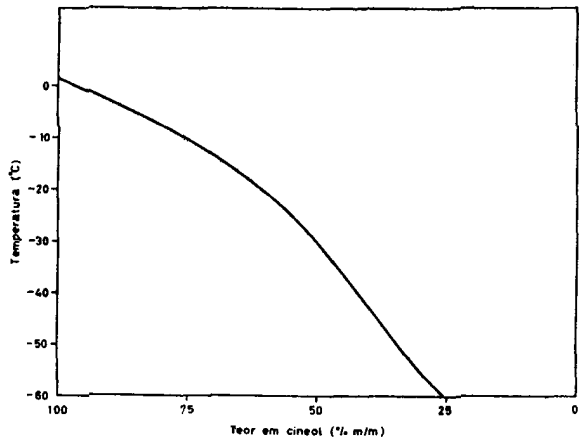

Fig. 8 - Teor em 1,8-cineol vs. temperatura no topo

Através de outro programa de cálculo,igualmente explorado em computador, foi possível estabelecer " campos de operação", em que a combinação das variáveis analisadas e do rendimento pretendido permitem a obtenção do produto especificado. Dos vários " campos" estudados o mais interessante e de utilização mais simples é apresentado na fig. 10 . Por exemplo, só se garante $Z_r \geqslant 70\%$ à direita da curva assinalada (Z_r= 70%); por outro lado só à esquerda da curva X= 80% se garante a qualidade do produto,com esta alimentação. Para X= 80% são possíveis as seguintes combinações:

T= - 28ºC ; R= 1,1 ; Z_r = 70%

T= - 57ºC ; R= 2,5 ; Z_r = 90%

(além de muitas outras intermédias). O "campo de operação" possível para X⩽80% e $Z_r \geqslant 70\%$ é o campo inferior delimitado pelas duas curvas, de que o extremo superior é a primeira daquelas combinações.

Para $Z_r \geqslant 90\%$ uma combinação possível, além da já assinalada (X= 80%, R= 2,5 , T= -57 ºC) é:

T= - 35ºC ; R= 4,2 ; X= 90% .

(Seria difícil garantir no cristalizador a temperatura de -57 ºC que exigiria uma temperatura do fluido frigorífico inferior a -70ºC).

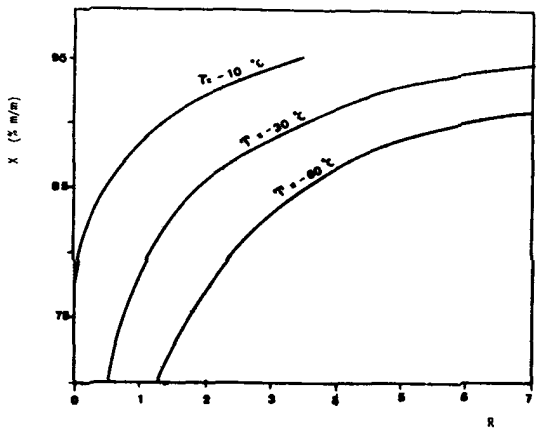

Fig.9- Valores máximos de R para a pureza de 100% em função de X e de T

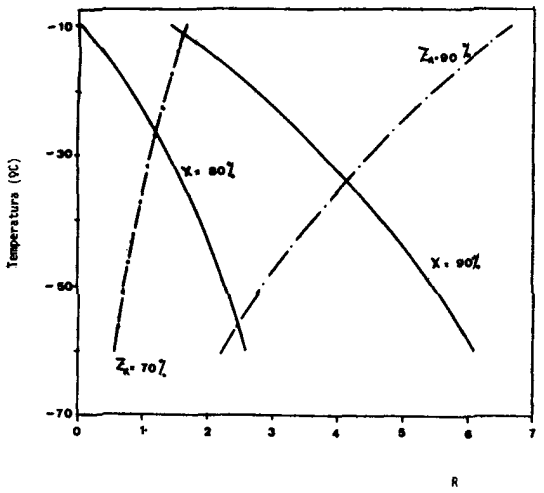

Fig.10 -Valores limites de R para a pureza de 100% em função de T, X e Z_r

É pois difícil compatibilizar um teor médio de alimentação com temperaturas não muito baixas e com rendimentos razoáveis nesta única operação de CCC, e daí o interesse do processo integrado em que a reciclagem para outra operação de separação da corrente esgotada permite valores elevados do rendimento com temperaturas no cristalizador técnica e economicamente viáveis.

Análise do processo integrado

Um processo integrado de produção de eucaliptol deve incluir pelo menos uma rectificação, além da CCC; há no entanto razões para optar por um processo com duas rectificações descontínuas (fig.11), já proposto em anteriores trabalhos (7,9).
A análise deste processo,feita por cálculo manual dada a dificuldade de modelar as complexas rectificações descontínuas, partiu de modelos heurísticos para estas operações e estabeleceu balanços de massa para diferentes valores de R , suposta a única variável de actuação sobre a CCC (7,9).Nesta análise consideraram-se nulas as correntes 52 e 81 (saídas para a composição de óleos rectificados). Estas hipóteses restringem o campo de operação que poderia ser encarado a priori , mas não excluem a zona mais interessante para a potencial exploração industrial ou para o estudo da influência da reciclagem no rendimento do processo.
Dos valores calculados, são apresentados na Tab.3 os que respeitam ao balanço da CCC; para a sua interpretação estabeleceu-se a Tab.4, que demonstra ser o rendimento final,em larga medida , independente de R.: um reduzido rendimento por passe,originado por um R baixo, é compensado por uma razão de reciclagem elevada. Claro que R baixo e elevada razão de reciclagem fazem aumentar as dimensões do equipamento, aumentando o investimento, mas permitem temperaturas no cristalizador mais elevadas ,o que diminue o custo do arrefecimento.
O processo revela-se viável numa gama larga de valores de R com elevados rendimentos finais; a escolha da zona óptima de operação e o projecto do equipamento implica análise económica pelo balanço custos directos / custos indirectos. Tal zona deve cair dentro dos limites ensaiados, já que razões de reciclagem superiores a 0,6 ou temperaturas efectivas no cristalizador inferiores a - 35ºC parecem a priori pouco interessantes; é provável que o óptimo técnico-económico caia na gama $1,5 \leq R \leq 2,0$ para a qual as temperaturas

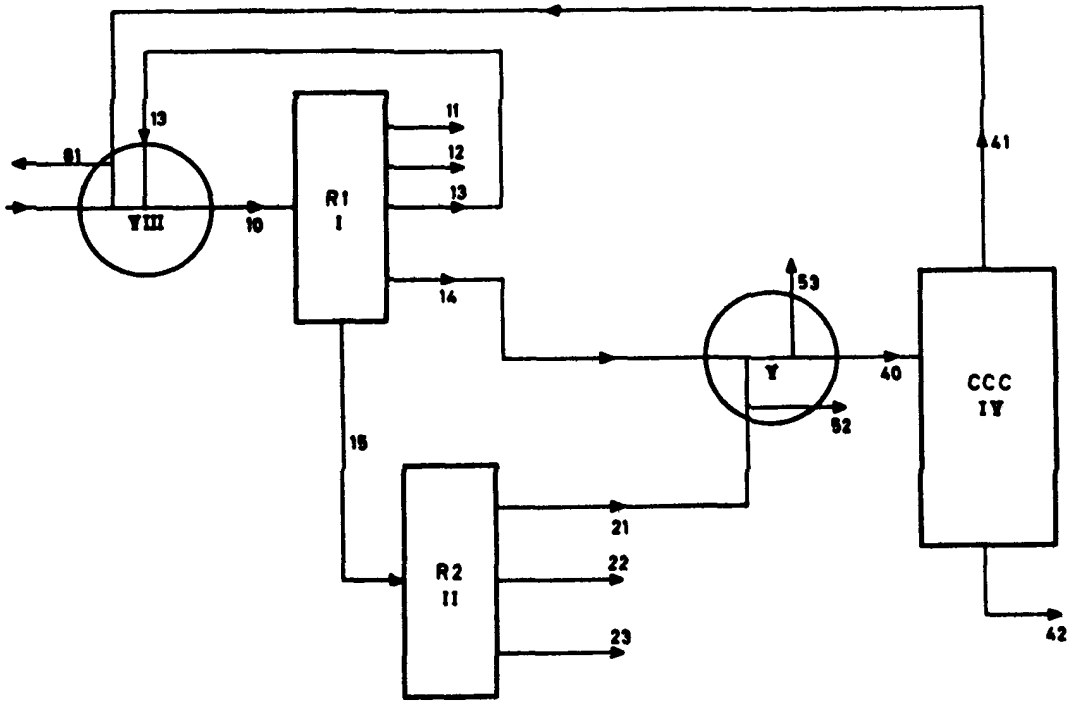

Fig. 11 - Processo integrado de produção de eucaliptol

TABELA 3

Balanço de massa sobre a CCC no processo integrado

R	Componentes	Corrente		
		40	41	42
1,0	TOTAL	124,1	60,7	63,4
	. terpenos	15,8	15,2	0,6
	. cineol	106,3	43,5	62,8
	. pinocarveol	2,1	2,1	-
1,5	TOTAL	105,3	42,1	63,2
	. terpenos	13,4	12,8	0,6
	. cineol	90,1	27,5	62,6
	. pinocarveol	1,8	1,8	-
2,0	TOTAL	95,8	32,0	63,8
	. terpenos	12,1	11,5	0,6
	. cineol	82,0	18,8	63,2
	. pinocarveol	1,7	1,7	-
2,5	TOTAL	85,3	21,3	64,0
	. terpenos	10,7	10,1	0,6
	. cineol	72,9	9,5	63,4
	. pinocarveol	1,7	1,7	-

. Todos os valores em Kg

. Base: 100 Kg de alimentação fresca contendo 65 Kg de 1,8-cineol, 20 Kg de terpenos (∝- pineno e d-limoneno), 6 Kg de pinocarveol, 4 Kg de compostos voláteis e 6 Kg de "outros" compostos (menos voláteis que o pinocarveol).

TABELA 4

Análise do processo integrado

	Teor de cineol (% m/m)			Rendimento real (%)		Razão de reciclagem	Temperatura no cristalizador(°C)
	10	40	41	por passe	final		
R = 1,0	67,4	85,6	71,7	59,1	96,7	0,61	-14
R = 1,5	64,7	85,6	64,9	69,6	96,4	0,48	-19
R = 2,0	63,3	85,6	58,8	77,1	97,2	0,42	-24
R = 3,0	61,4	85,4	44,7	86,9	97,5	0,35	-35

no cristalizador podem ser obtidas com unidades frigoríficas de um único andar e sem recurso a refrigerantes especiais.

CONCLUSÕES

O trabalho anterior permite concluir que os processos de separação com CCC são viáveis para a separação de um componente dominante em misturas complexas quando houver um campo eutético extenso que permita o esgotamento da corrente de topo. Nesta operação o rendimento por passe é limitado pela temperatura no cristalizador e pela extensão do campo eutético.

As determinações de esl para o ou os principais sistemas que a mistura complexa inclui são indispensáveis; é muito útil traduzir tais equilíbrios por correlações analíticas que permitem uma simulação do processo e a análise dos resultados da experimentação piloto. A experimentação piloto pode ser realizada em colunas de 2", devendo a unidade piloto permitir a obtenção de dados de base para a extrapolação a escala superior e dimensionamento desta (taxa de retenção e razão de refluxo).

A experimentação deve ser programada para determinar a influência sobre a pureza do produto obtido das variáveis controladas : razão de refluxo, razão base/topo, riqueza da alimentação, temperatura no cristalizador. caudal da alimentação, velocidade do rotor. Não se julga importante a obtenção de dados experimentais sobre a riqueza das fracções esgotadas e rendimentos da operação , que devem ser obtidos por cálculo para a escala industrial. Acessoriamente a experimentação piloto pode permitir encontrar grandezas físicas que, variando significativamente com a pureza do produto de base e com o esgotamento da corrente de topo, tornem possível o controle contínuo do processo.

A um outro nível, demonstrou-se que, das várias definições possíveis de rendimento para separações que recorrem à CCC , a de rendimento real é a mais válida; a sua utilização na análise da operação (rendimento por passe) ou do processo (rendimento final) permite definir campos de operação possíveis para a CCC.

Em particular, na aplicação à separação do óleo de eucalipto, concluiu-se ser a produção de 1,8-cineol a 99% viável ; para atingir um rendimento final elevado é indispensável a reciclagem da corrente esgotada para outra operação de separação. O campo de operação da CCC depende do teor da alimentação e do rendimento por passe pretendido; este campo é definido por uma gama de razões base/topo e de temperaturas no cristalizador. O rendimento final do processo integrado proposto é, em larga medida, independente do rendimento por passe; o valor óptimo deste depende do balanço económico custo de arrefecimento / investimento.

NOMENCLATURA

M- composto presente num binário de solubilidade sólida nula em teor que excede o do eutético;

N- composto presente num binário de solubilidade sólida nula em teor inferior ao do eutético;

P- teor em 1,8-cineol do produto de base (%m/m);

R- razão entre os caudais mássicos das correntes de base e de topo (razão base/topo);

q_a- caudal mássico da alimentação ;

q_b- caudal mássico da corrente de base;

q_t- caudal mássico da corrente de topo;

T - temperatura no cristalizador;

X - teor em 1,8-cineol da alimentação;

x_a- teor em M da alimentação;

x_b- teor em M da corrente de base;

x_t- teor em M da corrente de topo;

Y - teor em 1,8-cineol da corrente esgotada;

Z_a- rendimento aparente;

Z_i- rendimento industrial;

Z_r- rendimento real.

AGRADECIMENTOS

Este trabalho foi realizado no âmbito do Grupo de Estudos de Processos de Separação, que o Instituto Nacional de Investigação Científica vem apoiando, como Projecto de Investigação TLE/6 e,posteriormente, como Linha 1 do Centro de Processos Químicos das Universidades de Lisboa.

BIBLIOGRAFIA

1- Redlich, O.; A. Kister - J. Am. Chem. Society, 71 (1949), 505.

2 - Leprince,P.;A. Chaurel; J. Catry ; L.Costex-

" Procédés de pétrochimie" - Éditions Technip , Paris (1971).
3- Albertins, R. ; W. Gates; J.Powers - "Column Crystallisation" - cap. 11 de "Fractional Solidication " (M. Zief, W. Wilcox), Marcel Dekker , New York (1967).
4 - Marwill, S.; S. Kolner - Chem. Engng. Progress 59 (1963), n.º 2(Fev.), 60-65.
5- Mckay, D.;G.Dale ; D.Tabler - Chem. Engng. Progress 62 (19660, nº 11 (Nov.),104-112.
6- Weedman, J.;R. Findlay- Petroleum Refiner 37 (1958), nº 11(Nov.) 195-200.
7- Gomes, Aquiles - " Processos de Separação para Óleos essenciais", - tese de doutoramento,Lisboa , 1973 .
8- Gomes. Aquiles; Fátima Farelo - comunicação à Chempor 78
9- Gomes, Aquiles -comunicação ao II Congresso da Ordem dos Engenheiros, Porto, 1978.
10- Betts, W. (Coal Tar Research Association) - Comunicação pessoal, 1973.